U.PORTO
FEUP FACULDADE DE ENGENHARIA
UNIVERSIDADE DO PORTO

DEPARTAMENTO DE ENGENHARIA MECÂNICA E GESTÃO INDUSTRIAL

FILM THICKNESS AND FRICTION IN GREASE LUBRICATED CONTACTS: APPLICATION TO ROLLING BEARING TORQUE LOSS

TIAGO COUSSEAU

2013

TIAGO COUSSEAU

FILM THICKNESS AND FRICTION IN GREASE LUBRICATED CONTACTS: APPLICATION TO ROLLING BEARING TORQUE LOSS

A DOCTORAL THESIS SUBMITTED TO THE
FACULDADE DE ENGENHARIA DA UNIVERSIDADE DO PORTO
FOR THE *PROGRAMA DOUTORAL EM ENGENHARIA MECÂNICA*

Supervisor: Prof. Jorge H. O. Seabra
Co-supervisor: Prof. Armando J. V. Campos

DEPARTAMENTO DE ENGENHARIA MECÂNICA
FACULDADE DE ENGENHARIA
UNIVERSIDADE DO PORTO

Acknowledgements

I would like to express my sincere gratitude to my supervisor, Professor Jorge Seabra, and to my co-supervisor, Professor Armando Campos, for their patient guidance and permanent support throughout the course of this work.

My thanks also go to FEUP and to CETRIB/INEGI for providing the material means for carrying out this work.

I wish to thank to my remarkable colleagues and friends at CETRIB for making this work so enjoyable and interesting: Beatriz Graça, Ramiro Martins, Jorge Castro, José Brandão, Luís Magalhães, Jorge Seabra, Armando Campos, David Gonçalves, Carlos Fernandes, André Gama and Pedro Marques.

My special thanks to my family for their permanent availability and constant encouragement even when we were an ocean apart.

This work was developed within the scope of three research projects and an individual Doctoral Degree grant supported by the European Commission and by the Portuguese "Fundação para a Ciência e Tecnologia - FCT" of the Portuguese administration. As a significant part of this work was carried out developed at Luleå University of Technology - Sweden, supervised by Professor Roland Larsson and at the SKF Engineer and Research Center - The Netherlands, supervised by Dr. Piet Lugt, I wish to thank:

- the European Commission for its funding of the project entitled "BIOMON - Toward long-life biolubricants using advanced design and monitoring tools", Contract Reference n. BIOMON-COOP-508208.

- FCT for the economical support:

    - to the project entitled "Low friction, biodegradable and low toxicity greases for rolling bearings", Contract Reference n. PTDC/EME-PME/72641/2006;

    - to the project entitled "Rheology, starvation and tribofilms in grease lubricated rolling bearings", Contract Reference n. PTDC/EME-PME/122271/2010;

    - and for the individual Doctoral Degree grant "Power loss in grease lubricated rolling bearings", Contract reference n. SFRH/BD/70684/2010.

- the machine elements department of Luleå University of Technology - Sweden, and most especially, Professor Roland Larsson and his team for their scientific collaboration and for making the Luleå laboratory of tribology permanently available for carrying out the experimental work presented in Chapter 4.

- the SKF Engineer and Research Center, in special Dr. Piet Lugt and the Lubricant & Metallic Materials team for their scientific collaboration in this work and for providing the means for performing the experimental work presented in Chapter 7.

to my family

Abstract

Nowadays, energy saving and environmental awareness are global requirements for creating a sustainable society.

Every year billions of rolling bearings are manufactured in the world, of which approximately 90 % are lubricated by grease. There is a consensus in the tribological community, however, that grease lubrication is not as well understood as oil lubrication. As predictions of grease performance have not yet been established, increasing our knowledge of grease lubricated rolling bearings can be considered an efficient way of reducing power loss, lubricant consumption and environmental pollution.

The purpose of this work is to study the mechanisms of grease lubricated rolling contacts and the influence of grease formulation on rolling bearings performance, especially in the early stages of grease life when the availability of the oil released from the grease is sufficient to ensure full film formation.

These are the principal axes around which the present work is constructed:

- study of the grease lubrication mechanisms over grease life, with emphasis on the early stages of grease lubrication;
- characterization of the grease properties found to be closely related to grease performance in the early stages of lubrication, namely bleed-oil viscosity;
- analysis of the operating conditions' influence on film thickness and traction behaviour of lubricating greases in single contact tests;
- rolling bearing friction torque measurements and predictions based on single contact test results and on the SKF friction torque model.

Furthermore, due to the significant changes on grease lubrication mechanisms and performance with running time, the authors also include a brief study of degraded greases in order to better understand how grease functions in its later stages of life.

Sumário

Hoje em dia a redução do consumo energético e a consciência ambiental são requísitos mínimos para alcançar uma sociedade sustentável. O aumento do nível de conhecimento dos mecanismos de lubrificação de rolamentos lubrificados por massa é um modo eficiente de reduzir as perdas de potência, o consumo de lubrificantes e a poluição ambiental, uma vez que milhares de milhões de rolamentos são produzidos todos os anos, e que aproximadamente 90 % destes são lubrificados por massa.

Para além disso, existe um consenso geral na comunidade tribológica que os mecanismos de lubrificação da massa não são tão bem conhecidos como os dos óleos. Consequentemente, as ferramentes que prevêem o desempenho dos elementos mecânicos lubrificados por massa não estão bem consolidadas.

Por tanto, o presente trabalho destina-se ao estudo dos mecanismos de lubrificação das massas e da influência da sua formulação no desempenho de rolamentos durante a fase inicial de lubrificação, e foi desenvolvido em volta de quatro eixos principais:

- Estudo dos mecanismos de lubrificação das massas consoante o tempo de operação;
- Caracterização das propriedades das massas que estão intimamente relacionadas com a seu desempenho na fase inicial de lubrificação, nomeadamente a viscosidade do óleo extraído da massa;
- Análise da influência das condições de operação na formação de filme e no coeficiente de atrito medido num contato bola-disco;
- Medição do momento de atrito interno de rolamento, e a previsão deste baseada nos resultados experimentais obtidos nos testes bola-disco e no modelo desenvolvido pela SKF.

Para além disso, devido as significantes alterações no desempenho e nos mecanismos de lubricação das massas com o tempo de operação, um breve estudo sobre massas degradadas relacionando a vida útil destas com os seus mecanismos de lubrificação será apresentado.

Sommaire

Aujourd'hui, économies d'énergie et préoccupations écologiques sont des ingrédients nécessaires au soutien dun développement durable.

Chaque année, des milliards de roulements sont fabriqués dans le monde, $\approx$ 90 % d'entre eux lubrifié á la graisse. Toutefois, la communauté des tribologues s'accorde à affirmer que la lubrification la graisse n'est pas aussi bien comprise que la lubrification à l'huile. Par conséquent, la prévision de la performance des graisses n'est pas encore rigoureusement établie. L'accroissement des connaissances sur les roulements lubrifiés à la graisse est alors un moyen efficace de réduire la perte de puissance, la consommation de lubrifiant et la pollution.

Pour toutes ces raisons, le présent travail vise à étudier les mécanismes du contact roulant lubrifié à la graisse; ainsi que l'influence de la formulation de la graisse sur la performance des roulements, particulièrement dans les premiers stades de la vie de la graisse, quand la disponibilité de l'huile libérée de la graisse est suffisante pour assurer la formation d'un film complet.

Les principaux axes autour desquels le présent ouvrage est construit sont les suivants:

- Étude des mécanismes de lubrification à la graisse durant la vie de la graisse, en mettant l'accent sur les premiers stades de graissage;
- Caractérisation des propriétés de la graisse, qui se trouvent être étroitement liées à la performance de la graisse dans les premiers stades de la lubrification, à savoir la viscosité de l'huile de purge;
- Analyse de l'influence des conditions de fonctionnement sur l'épaisseur de film et le comportement de traction des graisses dans des tests de contact unique;
- Mesure des couples de frottement de roulements à billes et leur prédiction, basées sur les résultats des tests de contact unique et sur le modèle de couple de frottement SKF.

En outre, en raison des changements importants qui se produisent au long du temps sur les mécanismes de lubrification à la graisse et leur performance, une brève étude sur les graisses dégradées est également présentées afin de comprendre comment fonctionne la graisse dans les derniers stades de sa vie.

Keywords

Lubricating greases
Bleed-oil
Rolling bearings
Rheology
Film thickness
Rolling bearing friction torque
Grease degradation

Palavras chave

Massas lubrificantes
Bleed-oil
Rolamentos
Reologia
Espessura de Filme
Momento de atrito de rolamento
Deterioração da massa

Mots-clés

Graisse
Bleed-oil
Roulements
Rhéologie
L'paisseur de film
Couples de frottement de roulements billes
Graisses dgrade

Contents

Acknowledgements v
Abstract ix
Sumário xi
Sommaire xiii
Keywords xv
Table of Contents xvi
List of Figures xxi
List of Tables xxvii
List of Symbols xxix

1. Introduction **1**
1.1. Aim and Thesis Outline 2
1.2. Integration in the R&D activities of the Research Group (CETRIB-INEGI) 4

2. Grease composition and properties **7**
2.1. Introduction 7
2.2. Importance of lubrication 8
2.3. History of grease lubrication 11
2.4. Grease definition 12
2.5. Grease base oil 12
2.5.1. Solubility 13
2.5.2. Oxidation stability 13
2.5.3. Evaporation loss 13
2.5.4. Low temperature properties 13
2.5.5. Viscosity 13
2.5.6. Base oil types 20
2.6. Grease thickener 22
2.6.1. Thickener morphology 23
2.6.2. Thickener types 24

2.7. Additives 26
2.7.1. Corrosion inhibitors - CI 28
2.7.2. Extreme pressure - EP 28
2.7.3. Anti-wear - AW 29
2.7.4. Antioxidants - AO 29
2.8. Grease performance and characterization 30
2.9. Penetration / Grease consistency 32
2.10. Rheological properties 33
2.10.1. Yield stress 33
2.10.2. Oscillatory tests 35
2.10.3. Flow tests 36
2.10.4. Influence of grease formulation on grease rheology 40
2.11. Bleed-oil 41
2.12. Grease manufacturing 42
2.13. Summary 43

3. Experimental characterization of the lubricating greases 45
3.1. Introduction 45
3.2. General characteristic of the used lubricating greases 46
3.3. Scanning Electron Microscopy - SEM 46
3.4. Static bleed test - IP 121/75 50
3.5. X-ray fluorescence - XRF 51
3.6. Remaining oil percentage, or thickener/oil ratio 53
3.7. Fourier transform infrared spectroscopy - FTIR 55
3.8. Rheometry 63
3.8.1. Base and bleed oil flow properties 65
3.8.2. Creep tests 69
3.8.3. Oscillatory tests 73
3.8.4. Flow tests 75
3.9. Other properties 81
3.10. Discussion and conclusions on grease properties 82

4. Lubricant film thickness in a grease and oil lubricated contact 87
4.1. Introduction 87
4.2. Materials and methods 89
4.2.1. Test Specimens 90
4.2.2. Test procedures 91

4.3. Results of fully flooded film thickness measurements 92
4.3.1. Base oil film thickness - Background 92
4.3.2. Base oil film thickness - Results 93
4.3.3. Bleed-oil film thickness - Background 95
4.3.4. Bleed-oil film thickness - Results 97
4.3.5. Grease film thickness - Background 98
4.3.6. Grease film thickness - Results 100
4.4. Discussion on fully flooded film thickness results 102
4.5. Results and discussion on grease thin-films under fully flooded lubrication 108
4.5.1. Grease thin-films - Background 108
4.5.2. Grease thin-films - Results 109
4.6. Results and discussion on grease film thickness under starved lubrication 110
4.6.1. Grease film thickness under starved lubrication - Background . 110
4.6.2. Grease film thickness under starved lubrication - Results . . . 112
4.7. Discussion and conclusions on grease film thickness 114

5. Traction coefficient in a grease lubricated contact 117
5.1. Introduction 117
5.2. Materials and methods 118
5.2.1. Test specimens 118
5.2.2. Test procedure 119
5.3. Friction map analysis 119
5.4. Results 121
5.4.1. Fully flooded tests 121
5.4.2. Starved tests 124
5.4.3. Influence of temperature 126
5.5. Discussion and conclusions on grease traction coefficient 129

6. Rolling bearing friction torque 131
6.1. Introduction 131
6.2. Materials and methods 132
6.2.1. Rolling bearing assembly 133
6.2.2. Test procedure 135
6.3. Experimental results 137
6.4. Friction torque - SKF Model 138
6.5. Lubricant film thickness inside the THBB 51107 145
6.6. Friction torque model results 150
6.6.1. Rolling torque - M'_{rr} 152

6.6.2. Sliding torque - M_{sl} 154
6.7. Discussion and conclusions on rolling bearing friction torque 155

7. Grease degradation **161**
7.1. Introduction 161
7.2. Aging: Practical approach 162
7.3. Results: Comparison between aged and fresh greases 166
7.3.1. FTIR 166
7.3.2. X-ray fluorescence - XRF 172
7.3.3. Remaining oil percentage and bleed-oil viscosity 173
7.3.4. Rheometry 176
7.3.5. Grease film thickness measurements 180
7.3.6. Traction coefficient measurements 184
7.3.7. Rolling bearing friction torque measurements 186
7.4. Discussion and conclusions on grease degradation 189

8. General conclusions and future work **191**
8.1. Conclusions 191
8.2. Future work 193

Bibliography **195**

A. Data correction of the rheological measurements **217**
A.1. Edge effects, wall slip, parallelism, concentricity and flatness of the plates 217
A.2. Gap error 217
A.3. Non-constant shear rate 219

B. Rolling bearing friction torque **221**
B.1. SKF rolling friction torque model 221
B.1.1. Rolling torque - M_{rr} 221
B.1.2. Sliding torque - M_{sl} 224

C. Degradation process (Confidential) **229**

D. Publications **231**
D.1. Articles in international peer reviewed scientific journals 231
D.2. Articles in conference proceedings 233
D.3. Master thesis 234
D.4. Products development 234

List of Figures

2.1. Laminar flow between two planar surfaces. 14
2.2. Kinematic viscosity versus temperature for a mineral oil using different viscosity laws. 16
2.3. Schematic representation of the viscosity index definition. 17
2.4. Photographs of the grease thickener structure using different techniques for similar Lithium mineral based greases. SEM (left), AFM (center) and TEM (right). 24
2.5. Creep Test - Shear strain versus time for different applied shear stresses. 35
2.6. Storage (G') and Loss (G'') moduli versus oscillatory stress. 36
2.7. Shear stress and apparent viscosity versus shear rate of a Newtonian fuild at 40 °C (Base oil). Measurements ($\diamond$); Rheological model (—). . 37
2.8. Shear stress and apparent viscosity versus shear rate of a non-Newtonian fuild at 40 °C (Grease). Measurements ($\diamond$); Rheological model (—). . 37
2.9. Schematic representation of the apparent viscosity versus shear rate for lubricating greases. Non-Newtonian behaviour. 38
2.10. Schematic representation of the shear stress versus shear rate for lubricating greases. Non-Newtonian behaviour. 40

3.1. SEM photographs of the grease thickener structure. LiM1 - Lithium 12-hidroxy stearate. 47
3.2. SEM photographs of the grease thickener structure. LiCaE - Lithium-Calcium thickener of stearate derivatives. 47
3.3. SEM photographs of the grease thickener structure. PPAO - Polypropylene. 47
3.4. SEM photographs of the LiM1 (top), LiCaE (middle) and PPAO (bottom) grease thickener structure. 49
3.5. Bleed-oil Separation Apparatus - IP 121; oil container; 240 mesh filter cone; metallic mass 100 g. 50
3.6. Remaining oil percentage method. 54

3.7. FTIR spectrum of LiM1: grease (top), bleed-oil (middle) and thickener (bottom). 57
3.8. FTIR spectrum of LiM1: comparison between base oil and bleed-oil spectra in the finger print zone. 58
3.9. FTIR spectrum of LiCaE: grease (top), bleed-oil (middle) and thickener (bottom). 59
3.10. FTIR spectrum of LiCaE: comparison between base oil and bleed-oil spectra in the finger print zone. 60
3.11. FTIR spectrum of PPAO: grease (top), bleed-oil (middle) and thickener (bottom). 61
3.12. FTIR spectrum of PPAO: Comparison between base oil and bleed-oil spectra in the finger print zone 62
3.13. Concentric cylinder (a), Vane-cylinder (b), Parallel plates (c) and Cone-plate (d) geometries for a shear rheometer [1]. 63
3.14. Base and bleed-oil viscosity and shear stress vs. shear rate at 40 °C . 67
3.15. Relative percentage difference between base oil and bleed-oil viscosity at 40 °C 67
3.16. Technical data sheet of PPAO (Commercial name: NOION 632 EPB). 68
3.17. Creep test: shear strain versus time for different applied shear stresses. Grease LiM1. 70
3.18. Creep test: shear strain versus time for different applied shear stresses. Grease LiCaE. 71
3.19. Creep test: shear strain versus time for different applied shear stresses. Grease PPAO. 72
3.20. Storage and loss moduli versus oscillatory stress at 40 °C 73
3.21. Complex modulus (G^*) versus oscillatory stress at 40 °C 74
3.22. Phase angle $tan(\delta)$ versus oscillatory stress at 40 °C 74
3.23. Grease viscosity versus shear rate: Comparison between experimental and calculated values at 40 °C 77
3.24. Viscosity versus shear rate: Comparison between the lubricating greases at 40 °C 77
3.25. Grease shear stress versus shear rate: Comparison between experimental and calculated values at 40 °C 79
3.26. Shear stress versus shear rate: Comparison between experimental and calculated values at 40 °C 80
3.27. Shear stress versus shear rate: Comparison between PPAO base oil and bleed-oil at 40 °C 80

4.1. Elasto-hidrodynamically lubricated contact operating at fully flooded (left) and starved conditions (right) [2] 89
4.2. View of the WAM 11A ball-on-disc test apparatus. Luleå University of Technology. 90
4.3. Film thickness versus entrainment speed: Experimental and predicted values at 40, 60 and 80 °C . Base oils. 94
4.4. Application of Carreau model to the PPAO bleed-oil viscosities measured at ≈ 40, 60 and 80 °C 96
4.5. Film thickness versus entrainment speed: Experimental and predicted values at 40, 60 and 80 °C . Bleed-oils. 97
4.6. Film thickness versus entrainment speed: Experimental values at 40, 60 and 80 °C . Greases. 101
4.7. Film thickness versus entrainment speed: Comparison between grease, base oil and bleed-oil at 40, 60 and 80 °C . LiM1. 103
4.8. Film thickness versus entrainment speed: Comparison between grease, base oil and bleed-oil at 40, 60 and 80 °C . LiCaE. 104
4.9. Film thickness versus entrainment speed: Comparison between grease, base oil and bleed-oil at 40, 60 and 80 °C . PPAO. 105
4.10. $\Delta h\,[\%]$ − Relative film thickness increment between base and bleed-oils. 106
4.11. Film thickness results for greases, base oils and bleed products [3]. . . 106
4.12. Avarage lift-off speed (left) and break-through-speed (right) for pure base oil, bleed-oil and grease [4]. 107
4.13. Thin film thickness measurements versus entrainments speed at 40 °C and P_0 = 0,5 GPa. Greases. 110
4.14. Characteristic starvation behaviour for grease lubrication [5]. 112
4.15. Grease film thickness versus time under starved conditions at P_0 = 0.5 GPa, T = 40 °C and Ue = 100 mm/s. 113

5.1. WAM 11A ball-on-disc test device: Traction measurement arrangement. Luleå University of Technology. 118
5.2. Typical 3D friction map obtained under fully flooded lubrication with the different traction regimes highlighted. 121
5.3. LiM1 friction map at 40, 60 and 80 °C . Fully flooded lubrication. . . 122
5.4. LiCaE friction map at 40, 60 and 80 °C . Fully flooded lubrication. . 122
5.5. PPAO friction map at 40, 60 and 80 °C . Fully flooded lubrication. . 122
5.6. Specific film thickness at 40, 60 and 80 °C of all lubricating greases. Fully flooded lubrication 123
5.7. Traction curves at very low $SRR's$, T =80 °C , Ue = 2.8 m/s. 124

5.8. LiM1 friction maps at 40, 60 and 80 °C . Starved lubrication. 125
5.9. LiCaE friction maps at 40, 60 and 80 °C . Starved lubrication. 125
5.10. PPAO friction maps at 40, 60 and 80 °C . Starved lubrication. 125
5.11. Difference in percentage between the traction coefficient values at 40 °C and 80 °C under fully flooded conditions. 127
5.12. Maximum traction coefficient at 40, 60 and 80 °C of each grease under fully flooded lubrication. 128

6.1. Schematic view of the rolling bearing assembly with a THBB 51107. . 134
6.2. THBB 51107 schematic view and dimensions. 135
6.3. Friction torque and operating speed versus time at 1000 rpm and 7000 N. 136
6.4. (a) Friction and (b) operating temperature versus rotational speed . . 137
6.5. (a) Friction torque measurements and predictions versus rotational speed; (b) Operating temperature and base oil kinematic viscosity versus rotational speed. 139
6.6. Operating temperature and kinematic viscosity versus rotational speed. Inputs to run SKF Bearing BEACON. 141
6.7. Friction torque versus rotational speed: comparison between the results from SKF BEACON and from SKF GC 6000. 142
6.8. PPAO bleed-oil viscosity versus shear rate. Measured values (markers), Carreau equation 4.10 (lines). 143
6.9. LiM1: μ_{EHL2} values extrapolated from Figure 5.3 with $R^2 = 0{,}94$. The markers represent the μ_{EHL2} for each bearing operating condition. . . 144
6.10. LiCaE: μ_{EHL2} values extrapolated from Figure 5.4 with $R^2 = 0{,}97$. The markers represent the μ_{EHL2} for each bearing operating condition. 144
6.11. PPAO: μ_{EHL2} values extrapolated from Figure 5.5 with $R^2 = 0{,}97$. The markers represent the μ_{EHL2} for each bearing operating condition. 145
6.12. Operating temperature and bleed-oil kinematic viscosity versus rotational speed. 146
6.13. Pressure-viscosity coefficient versus operating viscosity calculated from the film thickness measurements (markers) and extrapolated with Eq. 6.6 (continuous lines). 147
6.14. Dynamic viscosity and pressure-viscosity coefficient versus rotational speed. 148
6.15. Specific film thickness versus rotational operating speed. 149
6.16. Weighting factor for the sliding friction coefficient (φ_{bl}) versus rotational speed. 149
6.17. Viscosity ratio versus bearing operating speed. 150

6.18. LiM1: Measured and predicted rolling bearing friction torque versus rotational speed. 151
6.19. LiCaE: Measured and predicted rolling bearing friction torque versus rotational speed. 151
6.20. PPAO: Measured and predicted rolling bearing friction torque versus rotational speed. 152
6.21. Rolling Torque ($M_{rr'}$) versus rotational speed. 153
6.22. (a) Rolling Torque ($M_{rr'}$) and (b) Reduction factors product ($\varphi_{rs} \times \varphi_{ish}$) versus the parameter ($\nu \times n \times d_m$). 153
6.23. (a) Sliding Torque - M_{sl1} and (b) M_{sl2} versus versus rotational speed. 154
6.24. (a) μ_{EHL1} and (b) μ_{EHL2} versus versus rotational speed. 155
6.25. Operating temperature T, bleed-oil viscosity ν_{bleed}, viscosity ratio k, total experimental friction torque $M_t \equiv M_{exp}$, rolling torque M'_{rr} and sliding torque M_{sl} versus rotational speed 156

7.1. (a) Grease, (b) Bleed-oil and (c) Thickener spectra. 167
7.2. (a) Grease, (b) Bleed-oil and (c) Thickener spectra. 169
7.3. (a) Grease, (b) Bleed-oil and (c) Thickener spectra. 171
7.4. Fresh bleed-oil dynamic viscosity versus oil loss ($\eta_{\text{bleed-oil}} \times |\Delta_{oil}|$). . . 174
7.5. Bleed-oil viscosity at 40 °C . Comparison between fresh and aged samples.174
7.6. Absolute value of the relative dynamic bleed-oil viscosity versus oil loss ($|\Delta\eta| \times \Delta_{oil}$). 175
7.7. Creep test: Shear strain vs. time for different applied shear stresses. Comparison between fresh and aged sample of LiM1 grease. 176
7.8. Creep test: Shear strain vs. time for different applied shear stresses. Comparison between fresh and aged sample of LiCaE grease. 177
7.9. Creep test: Shear strain vs. time for different applied shear stresses. Comparison between fresh and aged sample of PPAO grease. 177
7.10. Storage G' (—) and Loss G'' ($\cdots$) moduli. Comparison between fresh and aged grease samples. 178
7.11. Shear stress versus shear rate. Comparison between fresh and aged samples. 179
7.12. Film thickness versus entrainment speed. Comparison between fresh and aged samples (a) LiM1, (b) LiCaE and (c) PPAO. 182
7.13. Traction coefficient. Comparison between fresh and aged samples (a) and (b) LiM1, (c) and (d) LiCaE, (e) and (f) PPAO. 185
7.14. Rolling bearing friction torque versus entrainment speed. Comparison between fresh and aged samples (a) LiM1, (b) LiCaE and (c) PPAO. 187

A.1. Gap correction graph at 40°C - Newtonian oil. 218

B.1. Rolling resistance due to pressure distribution and elastic deformation [6].222
B.2. Typical variation of the reduction factors φ_{ish} and φ_{rs} with the operating parameter $\nu \times n \times d_m$. 223
B.3. Typical variation of the rolling torque M'_{rr} and M_{rr} with the operating parameter $\nu \times n \times d_m$. 224
B.4. Sliding resistance due to elastic deformation in a rolling element with a curved contact surface [6]. 225
B.5. Typical variation of the weighting factor (φ_{bl}) with the operating parameter $\nu \times n \times d_m$. 226
B.6. Typical variation of the sliding torque (M_{sl}) with the operating parameter $\nu \times n \times d_m$. 227
B.7. Typical variation of the total torque (M_t) with the operating parameter $\nu \times n \times d_m$. 227

List of Tables

2.1. Number of papers published in Journals of Tribology with the highest SRJ factor from 1999 to 2011. 10
2.2. Properties used for comparing thickeners. 23
2.3. Thickener properties. Comparison between the tested greases. 27
2.4. Twelve phenomena and twenty-four properties of lubricating greases [7]. 31
2.5. NLGI grades and the penetration ranges of worked greases. 32

3.1. Oil bleed rate according to IP 121 standard: T = 40 °C and t = 42 h. 50
3.2. Concentration in percentage of total mass [wt % $\times 10^{-3}$] of the grease chemical content. 52
3.3. Thickener and oil content of LiM1 grease. 54
3.4. Thickener and oil content of LiCaE grease. 55
3.5. Thickener and oil content of PPAO grease. 55
3.6. Yield stress limits at 40 °C . Creep tests. 69
3.7. Yield stress limits at 40 °C . Oscillatory tests. 75
3.8. Inputs and calculated rheological parameters of lubricating greases at 40 °C . Obtained by fitting the viscosity measurements (Figure 3.23) and Equation 3.6. 78
3.9. Inputs and calculated rheological parameters of lubricating greases at 40 °C . Obtained by fitting between the shear stress measurements (Figure 3.25) and Equation 3.7. 81
3.10. Density and refractive index of the lubricating greases and of their corresponding base oils and bleed oils. 82
3.11. Summary of the physicochemical properties of lubricating greases and their constituents. 84

4.1. Ball and disc data. 91
4.2. Pressure-viscosity coefficients of the base oils at ≈ 40, 60 and 80 °C . 94
4.3. Bleed-oil parameters for the Carreau viscosity model at ≈ 40, 60 and 80 °C 96
4.4. Pressure-viscosity coefficients of the bleed-oils at ≈ 40, 60 and 80 °C . 97

4.5. Comparison between film thickness calculated with Equations 4.11 to 4.13 and the measured values presented at Figure 4.6. Grease PPAO, U_e = 0,5 m/s. 100
4.6. Film thickness versus time under starved lubrication. P_0 = 0.5 GPa, T = 40 °C , Ue = 100 mm/s. 113

5.1. Ball and disc data. 119

6.1. Main characteristics of the thrust ball bearing SKF ref. 51107. 135
6.2. SKF parameters for bearing friction torque predictions [8]. 139
6.3. Input parameters for friction torque predictions. 141
6.4. Parameters n and t for all bleed-oils. 147
6.5. Geometric and material parameters of the THBB 51107 for film thickness prediction. 149
6.6. Bleed-oil viscosity, viscosity ratio and friction torque values at 1000 and 2000 rpm. 158
6.7. Characterization and properties of seven lubricating greases. 159

7.1. Concentration in percentage of total mass [wt % $\times 10^{-3}$] of the chemical content of fresh and aged grease samples. 172
7.2. Oil Content. Comparison between fresh and aged grease samples. . . 173
7.3. Thickener Content. Comparison between fresh and aged grease samples.173
7.4. Bleed-oil viscosity at 40 °C . Comparison between fresh and aged samples.175
7.5. Yield stress limits. Comparison between fresh and aged sample at 40 °C 176
7.6. Storage and loss moduli versus oscillatory stress. Comparison between fresh and aged samples at 40 °C in the LVE region. 178
7.7. Used parameters for friction torque predictions. 188
7.8. Friction torque predictions at 40 °C . Comparison between fresh and aged samples. 188

List of Symbols

Symbol	Unit	Designation
C_o	-	influence of ellipticity - $C_0 = 1 - 0,61 \times e^{(-0,752\times(R_x/R_y)^{0,64})}$
d	mm	rolling bearing inner diameter
d_m	mm	rolling bearing mean diameter
D	mm	rolling bearing outer diameter
E	Pa	modulus of elasticity
E^*	Pa	effective elastic modulus - $1/E^* = (1-\nu_1^2)/E_1 + (1-\nu_2^2)/E_2$
E_k^*	Pa	effective elastic modulus - $1/E_k^* = 0.5\times((1-\nu_1^2)/E_1 + (1-\nu_2^2)/E_2)$
F_a	N	axial force
F_N	N	normal force
G	-	dimensionless material parameter - $G = 2 \times \alpha \times E^*$
G_k	-	dimensionless material parameter - $G_k = \alpha \times E_k^*$
G_{cr}	Pa	critical stress (Newtonian limit)
$G_{rr,sl}$	-	factor that depends on the bearing type, bearing mean diameter and applied load
G'	Pa	storage modulus
G''	Pa	loss modulus
G^*	Pa	complex modulus
h	m	central film thickness
H_{oc}	m	central film thickness with inlet shear heating correction - Eq 4.7
H_{ock}	m	central film thickness with inlet shear heating and shear thinning corrections - Eq 4.9
k	-	Viscosity ratio
K	-	model constant of Eq. 2.14
K_f	w/m°C	lubricant thermal conductivity
K_{rs}	-	replenishment/starvation constant

Symbol	Unit	Designation
K_z	-	bearing type related geometry constant
m	-	model constant of Eq. 2.14
m	g	mass of separated oil - Eq. 3.1
M	g	initial mass of the grease sample - Eq. 3.1
M_{exp}	N.mm	rolling bearing friction torque measured experimentally
M_{rr}	N.mm	rolling friction torque
M_{sl}	N.mm	sliding friction torque
M'_{sl1}	N.mm	sliding friction torque calculated using μ_{EHL1} from Eq. 6.4
M'_{sl2}	N.mm	sliding friction torque calculated using μ_{EHL2} from Figures 6.9 to 6.11
M_t	N.mm	total rolling bearing friction torque
n	rpm	rotational speed Chapters 6 and 7
p	Pa	pressure
P	N	load
P_o	Pa	maximum Hertzian pressure
R_x	m	equivalent radius of contact in the X direction - $1/R_x = 1/2 \times (1/R_{x1} + 1/R_{x2})$
R_{xk}	m	equivalent radius of contact in the X direction - $1/R_{xk} = 1/R_{x1} + 1/R_{x2}$
$R_{x1,2}$	m	radius of surfaces 1 and 2 in the X direction
R_y	m	equivalent radius of contact in the Y direction
R_{yk}	m	equivalent radius of contact in the Y direction
$R_{y1,2}$	m	radius of surfaces 1 and 2 in the Y direction
R_1	-	geometry constant for rolling frictional moment
$\bar{R}$	-	shear thinning factor
S_1	-	geometry constant for sliding frictional moment
S_{oil}	% w	separeted oil
SRR	-	slide-to-roll ratio
t	s	time
T	°C	temperature

Symbol	Unit	Designation
$tan(\delta)$	-	phase angle
TV	-	traction values
U	-	dimensionless speed parameter - $U = \eta_0 \times (U_1 + U_2)/(2 \times R_x \times E^*)$
U_e	m/s	entrainment speed
Uh_{min}	m/s	speed value in which the film thickness change its trend
U_k	-	dimensionless speed parameter - $U_k = \eta_0 \times (U_1 + U_2)/(R_{xk} \times E_k^*)$
$U_{1,2}$	m/s	tangential speed of the body contacts 1 and 2
v	m^3	sample volume
$V.I.$	-	viscosity index
W	-	dimensionless load parameter - $W = 2 \times F_N/R_x^2 \times E^*)$
W_k	-	dimensionless load parameter - $W_k = F_N/(R_{xk}^2 \times E_k^*)$
α	Pa^{-1}	pressure-viscosity coefficient
α_{film}	Pa^{-1}	pressure-viscosity coefficient obtained from the film thickness measurements
δ	-	loss factor
Δh	%	relative film thickness between base oil and bleed-oil (Chaper 4) and between fresh and aged grease samples (Chapter 7)
Δ_{oil}	%	relative oil content between fresh and aged grease samples
Δ_{thick}	%	relative thickener content between fresh and aged grease samples
$\Delta\alpha_{film}$	%	relative pressure-viscosity coefficient between fresh and aged samples
$\Delta\eta$	%	relative dynamic viscosity between base oil and bleed-oil (Chapter 3) and between fresh and aged bleed-oils (Chapter 7)
$\Delta\tau$	%	relative shear stress between base oil and bleed-oil
φ_{bl}	-	weighting factor for the sliding friction coefficient
φ_{ish}	-	inlet shear heating reduction factor
φ_{rs}	-	kinematic replenishment / starvation reduction factor
$\dot{\gamma}$	s^{-1}	shear rate
η	Pa.s	dynamic viscosity
η_0	Pa.s	dynamic viscosity at very low shear rate
η_∞	Pa.s	dynamic viscosity at very high shear rate

Symbol	Unit	Designation
Λ	-	Specific film thickness
μ_{bl}	-	boundary coefficient of friction
μ_{EHL}	-	friction coefficient in full film conditions
μ_{sl}	-	sliding friction coefficient
ν	mm^2/s	kinematic viscosity
ρ	kg/m^3	density
σ	m	surface roughness - arithmetic average
σ_s	m	composite surface roughness
τ	Pa	shear stress
τ_{co}	Pa	cross over shear stress
τ_{os}	Pa	oscillatory shear stress
τ_y	Pa	yield stress
ω	s^{-1}	frequency

Acronyms	Meaning
$AGED$	lubricant sample obtained after the Aging Procedure
AO	anti oxidant additive
AW	anti wear additive
CI	corrosion inhibitor additive
EP	extreme pressure additive
$FRESH$	lubricant sample before submitted to any kind of stresses
$FTIR$	Fourier Transform Infrared Spectroscopy
LVE	linear viscoelastic region
ROF	lubricant sample obtained after the ROF test
SEM	Scanning Electron Microscopy
XRF	X-ray Fluorescence Spectrometry

1. Introduction

Ever since rolling bearings and lubricating greases were first used there has been a constant demand for increasing their lifetime, power density and efficiency. Furthermore, growing environmental awareness has led to an increasing interest in biodegradable non-toxic lubricants. Likewise, new grease formulations and bearing designs have been developed and significant efforts have been directed at predicting grease performance in rolling bearings.

Furthermore, grease lubrication mechanisms and, mostly, new grease formulations are very complex and not yet well understood. Consequently, predictive tools are not as well established for grease lubricated contacts as they are for oil lubricated contacts.

Nowadays, nearly 90 % of the rolling bearings are grease lubricated [9]. Since the main function of these rolling bearings is to transmit load at very low friction, the importance of understanding internal friction in rolling bearings becomes relevant when energy saving is a global requirement in our society.

During the last decades intensive research work has been done regarding the tribological and structural changes that take place on Lithium-thickened mineral-based greases under some influencing parameters (temperature, speed, shear stress, grease formulation, contamination, etc.) [10–16]. There have been significant advances and the assumption that grease rolling contacts operating under high shear rates are lubricated mostly by the grease base oil on the top of a thin sheared thickener layer is well-accepted by many researchers [17]. Subsequently, most of the analytical tools developed to predict grease film thickness [18–21], traction behaviour [22,23] and rolling bearing friction torque [8, 24] only take into account the grease base oil properties and neglect the interaction between thickener, additives and base oil.

It has already been shown, however, that the oil released from the grease, which carries information regarding the thickener-additive-base oil interaction, can possess significantly different properties from the base oil [3, 4, 25]. This suggests that a different approach should be used in order to characterize the grease behaviour in an EHL contact.

1.1. Aim and Thesis Outline

TThe main purpose of this work is to investigate the influence of grease formulation on rolling bearing performance in the early stages of grease life. The work is also directed at increasing knowledge of the field of grease lubrication rolling contacts, thereby contributing to the understanding of grease lubrication mechanisms and to the development of predictive tools, in particular those related to film formation and rolling bearing friction torque. These objectives were approached in four parts.

The first part analyses grease lubrication mechanisms and how they affect bearing performance and it is based on friction torque experiments and literature review. From that, it was verified that the oil released from the grease is most probably the dominant lubrication mechanism during the early stage of grease life (first few hours / days).

IIn the second part, the lubricating greases, their corresponding thickeners, base oils and bleed-oils[1] were characterized in order to determine the influence of grease formulation on the bleed-oil physical and chemical properties. Film thickness measurements were then performed with the lubricating greases, their base oils and bleed-oils to verify whether bleed-oil can indeed be considered the active lubricant[2] in grease lubricated contacts when operating under the fully-flooded conditions that occur in the early stage of grease life.

In the third part, traction coefficient measurements of the lubricating greases were carried out with a view to understanding traction behaviour under controlled temperatures, entrainment speed, slide-to-roll ratio and replenishment conditions.

Lastly, in the fourth and last part, full rolling bearing tests were performed with a view to measuring the bearing friction torque and bearing operating temperatures. These measurements were related, by means of the new SKF friction torque model, to the results obtained in the first three parts. Important correction factors were thus integrated in the rolling bearing friction torque model, optimizing it for thrust ball bearings.

Although this thesis focuses on understanding grease lubrication mechanisms and their impact in rolling bearing performance during the initial stages of grease life, a brief study of degraded greases is also presented with a view to understanding the lubrication mechanisms nearer the end of grease life.

This Thesis consists of eight chapters including this *Introductory Chapter*, which justifies the importance of increasing our knowledge of grease lubrication in rolling bearings, and consequently of this work. The work briefly presents an overview of

[1] Oil released from the grease under static or dynamic conditions.

[2] The lubricant that enters in the contact, thus forming the film thickness and generating friction.

current knowledge of grease lubrication mechanisms, identifies areas needing improvement and, lastly, presents a strategy for understanding grease formulation influence on the early stages of bearing performance.

Chapter **2 Grease composition and properties** briefly summarizes the importance of lubrication, the history of lubricating greases and the principle characteristics of the different types of lubricants. This is then followed by a general study of lubricating greases and their components (base oil, additives and thickener), mostly related to the typical physico-chemical properties and rheological response of greases and their base oils. Finally, the base oil, thickener and additive types and main characteristics are briefly described, and the importance of the manufacturing process is outlined.

Chapter **3 Experimental characterization of the lubricating greases** presents the experiments performed to characterize the lubricating greases and their constituents, as well as the test procedures and the pre and post-test analyses that were performed.

In Chapter **4 Lubricant film thickness in a grease and oil lubricated contact**, film thickness measurements carried out in a ball-on-disc device with the lubricating greases, their base oils and bleed-oils are presented. Film thickness predictions of Newtonian and non-Newtonian fluids are discussed and applied to the experimental results. Test procedures, pre and post-test analyses are also presented.

In Chapter **5 Traction coefficient in a grease lubricated contact**, the friction behaviour of lubricating greases is described in a wide range of operating conditions. Test procedures, pre and post-test analyses are also presented.

Chapter **6 Rolling bearing friction torque** presents the friction torque measurements. The new SKF friction torque model is explored by adding the knowledge obtained in Chapters 3, 4 and 5. The friction torque device, the procedures, pre and post test analyses are also presented.

Chapter **7 Grease degradation** describes an aging procedure developed for simulating lubricating greases during their later stage in life. All the lubricating greases were then aged and the techniques described in Chapters 3 to 6 were applied. A comparison between fresh and aged greases is presented.

The Chapter **8 General conclusions and future work** discusses the main conclusions of this work and suggests some ideas for future work.

1.2. Integration in the R&D activities of the Research Group (CETRIB-INEGI)

The research work presented in this thesis was developed and performed whilst the author and the Research Group participated in three research projects:

- **BIOMON - Toward long-life biolubricants using advanced design and monitoring tools**. The aim of this R&D project was to develop long life bio lubricants based on high-performance native esters and high temperature and oxidation-resistant biodegradable greases based on polyurea thickeners mixed with native esters. The purpose of the project was directed at increasing speed limits and performance by 10-20 %, reducing wear by 20 % and improving life proportionally by comparison to actual lubricants. The use of advanced tools and a 10 % decrease in the amount of lubricant used should help to reduce maintenance costs by approximately 30 %. This R&D project received financial support from the European Union through Contract Reference n. BIOMON-COOP-508208.

- **Low friction, biodegradable and low toxicity greases for rolling bearings**. The aim of this R&D project was to evaluate and compare biodegradable non-toxic greases for rolling bearings to conventional ones in terms of wear and power loss. Researchers hoped to develop/optimize a rolling bearing energetic (energy loss vs. heat evacuation) model that incorporates different sources of friction and takes the grease formulation into account. This R&D project received financial support from the Portuguese "Fundação para a Ciência e Tecnologia - FCT" through Contract Reference n. PTDC/EME-PME/72641/2006.

- **Rheology, starvation and tribofilms in grease lubricated rolling bearings**. The purpose of this on-going R&D project is to understand and quantify lubricant replenishment and contact starvation with regards to three major parameters: bearing geometry, bearing kinematics and bleed oil characteristics. It also aims at quantifying how thickener fibres (Lithium, Polypropylene, ...), base oil nature (mineral, PAO, Ester) and additives influence the generation/removal mechanisms of tribofilms inside the contact, as well as tribofilm influence on friction generation. This R&D project has received financial support from the Portuguese "Fundação para a Ciência e Tecnologia - FCT" through Contract Reference n. PTDC/EME-PME/122271/2010.

This research work was also supported by FCT, through the following individual Doctoral Degree grant (Contract reference n. SFRH/BD/70684/2010):

- **Power loss in grease lubricated rolling bearings**. The purpose of this grant was to continue the work developed on the previous projects, focusing on bleed-oil properties and their influence on grease tribological performance.

The authors research papers referred to in this thesis were based on his work as a member of the aforementioned projects, with a view to disseminating the said projects, and in agreement with the respective contracts.

More than 10 lubricating greases were studied under these projects and the thesis work. Because of time and test rig constraints, however, only three of these greases were analysed in full detail and are presented in this thesis. Nevertheless, some of the results obtained with the other greases were used because certain conclusions were more consistent when several, instead of only three, greases were compared.

2. Grease composition and properties

2.1. Introduction

The main purpose of using a lubricant is to reduce friction and minimize wear between two or more surfaces in relative motion. Theoretically, any substance - solid, liquid or gas - interposed between two surfaces to facilitate their relative slip is a potential lubricant. Many other characteristics, however, are often demanded of the lubricants: generation of a separation of the surfaces, low shear strength, good thermal conductivity, good oxidation and corrosion protection ability. Furthermore, environmental concerns have added biodegradability and low-toxicity requirements to the lubricants.

In an elasto-hydrodynamic contact the lubricant flows extremely swiftly ($\approx$ 1 ms) through the contact, suffers a pressure shock of $\approx$ 1 GPa or higher, is submitted to deformation rates that can reach $\approx 10^{+7}$ s^{-1}, and temperature rises above 100 °C . Such conditions, characterized by high and rapid variations in pressure and temperature, dramatically alter the properties of the lubricant. Consequently, characterization of the physical, chemical, rheological and tribological behaviour of the lubricant inside the contact is challenging.

Such characterization is even more complex when greases are used as lubricants, since their lubrication mechanisms are not as well understood as compared to oil lubrication mechanisms [17]. Furthermore, it is known that the properties of lubricating greases may change significantly and very quickly over time depending on the operating conditions [26, 27]. Some greases after running less than 1 % of their lifetime in rolling bearings can present rheological differences greater than 100 % with few chemical changes, as will be shown in Chapter 7.

Such complexity is expressed by the significant number of standard and nonstandard test methods used to qualify lubricating greases and their constituents, of which most are very demanding in terms of consumables, time and people.

A brief description of the importance of lubrication, the history of lubricating greases and their main characteristics are presented in this chapter. This is followed by a more in-depth explanation of some of the many tests often used to characterize

lubricating greases and their constituents.

2.2. Importance of lubrication

At the engineering level, the main functions of lubricants are friction control and wear minimization by reducing the metal-to-metal contact between components. In elasto-hydrodynamic lubrication, however, the lubricant also has several other secondary functions, such as:

- Cleaning: lubricants maintain internal cleanliness by suspending contaminants within the fluid or by preventing the contaminants from adhering to the operating surfaces;
- Cooling: by reducing friction, minimizes heat generated by the moving parts, which lowers the overall operating temperature of the equipment. Lubricants also absorb heat from the contacting surfaces and transport it to locations where it can be safely dispersed, such as the oil sump;
- Protection: a lubricant must be able to prevent or minimize internal component corrosion. Lubricants accomplish this either by chemically neutralizing corrosive products or by creating a barrier between the components and the corrosive material;
- Sealing: lubricants act as a dynamic seal like grease on rolling bearings, which prevents external contamination from coming into the bearing;
- Dampening Shock: a lubricant can cushion the blow of mechanical shock. A highly functional lubricant film can resist rupture and absorb and disperse energy spikes over a broad contact area. As mechanical shock on components is dampened, wear and damaging forces are minimized, thus extending the overall operating life of the components.

The economic relevance of lubrication was put into evidence in 1966 through the so called Jost Report [28], which estimated savings of about 700 millions of pounds per year if the concepts of correct lubrication were used. From then on research in tribology has grown every year.

It is estimated that nowadays, approximately one third of all energy used in industrial countries goes to overcome friction [29]. High friction often results in high wear and machinery breakdown and more than 30 % of production in industry goes to replace worn-out products with new ones. Furthermore, machinery breakdown

of may also result in safety risks and environmental pollution. Therefore, reducing friction and controlling wear is a major challenge in our attempt to achieve a sustainable society with low energy consumption and reduced environmental climate change effects [29].

As described earlier, friction and wear control are often secured by lubrication. It is also important to point out, however, that lubricants are a common pollutant in a wide range of industries [30]. In some cases, lubrication systems are designed to compensate for lubrication loss with periodic re-lubrication; unfortunately, the lubricants are released into the environment without treatment, thus forming a significant source of water and earth pollution. Although lubricants are already formulated with a special regard for biodegradability and ecotoxicity, replacement of conventional lubricants by biodegradable formulations has been very slow.

Growing concerns for the need to reduce friction and wear are demonstrated by the increasing number of papers published in the field of Tribology in the last decade (increasing at a rate of approximately 60 %). According to SJR[1] [31], more than 11,000 papers were published in tribology journals with higher SJR, such as: Wear, Tribology International, Tribology Letters, Journal of Tribology, Tribology Transaction and Journal of Engineering Tribology, Part J. These data were obtained in December 2012 and are presented in Table 2.1.

Of these 11,000 papers published, although approximately 9,000 are related to lubricating oils and greases, only 1 in every 6 to 9 papers refers to lubricating greases[2]. It was already to be expected since the global business for grease, which represent only 9 % of the estimated total lubricant consumption in the world (data from 2004) [32], does not allow for large research programs.

[1]SCImago Journal Rank indicator. A measure of a journals impact, influence or prestige, it expresses the average number of weighted citations received in a given year according to the number of papers published in the journal in the three previous years.

[2]Data obtained from Scopus (www.scopus.com) and ISI Web of Knowledge (apps.webofknowledge.com). The constrains used as input in both websites were: Lubricating grease(s) and Lubricating oil(s). The search ran between 1999 and 2011.

Table 2.1.: Number of papers published in Journals of Tribology with the highest SRJ factor from 1999 to 2011.

	Number of papers published per year												
Scientific Journals	1999	2000	2001	2002	2003	2004	2005	2006	2007	2008	2009	2010	2011
Tribology Letters	58	47	74	69	87	153	130	133	133	104	106	200	147
Journal of Tribology	138	124	114	112	108	110	110	114	119	92	117	92	53
Tribology International	79	98	91	90	125	117	123	209	203	142	224	310	226
Wear	393	240	369	240	315	277	393	325	384	381	467	318	505
IMechE, Part J: Journal of Engineering Tribology	41	49	47	36	40	51	40	80	82	105	116	119	76
Tribology Transactions	121	115	95	77	80	70	70	38	41	44	92	62	41
Total of publications	**830**	**673**	**790**	**624**	**755**	**778**	**866**	**899**	**962**	**868**	**1122**	**1101**	**1048**

2.3. History of grease lubrication

The technology of lubrication has been used since ancient times, when massive rock slabs were moved to build the pyramids. The recorded use of lubricants animal fats or vegetable oils - dates back almost to the birth of civilization.

Ancient inscriptions dating back to 3500 to 2500 B.C. suggests that grease-like lubricants were already known to the Sumerians who used them in their wheeled vehicles [33]. As early as 1400 B.C., Egyptians are said to have used grease made from olive oil or tallow (animal fats) and lime to lubricate the axles on the chariot wheel [34]. From these very early roots, efforts to reduce friction depended on relatively abundant animal fats and vegetable-based oils.

During the Middle Ages (450-1450 A.D.) there was a steady development in the use of lubricants, but it was not until 1600-1850 A.D. (particularly during the industrial revolution in 1750-1850 A.D.) that the value of lubricants in decreasing friction and wear was recognized.

The first grease of the industrial age, a calcium grease made from olive oil or tallow, was probably patented by Partridg [35] in 1835. About 10 years later, greases based on mineral oils and thickened with soaps were probably first proposed by Raecz [36]. In 1849,, William Little [37] patented a sodium grease made from tallow and from then on, many other grease types were developed. During the 1930s and 1940s calcium, lithium and barium-thickened greases were developed as multi-purpose lubricants. The 1950s was the age of aluminium complex greases and the 1960, that of lithium complex thickened greases. Later, the 1980s saw the first use of polyurea and the 1990s, the development of polypropylene greases.

Further developments in grease lubrication are expected due to ever-increasing demands for long life, higher speed, higher running temperatures, higher performance in different types of materials (steel, aluminium, composites, etc.) and compatibility with the mechanical seals, as well as increasing global environmental concerns, that the future will bring.

According to specialists from the European Lubricating Grease Institute (ELGI), fundamental research able to describe the basic principles of grease lubrication is still just in its infancy and presents a major challenge for current and future researchers and grease manufacturers [38].

2.4. Grease definition

The most common definition of lubricating grease is the one put forward by The American Society for Testing and Materials (ASTM D 288): "*A solid to semi fluid product of a thickening agent in a liquid lubricant, other ingredients imparting special properties may be included.*" [39].

This means that a lubricating grease is a thickened (not a thick) oil. It also states that grease is based on a multiphase system consisting of at least two well-defined components, namely a thickener and a lubricant fluid. The "other ingredients" refers to additives and co-thickeners.

The typical distribution of these components is 65 to 95 wt % base oil, from 5 to 35 wt % thickener (and co-thickener) and from 0 to 10 wt % additives [40]. Nowadays, nano particles are also used in grease formulation as replacements for some additives [41–44].

These separate components form a multi-phase matrix and coexist like "water in a sponge", where the thickener system is the sponge and the base oil is the "water". Although not strictly scientific, this illustration is useful in conceptualising certain problems arising from the use of lubricating greases.

Such a composition endows the grease with a certain consistency and a viscoelastic semi-plastic behaviour that gives it many advantages over lubricant fluids. Although each of its components plays a very important role in the lubrication process, their effectiveness depends on their interaction and on the manufacturing process, which makes it quite difficult to characterize their individual influence on grease performance.

2.5. Grease base oil

As described in the previous section, lubricating greases typically contain about 65-95 % base fluid. Consequently, the base oil will exert considerable influence on the behaviour of the finished grease. In order to fulfil its role in a wide range of applications, the base oil must contain a combination of appropriate properties such as: solubility, oxidation stability, evaporation loss, low temperature properties and viscosity. Environmental and health aspects are also requirements. Base oils commonly used in grease formulation are mineral, triglyceride and synthetic oils.

2.5.1. Solubility

Perhaps the most important factor in the choice of the base oil is its solubility characteristics. For both the manufacturing process and the final performance characteristics of the grease, it is important that the solubility of the thickener and that of the base oil are properly balanced. Optimised solubility will result in:

- Better yield (less thickener is needed to obtain a specific consistency);
- Rapid mixing during manufacturing;
- Less oil separation;
- Better storage stability.

2.5.2. Oxidation stability

Oxidation stability is a lubricant's ability to resist oxidation. The oxidation process of lubricants has been already described elsewhere [45–47] and is briefly presented in Chapter 7. It is important to point out that the oxidation effects on the tribological performance of the grease is not well known. It is generally accepted, however, that oxidation reduces lubricant life.

2.5.3. Evaporation loss

The operating temperature of lubricating greases can be relatively high and oil loss takes place due to evaporation. A low loss of volatile components in the base oil is therefore desirable. Moreover, high oil losses make the grease too stiff and may lead to severe starvation conditions.

2.5.4. Low temperature properties

The low temperature properties of the grease are not directly dependent on the pour point (the lowest temperature at which base oil still flows), but they are significantly affected by it. Certain thickeners may reduce this temperature even more.

2.5.5. Viscosity

Viscosity and temperature, pressure and shear rate dependency are key base fluid requirements. Different levels of base oil viscosity have different properties. High viscosity base oils generally result in:

- Less oil bleed;
- Higher yield (less thickener is needed to obtain the preferred consistency);
- Better performance at the lowest speeds;
- Better load carrying capacity;
- Lower evaporation loss;
- Stronger adhesion;
- Better water resistance.

Low viscosity oils produce:

- Improved heat transfer;
- Better low temperature properties.

For example, high-speed bearings require relatively low viscosity oils and vice versa.

2.5.5.1. Definition of viscosity

The viscosity of a fluid is defined as the resistance opposed by the fluid to internal shear deformation. This opposing force can be calculated by applying *Newton's formula* to the laminar flow between a mobile surface with a velocity V and a fixed surface, as shown in Figure 2.1.

Since there is relative motion between both surfaces and the no-slip boundary condition needs to be verified, obviously there will be different "layers" of fluid moving at different speeds ranging from 0 to V.

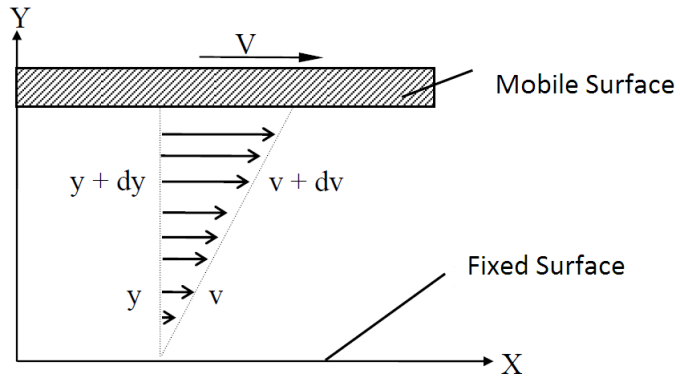

Figure 2.1.: Laminar flow between two planar surfaces.

At any distance y from the fixed surface, the speed of the fluid is v; at a distance $y + dy$ the speed will be $v + dv$. Thus, shear stress, represented by τ, can be given as

$$\tau = \eta \frac{dv}{dy} \tag{2.1}$$

where η is a characteristic coefficient of the fluid designated by dynamic viscosity and the derivative dv/dy is the variation of the fluid speed with height, referred as shear rate $\dot{\gamma}$.

The above hypothesis can be experimentally verified for many fluids. These types of fluids are known as *Newtonian fluids*. Common fluids such as water and several oils present this type of behaviour under laminar flow conditions. The presence of macro molecules or the extreme use (high loads) of these fluids may modify their behaviour so that the linear proportionality relation between shear stress and shear rate can no longer be verified. If the above linear relation is no longer valid, the fluid is then classified as *non-Newtonian*.

Dynamic viscosity (η) is measured in rotational rheometers and is given in Pascal second (Pa.s) in the International System.

Kinematic viscosity (ν) is often measured with an Engler Viscometer, but it can also be calculated from the dynamic viscosity with equation 2.2.

$$\nu = \frac{\eta}{\rho} \tag{2.2}$$

where ν is the kinematic viscosity in m^2/s, commonly represented in mm^2/s or cSt (centistokes) and ρ is the density of the fluid in Kg/m^3.

2.5.5.2. Viscosity dependence on temperature

Thermo viscosity is the change of viscosity under varying temperatures. An increase in temperature always has a thinning effect on lubricating oils; i.e., viscosity diminishes as the temperature rises.

Several models for this dependence have been developed. Thermo viscous behaviour is of significant interest to EHD lubrication because it is one of the two lubricant parameters used as an input for film thickness prediction, as will be shown in Section 4.3.1.

The simplest thermoviscosity law, given by Equation 2.3, was proposed by *Cameron* [48]. This equation, however, is only valid for small variations of the reference temperature.

$$\eta = \eta_0 e^{(-\beta \Delta T)} \tag{2.3}$$

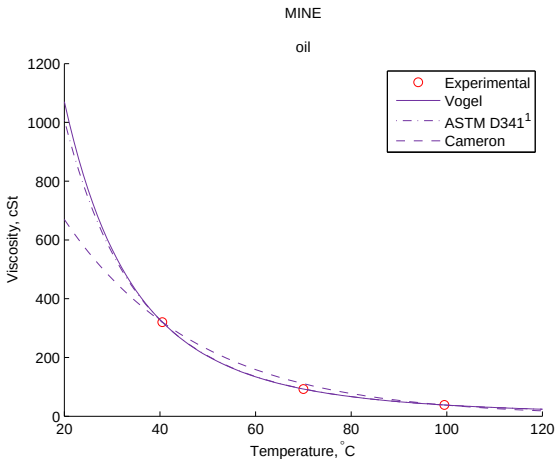

Figure 2.2.: Kinematic viscosity versus temperature for a mineral oil using different viscosity laws.

A more accurate equation that expresses the thermo viscosity of a lubricant is described in ASTM D341 standard [49], as shown in Equation 2.4.

$$LogLog(\nu + a) = n - mLog(T) \tag{2.4}$$

where ν is the kinematic viscosity, T is the temperature in Kelvin and m, n and a are experimentally determined lubricant dependent constants.

Many other laws such as Vogel's equation [50] describe the thermo viscous behaviour of lubricating oils. Vogel's equation is said to be a more realistic approximation for viscosity variation with temperature since three experimental points are required in order calculate the constants of the equation. Nonetheless, it gives very similar results as ASTM D341, which requires only two viscosity values that are usually provided in the technical data sheet for the lubricants.

Figure 2.2 compares the results obtained by means of the above laws.

An arbitrary measure for the change of viscosity with temperature is given by the viscosity index (VI) as a single number, standardized by ISO 2909 / ASTM D2270-10e1 [51]. This can be calculated with the following equation

$$V.I. = \frac{L - U}{L - H} \times 100 \tag{2.5}$$

where L and H, which correspond to the viscosity of the reference oil at 100 °C , are read from Table 2.2 from [51], and U is the viscosity at 40 °C of the oil of interest. A schematic representation of the viscosity index definition is given in Figure 2.3.

As shown in the Figure 2.3, high VI values represent low viscosity variations with temperature and vice versa.

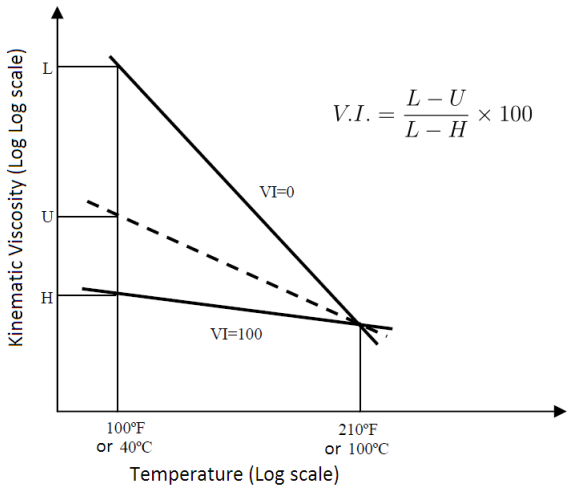

Figure 2.3.: Schematic representation of the viscosity index definition.

2.5.5.3. Viscosity dependence of pressure

Piezoviscosity is the change of viscosity under varying pressures. Unlike the effect of temperature, an increase in pressure is always followed by an increase in viscosity.

Several laws describing the viscosity dependence on pressure have been developed. Piezoviscosity, as well as thermo viscosity, is of significant interest in EHD lubrication as it is the second lubricant parameter used as an input for predicting film thickness, as will be shown in Section 4.3.1.

The simplest law describing the variation of viscosity with pressure was proposed by Barus [52] and is given by equation 2.6, or equation 2.7 when the thermo viscous effect is also included.

$$\eta = \eta_{0T} e^{(\alpha p)} \tag{2.6}$$

$$\eta = \eta_0 e^{(\alpha p - \beta \Delta T)} \tag{2.7}$$

where α is the pressure-viscosity coefficient used in the film thickness equation, given in Pa^{-1}, β is the thermoviscosity coefficient and p is the pressure that the lubricant is subjected to.

These equations consider that the piezoviscosity coefficient is pressure-independent and that it is defined at the oil temperature in the contact inlet. Although this is satisfactory for minor variations in pressure and temperature, it becomes inaccurate for pressures above 0.1 GPa and high temperatures.

Roelands [53] proposed another equation that is more accurate than Baruss equation for high pressures (above 0.1 GPa) and temperatures up to 200 °C ,

$$ln(\eta) = (ln(\eta_0) + 9,67) \times \left\{ \left(\frac{T - 138}{T_0 - 138} \right)^{-S_0} \times \left(1 + \frac{p}{0,196} \right)^{Z} - 1 \right\} \tag{2.8}$$

Bair [54] however, has criticized the use of Barus and Roelands equations since measurements at very high pressure have shown that for many liquids, the viscosity increase with pressure does not follow Barus and Roelands law. In fact, the viscosity increase with pressure is less than exponential up to a certain pressure (generally greater than 1 GPa) and greater than exponential after that. Although Bair then proposed an improvement on Barus and Roelands' equations, this has failed to be adopted by the tribology community because it requires very challenging and expensive low and high pressure viscosity measurements.

Consequently, Equations 2.7 and 2.8 are still the most widely used in lubrication literature, mostly because they are adequate for the resolution of Reynolds equation for film thickness calculations, as shown in 1959 by Downson and Higgindon's theoretical predictions [55] and later through Crook's experimental observations [56–59]. Still, even these equations require at least one measurement of the dynamic viscosity at a non-atmospheric pressure.

In case these measurements are not available, empirical equations have to be used, such those proposed by Gold *et al.* [60], So and Klaus [61], Fein [62], among others. As the values predicted by these equations, however, show very large differences (>95 %) for the same inputs, this is not advisable. This, together with the fact that high pressure rheological measurements are difficult and expensive, led to the extrapolation of the pressure-viscosity coefficient (α) from film thickness measurements. Van Leeuwen showed that such extrapolation produces a less than 5 % error of theα-value [63]. Bair, however, pointed out that such methodology leads to wrong α predictions, since it most likely adjust for the neglect of ordinary shear-thinning [64].

2.5.5.4. Viscosity dependence of shear rate

The viscosity dependence of the shear rate is evident in lubricating greases, as described in Section 2.10.3. However, even the base oil viscosity that exhibits a Newtonian behaviour under moderate pressures and shear rates, may present a non-Newtonian behaviour under extreme conditions, such as in EHL conditions where pressures are typically between $1,0 \leqslant P_0 \leqslant 3$ GPa and shear rates of $10^5 \leqslant \dot{\gamma} \leqslant 10^8$ s^{-1}.

This occurs up to the point where stress reaches a limiting shear stress. If lubricant behaviour during the journey through the contact were truly Newtonian and given a

nearly exponential increase of viscosity with pressure, very high shear stresses and, consequently, coefficient of frictions would have to be observed. But this is not the case, since 0.05 is a typical value for the coefficient of friction measured for such conditions.

The shear rate dependency in this situation used to be defined in terms of shear stress τ^* since at the high "pressure zone" of the contact, shear stress is an important parameter for determining the lubricant coefficient of friction. One of the many models used to describe the shear thinning effect, and probably the most frequently used is the Ree-Eyring model [65]:

$$\frac{\eta}{\eta^*} = \left(\frac{\tau^*}{\tau_E}\right)^{-1} \texttt{sinh}\left(\frac{\tau^*}{\tau_E}\right) \tag{2.9}$$

whereby, the viscosity is found to be temperature, pressure and shear rate dependent - $\eta(T, p, \dot{\gamma})$.

2.5.5.5. Other base oil properties

Bulk density

Bulk density is defined as the ratio between the mass of a body and its volume (kg/m^3); like viscosity, it also depends on pressure and temperature. Its approximate variation with temperature can be calculated using Equation 2.10 [47]:

$$\rho(T) = \rho(T_0) \times (1 - \frac{T - T_0}{1250}) \tag{2.10}$$

where T is temperature and $\rho(T_0)$ is the density measured at reference temperature T_0.

Density variation with pressure can be estimated using the empirical equation proposed by Hamrock [66]:

$$\rho(p) = \rho(p_0) \times \left(1 + \frac{0,6p}{1 + 1,7p}\right) \tag{2.11}$$

where p is pressure and $\rho(p_0)$ is density measured at the atmospheric pressure p_0.

Thermal conductivity

Thermal conductivity is the heat flow that is transferred when a unitary temperature gradient per unit of time flows in a normal direction to a unitary area surface. Higher thermal conductivity favours heat evacuation, (e.g. when the lubricant is

cooled on a heat exchanger). This property exhibits linear variation with temperature and is expressed in W/m°C .

Specific Heat

This property is of great importance as it defines how much energy is needed to create a temperature variation of one Kelvin for a unitary mass. For example, in the inlet zone of an EHD contact, a higher specific lubricant heat generates a lower temperature increase. Like thermal conductibility, specific heat varies linearly with temperature and is expressed in J/kgK.

Thermal diffusivity

Thermal diffusivity is the property that describes how temperature spreads on bodies; it is defined as the ratio between thermal conductivity and the product of bulk density by its specific heat. This property is expressed in m^2/s.

A full description of lubricating oil properties is given in [67].

2.5.6. Base oil types

2.5.6.1. Mineral oils

A mineral oil undergoes a series of processes, depending on the crude and the technology used in the refining. As a result, mineral oils contain a very wide variety of chemical components.

A carefully selected blend of different mineral oils based on the type of the carbon bond is used in lubricating greases:

- Aromatics, for their excellent solubility;
- Naphthenics, for their good low temperature properties;
- Paraffins, for their high viscosity index, low sulphur content and inherent good oxidative stability.

One of the lubricating greases (LiM1) studied was formulated with a relatively high viscous mineral base oil. High viscous base stocks contain small amounts of inactive sulphur that also positively affect the extreme pressure, anti-wear and anti-oxidant (EP/AW/AO) characteristics (additive effects are presented in Section 2.7).

2.5.6.2. Synthetic oils

In contrast to mineral oils, synthetic oils are prepared by the reaction of chemical compounds. As such, they can be tailored to provide properties that might be impossible to achieve using conventional mineral products.

Compared to mineral oils, synthetic base oils typically offer one or more of the following advantages:

- Higher Viscosity index[3];
- Improved thermal and oxidative stability[3];
- Low volatility[3];
- Improved low temperature flow behaviour;
- Lower internal friction;
- Improved wear performance and load carrying capacity;
- Enhanced corrosion protection;
- Lower toxicity risks due to the absence of aromatics;
- Eventually improved fire resistance.

Typical application areas for greases based on synthetic oils are those requiring a wider range of operating temperatures or enhanced chemical resistance. Compatibility with rubber or plastic components and seals, lubrication of non-metallic surfaces and improved electrical properties are all areas where synthetic base fluids can make a difference. Besides, environmental considerations such as biodegradability also lead to the use of synthetic oils. Large-scale use of synthetic base oils, however, has increased slowly because of their considerably higher cost and the relatively recent development of most of them.

Several groups of synthetic base fluids that may be applied to grease include: synthetic hydrocarbons (PAOs), alkylated aromatics, esters, polyglycols, silicone oils, perfluoropolyethers and many others.

Only esters and PAO characteristics are shown below because these are the types of synthetic base oils used in this work.

[3]Allows higher operating temperature

PolyAlphaOlefins (PAO)

PAOs meet many of the requirements of an ideal lubricant. They have high oxidative and thermal stability, high Viscosity Indexes (VI), low evaporation rates up to 160 °C and a very low pour point. Although their low polarity leads to poorer additive solvency, their response to antioxidants and EP/AW additives is better than that of mineral oils. PAOs are miscible with all mineral oils and esters. Due to their totally paraffinic structure, PAOs tend to polar shrink seals. To avoid this, they are usually blended with a small amount of polar oil, such as an ester. Although traditionally PAOs have been used in aerospace, nowadays they have gained importance in life time applications. Their relative cost is about three to five times that of mineral base oils.

Diesters and polyesters

Diesters and polyesters have very good ageing characteristics, favourable evaporation behaviour, excellent low temperature behaviour and viscosity indexes, good solubility, and are miscible with mineral oils and PAOs. Some of them also biodegrade rapidly.

Careful selection of sealing materials is necessary, however, and paint coatings may be affected. Their relative cost is about four to five times that of mineral base oils

2.6. Grease thickener

The thickener system is a key factor in providing a mechanically stable grease matrix, both over time and under the operating shear within the mechanical components. The system must offer a solid structure until operating conditions - such as load, shear and temperature - initiate a viscoelastic response in the grease. It is one of the characteristics because of which about 90 % of the rolling bearings are grease lubricated [9]. In rolling bearing applications, the solid structure of the grease forms a lubricant reservoir and provides a sealing action (grease attached to the seals and cage); grease under large shear rates has a viscosity decrease due to its shear thinning properties, which endows it with excellent flow and lubrication properties (grease surrounding the contact inlet).

Thickeners also contribute to the extreme pressure and anti-wear qualities of a grease and additionally, they produce a grease gel capable of carrying additives, extending their performance to those areas. Water resistance, surface adhesion/tackiness, dropping point and compatibility with other grease are all properties where the thickener plays an important role. Besides, as with all other grease components,

human toxicology, eco-toxicology and the biodegradability of lubricating greases are also thickener-related and have become important issues.

The thickener structure holds the base oil by mechanical entrapment and a combination of Van der Waals and capillary forces[4] [68]. Interaction between thickener molecules are dipole-dipole, including hydrogen bonding [69] or ionic and Van der Waals forces [70]. Although this is true for most of soap thickeners, in the case of non-soap thickeners like Polypropylene (PP) however, these interact only through Van der Waals forces, and their interaction with the oil is likewise different. The effectiveness of these forces depends on how these fibres contact each other [9]. When all their properties are taken into consideration, none of the commercially important thickeners stand out from the others (see Table 2.2). They are comparably competitive and suited for their tasks. The differences mainly lie in the more special demands that are made on them [32]. Besides, for the same application, a certain type of thickener can be better or worse than others in terms of efficiency (power loss and wear), depending on its interaction with the base oil and additives and the manufacturing process. The thickener by itself, although it provides several characteristics to the greases, does not lead the grease performance.

Table 2.2.: Properties used for comparing thickeners.

Thickener Properties			
High temperature	Compatibility	Tackiness	Shear
Low temperature	Oil loss	Flowability	Friction
Aging	Toxicity	Load	Wear

2.6.1. Thickener morphology

The morphology and dispersion of the grease structure is usually examined under Transmission Electron Microscopy (TEM), Scanning Electron Microscopy (SEM), Atomic Force Microscopy (AFM), Cryo-Scanning Electron Microscopy (cryo-SEM) and others. However, because of sample preparation, exposure time and incident energy of the electron beam on the sample, all requirements of the electron microscopy techniques, there is a real possibility that the thickener might be damaged or changed in the process.

[4] A capillary effect occurs because of attractive inter-molecular forces between the liquid and the solid surrounding surfaces. The effect depends on the surface tension and adhesive forces between oil and thickener

The AFM technique, in spite of its possibly not changing the grease structure, only shows the surface of a sample down the atomic scale; only thickener that is not dipped in the base oil can be observed. There are different types of light microscopy techniques where particles can be identified as clusters and agglomerates of several molecules, yet no evidence is found of fibres or a network structure as discovered by the SEM techniques [38].

EAlthough each technique offers some advantages over the others, none of them provides the "perfect picture" of the grease structure and it is possible that the "true structure" of the lubricating greases is still unknown [38].

Figure 2.4 shows some typical images of the structure of similar lithium greases formulated with mineral base oil obtained with SEM, AFM and TEM, respectively. Windows size corresponds to approximately 10 μm.

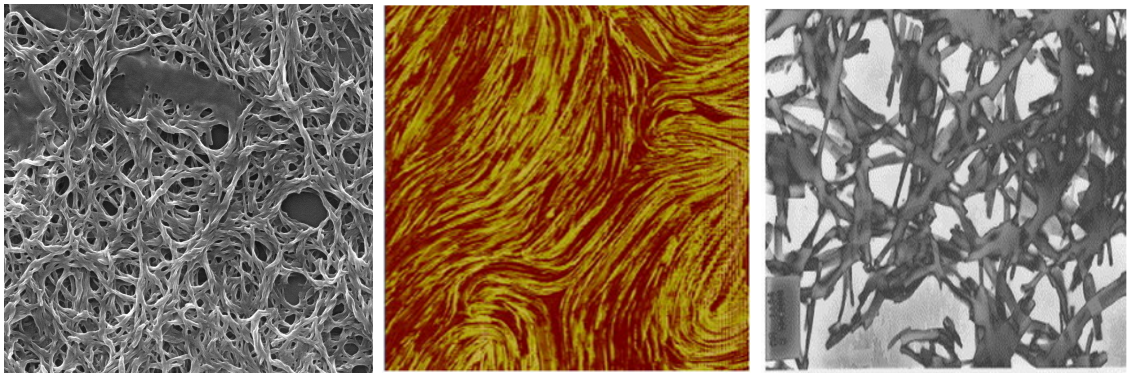

Figure 2.4.: Photographs of the grease thickener structure using different techniques for similar Lithium mineral based greases. SEM (left), AFM (center) and TEM (right).

2.6.2. Thickener types

Grease thickeners are usually classified as:

- Metal soaps;

  Simple soap thickener;

  Mixed soap based greases;

  Functional thickener;

- Non-soap thickener;

Of the many types of thickeners used for formulating greases, only those used in this work are presented here, namely Lithium and Lithium-Calcium soap thickeners and Polypropylene non-soap thickeners.

2.6.2.1. Lithium 12-hydroxy stearate

LiM1 is a lithium 12-hydroxy stearate thickened grease.

Catalysed by developments in the aircraft industry during the late 1930s, the introduction of lithium based greases was heralded as a significant step forward [5]. For the first time, lubrication engineers were provided with a grease which could be classified as "multipurpose".

Early lithium soaps were made from simple stearic acid, mainly derived from beef tallow. Today, almost all lithium greases are based on castor oil derivatives and 12-hydroxy stearic acid [71]. The capabilities of lithium greases include excellent mechanical stability, good water resistance, high dropping point and reasonably good high temperature performance up to 120 °C .

Lithium thickened greases also respond relatively well to many kinds of additives, which makes it easier to tailor them to specific conditions and environments.

The lower application temperature limit for a lithium soap thickened grease, as for all other greases, mainly depends on the physical properties of its base oil.

2.6.2.2. Lithium-Calcium thickener of stearate derivatives

LiCaE is a lithium-calcium thickened grease of stearate derivatives.

Calcium greases came before lithium ones and at the time they were produced by reacting lime with vegetable oils or animal fats in the presence of water. This grease was adequate for simple lubrication tasks such as cartwheel and waterwheel shafts and bearings. However, due to its low melting point (< 100 °C), calcium grease was not suitable for high operating temperatures. Nowadays, some calcium thickeners however, such as anhydrous calcium, have better qualities when compared to lithium 12-hydroxy stearate greases.

The availability of a range of soaps based on different metals encouraged grease formulators to investigate the effect of mixtures on the final grease. Mixed-based lithium-calcium greases, for instance, typically show better water resistance and often better shear stability than pure lithium greases, and they outperform pure calcium greases with their upper temperature limit. Their properties, however, depend largely on the relative proportions of two or more soaps. As the proportion of calcium / lithium is 15 / 85 %, the grease dropping point (185 °C) will be close to that of the lithium soap alone and its wear and friction performance will be better than those with pure lithium grades [72].

[5] patents issued to Clarence Earle in 1942-43.

2.6.2.3. Polypropylene

PPAO is thickened with high crystallinity polypropylene (isotactic and homopolymer) and an elastomer as a co-thickener. Lubricating grease PPAO was formulated with a new thickener technology based on polymer compounds with an optimised crystalline-amorphous balance. This polymer thickener consists of a combination of different polypropylenes and rubber, resulting in a non-ionic product with controlled oil separation.

According to Professor Emeritus Bo Jacobson from Lund University in Sweden, a "controlled" oil separation at low and ambient temperature was already achieved with this technology. This not only implied releasing the amount of oil at any low and/or ambient temperatures, but the properties of the released oil also. The amount and type of oil and even the amount of additives in the released oil could be controlled varying certain parameters in the production process. This technology made it possible to reduce or eliminate the risk of starvation to be reduced. Moreover, the temperature dependence of the oil released could be modified, thus endowing the products with exceptionally low temperature properties [6].

The non-ionic thickener system allows the active components in the additives to reach the metal surface. Whereas soap-based thickeners will interfere with the additives' reaction by competing for the surface, the polymer system will allow the additives to win the race for some metal to react with.

Because of the high adhesion and low solubility combination, polymer-based non-ionic products show good resistance against water and aggressive chemicals and increased surface and corrosion protection. Polymer systems are generally more resistant to oxidation, degradation and centrifugal forces than soap based products.

A comparison between grease thickeners is summarized in Table 2.3. As discussed earlier, as grease properties depend on its constituents, their interaction and the manufacturing process, the thickener properties classified in Table 2.3 do not necessarily translate the grease properties.

2.7. Additives

Almost all modern greases contain additives to enhance various aspects of lubricant performance. Some additives need to be available at the metal surface, whereas others perform their duty better by being thoroughly dispersed in the base oil or even in the thickener system.

[6] Private communication with Professor Emeritus Bo Jacobson, Lund University

Table 2.3.: Thickener properties. Comparison between the tested greases.

	Li-12-OH-stearate	Li-Ca	PP
Thermal stability	good	good	excellent
Shear stability	good	good	moderate
Water resistance	good	very good	very good
Load carrying capacity	good	very good	moderate
Additive response	good	good	excelent
Low temperatures behaviour	poor	good	very good
Compatibility with other greases	good	good	very good

Solubility and insolubility are key factors in this selection. It is not, however, a prerequisite in grease formulation once the solid gelled structure of lubricating greases is capable of retaining both soluble and insoluble additive components within its solid matrix. In lubricating oils, on the other hand, additives must be soluble or very highly dispersed in the liquid to avoid phase separation or sedimentation.

At high temperatures certain types of additives may degrade rapidly, thus requiring very special chemistries for high temperatures greases.

In a soap-thickened grease (LiM1 and LiCaE), additives which need to be present at the metal surface have to be able to compete with the polar molecules of the thickener system and/or the polar characteristics of the base oil. The soap itself may well have already fully coated the metal surface leaving nothing for the additives to react with. That is not the case of PPAO grease, which has a non-polar thickener.

Since the majority of additives are designed for optimum performance in liquid lubricants such as motor oils and hydraulic fluids, they are often highly polar substances and can therefore interfere with the thickening mechanisms within a grease. This interference leads to a breakdown in grease structure and catastrophic de-gelling as a result, hence the correct selection of functional additives is clearly very significant in enhancing grease performance.

The most common additives used in lubricating greases are: corrosion inhibitors, extreme pressure, anti-wear and friction modifiers, which are all surface active, and the antioxidants and viscosity modifiers, which are bulk active.

Additives used during grease manufacturing are generally unknown by the end-users and difficult to find out. That is the case of the lubricants analysed in this work.

2.7.1. Corrosion inhibitors - CI

The corrosion of grease lubricated steel bearing components, caused by the presence of atmospheric oxygen, moisture and other aggressive products, can lead to serious malfunctions. Acidic products that generate corrosion can be formed by thermal and oxidative decomposition of the lubricant; these already exist in the direct environment or can be caused by the specific application. The grease itself has a built-in rust inhibiting property but it is generally not enough.

Corrosion inhibitors for steel rolling bearings are anti-rust additives. These usually are highly polar oil-soluble compounds that function by absorption on the metal surface to form a thin protective film, which excludes air and water, thus protecting the surface from corrosion. Unfortunately, they compete for the metal surface with other polar additives and in the case of polar thickeners, especially with the thickener.

The most common corrosion inhibitors are zinc naphtenates and calcium sulphonates.

2.7.2. Extreme pressure - EP

With the right thickener and base oil combination, the load carrying capacity of a properly formulated grease can be achieved by the lubricant film itself. Extreme pressure additives should therefore only be expected to function in acute situations and to provide additional protection. Under such circumstances the film thins out and metal to metal contact can occur; the distribution of lubricating grease becomes uneven in the contact zone and metal asperities come together, generating heat and dramatically increasing friction. This usually happens at high temperatures, at low speeds or during extremely high loading.

All EP additives therefore need to be highly reactive with the metal surface. When the local temperature rises above a certain critical level, they react and change the chemistry of the metal surface. With most conventional extreme pressure additives, the high spot becomes brittle and simply breaks off. Other EP additives change the hardness of the metal creating smoother surfaces. These micro-mechanisms prevent the surfaces from welding together.

More traditional additives, based on lead, have already been replaced by sulphur and phosphorus compounds and these are, in turn, being replaced by more environmentally-acceptable products such as bismuth.

2.7.3. Anti-wear - AW

Anti-wear additives are similar in function to extreme pressure additives, however they operate at lower temperatures and under less stressful conditions.

These materials normally work by forming some kind of protective monomolecular film on the metal surface, often by physical adsorption. Thickeners based on metal soaps can actually provide a certain degree of anti-wear protection and, like soaps, many anti-wear additives are actually based on long chain, fatty molecules. Such types of additives can also be used as friction modifiers (FM) to optimise performance under less critical conditions.

The most common anti-wear additive used nowadays is zinc dialkyldithiophosphate, usually designated as ZDDP.

2.7.4. Antioxidants - AO

Oxidation can be seen as aging of the grease. The parameters initiating and/or accelerating this process are oxygen, heat, metals, light and contamination. Unfortunately almost all (or all) of these can be found in grease lubricated rolling bearings.

Lubricant aging can be divided into two different processes:

- reaction of the lubricant molecules with oxygen;
- thermal decomposition at high temperatures.

These processes significantly influence the life and properties of the lubricant.

The antioxidant fights the oxidation through different mechanisms and these can be split into two groups:

- primary antioxidants or the radical scavengers;
- secondary antioxidants or the peroxide decomposers.

Radical scavengers compete with the lubricant molecule for the reaction with the reactive radicals, forming stabilized products that are so unreactive that they will stop the propagation of the auto-oxidation. Peroxide decomposers, on the other hand, convert the hydro peroxides into non-radical products, thus also preventing the chain propagation reaction. As the antioxidants try to terminate the free-radical chain reaction, they are also gradually destroyed in the process

The most common antioxidants are phenol and/or amine derivatives, although compounds containing sulphur and phosphorus are also used.

The oxidation of lubricating greases is discussed in Chapter 7.

2.8. Grease performance and characterization

Theoretically, there are twelve main phenomena which must be considered for grease characterization. These phenomena result in twenty-four requirements for optimum performance (Table 2.4) [7]. It is out of question, however, to expect a real grease to meet all these requirements because there are several performance contradictions. The suitability of a grease for both high and low temperature applications is, for example, difficult to achieve.

There are more than 50 standard and non-standard grease qualifying tests that are usually performed when fully characterizing a lubricating grease. A complete collection of the standard tests is published regularly in the Annual Book of ASTM Standards [73]. Besides, several analytical methods are applied to the elemental analysis of lubricating greases:

- X-ray Fluorescence Spectrometry (XRF), Inductively Coupled Plasma atomic emission (ICP) and Atomic Absorption Spectrometry (AAS) are used for the quantitative determination of chemical elements. In the grease lubrication field, these techniques are mostly used to track contaminants, wear particle and additive analysis;

- Fourier Transform Infrared Spectroscopy (FTIR) is most suitable for tracking grease chemical changes due to degradation;

- Nuclear Magnetic Resonance spectroscopy (NMR) has been used to investigate how a gellant affects the diffusion coefficient of oil in a lubricating grease and structural issues;

- Thermogravimetry (TG) and Differential Scanning Calorimetry (DSC) are thermo analytical methods mostly used for antioxidant analysis. They monitor mass changes as a function of temperature and time and also, of pressure and gas composition;

- Gas Chromatography (GC) and High-Performance Liquid Chromatography (HPLC) are used to separate grease compounds in analytical chemistry and biochemistry with a view to identifying and quantifying the individual components.

The following sections summarize a few of the most important grease properties in terms of their lubricating ability under moderate operating conditions.

Table 2.4.: Twelve phenomena and twenty-four properties of lubricating greases [7].

Twelve phenomena	**Twenty-four properties**
High temperature	Maximum thermal stability
	Minimum evaporation loss
	Maximum viscosity
Low temperature	No (regular) crystallization
	Minimum viscosity
Aging	Maximum oxidation resistance
	Resistance to changes in structure
Compatibility	No reaction with non-ferrous metals
	Maximum corrosion inhibition
	Maximum polymer compatibility
	Immiscibility with foreign liquids
	Deflection of foreign solid matter
Oil loss	Optimum oil loss
Toxicity	No toxicity
	Biodegradability
Tackiness	Optimum tackiness
Flowability	Optimum relaxation
	Maximum pumpability
Load	Optimum elasticity
	Maximum lubricating film thickness
	Maximum emergency running properties
Shear	Maximum mechanical stability, or
	Optimum relaxation time
Friction	Minimum, or optimum friction
Wear	Minimum wear.

2.9. Penetration / Grease consistency

Lubricating greases are classified according to their consistency, which is defined by the NLGI grade. The cone penetration test of unworked and worked greases that defines the NLGI grade was established by the National Lubricating Grease Institute and standardized by ASTM D217 [74] and ASTM D1403 [75], respectively. Table 2.5 shows the nine NLGI grades.

The NLGI grade alone is not sufficient for specifying the grease required for a particular application. In combination with other test-based properties, however, it determines quite well the suitability of various greases for a specific application.

The lower the NLGI number, the softer the grease, and therefore, the better it flows. Greases with higher NLGI numbers are stiffer, tend to stay in place, and are a good choice when leakage is a concern.

Replacement of the cone penetration method by rotational viscosimetry has been discussed for several years [76]. Not just to determine yield stress τ_y, regarding which there have been many attempts to correlate it with cone penetration values, but also as a means of describing the viscoelastic semi plastic flow behaviour of lubricating greases.

Table 2.5.: NLGI grades and the penetration ranges of worked greases.

NLGI grade	**ASTM worked (60 strokes) penetration at 25 °C (0.1 mm)**	**Appearance**
000	445-475	fluid
00	400-430	semi-fluid
0	355-385	very soft
1	310-340	soft
2	265-295	“normal” grease
3	220-250	firm
4	175-205	very firm
5	130-160	hard
6	85-115	very hard

2.10. Rheological properties

The flow properties of lubricating greases are probably foremost when qualifying the performance of grease lubricated rolling bearings [17]. The viscoelastic and fluid-viscous behaviours are requirements for ensuring great lubricating conditions: lubricating greases should present a viscoelastic behaviour below low shear ($G' >> G''$), so that they do not flow out of the bearing (seals, cage) and provide a sealing action; they also should present fluid-viscous behaviour under high shear ($G'' > G'$), so that they do flow smoothly and endow the grease with excellent lubrication properties. To characterize these two behaviours of lubricating greases properly, one has to know their yield stress (τ_y), storage modulus (G'), loss modulus (G'') and flow curve (shear stress τ or viscosity η versus shear rate $\dot{\gamma}$).

There are many different techniques to measure such parameters, but unfortunately, they often lead to different results. In fact, the nonexistence of a standard measuring procedure imposes some difficulties in determining grease rheological parameters. It might be one of the reasons that there is an on-going discussion of rheological measurements, mainly yield stress, since it starts without a consensus [77]. An exception concerns the flow curve, which is standardised by ASTM D1092 [78], but fairly used by the tribology community because the test method covers only a low range of temperatures (from -54 to 38 °C).

Due to the lack of standards for obtaining some rheological parameters, the measured results always have to be accompanied by a full description of the methodology and operating conditions used for validating the data.

2.10.1. Yield stress

Yield stress (τ_y) can be determined and defined in several ways. It is also called "apparent yield stress" because even though an apparent yield stress could be measured, creep exists below this stress, and it may present Newtonian behaviour at very low stresses (Barnes [77]).

Yield stress is defined here as the stress that is required to brake a sufficient number of contact junctions in the thickener network so that flow will occur. Keentok [79] summarized the work of more than 12 authors and showed seven different ways usually used to measure yield stress in the early 1980s. He concluded that yield stress can be more accurately obtained by using cone or plate geometries with rough surfaces or with vane geometry[7]. The influence of the geometry on the rheological measurements is discussed in Section 3.8.

[7]Vane geometry could not be used due to the scanty amount of degraded grease obtained from rolling bearing tests.

In the present work the yield stress was determined in three different ways:

- Obtained from the flow curves. This is a value of the shear stress in the first plateau of the curve (transition between Zone 1 and 2 - see Figure 2.10). That is a traditional methodology for obtaining the yield stress [80].

- Obtained from the oscillatory curves. This is a value between the initial drop of the storage modulus G' (end of the LVE - Linear Visco-Elastic region) and the cross over stress τ_{co} when $G'/G'' = 1$ - see Figure 2.6) [81, 82]. It is important to note that test frequency can influence the yield stress measured according to the relaxation behaviour of the sample under test, and therefore, obtaining τ_y through oscillatory tests is considered a rough approach. The yield stress τ_y for some researchers is associated only to the initial drop of G' since it represents the onset of non-linearity and hence structure breakdown, while others consider the cross-over stress to be the yield point since it represents the transition from solid to liquid-like behaviour [83].

- Obtained from creep tests. This method has already been used by several authors and is briefly described below [38, 84, 85].

Creep test is a simple method to determine not just yield stress, but also the viscoelastic properties of the lubricating greases.

The mobile part of the arrangement (upper plate) is loaded against the grease sample. After some resting time, a constant shear stress (τ) is then applied for a certain period of time. The sample reacts to this force with a deformation, i.e. the material starts to creep. In the second part of the test, the grease is relieved from the shear stress for a certain period of time so that it may recover.

Figure 2.5 shows the shear strain over time when a constant shear stress is applied and released successively. In the example given, the shear stress is applied for 3 minutes and relieved for 2 minutes. This is performed twice for each shear stress (τ = 100, 200 and 400 Pa) at 40 °C with a lubricating grease NLGI grade 2.

In Figure 2.5, the first and second graphs (τ = 100 and 200 Pa, respectively) present a typical elastoplastic behaviour, where the elasticity of the grease is seen by the recovering of the shear strain. This indicates that the thickener network was not broken by the previous shearing ($\tau < \tau_y$). In the third graph (τ = 400 Pa), however, no strain recovering is observed, thus indicating a viscous fluid behaviour. In this graph the shear stress destroyed the internal structure of the grease and the material behaved like a fluid ($\tau > \tau_y$).

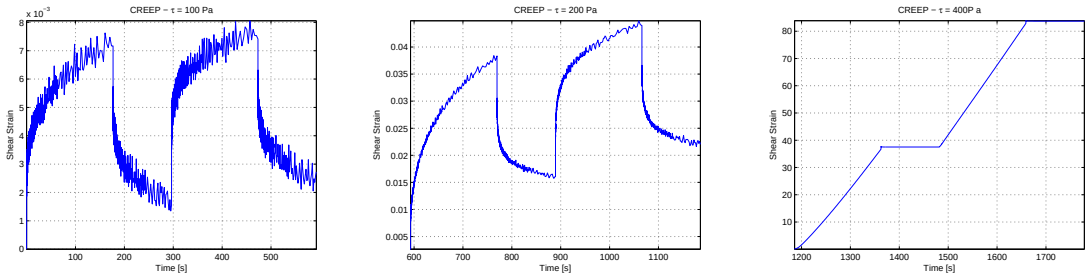

Figure 2.5.: Creep Test - Shear strain versus time for different applied shear stresses.

This indicates that the absolute value of the yield stress is somewhere between $\tau_{ymin} = 200$ and $\tau_{ymax} = 400$ Pa (graphs 2 and 3), where a transition from elastoplastic to fluid behaviour is observed.

2.10.2. Oscillatory tests

Small-amplitude oscillatory shear usually describes the linear viscoelastic properties of lubricating greases, where an oscillatory shear rate of increasing amplitude at constant frequency is applied at different temperatures. Storage (G') and loss (G'') moduli are obtained from these measurements (see Figure 2.6). For Newtonian fluids, storage modulus (G') is insignificant.

The storage modulus is related to the elasticity of the grease; the highest is the G'/G'' ratio, the highest is the grease stiffness. The loss modulus is related to the viscous part of the grease; the highest is the G''/G' ratio, the highest is the fluidity of the grease.

In the linear viscoelastic region - LVE (see Figure 2.6), the storage and loss moduli are independent of the magnitude of the applied stress/strain and a plateau zone is observed. At this level the dissipative modulus G'' presented much lower values than storage modulus G' ($G' >> G''$) and the grease behaviour was mainly controlled by its elastic properties, which depend on the type of grease constituents, their quantity and the interaction between them [3]. As amplitude increases, a rapid decay of G' is observed, which is imputed as a significant breakdown in grease structure. Here, the grease's capacity to store energy over the energy dissipated becomes less significant, as it reacts to the stress imposed on the internal structure of the. The storage and loss moduli curves fell off at different rates and crossed at a stress level which is often called the cross-over stress, τ_{co} (see Figure 2.6).

The complex modulus (G^*) and phase angle ($tan(\delta)$) can be calculated from G' and G''.

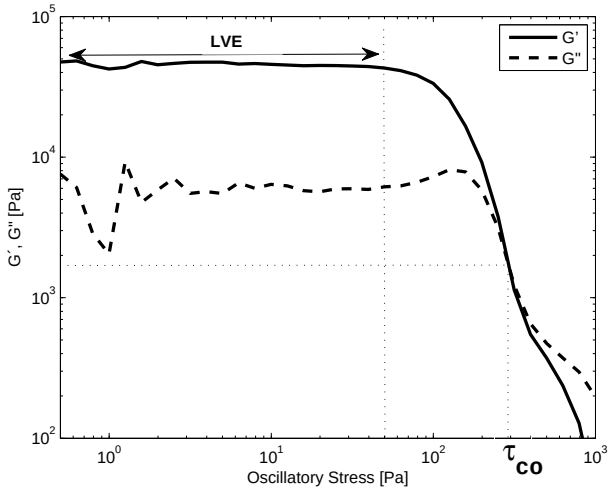

Figure 2.6.: Storage (G') and Loss (G'') moduli versus oscillatory stress.

The complex modulus is determined by the vector sum of the elastic and the viscous components of the greases as shown by Equation 2.12. This represents grease resistance to deformation. The phase angle $tan\,(\delta)$ expresses the balance between elastic and viscous behaviour, and is given by Equation 2.13.

$$G^* = \sqrt{G'^2 + G''^2} \tag{2.12}$$

$$tan\,(\delta) = \frac{G''}{G'} \tag{2.13}$$

2.10.3. Flow tests

Flow curves usually describe the shear stress (τ) and the apparent viscosity (η) behaviour within a large range of shear rates ($10^{-6} \leqslant \dot{\gamma} \leqslant 10^4$) and temperatures at low pressure. Under these operating conditions the Newtonian fluids (such as most of the base oils) present a linear increase of the shear stress with shear rate and do not present any change on the viscosity values in log-log scales. Such behaviour is depicted in Figure 2.7 for a mineral base oil (further described in Section 3.8.1). Non-Newtonian fluids (such as lubricating greases) however, typically show a non-linear increase of the shear stress and a reduction of the apparent viscosity with increasing shear rates This effect is designated as "shear thinning", and is depicted in Figure 2.8 for a mineral based grease (further described in Section 3.8.4)

There are several models for predicting the shear stress and apparent viscosity behaviour of lubricating greases. These models are mostly used by tribologists to

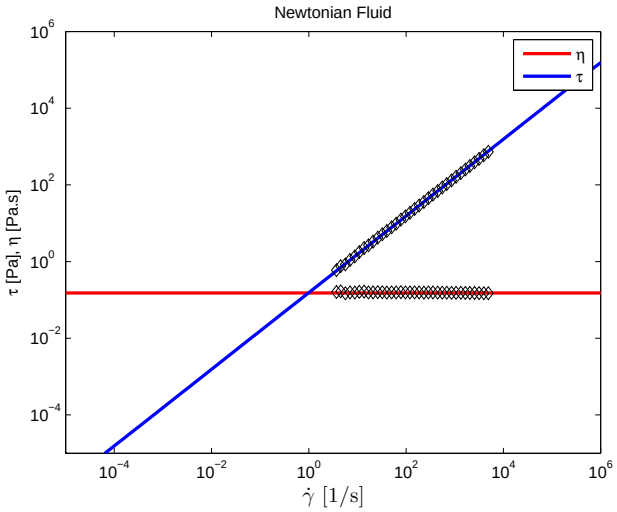

Figure 2.7.: Shear stress and apparent viscosity versus shear rate of a Newtonian fuild at 40 °C (Base oil). Measurements (⋄); Rheological model (—).

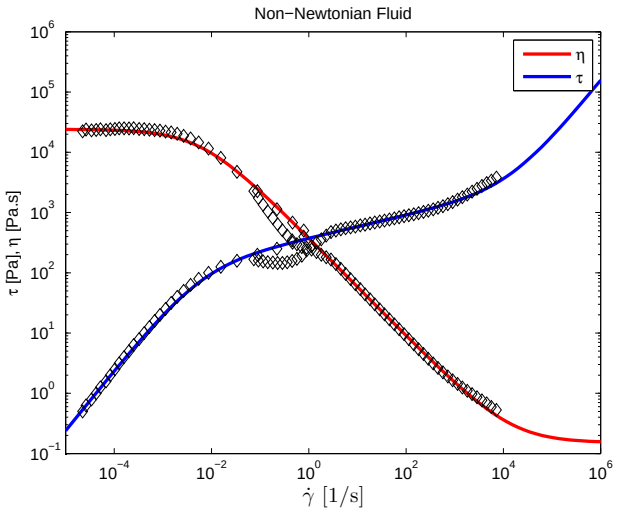

Figure 2.8.: Shear stress and apparent viscosity versus shear rate of a non-Newtonian fuild at 40 °C (Grease). Measurements (⋄); Rheological model (—).

extrapolate the values of τ and η from low to very high shear rates due to the difficulty to properly measure them at the range extremes (see Section 3.8), and because it allows for obtaining numbers from the flow curves, which is more straightforward for grease comparison. Such extrapolation aims at determining the grease properties in similar conditions to those observed in grease lubricated machine elements and using them to model the tribological behaviour of a given system. High-pressure and high shear rate rheology, however, have not yet been applied to lubricating greases and

therefore, two assumptions have to be made: *i)* grease and base oil viscosity and shear stress likewise vary with pressure; *ii)* grease viscosity and shear stress at very high shear rates are equal to those of its base oil. Such assumptions are well accepted since grease typically consists of 80-90 % base oil.

2.10.3.1. Apparent viscosity

The apparent viscosity of lubricating greases can be depicted as shown in Figure 2.9. At very low shear rates (Zone 1) NLGI-class 2 lubricating greases present a Newtonian behaviour, where the apparent viscosity does not depend on the shear-rate (or its dependence is insignificant). At this point viscosity is very high and only creep flow occurs. At slightly higher shear rates shear thinning occurs (Zone 2), reducing viscosity in orders of magnitude. As the shear rate rises further, shear thinning becomes less significant up to the moment that the apparent viscosity reaches the second Newtonian plateau. This second Newtonian behaviour (Zone 3) is believed to approach the base oil viscosity [86].

In the first zone, the grease behaves as Newtonian because there is no rupture of the thickener fibres (elastic regime). In the Zone 2, shear thinning may occur for many reasons as the shear rate increases. This goes from alignment of the fibres, loss of confluences between them, reduction in width and length due to the break off and rearrangement of the fibres [70]. In the last zone, the shear rate is so high that the thickener is completely broken into very small thickener material that is dispersed in the base oil, and therefore the grease response at that stage is governed by the base oil with little thickener material, which approaches the base oil behaviour (Newtonian).

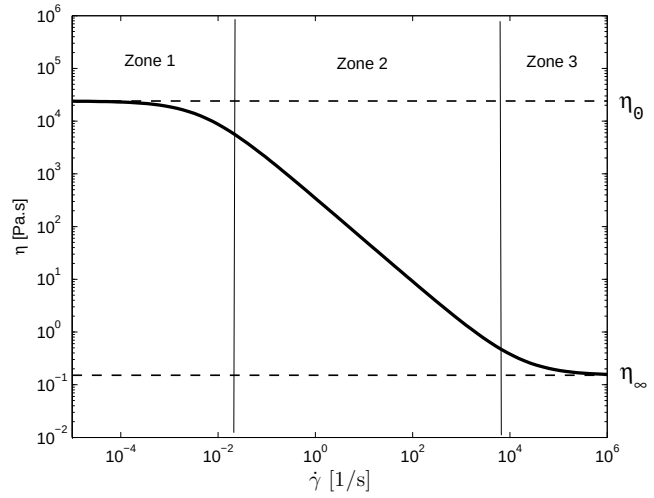

Figure 2.9.: Schematic representation of the apparent viscosity versus shear rate for lubricating greases. Non-Newtonian behaviour.

There are several models for predicting the variation of grease viscosity with shear rate. A complete overview of those models is provided in [87, 88]. When viscosity measurements for a large shear rate range are available, the Cross model for pseudo-plastic flow (see Eq. 2.14) [89] describes the variation of the viscosity for the full shear rate range with reasonable accuracy:

$$\eta = \frac{\eta_0 - \eta_\infty}{1 + (K\dot{\gamma})^m} + \eta_\infty \tag{2.14}$$

where η_0 is the viscosity at very low shear rates, η_∞ is the viscosity at very high shear rates, often assumed to be equal to the base oil viscosity, and K and m are model constants. In the present work, η_∞ is assumed to be equal to the bleed-oil viscosity due to some evidence noted during the film thickness measurements (see Section 4.4).

2.10.3.2. Shear stress

Shear stress of lubricating greases can be depicted as in Figure 2.10. A divergence between the continuous line (*model*) and the dash-dotted line (*Grease Meas.*) is observed in Zone 1. Such difference is due to an engineering assumption related to the yield stress - τ_y, described in Section 2.10.1.

Similarly to viscosity, at very low shear rates (Zone 1) NLGI-class 2 lubricating greases present a Newtonian behaviour, where the shear stress shows a linear increase with increasing shear rate in a log-log plot (the dash-dotted line - *Grease Meas.*). AAt this point shear stress is very low and only creep flow occurs. At slightly higher shear rates the "yield stress - τ_y" is reached (Zone 2), and the grease flows non-linearly with the shear rate. As the shear rate increases further, it reaches the second Newtonian plateau (Zone 3) and is believed to approach the base oil shear stress.

Most rheological models disregard the measured stress at Zone 1 (*Grease Meas.*) by adding yield stress τ_y (*Model*) to the rheological models, as shown in Figure 2.10 and Equation 2.15. This does not create any inaccuracy as long as the timescale is short enough [17]. Then again, as many mechanical transmissions work in start/stop periods of many hours (or even days), such assumption may lead to an incorrect understanding of the initial lubrication condition after a long stop period.

There are several models for predicting grease shear stress dependence on shear rate (see [87, 88]). In the present work the Cross model, given by Equation 2.14, was re-written in terms of shear stress as [68]

$$\tau = \tau_y + \left[\frac{\eta_0 - \eta_\infty}{1 + (K\dot{\gamma})^m} + \eta_\infty\right]\dot{\gamma} \tag{2.15}$$

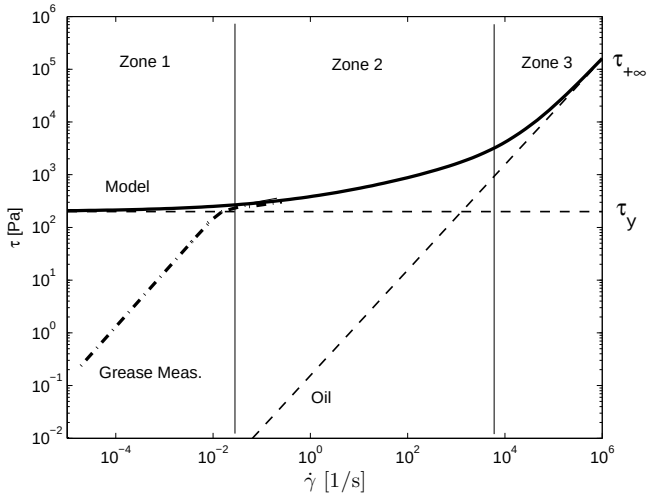

Figure 2.10.: Schematic representation of the shear stress versus shear rate for lubricating greases. Non-Newtonian behaviour.

where the yield stress term τ_y has been added to adjust for the apparent yield at low shear rates.

Model constants K and m can be determined from equations 2.14 and 2.15 by fitting them with the experimental results. The τ_y, η_∞, η_0, K and m are then used to characterize the grease flow behaviour.

2.10.4. Influence of grease formulation on grease rheology

When comparing the rheological response of lubricating greases to different formulations (thickener and oil type) and different manufacturing processes, the effect of the oil viscosity or thickener concentration on the rheological parameters is not clear. However, when all the grease manufacturing variables are kept constant and only the base oil viscosity and the thickener concentration are changed, that effect becomes clear. Delgado *et al.* [14] showed that with increasing thickener concentration:

- storage G' and loss G'' moduli increase significantly, but the phase angle $tan\,(\delta)$ varies relatively little;
- apparent viscosity η increases significantly;

and when base oil viscosity increases:

- storage modulus G' decreases;
- loss modulus G'' decreases at a lower rate than G';

- phase angle $tan\,(\delta)$ increases;
- apparent viscosity η at Zone 1 (see Figure 2.9) decreases;
- apparent viscosity η at Zone 2 (see Figure 2.9) barely change;
- apparent viscosity η at Zone 3 (see Figure 2.9) increases;

From these observations, one can state that grease flow behaviour is mostly controlled by the thickener at low shear rates, although at high shear rates the micro-structure of the grease is degraded and the oil released from the grease prevails in controlling flow behaviour. Actually, in the case of large deformations, lubricating greases consist of non-interacting aggregates of thickener, co-thickener and additive material dispersed into the lubricating oil, and this is the matter that controls flow behaviour at high shear rates.

Furthermore, thickener concentration prevails in controlling the viscoelastic behaviour of grease (very low shear rate); the oil solvency plays a role in structure reinforcement by changing grease micro-structure [3]. In this sense, a high oil viscosity acts as a mechanical barrier to the formation of physical entanglements and interaction among fibres that occurs during crystal growth in the final step of the grease manufacturing process, creating larger spaces between fibres [14].

2.11. Bleed-oil

Bleed-oil is the designation of the oil that "bleeds" from the grease. The grease releases oil (bleeds) either through mechanical and/or thermal stress (dynamic oil bleed) or during storage (static oil bleed).

Static oil bleed occurs naturally with all greases. This phenomenon is affected during storage by factors such as temperature changes, vibrations and an uneven grease surface. Under dynamic conditions the bleed rate is affected by operating and environmental conditions.

The oil bleed rate of the grease is adjusted by optimizing the composition (thickener and base oil type, properties and concentration, addition of polymers, additives, etc.) and through the manufacturing process (contactor, open kettle or continuous production) with a view to dialling in the appropriate amount of bleed needed by the application. Manufacturing process plays a key role in determining the distribution of the thickener matrix within the lubricating fluid and, consequently, the bleed characteristics of the finished lubricating grease. Thus, the ability of lubricating

greases to retain or release oil depends on their composition and on the manufacturing process.

Several oil bleed tests were developed in order to comprehend the root cause of bleeding and its influence on the grease performance. These tests can be classed into two groups: static and dynamic bleed tests. ASTM D1742 pressure bleed, ASTM D6184 cone bleed and IP 121 are static bleed tests that can be used for quality control in grease production. They determine the amount of oil separation from the grease, which can be related to the situation of the grease in its container during storage or in the pre-greased equipment when not in service. They are referred to as static tests because they operate on undisturbed grease exposed to relatively low stresses.

Dynamic bleed tests such as M1066 CGOR (Churned Grease Oil Release, in-house proprietary test), ASTM D4425 Centrifugal Oil Bleed and Trabon (Method 905A) determine the amount of oil separation after the grease is mechanically sheared, as would occur in rolling element bearings, or exposed to high levels of centrifugal stress, as typically found in shaft couplings and universal joints.

Different oil bleed rates are targeted depending on the end application of the lubricating greases. For very high speed or temperature applications where centrifugal forces are greatly important, greases are formulated to present a minimum separation of oil. On the other hand, for applications operating at low speeds or with a reciprocal motion of small amplitude there is a little churning of the grease, which requires grease designed to be sensitive to mechanical shear and to release oil under the effect of small stresses. High temperatures (up to a certain point - see Chapter 7) increase bleed rate, leading to rapid loss of oil (leakage, evaporation) and premature grease ageing. On the other hand, greases with a low although sufficient oil bleed at high temperatures, may under-perform at ambient temperatures because of oil starvation.

2.12. Grease manufacturing

Manufacturing of any lubricating grease is a complicated process requiring a high level of investment in terms of capital and manpower. Different greases require different manufacturing methods and each grease plant has its own particular detailed technology. According to some grease manufacturers, if formulations are regarded as proprietary and confidential, then the manufacturing processes must be classified as top secret.

The properties of the greases, especially those based on metal soaps depend not only on their composition, but also on the way in which the thickeners are prepared. Delgado *et al.* [14] manufactured lubricating greases, generating the soap thickener

in situ and with online viscosity and torque measurements. He also collected grease samples at different stages in the process for Scanning Electron Microscopy (SEM) and rheological analysis.

Delgado showed that the rheological properties of the grease, the morphology of the thickener structure and distribution changed considerably at different stages of grease production and therefore, lubricating greases with the same formulation but different manufacturing processes can have significant different properties. Therefore, grease performance cannot be evaluated solely by its base oil, or thickener, or additive package. It is their interaction plus the micro-structural characteristics achieved during processing that are determinant to the grease properties and probably, to their performance

Grease replenishment mechanisms for example, depend on the flow properties of the grease, its ability to release oil and its interaction with lubricated surfaces. In fact, all grease properties are related to the micro-structural characteristics achieved during processing and their composition, both of which are usually unknown

2.13. Summary

This chapter described the main characteristics of lubricating greases and how complex they are. Nowadays, it is not just the finished grease that is characterised, but also its components, especially the base oil. Many of the tests and measurements that are carried out to characterize lubricating greases are performed in the hopes of finding correlations with the tribological behaviour of grease lubricated systems, something which has not been fully achieved.

Scanning Electron Microscopy, for example, is an expensive and time-consuming technique that has being applied with a view to correlating grease micro-structure with grease lubrication mechanisms and to visualizing micro-structure changes due to thermal and mechanical effects. Nevertheless, there is no consensus regarding which kind of micro-structure is ideal for a given application.

Even some rheological properties that have been extensively studied, such as G', $G'', G^*, \tau_y, \tau, \eta, tan\,(\delta)$ have already been correlated with traction coefficients, wear and film thickness measurements, but without great success. To the author's knowledge, there is no general rule that states that some rheological property governs the friction or film formation.

On the other hand, all these techniques, when applied to grease characterisation, have helped grease developers achieve certain properties by applying scientific methodologies instead of *trial-and-error* methods and researchers to better understand the

grease mechanisms of lubrication. Moreover, as some grease rheological properties seem to correlate well with grease life, model constants K and m from Equation 2.14 have been used to predict film thickness. This, however, has not attracted the attention of many researchers so that grease film thickness prediction under fully-flooded lubrication is still determined the film thickness of its base oil.

3. Experimental characterization of the lubricating greases

3.1. Introduction

Of the many grease properties one can evaluate, some might not be useful for understanding grease lubrication mechanisms under certain specific operating conditions. Thus, grease characterization should be performed with a well-defined objective, which unfortunately is not always the case.

Characterization of base oil properties (ν, ρ, η, α) and bleed-oil properties (ν, ρ, $\eta, \alpha, \eta_0, \eta_\infty, G_{cr}, n$) was determined because they are required for film thickness and rolling bearing friction torque predictions.

The rheological parameters of lubricating greases (G', G'', G^*, K, m, τ_y, τ, η, tan (δ)) were measured / calculated to characterize thickener-oil interaction, grease flow and viscoelastic characteristics and determine their possible influence on grease traction behaviour, film thickness and rolling bearing friction torque.

The oil bleed rate of the greases was evaluated in order to correlate them with the grease rheological parameters and grease micro-structures, as measured by Scanning Electron Microscopy (SEM)

XRF was applied to determine the grease chemical content, mostly that related to the additive package.

FTIR was performed to compare the grease, thickener, base oil and bleed-oil spectra with a view to defining the grease components present in the bleed-oil but absent in the base oil.

Oil and thickener content were determined to help understanding the grease rheological behaviour.

All these techniques were also applied to degraded greases in Chapter 7, so that additive consumption (XRF), oxidation (FTIR), oil loss (remaining oil percentage, or thickener/oil ratio) and rheological changes could be evaluated and related to the level of degradation of each grease.

3.2. General characteristic of the used lubricating greases

Three lubricating greases with different formulations were analysed. The greases were named according to their chemical formulation (i.e., thickener + base oil): LiM1 was thickened with lithium and formulated with a mineral base oil; LiCaE was thickened with lithium and calcium and formulated with an ester base oil; PPAO was thickened with polypropylene, co-thickened with an elastomer and formulated with a polyalphaolefin base oil.

All these lubricating greases were fully formulated. The LiCaE grease passed the test for biodegradability (OECD 301F) and eco-toxicity (OECD 202).

The lubricating greases, their base oils and the physicochemical properties of the bleed-oils were measured; the results are presented at the end of this Chapter in Table 3.11. The test conditions and procedures used to obtain these properties are described in the following sections.

3.3. Scanning Electron Microscopy - SEM

Analysis of the grease micro-structure was performed with a JEOL JSM 35C/ Noran Voyager scanning electron microscope (SEM). This technique is not standard, which poses some difficulties for the measurements. As the SEM used operates in a high vacuum environment, wet samples could not be used and the base oil was separated from the grease. This process is believed to interfere with the thickener structure. Besides, the exposure time and incident energy of the electron beam on the sample, which is related to the image quality, can also modify the thickener structure [90].

So as not to add more entropy to the grease micro-structure analysis, exactly the same procedure was used to prepare the samples and to obtain the SEM images. A thin layer of each grease sample was spread on a glass substrate and a non-polar solvent was used (hexane) to carefully wash the base oil from the grease. The samples were not covered with any conductive coating film. SEM images were then taken with the same exposure time, magnifications of 2000X, 5000X and 20000X and a 5 kV electron beam. The SEM images are shown in Figures 3.1 to 3.3.

Three very different thickener micro-structures were encountered. Such differences could account for behavioural differences between greases since the micro-structures can have some effect on the thickeners ability to contain oil and insoluble additives by mechanical entrapment or capillary effects.

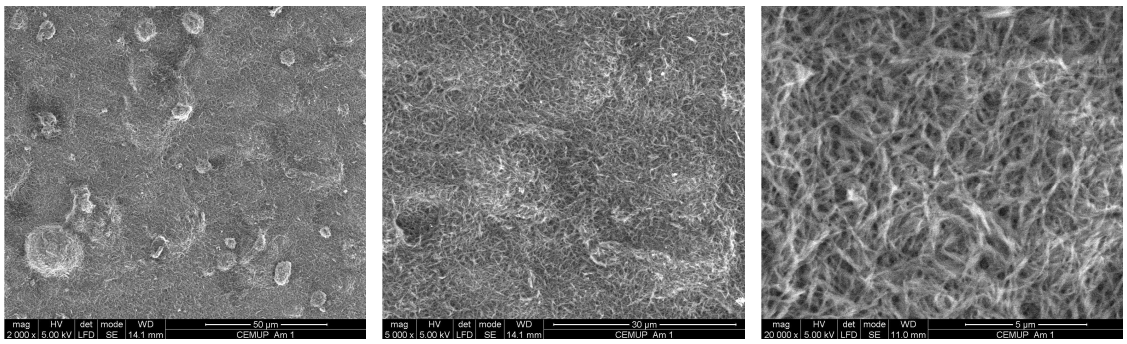

Figure 3.1.: SEM photographs of the grease thickener structure. LiM1 - Lithium 12-hidroxy stearate.

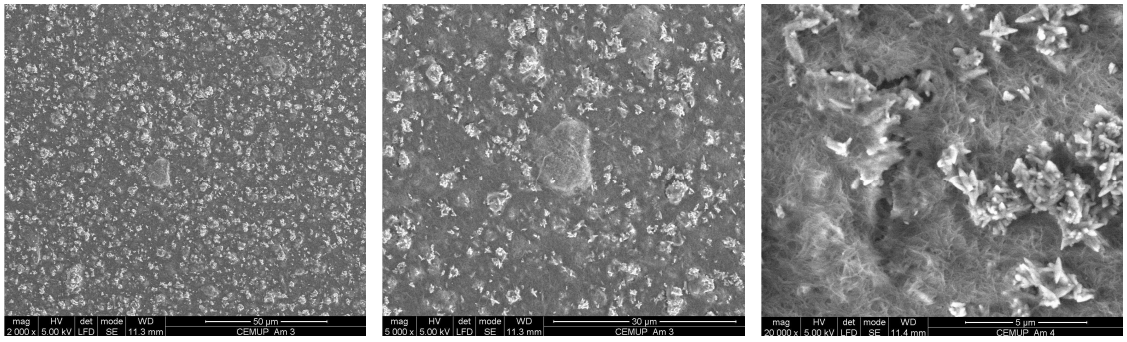

Figure 3.2.: SEM photographs of the grease thickener structure. LiCaE - Lithium-Calcium thickener of stearate derivatives.

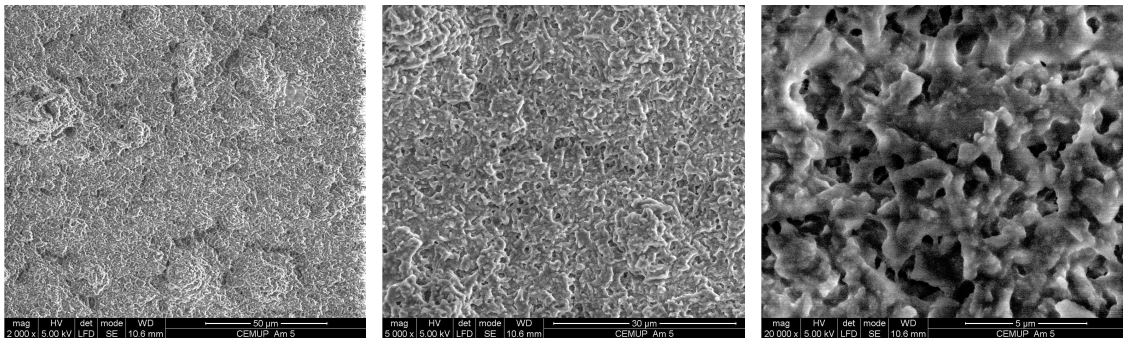

Figure 3.3.: SEM photographs of the grease thickener structure. PPAO - Polypropylene.

LiM1 presented a structured system based on entanglement networks with long and large lithium fibres. According to Scarlett [91], in most soap-based greases, the soap presents as fibres or ribbons varying in size from about 1 to 100 μm in length, with a length to diameter ratio of 10 to 100. In this case the mean diameters of several fibres were measured from Figure 3.4(a) and have values from 0.06 to 0.2 μm.

LiCaE greases also showed a structured system based on entanglement networks, however they contained several calcium crystals and the lithium fibres were shorter and thinner. The average diameter obtained from Figure 3.4(b) varied from 0.04 to 0.13 μm.

PPAO grease was thickened with polypropylene. The polypropylene micro-structure was very different from LiM1 and LiCaE. Instead of an entanglement network composed of fibres, short, thick elements connected to each other were randomly distributed. The average thickness of these elements was difficult to measure; it varied from 0.5 to 1.15 μm (Figure 3.4(c)).

Just by comparing the thickener micro-structure of these three greases, and as regards the thickener's ability to contain oil by mechanical entrapment, one could say that:

- PPAO thickener micro-structure is very dense and may constrain the oil molecules in a more intimate way than lithium fibres;

- As LiCaE thickener is shorter, thinner and the free space between the fibres is smaller when compared with LiM1, it constrains the oil in a more intimate way than LiM1.

There are other factors, however, that have to be taken into account when evaluating a thickener's ability to retain oil, such as the physical and chemical interaction between thickener and base oil.

According to Delgado *et al.* [92], the micro-structure also plays a key role in the rheological properties of greases. For lubricating greases with the same formulation but different manufacturing process, he determined that the high density of the physical entanglements among fibres leads to high consistency, apparent viscosity and viscoelastic properties (G', G''), "), whilst a lower density of the entanglements leads to the opposite. The major drawback of these findings is that the rheological measurements were obtained without a pre-shear program, which may significantly alter the rheological parameters (see Section 3.8).

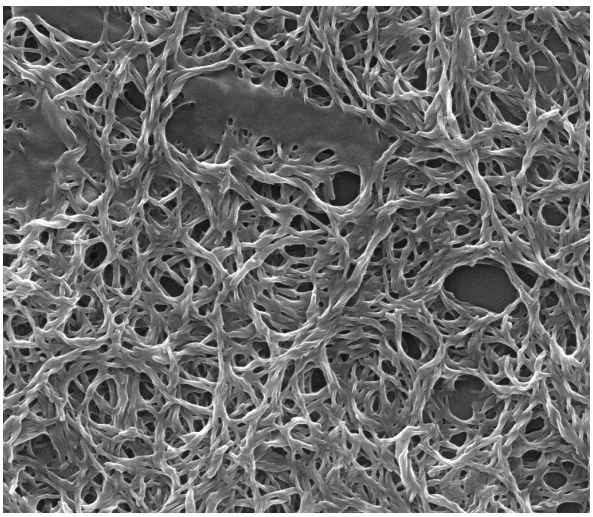

(a)

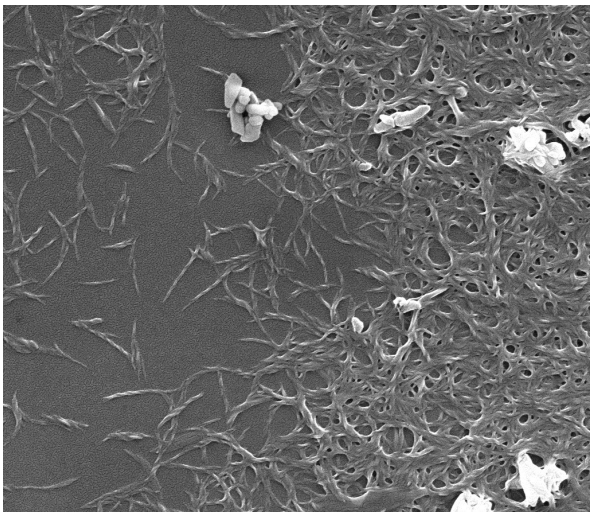

(b)

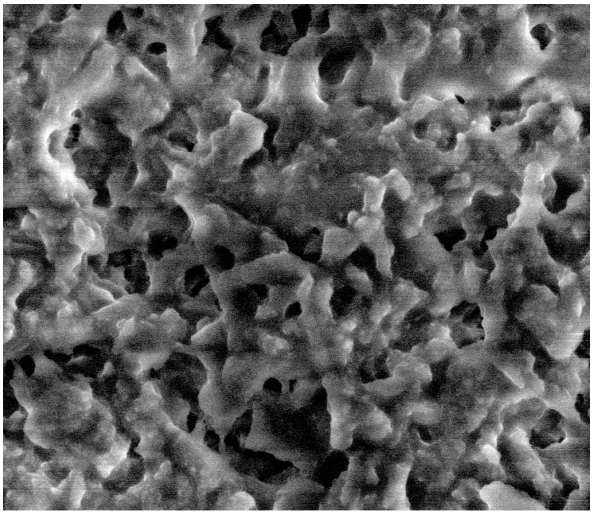

(c)

Figure 3.4.: SEM photographs of the LiM1 (top), LiCaE (middle) and PPAO (bottom) grease thickener structure.

3.4. Static bleed test - IP 121/75

The oil bleed rate was obtained with the static bleed oil test IP 121/75, which consists of a stainless steel separation cup with a cone-shaped 240 mesh (grid of ≈ 61 μm) woven wire cloth. OOil separation was obtained by placing the grease sample on the wire mesh and loading it with a 100 g mass during 42 or 168 hours at 40 °C . A picture of the equipment is shown in Figure 3.5.

The amount of oil separated S_{oil} is calculated by Equation 3.1 and presented in Table 3.1.

$$S_{oil} = 100 \times \frac{m}{M} \tag{3.1}$$

where M is the initial mass of the grease sample placed on the wire mesh and m is the mass of the separated oil measured after 42 or 168 hours.

Figure 3.5.: Bleed-oil Separation Apparatus - IP 121; oil container; 240 mesh filter cone; metallic mass 100 g.

Table 3.1.: Oil bleed rate according to IP 121 standard: T = 40 °C and t = 42 h.

	LiM1	LiCaE	PPAO
m [mg]	0,79	0,26	0,14
S_{oil} [wt %]	4,21	1,36	0,77

LiM1 grease released 5,5 times more oil than PPAO grease and 3,0 times more than LiCaE.

As described in Section 2.6, the thickener structure grasps the base oil by mechanical entrapment and a combination of Van der Waals and capillary forces. Van der Waals and capillary forces are difficult to evaluate since the grease chemical composition is not well known. However, mechanical entrapment, which may be related to the grease micro-structure (see Figures 3.4(a) to 3.4(c)), was in good agreement with the oil bleed rate, although such a comparison is too subjective.

Over the years, many researchers have claimed that the oil released from lubricating greases during operation is the major lubrication mechanism of the grease [19, 91, 93, 94], although not much attention has been spent to the study of bleed-oil properties and their performance.

Therefore, the main objective of performing the static bleed test was not to evaluate the oil bleed rate or to comprehend the root cause of the bleeding process and its influence on the grease properties, but to obtain a significant amount of bleed-oil to analyse its own characteristics and tribological performance. Accordingly, a modified IP 121 test was performed at 70 °C over a few weeks, where the grease sample was replaced by a new one every 2 days. Even so, only a few milligrams of bleed-oil were obtained. Further oil bleed tests were performed at different temperatures (20 to 70 °C) and under dynamic conditions in order to obtain a larger amount of bleed-oil in less time. The influence of temperature and centrifugal forces were found to be negligible in bleed-oil viscosity and FTIR spectrum.

3.5. X-ray fluorescence - XRF

X-ray fluorescence (XRF) is the emission of characteristic "secondary" (or fluorescent) X-rays from a material that has been excited by bombarding it with high-energy X-rays or gamma rays. It reveals the relation between the intensity of an element to its concentration in the sample. In lubricant analysis, XRF can be used for tracking chemical changes due to degradation and basic element analysis. A translation of X-ray photon count-rates into elemental concentrations is automatically obtained by the software of the device: WDX separates the X-ray lines efficiently, and the rate of generation of secondary photons is proportional to the element concentration. The number of photons leaving the sample, however, is affected by the physical properties of the sample and corrections may be needed. That was not the case because the procedure used was specially developed for grease analysis. The interested reader may find more about XRF applied to lubricating greases in [95].

The XRF (SPECTRO XEPOS) used provides, as output, a list of some chemical elements from Sodium (Z=11) to Uranium (Z=92) and their concentration as a percentage of total mass [wt %].

XRF of LiM1, LiCaE and PPAO greases were analysed at the SKF Engineering and Research Centre (Nieuwegein, The Netherlands) with a method specially developed for grease analysis. The lubricating greases were placed in appropriate pans and weighed before the analysis. An amount of approximately 3 g was used. The mass of the samples is an important input of the process, since the output is the relative percentage of the mass of each chemical element present in the sample. Two measurements were carried out and an approximately 10 % error was observed. Furthermore, some systematic errors can occur due to a matrix effect [96]. Although some techniques such as Inductively Coupled Plasma atomic emission (ICP) are known to give more reliable elementary information regarding lubricating greases, these techniques were not available.

Table 3.2 shows the most common elements used for grease additivation and their concentration as a function of the total mass [wt %].

Table 3.2.: Concentration in percentage of total mass [wt % $\times 10^{-3}$] of the grease chemical content.

Element	**LiM1**	**LiCaE**	**PPAO**
Phosphorus (P)	120	37	6
Sulphur (S)	1649	102	581
Calcium (Ca)	3	3145	22
Zinc (Zn)	285	29	-
Lead (Pb)	8	-	14
Bismuth (Bi)	-	-	717

As described in Section 2.7, some of the most common additives are:

- Antioxidants: the most common AO are phenol and/or amine derivatives, although compounds containing Sulphur and Phosphorus are also used.
- Corrosion inhibitors: the most common CI are Zinc naphtenates and Calcium sulphonates.
- Extreme pressure additives: the most traditional EP additives, based on lead, have already been replaced by Sulphur and Phosphorus compounds, and these, in turn, are being replaced by more environmentally acceptable products such as Bismuth-based additives.

- Anti-wear additives: the most common is Zinc dialkyldiphosphate (ZDDP), although Bismuth, Phosphorus and Sulphur are also common

Phenol and amine derivatives are not detected by XRF technique, but they may be present in all greases since all of them are fully formulated and their technical data sheets indicate a good protection against oxidation and corrosion.

LiM1 contains very high concentrations of Phosphorus, Sulphur and Zinc. It suggests very good EP capacity, AW protection and good protection against corrosion and oxidation.

PPAO contains very high concentrations of Bismuth and Sulphur, which should endow that grease with very good EP and AW properties. PPAO also has Calcium and Phosphorus in lower concentrations and therefore must contain good antioxidant and anti-corrosion properties.

LiCaE is less additivated than LiM1 and PPAO greases. Its lower additivation is hampered by low-toxicity and biodegradability requirements. Just like LiM1, this grease contains Phosphorus, Sulphur and Zinc, but in lower concentration. The high concentration of Calcium comes mostly from the thickener. Such additives will give the LiCaE grease relatively good EP and AW properties.

3.6. Remaining oil percentage, or thickener/oil ratio

The remaining oil percentage or thickener/oil ratio test gives the percentage of thickener and base oil for a lubricating grease [17]. This technique is usually applied as a control of the remaining oil in a grease sample after work.

The method consists of dissolving a certain amount of grease with a solvent (in this case Petroleum Ether, PE 40-60 °C was used) and forcing the dissolved grease through a filter with a 0,45 μm grid (see Figure 3.6). The oil and the solvent flow through the filter to a container whilst the thickener remains in the filter. The container with the mixture of oil and solvent is submitted to a low vacuum, low rotational speed and temperature of 60 °C to evaporate the solvent. The solvent remaining in the filter is also evaporated by subjecting the filter to temperatures of 60 °C . Both oil and thickener are then weighed. The percentage of each component is calculated by comparing the mass of the grease sample before separation to its components after separation.

To ensure that the thickener and oil were completely separated, the dissolved grease was forced several times through the filter. All the tests were repeated twice; errors were less than $\pm$ 1 %.

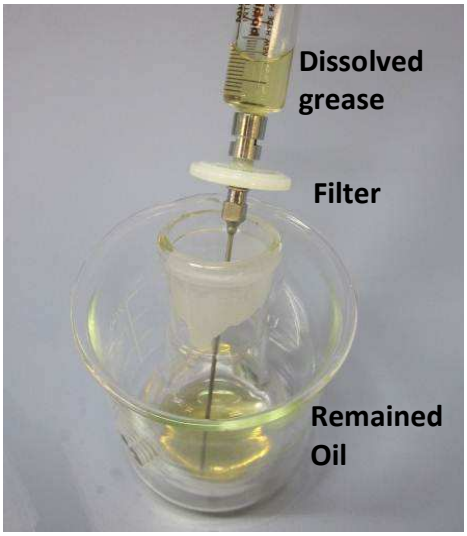

Figure 3.6.: Remaining oil percentage method.

The oil and thickener content are presented in Tables 3.3 to 3.5. LiCaE has the highest amount of thickener (≈ 22,1 wt %), followed by PPAO (15,3 wt %) and LiM1 (13,7 wt %), respectively.

From the ≈ 22 wt % thickener concentration of LiCaE grease, it is known than 5-10 wt % is Calcium[1], the remainder being Lithium.

The influence of the amount of thickener on grease properties (mainly rheological properties) is reasonably well known when comparing greases with the same formulations and manufacturing processes, where only the thickener amount is changed (see Section 2.10.4). The knowledge obtained from such studies (see [14, 92]), however, cannot be directly correlated to the rheological behaviour of lubricating greases with different formulations and manufacturing processes.

These results are compared to the thickener and oil content of their corresponding degraded greases in Chapter 7, with a view to determining the amount of oil loss occurring during the aging process.

Table 3.3.: Thickener and oil content of LiM1 grease.

Grease, g	Oil, g	Thickener, g	Oil, %	Thickener, %	Oil+Thickener, %
0.1609	0.1402	0.0220	87.16	13.67	100.83
0.2049	0.1767	0.0280	86.24	13.65	99.88
			86.70±0.5	**13.66±0.1**	**100.36±0.4**

[1]Information provided by grease manufacturer.

Table 3.4.: Thickener and oil content of LiCaE grease.

Grease, g	Oil, g	Thickener, g	Oil, %	Thickener, %	Oil+Thickener, %
0.3009	0.2378	0.0661	79.01	21.98	100.99
0.2437	0.1878	0.0542	77.06	22.25	99.32
			78,04±1.0	**22.12±0.2**	**100.16±0.9**

Table 3.5.: Thickener and oil content of PPAO grease.

Grease, g	Oil, g	Thickener, g	Oil, %	Thickener, %	Oil+Thickener, %
0.2320	0.1943	0.0354	83.75	15.26	99.01
0.2575	0.2186	0.0396	84.88	15.39	100.28
			84.32±0.5	**15.32±0.1**	**99.64±0.7**

3.7. Fourier transform infrared spectroscopy - FTIR

Fourier Transform Infrared Spectroscopy (FTIR) is a non-destructive technique used to collect the infrared spectrum of materials in a wide spectral range. Its goal is to measure how well a sample absorbs light at each wavelength. More about FTIR can be seen in [97].

In grease research two main routes have been singled out for the use of FTIR:

- Study of the composition of lubricating greases and their components such as thickeners, base oils and additives [98–101].
- Evaluation of changes (oxidation, depletion of additives, absorption of water, etc.) that occur in greases during service, storage and manufacturing processes [11, 69, 102, 103].

FTIR was performed to verify both of the above circumstances. In the case of the study of grease composition, it was intend only to obtain the spectra of grease, base oil, thickener and bleed-oil in order to determine the peaks related to the thickener and to the oil in the grease spectrum, as well as to compare the chemical properties of the base and bleed-oils. In the second case, FTIR was used to analyse grease changes after severe working conditions by comparing the fresh and degraded grease spectra. More about grease degradation is presented in Chapter 7.

A Spectra-Tech Nicolet Continuum Infrared Microscope connected to a Nicolet Nexus 670 FTIR spectrometer was used for these characterizations. Background spectra were taken from NaCl windows. All spectra were collected using 64 scans at a 2 cm^{-1} resolution at room temperature. All spectra were normalized to the CH_2 peak at approximately 1460 cm^{-1} to prevent disparities between spectra due to different sample thicknesses. To ensure that the results found with FTIR spectroscopy were representative of the composition, each spectrum was taken at least twice. This procedure was carried out for all greases tested and their corresponding thickeners, base oils and bleed-oils. The grease chemical characteristics were inferred by the appearance and magnitude of the peaks in a given wavelength range.

Figure 3.7 gives the spectrum of the LiM1 grease, its bleed-oil and thickener. The thickener was obtained with the process described in Section 3.6 and the bleed-oil with the process described in Section 3.4.

The main observations from Figure 3.7 are summarized bellow:

- The broad peak at 3340 - 3330 cm^{-1} is seen in the grease and in the thickener spectra, but absent in the bleed-oil, indicating that it belongs to the lithium thickener. This is usually observed in lubricating greases formulated with soap thickeners, as shown in [104];

- The strong absorption band in the area (2800 - 3000 cm^{-1}) consisting of an asymmetric C-H stretch of CH_2 and CH_3 molecules is a hydrocarbon structure that is present in both oil and thickener [99];

- The bands at 1580 and 1560 cm^{-1} stem from the soap thickener and are signed as COO^-. This is confirmed by their absence in the bleed-oil spectrum [105].;

- The CH_2 deformation solely attributed to the thickener occurs at 1450 cm^{-1}, whereas that of the base oil is 1461 cm^{-1}. The average wavenumber is therefore reduced to 1456 cm^{-1} in the bulk grease spectrum [102];

- The CH_2 and CH_3 groups of the base oil are primarily responsible for peaks at $\approx$ 2953, 2923, 2850, 1456, 1377 and 721 cm^{-1} in the grease spectrum. Also, the hydrocarbon soap thickener will contribute to these absorptions [99, 102].

Figure 3.8 compares the base oil and bleed-oil spectra in the fingerprint zone (1600 - 700 cm^{-1}) since the differences at higher wavelengths are negligible. Among the few differences observed, one can see that only the bleed-oil spectrum has a peak (or at least a more pronounced peak) at 1600, 1516, 1164 and 1004 cm^{-1}. All these peaks are most likely related to the additive package. The phenolic and amine antioxidants

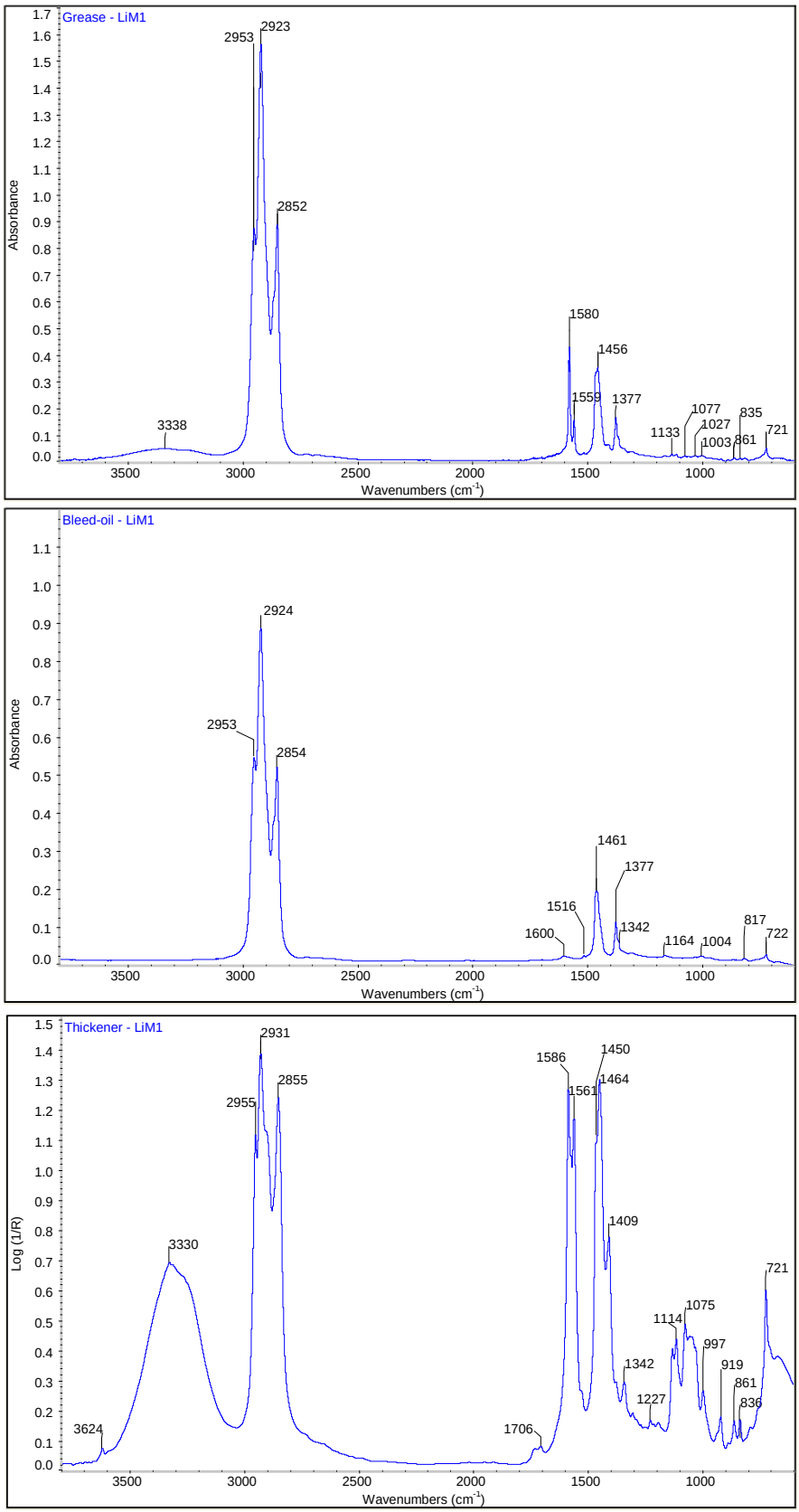

Figure 3.7.: FTIR spectrum of LiM1: grease (top), bleed-oil (middle) and thickener (bottom).

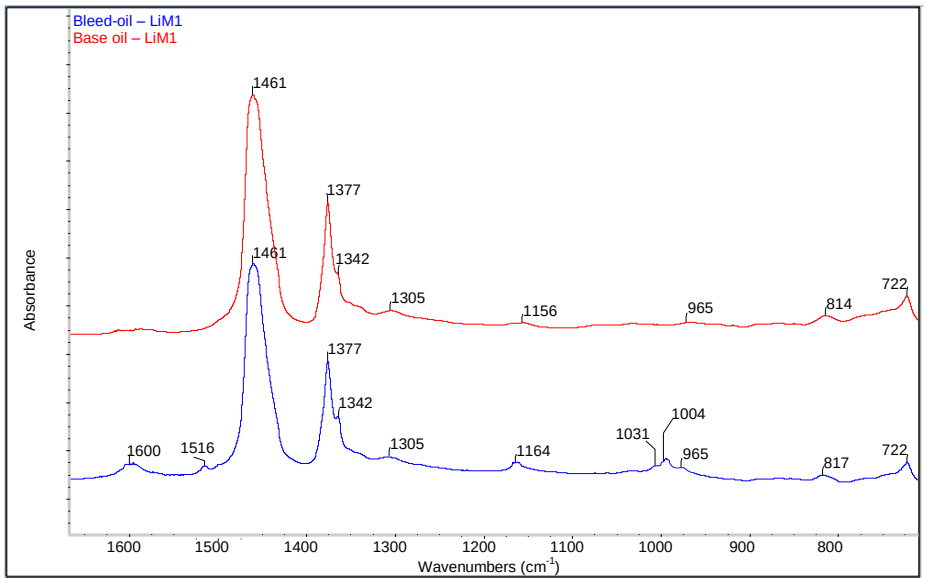

Figure 3.8.: FTIR spectrum of LiM1: comparison between base oil and bleed-oil spectra in the finger print zone.

are observed at ≈ 1600 cm^{-1} and ≈ 1516 cm^{-1} [106–109], the viscosity improvers at ≈ 1162 cm^{-1} [106], and the ZDDP, which also acts as antioxidant at ≈ 1004 cm^{-1} [11, 110].

Likewise, the analysis of LiCaE grease and its components is given in Figures 3.9 and 3.10. This grease is substantially different from LiM1. It is formulated with ester base oil and thickened with lithium and calcium. The main difference in the thickener spectrum is the calcium-intense broad band centring at ≈ 1430 cm^{-1} and its sharp bands at ≈ 1795, 874 and 712 cm^{-1} [111] and in the bleed-oil spectrum, the ester bands at ≈ 1744, 1238 and 1158 cm^{-1} [112]. Nevertheless, the main lithium bands are still present at the 1580 and 1560 cm^{-1} peaks, which can be shown in the grease and thickener spectra.

Some differences between base and bleed-oil were also observed. The 1789 cm^{-1} peak in the bleed-oil spectrum is absent in the base oil. This could be related to the band associated with calcium in the 1795 cm^{-1} peak (see Figure 3.10), thereby suggesting thickener transference to the oil during the bleeding process. Other peaks seen in the bleed-oil, but absent in the base oil and thickener spectra are the ones with low intensity absorbance at 1600 and 1517 cm^{-1}, which was also observed in the LiM1 bleed-oil spectrum and attributed to antioxidant additives. Merging of the base oil peaks at 1246 and 1226 cm^{-1} in the bleed-oil peak at 1237 cm^{-1} might indicate the addition of other constituents in the bleed-oil, either thickeners or additives.

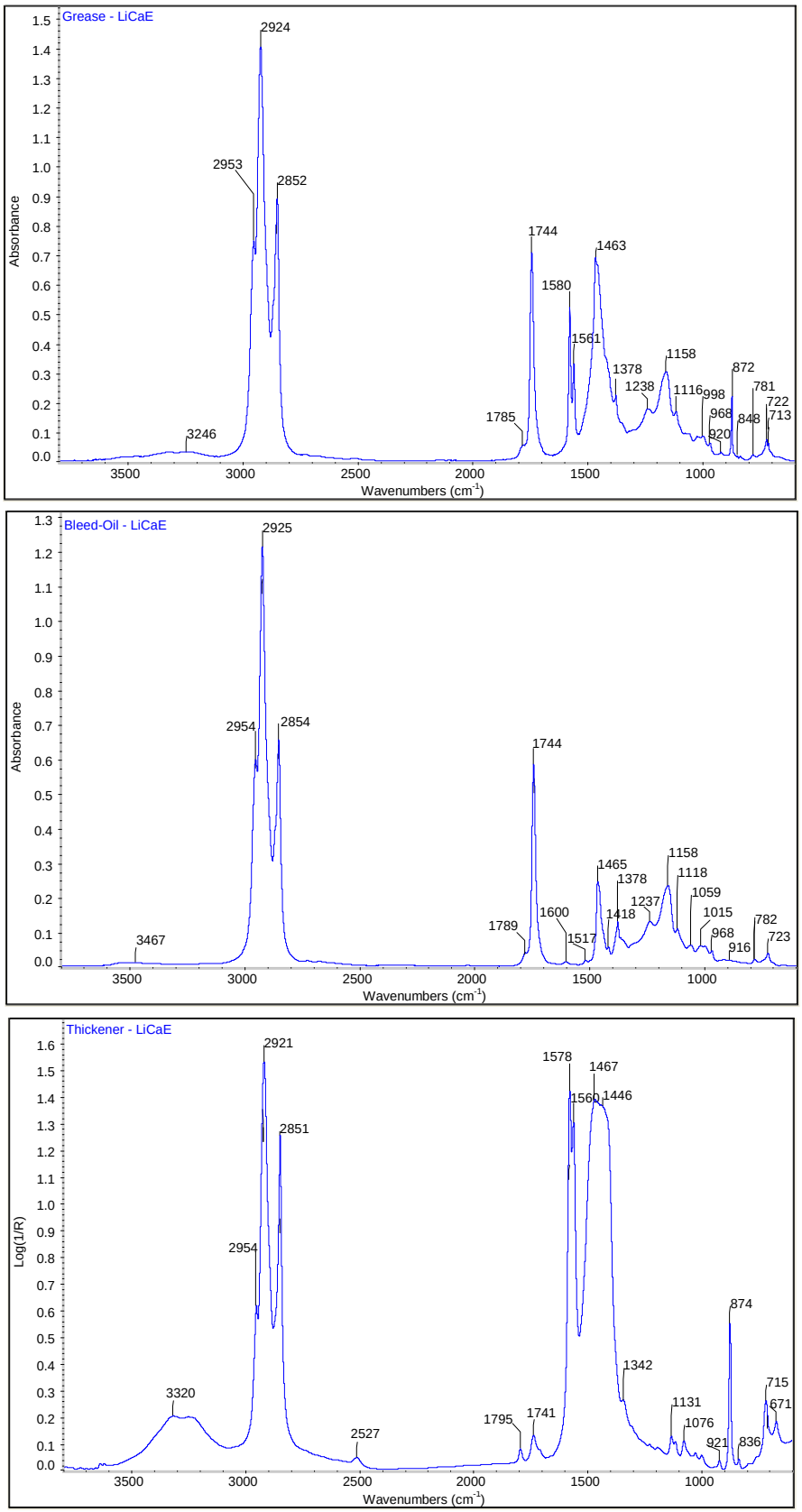

Figure 3.9.: FTIR spectrum of LiCaE: grease (top), bleed-oil (middle) and thickener (bottom).

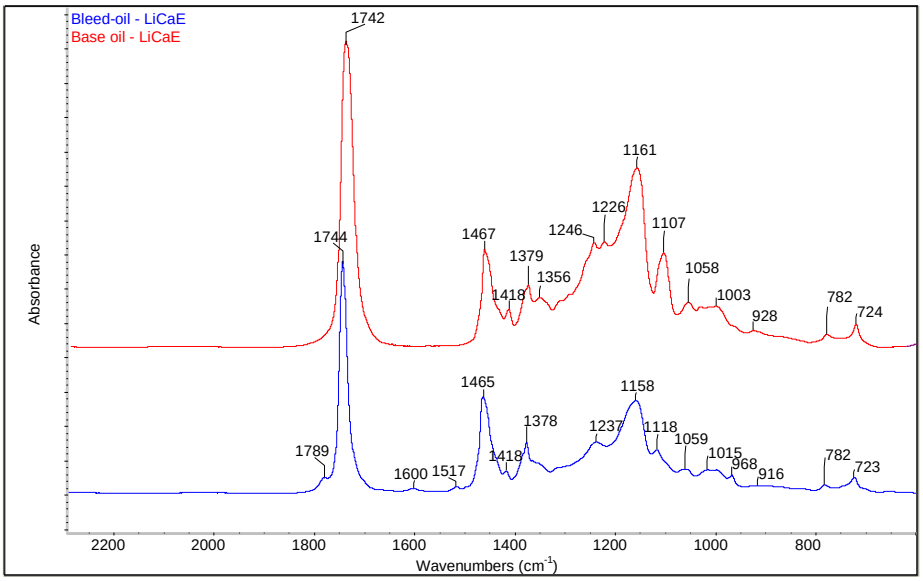

Figure 3.10.: FTIR spectrum of LiCaE: comparison between base oil and bleed-oil spectra in the finger print zone.

PPAO grease and its components are analysed in Figures 3.11 and 3.12. This grease has a different formulation from the greases previously described; it is formulated with polyalphaolefin base oil, thickened with polypropylene and co-thickened with an elastomer.

Different from the other greases, PPAO does not present a broad peak at 3340 - 3330 cm^{-1} because its thickener is polypropylene (non-soap thickener). The presence of isotactic polypropylene (iPP) in the grease is seen at approximately 1330, 1303, 1220, 1167, 1100, 998, 973, 940, 900, 841, and 808 cm^{-1} [113]. Most of those bands are seen only in the grease and thickener spectra.

Figure 3.12 also showed some differences between the base and bleed-oil spectra of PPAO grease. Among these differences, one notes that only the bleed-oil spectrum has the 1747, 1710, 1600, 1517, 1164, 822 and 700 cm^{-1} bands.

The 1600 and 1517 cm^{-1} bands found in all the lubricating greases, are attributed to antioxidant additives. At the band of 1747 cm^{-1} is found carbonyl (C=O) of the ester group, which is often used in AW additives [69]. The peak at 1164 cm^{-1} is attributed to viscosity improvers, and this was also observed in the LiM1 grease. The peak at 1710 cm^{-1} is Bismuth, also an EP/AW additive, which is known to be part of the grease additivation (see Table 3.2); the small hump on the 722 cm^{-1} peak around 700 cm^{-1} is caused by the co-thickener (rubber) [2].

[2]Information provided by the manufacturer.

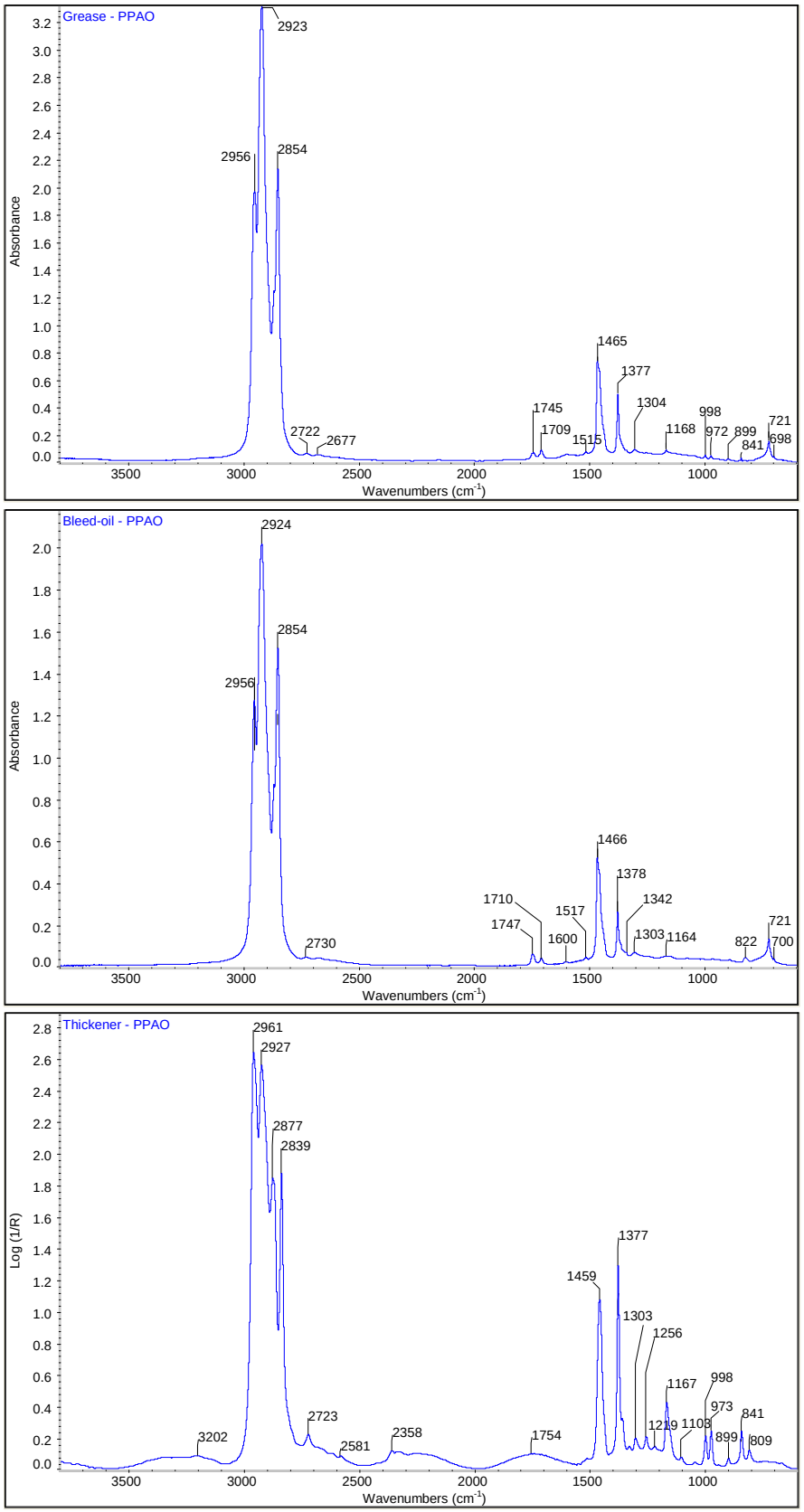

Figure 3.11.: FTIR spectrum of PPAO: grease (top), bleed-oil (middle) and thickener (bottom).

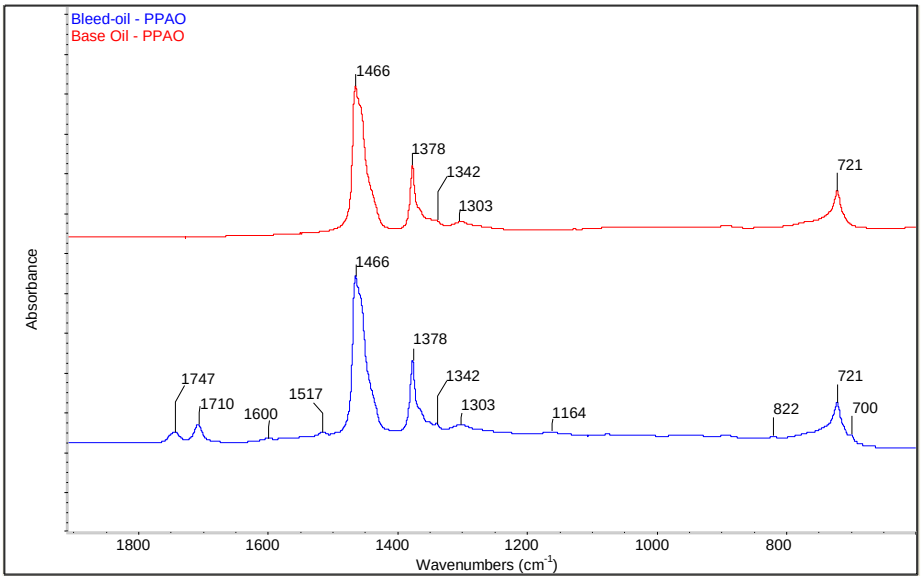

Figure 3.12.: FTIR spectrum of PPAO: Comparison between base oil and bleed-oil spectra in the finger print zone

The results presented above provided information regarding the grease peaks from the base oil and those from the thickener. They also demonstrated that most of the additives remain with the oil during the bleeding process.

Comparison between base oils and bleed-oil showed several differences between their spectra and these differences were shown to be dependent on the grease formulation. In fact, the co-thickener and the additives may have a large affinity with the oil, bleed out together during the bleeding process and generate a bleed-oil that is significantly different from the base oil. Furthermore, during the bleeding process the thickener may pass through the mesh due to the imposed stress and temperature. Hence, bleed-oil may contain additives, thickener and co-thickener material that is not present in the base oil, and their amount depends on the formulation of the grease.

Furthermore, the bleeding process also depends on the grease micro-structure that interacts in different ways with the macromolecules of the oil and the additives; consequently, the bleed-oil properties also depend on the grease manufacturing process [3].

The FTIR spectrum is not easily interpreted as there are many components that instead of giving rise to a new peak, only shift or change the intensity of an already existent peak and in some cases, are not even perceptible due to their small percentage in the sample. Even so, many additives were detected, as were a few traces of thickener and co-thickener in the bleed-oil that were absent in the base oil.

3.8. Rheometry

Rheometry generically refers to the experimental techniques used to determine the rheological properties of materials, that is, the quantitative and qualitative relationships between deformations and stresses and their derivatives.

By far the most frequently used method for measuring non-Newtonian grease rheology is shear rheometry. These rheometers control the shear stress or shear rate, and may have different geometries, e.g. concentric cylinders (Figure 3.13(a)), vane-cylinder (Figure 3.13(b)), parallel plates (Figure 3.13(c)), cone-plate (Figure 3.13(d)) and different surface finishings that vary from very smooth to very rough surfaces. A complete description of shear rheometers is found in the ELGI book [38].

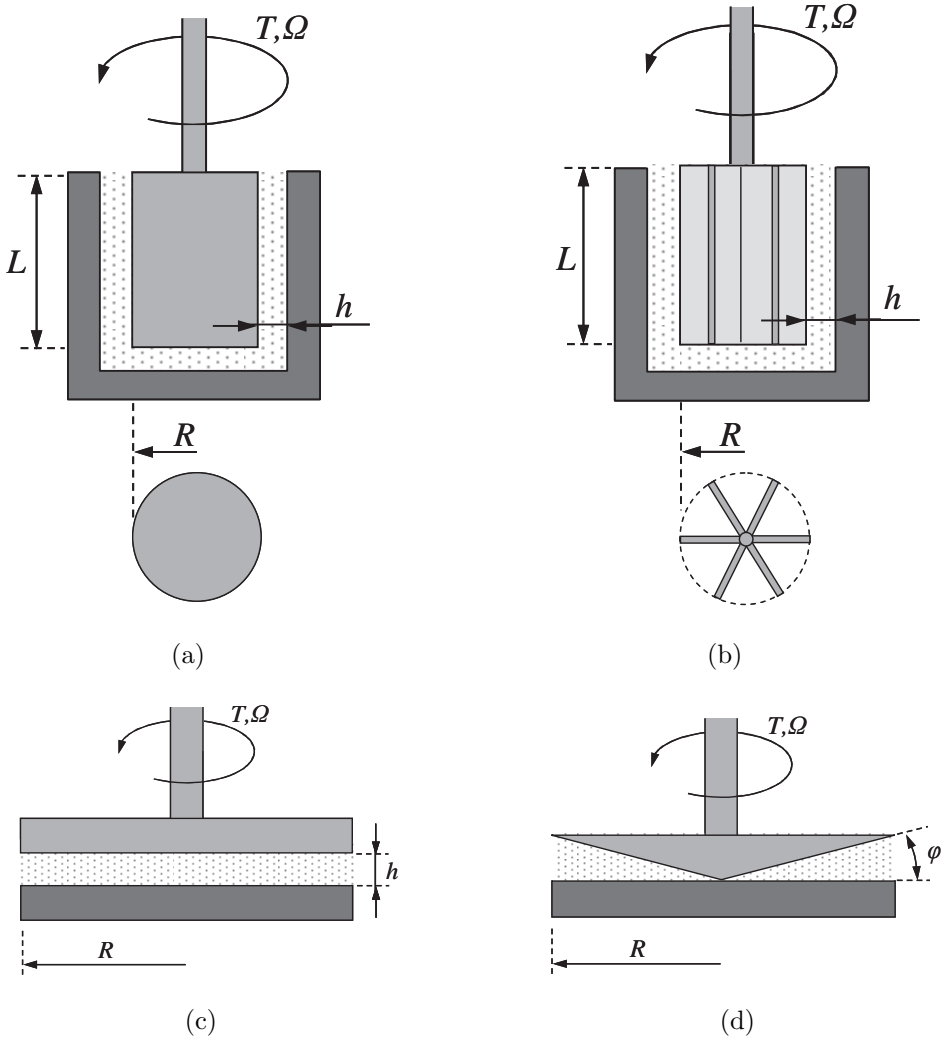

Figure 3.13.: Concentric cylinder (a), Vane-cylinder (b), Parallel plates (c) and Cone-plate (d) geometries for a shear rheometer [1].

The selection of the appropriate shear rheometer, geometry type, surface finishing and operating conditions depends on the desired outputs and the sample characteristics.

For grease characterization a large range of shear rate ($10^{-6} \leqslant \dot{\gamma} \leqslant 10^{+7}$) is very important. There are, however, many errors associated with range extremes. Wall slip is frequently observed at very low shear rates whilst grease leakage and edge effects occur at very high shear rates. Controlled stress rheology is particularly useful for probing the region of flow behaviour where flow actually starts (very low shear rate), which is of great interest for obtaining accurate yield stress (τ_y). With the controlled stress rheometer (CSR), a precisely controlled, operator-selected torque is applied to a rotating shaft and measurement geometry is in contact with the sample material; the resultant strain properties are then measured. The applied torque (stress) can be ramped up or down or held steady to evaluate flow and viscosity under steady (unidirectional) shear, as well as to evaluate the effects of oscillatory dynamic motion and creep.

As to the geometries, parallel plates (Figure 3.13(c))have some advantages over others: they are less sensitive to grease leakage and edge effects due to their geometry and they are the only ones that allow gap-height control, hence a larger range of shear rates. Regarding the surface finishing of the geometry, rough surfaces are preferred over smooth ones as they are less susceptible to wall slip [77, 114, 115]. Extremely rough surfaces, however, may be less reliable in filling the gaps and may promote fractures caused by the occurrence of secondary flows in the sample [116]. Taking this all into account, all the measurements were carried out with a controlled stress rheometer and $2R = 25$ mm diameter rough parallel plates with a $Ra \approx 20\mu$m.

Nevertheless, the right selection of the equipment does not ensure correct measurements. In view of the fact that grease is also a thixotropic material, as sample history usually plays an important role in determining data (mainly at low stress), sample preparation should be properly done.

Before each experiment the environmental rheometer chamber was heated to the required temperature in order to ensure a homogeneous temperature in the plates and surroundings. The zero gap was then set with the standard rheometer gap-zeroing procedure (gap height = 0 when the plates touch each other until a normal force of 5 N is measured). After that, an excessive amount of grease was loaded into the geometry to ensure fully filling the gap between the plates, which was subsequently set to the required gap height. As the minimum gap size was set in order to minimise artefacts from the walls, the gap had to be one order of magnitude above the thickener size [115, 117]. Since the excess grease had to be pushed out, some internal stresses

were produced in the sample. This surplus of grease was carefully removed from the edge. Next, a pre-shear program was performed to remove the internal stress (sample history). In order to maintain consistency in all measurements, all samples were pre-sheared in the same way. The pre-shear should not reach too high speeds or last too long to prevent unintended grease loss from the edges, edge fracture or excessive shear degradation [118]. It should nevertheless last long to overlap sample history. After the pre-shear program, the grease was left to rest until strain stabilization was observed (15 minutes for the greases studied) and only then were the measurements performed. The edge was examined for grease loss and edge fracture after the experiment.

Additionally, the small gaps and high speeds required to reach high shear rates may introduce several errors due to a non-constant shear rate distribution, inertia of the grease sample, errors in gap settings, viscous heating of the sample and edge fracture [115]. Although some of these errors are automatically corrected by the most modern rheometers, others need to be corrected afterwards.

In this work, the minimum gap size was taken into account when obtaining and processing all the rheological data in order to minimise artefacts from the walls, the non-constant shear-rate over the plate radius, uncertainty in the gap error and the thixotropic/historic effects (See Appendix A).

Viscous shear heating was not taken into account since Davies and Stokes [115] showed that the heat generated in the sample is rapidly dissipated into the plates due to the small gap height and therefore, no significant temperature gradients in the rheometer sample are expected.

Wall slip was visually identified in the flow curves after all corrections were applied, and disregarded when necessary. A plot combination of sweep (very low to medium shear rates) and flow tests (medium to high shear rates) was used for this identification.

The equipment/procedure used was validated by comparison with base oil viscosity measurements carried out according to ASTM D445-12 [119]. Furthermore, all the tests were performed twice; their differences were less than 10 %.

3.8.1. Base and bleed oil flow properties

Base and bleed-oil dynamic viscosity and shear stress were measured in an AR 1000-N rheometer from TA Instruments with rough plate-plate geometry ($2R$ = 25 mm; Ra = 20 μm) at two different temperatures (40 °C and 80 °C). Flow tests were performed with increasing levels of shear rate ($10^{-2}\mathrm{s}^{-1} < \dot{\gamma} < 10^{4}\mathrm{s}^{-1}$) whilst shear stress ($\tau$) and apparent viscosity (η) were measured. Under these conditions, all the base oils and the bleed-oils of the LiM1 and LiCaE greases presented a Newtonian

behaviour but different viscosity/stress values, whilst the PPAO bleed-oil showed a shear thinning behaviour, as indicated in Figure 3.14. The relative viscosity and shear stress difference observed in this figure was calculated by Equations 3.2 and 3.3, respectively. In the case of PPAO bleed-oil the η_{bleed} and τ_{bleed} are the average values at the low shear rate range ($\dot{\gamma} < 10^2$ s^{-1}).

$$\Delta\eta\,[\%] = \frac{\eta_{bleed} - \eta_{base}}{\eta_{base}} \times 100 \tag{3.2}$$

$$\Delta\tau\,[\%] = \frac{\tau_{bleed} - \tau_{base}}{\tau_{base}} \times 100 \tag{3.3}$$

Three different trends were observed when base oil and bleed-oil viscosities were compared at 40 °C . LiCaE grease presented similar values for base and bleed oil viscosities. In the case of LiM1 grease, the viscosity of the bleed-oil was 16.9 % lower than the viscosity of the base oil, while in the case of PPAO grease the viscosity of the bleed oil was 1150 % higher than the viscosity of the base oil. Such different behaviours are better seen in Figure 3.15.

The IR-spectra had already shown different compositions between base and bleed-oils, and therefore it was already expected some difference on the bleed-oil physical and rheological properties.

The very high viscosity of the PPAO bleed-oil was attributed to its co-thickener, an elastomer (rubber) with a high affinity with the base oil that bleeds out with it during the bleeding process[3]. The co-thickener was characterized as a small hump on the 722 cm^{-1} peak around 700 cm^{-1} in the FTIR spectrum (see Figure 3.12). Base and bleed-oil viscosity values of PPAO were also measured by the grease manufacturer and are presented in the technical data sheet of the product, as shown in Figure 3.16. There, bleed-oil viscosity values were found to be higher than the ones presented in Figure 3.15.

The $\Delta\eta$ of LiM1 and LiCaE are related to their different compositions as well. It is not clear, however, whether there is a direct association between $\Delta\eta$ and a specific spectra difference (as in the case of PPAO - 700 cm^{-1}).

[3]Information provided by the grease manufacturer.

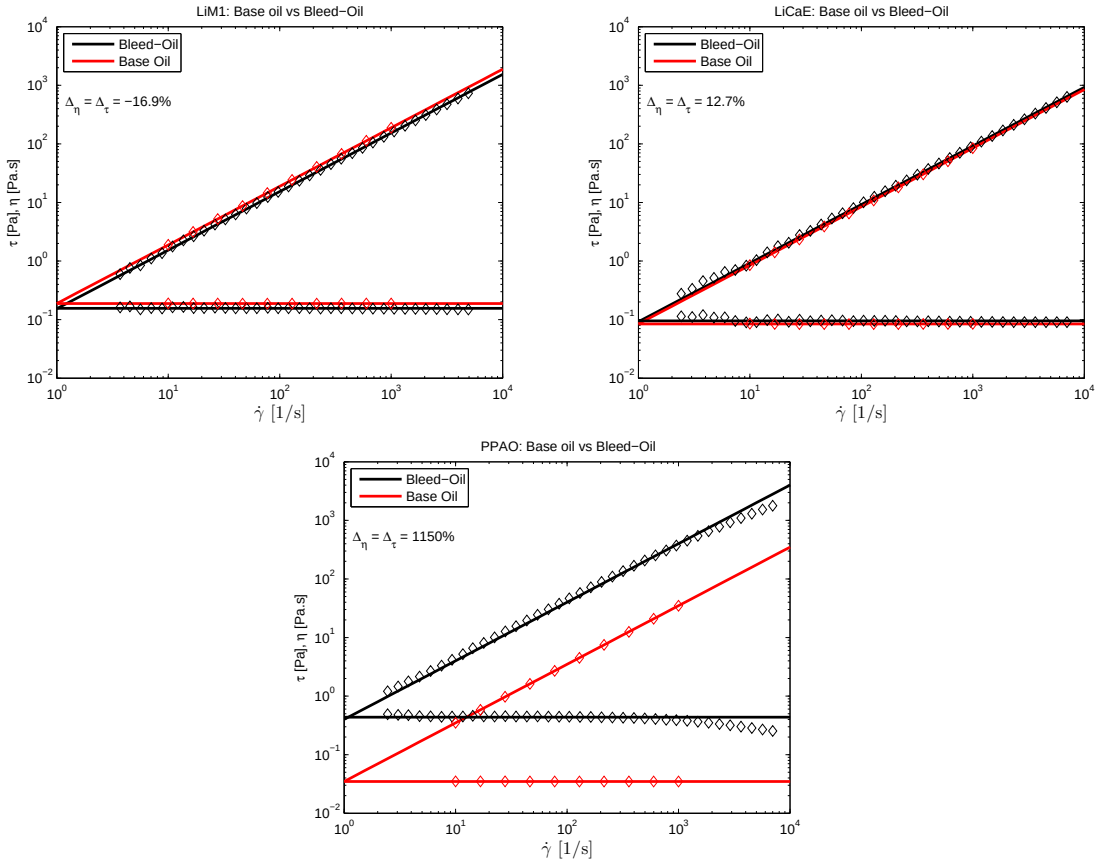

Figure 3.14.: Base and bleed-oil viscosity and shear stress vs. shear rate at 40 °C .

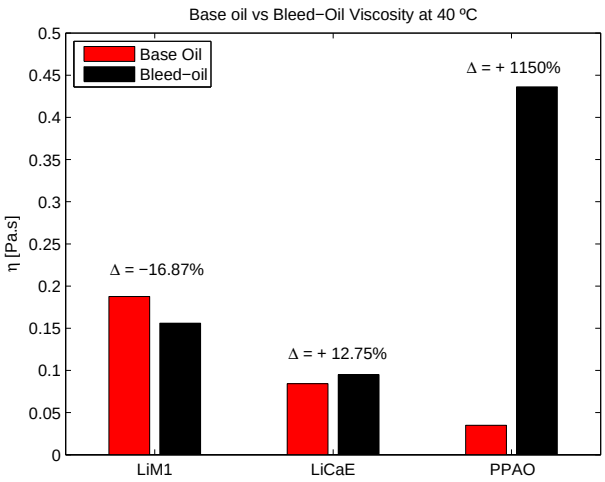

Figure 3.15.: Relative percentage difference between base oil and bleed-oil viscosity at 40 °C .

NOION 632 EPB

PRODUCT DESCRIPTION

NOION 632 EPB is a modern polymer-thickened lubricant incorporating AXEL's patented Epoch™ technology into an optimal blend of synthetic fluids and functional additives. The carefully selected additive package includes antioxidants, corrosion inhibitors and a unique EP/AW system based on bismuth chemistry.

This novel Epoch™ technology provides considerable advantages over conventional soap-based greases. The polymeric thickener is non-ionic, inert and contributes to an increased film thickness. This, in turn, results in longer life and easier and more secure maintenance. Due to the inertness of the thickener system, the product is also compatible with most types of conventional lubricating greases.

- Long life
- Inert thickener
- Excellent water resistance
- Controlled oil separation
- Excellent pumpability

In addition, Epoch™ technology provides high adhesion and low solubility resulting in excellent resistance to water and aggressive chemicals.

NOION 632 EPB is a unique high performance synthetic lubricant suitable for a wide variety of applications where long life is of critical importance. Improved lubrication of sensitive materials such as aluminium, ceramics, and elastomers are additional features emanating from the non-ionic thickener. In addition, Epoch™ technology provides enhanced functionality at low and ambient temperatures including pumpability in most modern centralised lubrication systems.

TYPICAL TECHNICAL DATA

Thickener		EPOCH™
Base oil		Synthetic oil
Colour	Visual	Beige
Base oil viscosity at 40°C	ISO 12058	47 mm^2/s
Base oil viscosity at 100°C	ISO 12058	8 mm^2/s
Viscosity of the bleed oil at 40°C	ISO 12058	640 mm^2/s
Viscosity of the bleed oil at 100°C	ISO 12058	72 mm^2/s
Dropping point	IP 396	>140°C
4-ball weld load	DIN 51350:4	3600 N
Temperature range		-35°C to +120°C

AXEL
AXEL CHRISTIERNSSON

Figure 3.16.: Technical data sheet of PPAO (Commercial name: NOION 632 EPB).

3.8.2. Creep tests

All the creep tests were performed with a 250 μm gap after a flow-type pre-shear and a 15 minutes resting time. The pre-shear consisted of applying a shear rate from 1 to 10 s^{-1} and then from 10 to 1 s^{-1} during 4 minutes.

The creep curves are presented in Figures 3.17 to 3.19, and the yield stress limits (τ_{ymin} and τ_{ymax}) are given in Table 3.6. These results showed that under low shear stress LiM1 grease offers the least resistance to flow, PPAO grease offers the highest and LiCaE grease is in between.

High or low yield stress values can be either beneficial or harmful for bearing application. On the one hand, high yield stress values can lead to bearing failure due to excessively low rates of replenishment, as once the standing lubricating grease in the cage pockets and side tracks of the rolling bearings will not flow back to the contact zone. On the other hand, lubricating greases with a very low yield stress might flow out of the box/bearing/cage, resulting in starvation and seizure of the bearings.

The influence of temperature on the yield stress was not studied here, but some measurements carried out by Gow [120], Karis *et al.* [121] and Froishteter *et al.* [122, 123] indicate that yield stress decreases by a factor between 2 and 6 for each 50 °C .

Table 3.6.: Yield stress limits at 40 °C . Creep tests.

	LiM1	LiCaE	PPAO
τ_{ymin}, [Pa]	100	200	600
τ_{ymax}, [Pa]	200	400	800

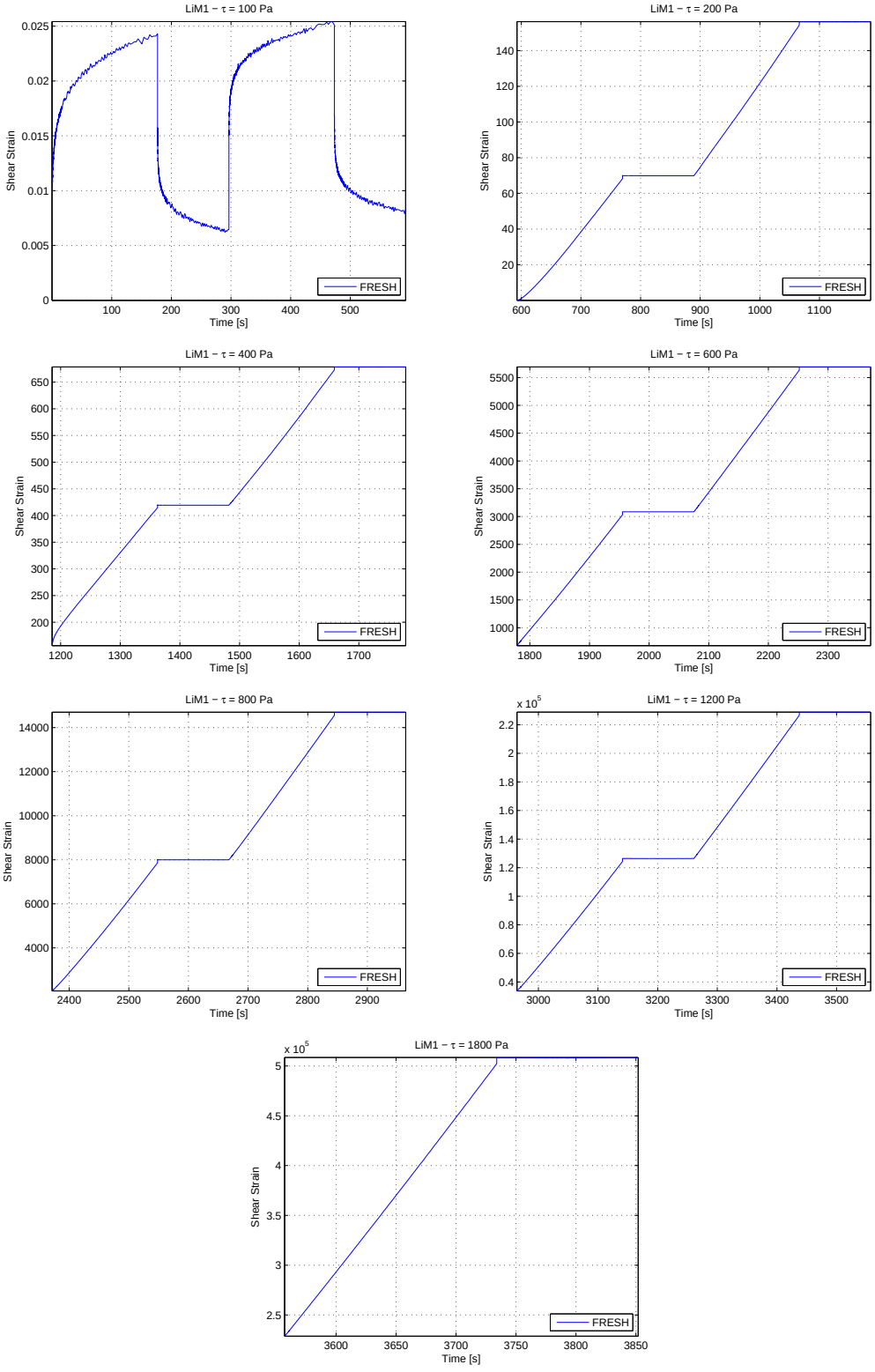

Figure 3.17.: Creep test: shear strain versus time for different applied shear stresses. Grease LiM1.

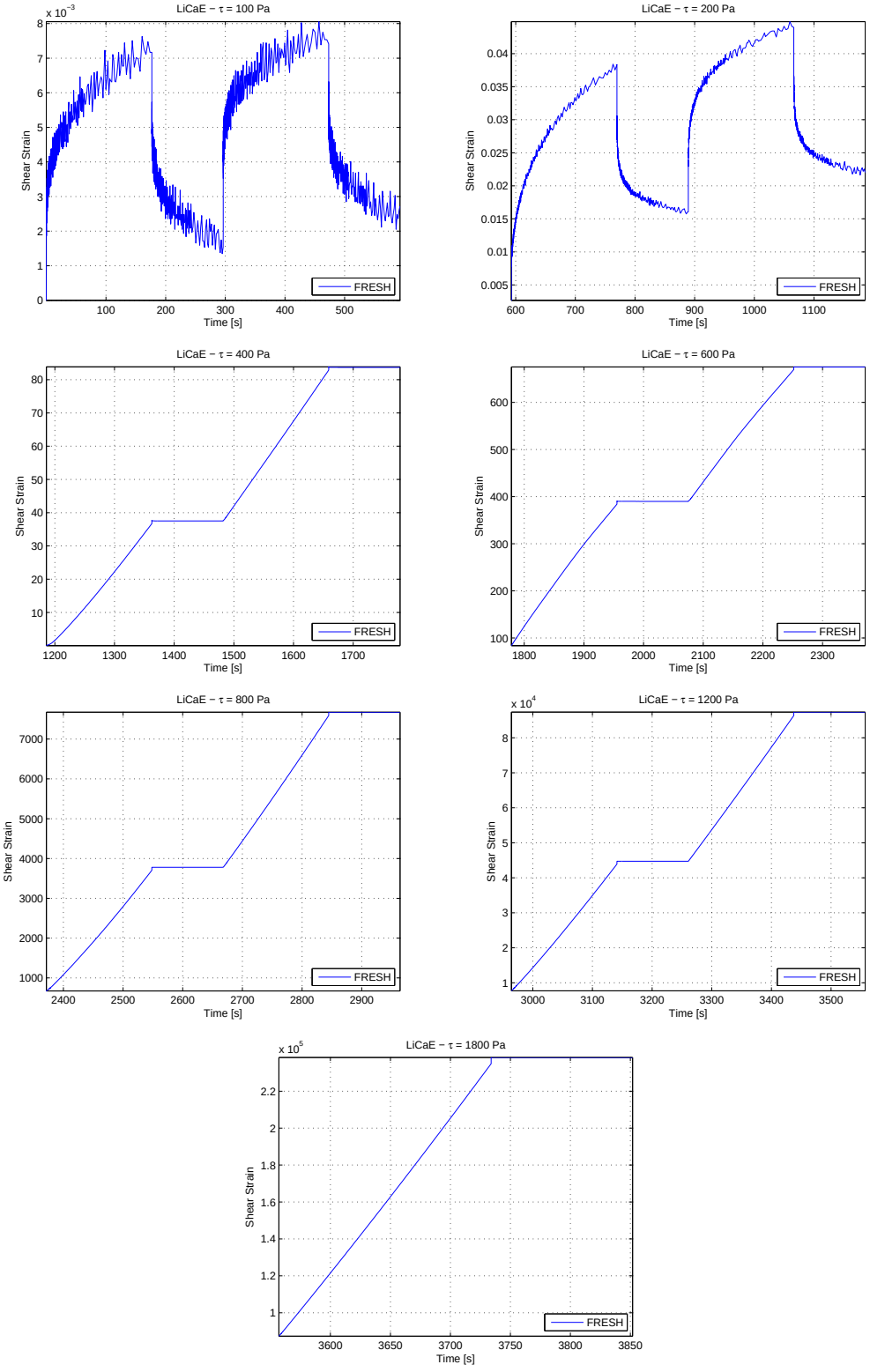

Figure 3.18.: Creep test: shear strain versus time for different applied shear stresses. Grease LiCaE.

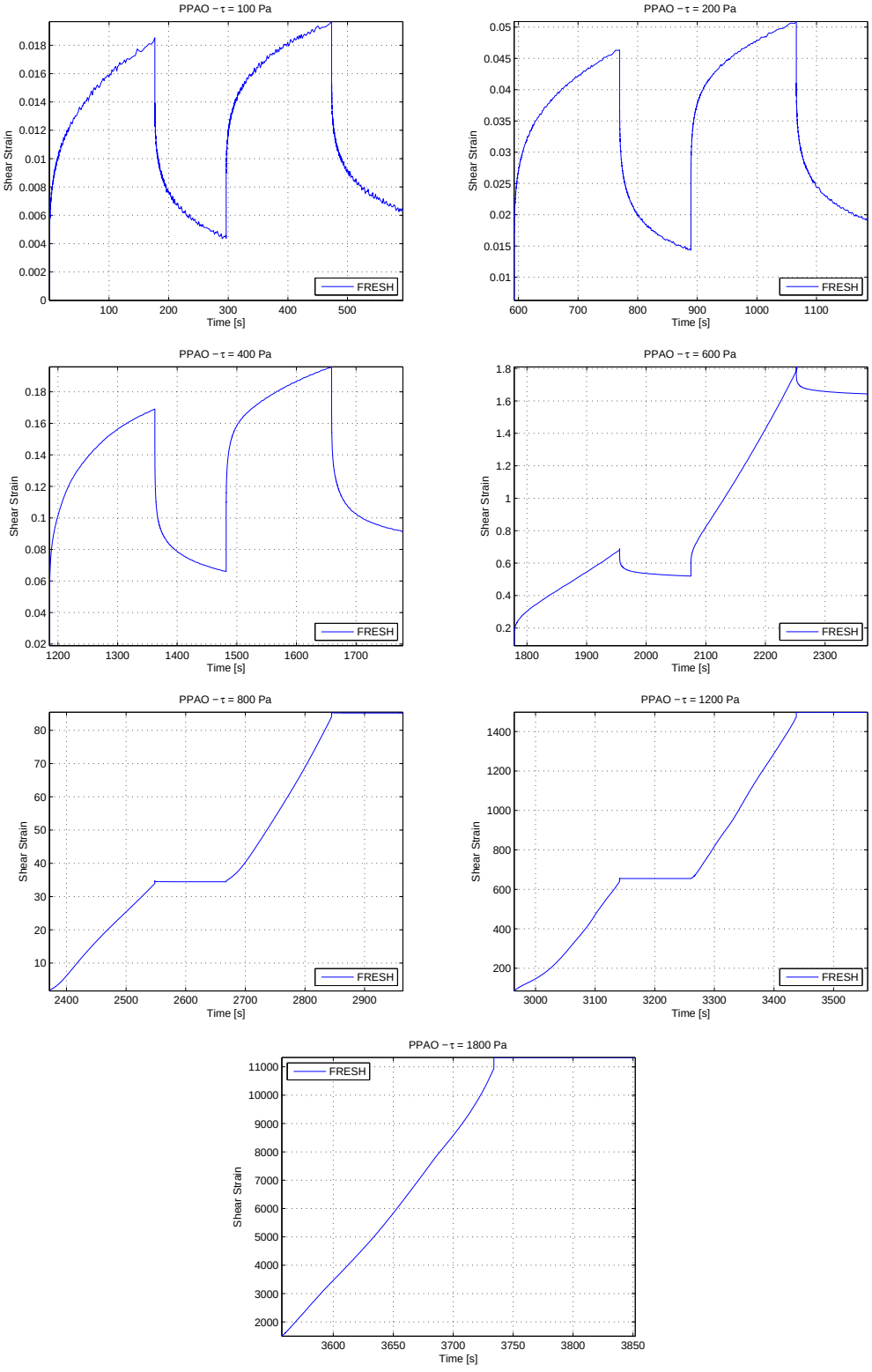

Figure 3.19.: Creep test: shear strain versus time for different applied shear stresses. Grease PPAO.

3.8.3. Oscillatory tests

All the oscillatory tests were performed with a 250 μm gap after an oscillatory-type pre-shear and a resting time of 15 minutes. The pre-shear was applied between the end of the linear visco-elastic region (LVE) and the cross over stress (τ_{co}). The pre-shear program consisted of applying an oscillatory rotational speed with a 0.01 to 0.2 strain during 5 minutes. The oscillatory stresses corresponding to a strain equal to 0.2 were 130, 205 and 255 Pa for LiM1, LiCaE and PPAO, respectively.

The storage G' and loss G'' moduli are plotted against the oscillatory stress τ_{os} in Figure 3.20.

The complex modulus G^* (Figure 3.21), given by equation 2.12, follows the same trend as G' and G''. In these figures one can see that all the greases maintain their resistance to deformation until they reach the yield stress[4], whereupon they undergo rapid transition from high to low G', G'' and G^* values. This rapid transition is observed by an increase in phase angle $tan(\delta)$, as shown in Figure 3.22, and is due to a breakdown of the internal elastic structure as the imposed stress was increased.

Figure 3.20 and 3.21 shows that LiCaE has the highest values of storage, loss and complex moduli. LiM1 and PPAO greases are quite similar, although PPAO has slightly higher values.

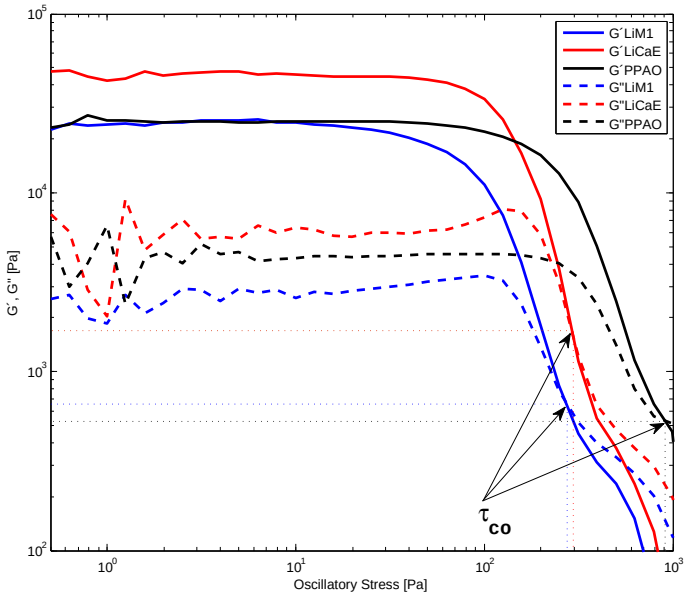

Figure 3.20.: Storage and loss moduli versus oscillatory stress at 40 °C .

According to Couronné *et al.* [3], storage modulus G' can be considered as an evidence of the intensity of the interaction between the grease components and that

[4]In case the yield stress is considered at the end of the LVE region.

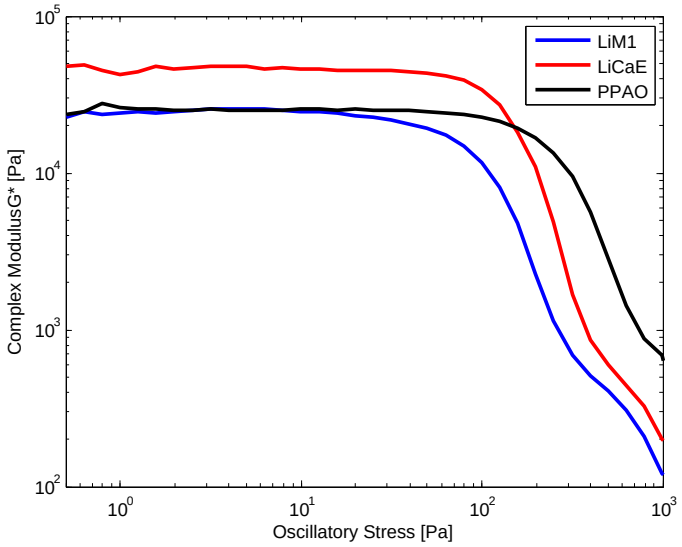

Figure 3.21.: Complex modulus (G^*) versus oscillatory stress at 40 °C .

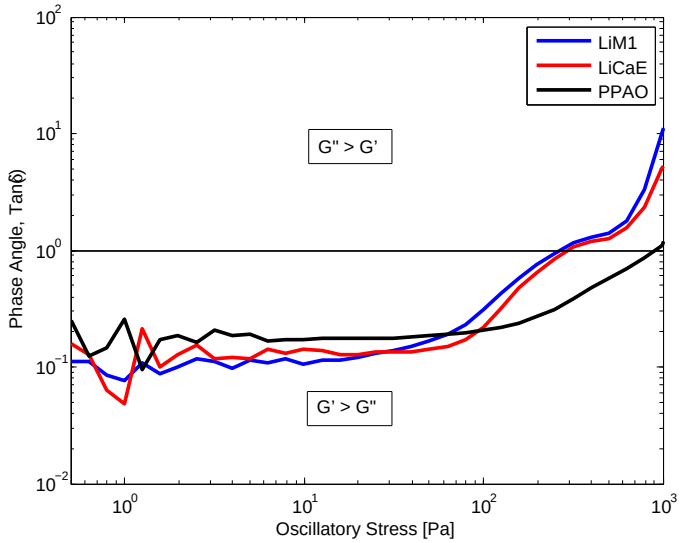

Figure 3.22.: Phase angle $tan(\delta)$ versus oscillatory stress at 40 °C .

lubricating greases with low G' values have a greater capacity to form and sustain a thick film than lubricating greases with high values. Couronné also claimed that no other rheological property (τ_y, η, τ_{co} and δ) correlates with the film formation. Her film thickness results were obtained with 4 fresh greases, a temperature around 20 °C , moderate speed, short time tests, light load and good supply of lubricant to the contact at the beginning of the test. If such considerations were brought to the results shown in 3.20, one would expect that PPAO and LiM1 greases had a better capacity to sustain a film than LiCaE grease. The effect of grease properties in film formation are discussed in Section 4.6.

Delgado *et al.* [92] found that, in general, the higher the plateau modulus G_N^0 [5]the lower the traction coefficient. This conclusion was based on the rheological and tribological evaluation of 14 lubricating greases formulated with lithium and a naphthenic base oil under flooded lubrication, short period tests, moderate loads (0.8 GPa), moderate speeds and at ambient temperature. Again, if such a consideration were brought to the results shown in Figure 3.20, one would expect that LiCaE grease would present a lower friction factor than LiM1 and PPAO.

As described in Section 2.10.1, yield stress has a value somewhere between the initial drop in G' and the cross-over stress τ_{co}. Applying this concept to the results presented in Figure 3.20, the yield stress would have a value somewhere between the values presented in Table 3.7.

Table 3.7.: Yield stress limits at 40 °C . Oscillatory tests.

	LiM1	LiCaE	PPAO
τ_{ymin}, [Pa]	15	40	60
τ_{ymax}, [Pa]	270	295	915

3.8.4. Flow tests

3.8.4.1. Grease viscosity

All the flow tests were performed with a 175 μm gap after a flow-type pre-shear and a resting time of 15 minutes. The pre-shear consisted of applying a shear rate from 1 to 10 s^{-1} and then from 10 to 1 s^{-1} during 4 minutes.

Grease viscosity was measured in flow tests from medium to high shear rates and in oscillatory tests from low to medium shear rates. The equation developed by

[5]The value of the storage modulus at the minimum frequency for loss tangent ($\tan\delta = G''/G'$).

Doraiswamy *et al.* was used [124] to obtain the steady shear viscosity from oscillating shear

$$\eta(\gamma_m \times \omega) = \eta(\dot{\gamma}) \quad \text{for} \quad \gamma_m \times \omega = \dot{\gamma} \tag{3.4}$$

where γ_m is the amplitude of the shear strain at which the angular frequency ω was imposed. In the particular case, a 1 Hz frequency was used, therefore

$$\eta(\gamma_m \times \omega) = \tau_{os}/(\gamma_m \times \omega) \tag{3.5}$$

The K and m constants of Equation 2.14 were obtained by combining both measurements and by using a non-linear fitting procedure. This equation is re-written below.

$$\eta = \frac{\eta_0 - \eta_\infty}{1 + (K\dot{\gamma})^m} + \eta_\infty \tag{3.6}$$

η_∞ is the measured bleed-oil viscosity (Figure 3.15) and η_0 is read from the experimental results of the oscillatory tests after applying Equation 3.4. In the case of PPAO bleed-oil, η_∞ represents the average viscosity values at the low shear rate range ($\dot{\gamma} < 10^2$ s^{-1}).

The measured ($\diamond$) and calculated grease viscosity (—) versus the shear rate at $T = 40$ °C are shown in Figure 3.23 for each lubricating grease. The measured ($\square$) and calculated bleed-oil viscosity (- -), as well as the first Newtonian viscosity - η_0 ($\cdots$) are also shown in this figure. Input parameters (η_0 and η_∞), the model constants obtained by a non-linear fitting process (m and K) and the R^2 are shown in Table 3.8.

A comparison between the lubricating greases is shown in Figure 3.24.

Figure 3.24 shows that at very low shear rates, LiCaE presented the highest viscosity, followed by PPAO and LiM1 with very similar values. At high shear rates, an inversion is observed and PPAO showed the highest viscosity, followed by LiM1 and LiCaE. Viscosity values at high shear rates are conditioned by the assumption that lubricating greases reach their bleed-oil viscosities at high shear rates. However, some bleed-oils (or even base oils) might present a shear thinning behaviour, which would produce lower η_∞ and consequently lower values for the grease viscosity at high shear rates, thus slightly changing the K and m model constants.

Model constants K and m are associated with the rupture of grease linkages and shear thinning behaviour, respectively [89].

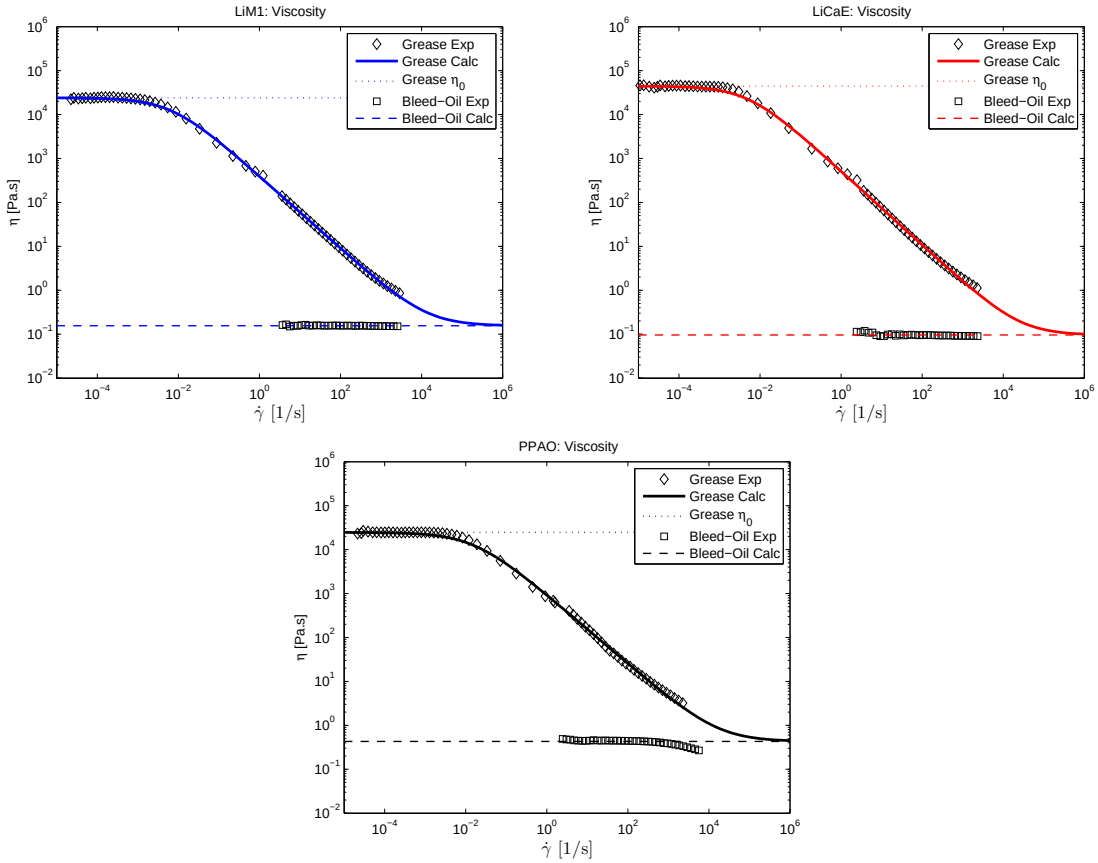

Figure 3.23.: Grease viscosity versus shear rate: Comparison between experimental and calculated values at 40 °C .

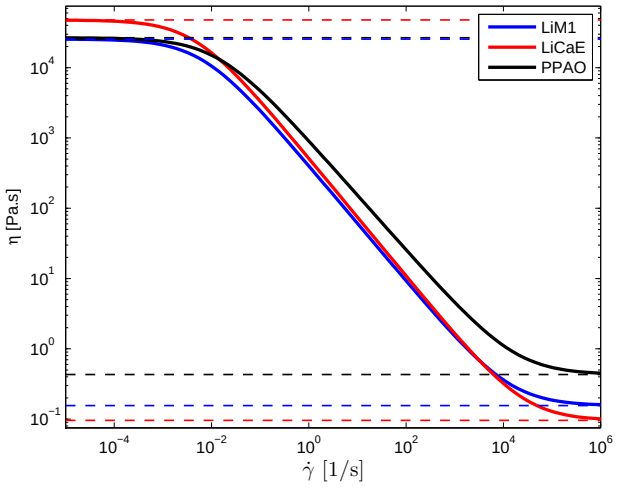

Figure 3.24.: Viscosity versus shear rate: Comparison between the lubricating greases at 40 °C .

Table 3.8.: Inputs and calculated rheological parameters of lubricating greases at 40 °C . Obtained by fitting the viscosity measurements (Figure 3.23) and Equation 3.6.

	LiM1	LiCaE	PPAO	Unit
η_0	25062	44364	24675	Pa.s
η_∞	0.1558	0.0960	0,4317	Pa.s
K	146.17	198.40	61.77	Pa.s^m
m	0.8235	0.8374	0.7850	-
R^2	0.948	0.946	0.944	-

3.8.4.2. Grease shear stress

Similarly, shear stress was also measured with flow and oscillatory tests. The K and m constants of Equation 2.15 were obtained by combining both measurements and using a non-linear fitting procedure. This Equation is re-written below.

$$\tau = \tau_y + \left[\frac{\eta_0 - \eta_\infty}{1 + (K\dot{\gamma})^m} + \eta_\infty\right]\dot{\gamma} \tag{3.7}$$

Due to the difficulty in determining absolute yield stress τ_y, Equation 3.7 was solved by using $\tau_y = 0$ and and its minimum and maximum values obtained in the creep tests (see Table 3.6). These ranges are within the values observed in the flow curves (Figure 2.10, transition from Zone-1 to Zone-2). Yield stress limits obtained with the oscillatory tests were disregarded, given their too extensive limits and their inconsistency with the values observed through the creep and flow tests.

It is important to note that adding yield stress to the transposition of Equation 2.14 to 2.15 (or Equation 3.6 to 3.7) significantly changes the K and m model constants. Furthermore, one needs to know that K and m depend greatly on the chosen model and therefore, one cannot compare such parameters when they have been obtained by different models.

Figure 3.25 shows the shear stress measured (▫) and calculated for the bleed-oil (- -), the shear stress measured for the grease(◇), and the shear stress for the grease calculated with Equation 2.15 when $\tau_y = 0$ (__), $\tau_y = \max$ ($\cdots$) and $\tau_y = \min$ (—). The parameters used and the R^2 are given in Table 3.9.

A comparison between lubricating greases is shown in Figure 3.26 .

As demonstrated in Section 2.10.3.1, grease viscosity at high shear rates was set equal to the bleed-oil ($\eta_\infty = \eta_{\text{bleed-oil}}$), instead of the usual assumption where $\eta_\infty = \eta_{\text{base-oil}}$, due to the evidence observed in the film thickness measurements (see Section 4.4).

In fact, when comparing the PPAO grease flow curves obtained considering $\eta_\infty = \eta_{\text{base oil}}$ (—) and $\eta_\infty = \eta_{\text{bleed-oil}}$ (—) with the grease measurements (◇), one can see that the shear stress calculated using $\eta_\infty = \eta_{\text{bleed-oil}}$ approaches the measured values at high shear rates in a more realistic way than the shear stress calculated using $\eta_\infty = \eta_{\text{base oil}}$, as shown in Figure 3.27. Furthermore, correlation factor R^2, although not very significant, is slightly higher when using the bleed-oil viscosity (R^2 =0,99) instead of the base oil viscosity (R^2 =0,97).

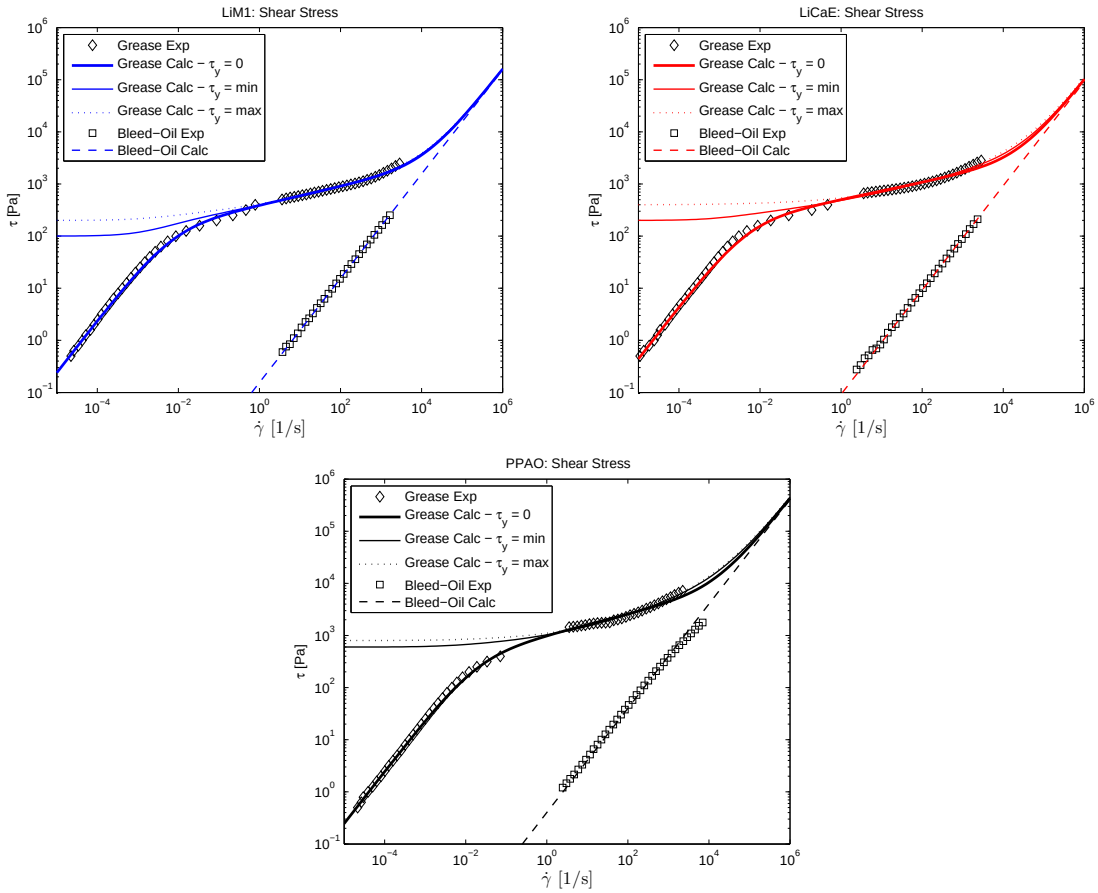

Figure 3.25.: Grease shear stress versus shear rate: Comparison between experimental and calculated values at 40 °C .

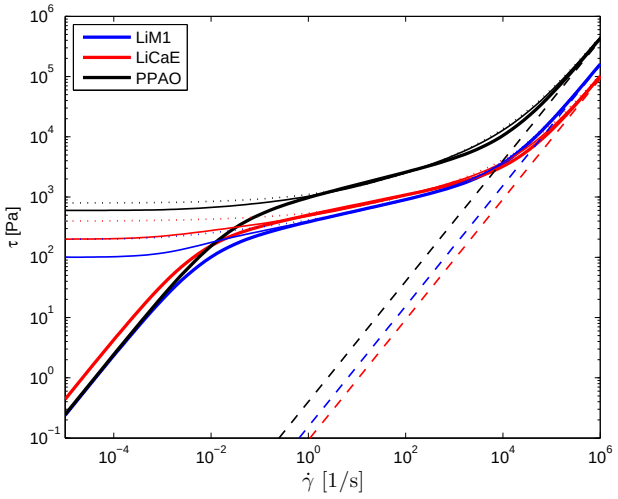

Figure 3.26.: Shear stress versus shear rate: Comparison between experimental and calculated values at 40 °C .

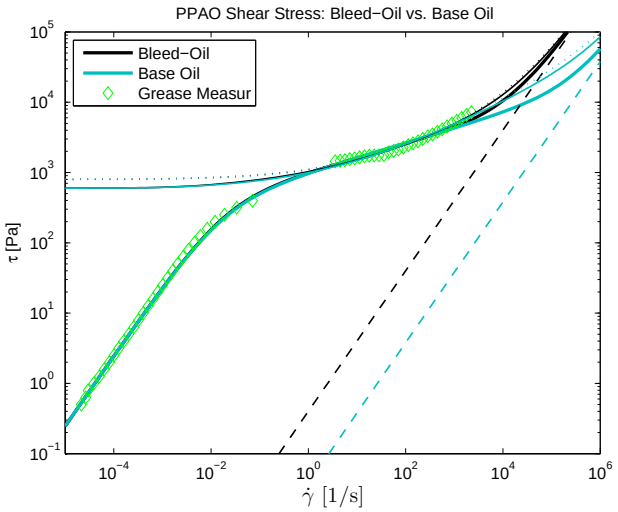

Figure 3.27.: Shear stress versus shear rate: Comparison between PPAO base oil and bleed-oil at 40 °C .

Table 3.9.: Inputs and calculated rheological parameters of lubricating greases at 40 °C . Obtained by fitting between the shear stress measurements (Figure 3.25) and Equation 3.7.

	LiM1	LiCaE	PPAO	Unit
		when $\tau_y = 0$		
K	146.17	198.40	61.77	Pa.s^m
m	0.8235	0.8374	0.7850	-
R^2	0.99	0.97	0.97	-
		when τ_y =min		
K	265.84	758.96	369.34	Pa.s^m
m	0.7875	0.7607	0.6826	-
R^2	0.99	0.98	0.99	-
		when τ_y =max		
K	518.58	4900	963.18	Pa.s^m
m	0.7528	0.6760	0.6375	-
R^2	0.99	0.98	0.99	-

3.9. Other properties

Grease, base oil and bleed-oil density were measured by weighting a 5 cm^3 of a sample at ambient temperature (21.1 °C). Three different syringes were filled with the lubricant sample and weighed three times each. The averages of the 9 values calculated ($\rho = m / V$) are presented in Table 3.10. The maximum error for the measurements was 2 %. The density values of the base oil were in agreement with the ones provided by the manufacturer. Density measurements were used to calculate the kinematic viscosity.

The refractive index of the lubricants was measured with an Abbot refractometer at ambient temperature. Such measurements were used as input for film thickness measurements.

All the measured lubricant properties presented in this Chapter are summarized in Table 3.11.

Table 3.10.: Density and refractive index of the lubricating greases and of their corresponding base oils and bleed oils.

Designation	***LiM1***	***LiCaE***	***PPAO***
	Grease properties		
Density [g/cm^3]	0,909	0,919	0,886
Refractive Index at 25 °C	1,4948	1,4744	1,4639
	Bleed oil properties		
Density [g/cm^3]	0,909	0,919	0,843
Refractive Index at 25 °C	1,4948	1,4744	1,4639
	Base oil properties		
Density [g/cm^3]	0,903	0,952	0,828
Refractive Index at 25 °C	1,4956	1,4562	1,4592

3.10. Discussion and conclusions on grease properties

Several properties can be evaluated when describing a lubricating grease, although to date, none of the most common characterisations provides parameters to predict the performance of grease lubricated contacts.

Many authors have incorporated the grease shear thinning effect through parameters K and m (or equivalents, depending on the rheological law used to describe the grease viscosity dependence of the shear rate) to predict grease film thickness under fully flooded lubrication [18, 20, 125, 126]. These models, however, are not widely accepted and their application does not correlate with the experimental results presented in Chapter 4. Besides, the belief that lubricating greases approach their base oils in terms of viscosity and shear stress at very high shear rates, leads many researchers to assume that the fully flooded film thickness of a grease can be simply calculated from the oil film thickness equations on the assumption that the grease viscosity is equal to the base oil viscosity [17].

A number of film thickness measurements performed with greases and their base oils under fully flooded lubrication, however, have showed that this does not happen [19, 127, 128].

This shows that different approaches should be used to characterize lubricating greases when one aims to define the grease properties related to their performance in an elastohydrodynamic contact.

In this Chapter, aside from the grease analysis through FTIR, XRF, SEM, oil bleed

rate, rheometry, thickener/oil ratio, which provided a significant amount of information that may be related to the grease mechanisms of lubrication, it was performed an analysis of the bleed-oil properties since over the years many researchers have suggested that the oil released from the grease is its major lubrication mechanism. Furthermore, although grease rheology has been widely studied, in fact there is no direct relationship between the low pressure / low shear rate rheometry (1 atm $\approx$ 0,1 MPa / $\dot{\gamma} < 10^5$ s^{-1}) of NLGI-grade 2 lubricating greases and their tribological performance (traction behaviour and film thickness) that is well known and widely accepted.

Delgado *et al.* [16] for example, compared 14 lubricating greases with exactly the same formulation (additive-free, 14 wt % lithium thickener and naphthenic base oil) but different manufacturing process conditions, in terms of their rheological, tribological and mechanical behaviour. The variants of the manufacturing process were rotational speed, maximum temperature, cooling profile and homogenisation time, speed and temperature. Of the 14 manufactured greases, 6 ended up with a NLGI class-2 consistency. Even with the same NLGI class and constituents, the rheological parameters measured showed a very significant difference between their maximum and minimum values:

- 3,6 times of strain, at $\delta = 1$;
- 1,45 times the storage modulus G' in the LVE region;
- 1,7 times the phase angle $tan(\delta)$ in the LVE region;
- 1,25 times the power law consistency index K;
- 2,2 times the power law flow index n;
- 1,25 times the apparent viscosity η, at shear rate of 100 s^{-1}.

For the same 6 greases, Delgado also measured the traction values using a tribometer (ball-on-disc device) under fully flooded conditions. Despite the major differences observed in the rheological parameters, maximum differences in the traction values measurements were below 4.5 %. This indicates that attempts to correlate grease composition with its rheological behaviour can lead to wrong assumptions when the manufacturing process is not the same. It also shows that the rheological parameters obtained under low pressure and low shear rate conditions do not significantly affect the tribological behaviour of lubricating greases under fully flooded conditions, although they may be significant after the bleeding stage, mainly as regards the replenishment and sealing mechanisms [3], as well as grease/bearing life [10, 129].

Table 3.11.: Summary of the physicochemical properties of lubricating greases and their constituents.

Designation	***Symbol***	***unit***	***LiM1***	***LiCaE***	***PPAO***
Grease constituents					
Base oil	-	-	Mineral	Ester	PAO
Thickener	-	-	Li	Li & Ca	PP
Co-thickener	-	-	-	-	Elastomer
Phosphorus	P	wt % $\times 10^{-3}$	120	37	6
Sulphur	S	wt % $\times 10^{-3}$	1649	102	581
Zinc	Zn	wt % $\times 10^{-3}$	285	29	-
Bismuth	Bi	wt % $\times 10^{-3}$	-	-	717
Base oil properties					
Density at 21.1 °C	ρ	g/cm^3	0.903	0.952	0.828
Base oil viscosity at 40 °C	ν_{40}	mm$^2/s$	211.05	89.84	42.78
Base oil viscosity at 80 °C	ν_{80}	mm$^2/s$	34.49	25.11	12.36
Base oil viscosity at 100 °C	ν_{100}	mm$^2/s$	18.47	15.73	7.93
Viscosity Index	VI	-	97	187	159
Piezoviscosity coefficient at 40 °C	α_{40}	GPa^{-1}	28.52	16.46	20.43
Piezoviscosity coefficient at 80 °C	α_{80}	GPa^{-1}	23.71	12.23	11.53
Bleed oil properties					
Density at 21.1 °C	ρ	g/cm^3	0.909	0.919	0.843
Bleed-oil viscosity at 40 °C	ν_{40}	mm^2/s	186.20	107.79	529.80
Bleed-oil viscosity at 80 °C	ν_{80}	mm^2/s	30.26	26.22	140.67
Bleed-oil viscosity at 100 °C	ν_{100}	mm^2/s	16.25	15.76	84.28
Viscosity Index	VI	-	90	156	246
Piezoviscosity coefficient at 40 °C	α_{40}	GPa^{-1}	43.27	28.39	25.81
Piezoviscosity coefficient at 80 °C	α_{80}	GPa^{-1}	36.28	20.20	11.76

Designation	***Symbol***	***unit***	***LiM1***	***LiCaE***	***PPAO***
Grease general properties					
Biodegradability OECD301F / SS155470 class B	-	%	-	> 60	-
Toxicity - OECD 202	-	%	-	> 45	-
NLGI Number (DIN 518181)	-	-	2	2	2
Dropping point	-	°C	185	>180	>140
Operating temperature	T_{op}	°C	-20 / +130	-30 / +120	-35 / +120
Oil Content	Oil %	% wt	86,7 ± 0.5	78.04 ± 1	84.32 ± 0.5
Thickener content	Thick %	% wt	16.6 ± 0.1	22.12 ± 0.2	15.32 ± 0.7
Grease flow properties at 40 °C					
Yield stress	τ_y	Pa	100-200	200-400	600-800
Consistence index with $\tau_y = 0$	K	Pa.s^n	146.17	198.40	61.77
Consistence index with $\tau_y = min$	K	Pa.s^n	265.84	758.96	369.34
Consistence index with $\tau_y = max$	K	Pa.s^n	518.58	4900	963.18
Flow index with $\tau_y = 0$	m	-	0.824	0.837	0.785
Flow index with $\tau_y = \min$	m	-	0.788	0.761	0.683
Flow index with $\tau_y = \max$	m	-	0.753	0.676	0.638
Viscosity zero	η_0	Pa.s	25062	44364	24675
Viscosity inf	η_∞	Pa.s	0.1558	0.096	0.4317
Grease oscilatory properties at 40 °C					
Storage modulus at LVE	G'	Pa	23690	44893	24957
Loss Modulus at LVE	G''	Pa	2778	5895	4394
Complex Modulus at LVE	$G*$	Pa	23852	45278	25341
Storage and Loss moduli at τ_{co}	G', G''	Pa	660	1460	530
Complex Modulus at τ_{co}	$G*$	Pa	933	2065	750
Oscillatory Stress	τ_{co}	Pa	450	560	800

4. Lubricant film thickness in a grease and oil lubricated contact

4.1. Introduction

The accurate prediction of EHL film thickness, under actual operating conditions and for a wide variety of lubricants, is extremely important to ensure complete separation of the mating surfaces, because it leads to an increase of energy efficiency and useful life service of the mechanical components.

Over the past fifty years, both experimental and numerical tools have been significantly improved to predict film thickness and many researchers have presented film thickness formulas based on the regression of their numerical results. Katyal and Kumar [130] summarized 15 central film thickness formulas for point contacts, developed from 1965 to 2000. All of them work with some accuracy for Newtonian fluids (that remain Newtonian within the inlet zone) within a certain range of pressure, entrainment speed and slide-to-roll ratio. More improvements have been achieved over the past decades in order to add shear thinning, viscous heating and thixotropy (shear degradation) phenomena to the film thickness equations [130–136]. Such phenomena are seen in some lubricating greases and in a new generation of lubricating oils with high polymer contents and other blends.

In general, these are film thickness formulas derived from solving Equations 4.1 to 4.5 simultaneously or iteratively, with boundary conditions at atmospheric pressure in the inlet and an appropriate cavitation model to prevent large negative pressures in the exit region, or through experimental measurements. As one can see, Equations 4.3 and 4.4 are not explicit, because there are several equations that relate viscosity and density to pressure and temperature (and shear rate, thixotropy and shear degradation). Different film thickness results are obtained depending on the model chosen to describe the viscosity and density with the operating conditions (Equations 4.3 and 4.4)

$$\frac{\partial}{\partial x}\left\{\frac{\rho h^3}{\eta}\frac{\partial p}{\partial x}\right\}+\frac{\partial}{\partial y}\left\{\frac{\rho h^3}{\eta}\frac{\partial p}{\partial y}\right\}=12\left\{\frac{\partial\left(\rho U h\right)}{\partial x}+\frac{\partial\left(\rho U h\right)}{\partial y}+\frac{\partial\left(\rho h\right)}{\partial t}\right\}, \tag{4.1}$$

$$w\left(x,y\right)=\frac{1}{2\pi E'}\int\int_{A}\frac{p(x',y')}{r}dx'dy', \tag{4.2}$$

$$\eta=f(p,T), \tag{4.3}$$

$$\rho=f(p,T), \tag{4.4}$$

$$W=\int\int_{A}pdxdy, \tag{4.5}$$

In addition to the uncertainty regarding which pressure-viscosity relationship to use, determining the pressure-viscosity coefficient () is challenging and expensive, as described in Section 2.5.5.3. This situation, which leads many researchers to derive the α-value from EHL film thickness measurements in conjunction with an appropriate EHL film thickness equation, was shown to be accurate for Newntonian fluids [63]. Krupka [137], however, showed that α-values obtained with this technique depend on the contact geometry (ball diameter), and therefore the use of such an α-values to predict film thickness for different geometries may significantly over or under-estimate film thickness. The solution proposed by Krupka requires high pressure viscosity measurements.

At present, therefore, the main frontier of research in full film EHL modelling lies in characterizing the nature and properties of the lubricant films and on determining an accurate model of fluid rheology under the extreme conditions present in EHL contacts. Another challenge is predicting film thickness under starved conditions, since it is very difficult to accurately foresee how the lubricant replenishes the contact [138].

Film thickness measurements in grease lubricated contacts have been performed for more than 40 years [139]. Nowadays, thin film interferometry allows mapping of the film thickness with a 1nm resolution in a 1 to 800 nm [140]. This technique was used to study the base oil, bleed-oil and grease film formation for a broad range of operating conditions under fully flooded and starved lubrication. Figure 4.1 shows a schematic view of a contact operating under these conditions.

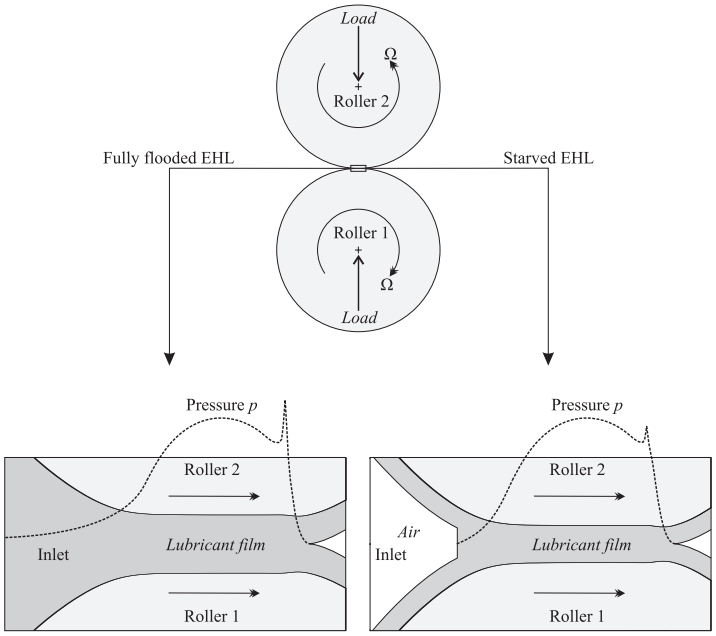

Figure 4.1.: Elasto-hidrodynamically lubricated contact operating at fully flooded (left) and starved conditions (right) [2]

4.2. Materials and methods

Film thickness measurements were performed with a WAM (Wedeven Associates Machine) ball-on-disc test apparatus equipped with optical interferometry. The glass disc had a chromium semi-reflecting coating on top of which a spacer layer of transparent silica was deposited ($CrSiO_3$).

Optical interferometry measurements of lubricant film thickness have already been described by several authors. Details of this technique have been reported elsewhere [140–142] and only a brief description will be given here.

The lubricated contact is formed by the reflective steel ball and the flat surface of the glass disc. The load is applied by moving the disc downwards towards the ball. The disc is mounted on a shaft driven by an electric motor. The steel ball is also controlled by an electric motor, making it possible to run the tests under rolling/sliding conditions. The glass disc is coated with a semi-reflecting chromium coating on top of which a spacer layer of transparent silica is deposited ($CrSiO_3$).

White light is shone through the glass disc into the contact. Part of the light is reflected back by the chromium layer, while the rest passes through the silica layer and any oil film present, before being reflected back by the steel ball. Since the light has travelled different distances, upon recombination the two beams interfere optically at wavelength values that depend on differences in the path, thus making

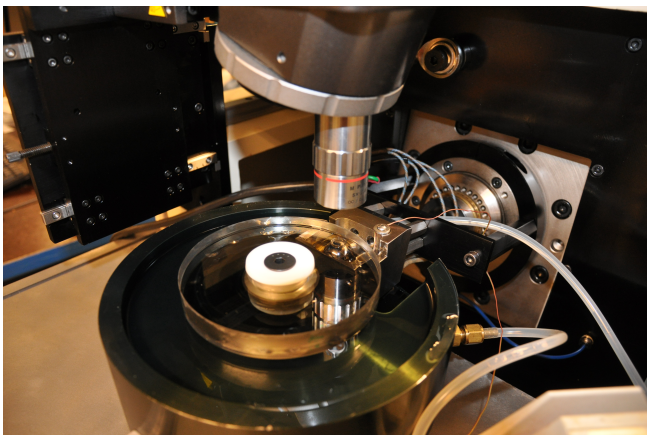

Figure 4.2.: View of the WAM 11A ball-on-disc test apparatus. Luleå University of Technology.

it possible to measure the thickness of the film. The colour interference image is detected by a CCD camera attached to a frame grabber so that images of the contact region can be taken.

The method used for translating the optical phase difference map into film thickness has been described by several authors, such as [140, 143, 144]. The method used here is the Lab-method described by Hartl *et al.* [144]. This technique can also be applied when a spacer layer is used. The spacer layer imaging method permits mapping of the film thickness with a 1 nm resolution at a 1 nm to 800 nm range. This technique is useful for grease film thickness measurements since the starved conditions are quickly reached and film thickness values are in general lower than 80 nm under these conditions. With white light and without spacer layer discs it is very difficult to measure film thicknesses below 80 nm.

4.2.1. Test Specimens

The standard ball specimen has a 13/16" (20,637 mm) diameter and is made from AISI 52100 bearing steel. The roughness of the balls was measured with a Wyko NT1100 optical profiling system from Veeco. Measurements were done using 10× magnification and 0,5× field of view (FOV).

The discs were made from glass that supports a maximum Hertz pressure of approximately 0.6 GPa. The silica spacer layer has a refractive index of 1.4785 according to the manufacturer.

The ball and disc properties are presented in Table 4.1 and the properties of the lubricants are presented in Table 3.11.

Table 4.1.: Ball and disc data.

	Ball	Disc
Elastic Modulus - E [GPa]	210	64
Poison Coefficient - ν [-]	0.29	0.2
Radius - R [mm]	10.3185	50
Surface roughness - Ra [nm]	20	≈ 5
Spacer layer thickness - [nm]	-	≈ 160
Spacer layer refractive index - [-]	-	≈ 1.4785

4.2.2. Test procedures

A set of lubricant film thickness measurements was carried out under fully flooded lubrication for all lubricating greases and their base oils and bleed-oils.

To ensure that starvation does not occur, a scraper was used to re-distribute the grease back to the rolling track and generate fully-flooded lubrication. Thus, the inlet lubricant supply, which has a large influence on film formation, was the same for greases, base oils and bleed-oils. The load applied was 25.71 N, which corresponds to a maximum Hertz pressure of $P_0 = 0{,}5$ GPa. Three operating temperatures were used: 40, 60 and 80 °C . The tests were carried out with a 3 % slide-to-roll ratio (SRR), in pure rolling conditions. The results were very similar; only the values under pure rolling condition are presented here. SRR is defined by

$$SRR[\%] = 2 \times \frac{(U_{disc} - U_{ball})}{(U_{disc} + U_{ball})} \times 100 \tag{4.6}$$

The entrainment speed range was different for each lubricant. The lowest entrainment speed was selected so that a film thickness not lower than 100 nm was measured, thus ensuring that ball-disc contact does not occur. The highest entrainment speed was limited by two factors, the maximum measurement range of the optical device (around 800 nm) and the volume of lubricant available. In the case of the tests performed with bleed-oil, the oil amount available was not enough to keep the oil reservoir filled during the whole test. Therefore, low entrainment speeds were used to avoid emptying the oil reservoir.

In the case of the tests with greases, the operating temperature was maintained by enclosing the ball-on-disc device with a plastic chamber and blowing hot air into this chamber. To ensure a homogeneous temperature (on the ball, disc, lubricant

and chamber) three thermocouples were strategically positioned inside the chamber and the hot air was applied during at least 40 minutes before each measurement. The largest measured temperature deviation from the target was ± 1,5 °C during the 80 °C tests.

AA different procedure was used for the oils since a different arrangement had to be used. In this case the lubricant was heated in two different containers connected by a tube. The small container, where the ball is partially submerged (up to the centre of the ball), was filled with around 10 ml of lubricant. The larger one, which supplies the small one through a pump, stored up to 200 ml. The base oil tests carried out with this configuration presented a slightly higher temperature deviation of ± 2,0 °C during the 80 °C test. In the case of the bleed-oils, the temperature deviation was higher since there was not enough lubricant to fill both containers. In this case, the highest temperature fluctuation was ± 2,9 °C during the 80 °C tests.

The temperature oscillations were considered when calculating all the parameters shown in Sections 4.3.1 to 4.3.5. For each operating temperature, the film thickness was measured from the lowest to the highest entrainment speed, with increments of 0.05 m/s and then from the highest to the lowest entrainment speed. This procedure was repeated for each temperature and lubricant, for a total of at least four measurements for each entrainment speed. The scatter observed in the film thickness measurements is mainly due to the temperature variations and the low stability of the machine at low entrainment speeds $<$ 0,1 m/s and low load ($P \approx$ 25,71 N).

A different set of grease film thickness measurements was performed a year later under fully flooded and starved conditions in order to study grease behaviour under very low entrainment speeds and the influence of grease properties on starved film formation. These measurements were carried out in a WAM 6A, with a different ball diameter ($2R = 19,25$ mm) and at 40 °C only. The contact pressure was kept $P_0 =$ 0,5 GPa. The fully flooded tests followed the previous procedure, while the starved tests were performed without the scraper during t = 30 min at constant a speed of $U_e = 0,1$ m/s.

4.3. Results of fully flooded film thickness measurements

4.3.1. Base oil film thickness - Background

Film thickness measurements and predictions for the base oils with Newtonian behaviour are accurate and understood, since, in general, base oils do not exhibit

significant shear thinning, shear degradation and thixotropy behaviour under typical EHL conditions.

There are several equations that predict the film thickness for base oils [145–150]. The main differences between them are the rheological models relating the viscosity and density with pressure and temperature.

Van Leeuwen [63] recently compared accurate film thickness measurements with the values predicted by eleven (11) different equations proposed in the literature for two different base oils. The pressure-viscosity coefficient (α) of one of the oils was known in advance. Van Leeuwen showed that the central film thickness equations for point contacts proposed by Chittenden *et al.* [148] and Hamrock *et al.* [149] presented a correlation factor $R^2 > 97$ % for the lubricant with a known $\alpha-$value. Consequently, the pressure-viscosity coefficient of other base oils should be calculated with these equations when similar operating conditions are used. As discussed before, this appears to be the best way to determine $\alpha-$value when high pressure viscosity measurements are not available.

The equations presented by Chittenden *et al.* and Hamrock *et al.* use the Roelands equation [53] to describe viscosity dependence on pressure and on temperature and take into account that the fluid is compressible, according to Dowson and Higginson [151].

The film thickness equation proposed by Hamrock *et al.* is given by Equation 4.7 [149]. Thermal correction ϕ_T was considered according to Gupta *et al.* [152], as shown in Equation 4.8. The use of these equations and film thickness measurements determine the pressure-viscosity coefficient (α_{film}) that gives the best R^2 fit with the measured results. With α_{film}, film thickness can be estimated on the basis of the data provided in Table 3.11 and Equation 4.7.

$$H_{oc} = \phi_T \times 1,345 \times R_x \times U^{0,67} \times G^{0,53} \times W^{-0,067} \times C_0 \tag{4.7}$$

$$\begin{aligned} \phi_T &= \frac{1 - 13,2 \cdot (p_0/E) \cdot L^{0,42}}{1 + 0,213\,(1 + 2,23 \cdot SRR^{0,83}) \cdot L^{0,64}} \\ L &= \frac{-\partial\eta}{\partial T} \cdot \frac{Ue^2}{K_f} \end{aligned} \tag{4.8}$$

4.3.2. Base oil film thickness - Results

Figure 4.3 shows the film thickness measurements versus the entrainment entrainment speed for all base oils at $\approx$ 40, 60 and 80 °C . Predictions of the film thickness considering the measured temperatures are also presented in the figure. In all

cases, film thickness measurements increased with the entrainment speed at a rate of $\approx U^{0,67}$, as predicted by most of the film thickness equations. LiM1 base oil had the highest film thickness, PPAO base oil the lowest one, while LiCaE appeared between the other two.

The pressure-viscosity coefficients, determined on the basis on a best $\mathbf{R}^2$ fit between measurements and predictions, are shown in 4.2 for each operating temperature.

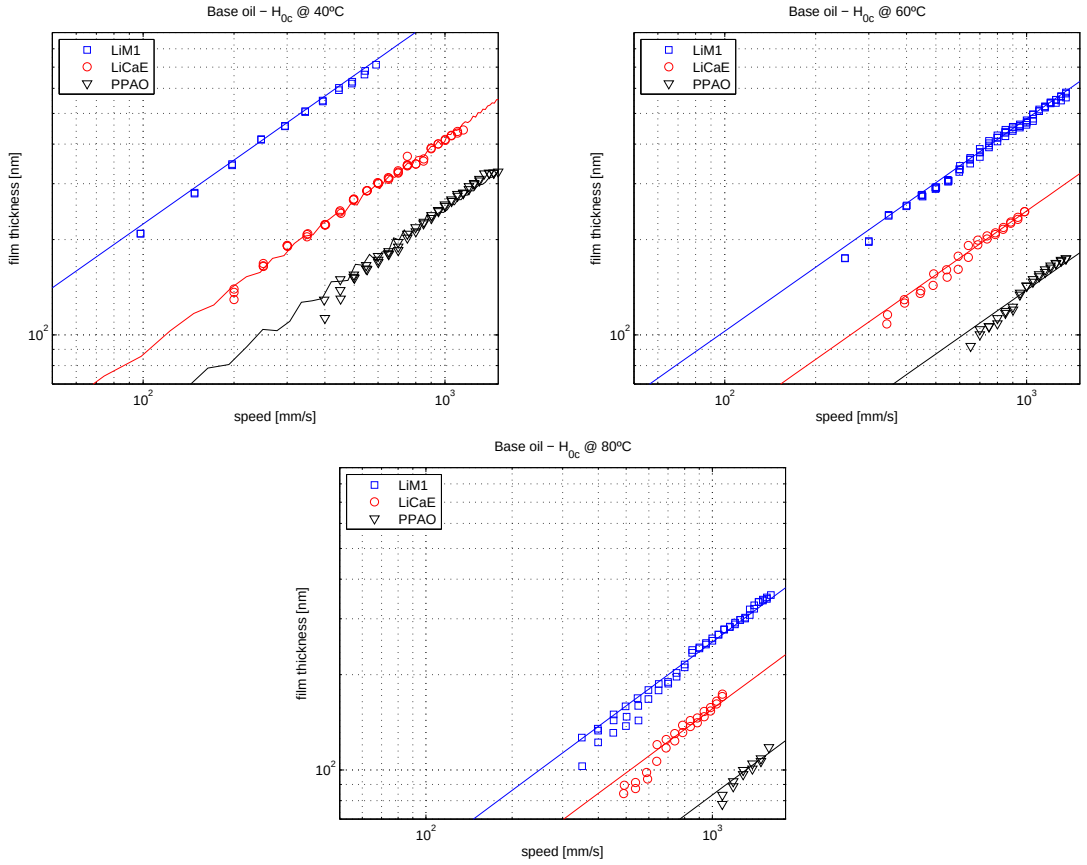

Figure 4.3.: Film thickness versus entrainment speed: Experimental and predicted values at 40, 60 and 80 °C . Base oils.

Table 4.2.: Pressure-viscosity coefficients of the base oils at ≈ 40, 60 and 80 °C .

α_{film}·[GPa^{-1}]	LiM1	LiCaE	PPAO
≈ 40 °C	28,9	16,4	20,0
≈ 60 °C	25,6	14,4	15,2
≈ 80 °C	23,9	12,1	11,4

4.3.3. Bleed-oil film thickness - Background

As described in Section 3.4, significant attention has been paid to "controlling / understanding" the oil bleed rate. To the best of the authors' knowledge, however, few scientific studies have been published concerning the bleed-oil properties and their influence on tribological behaviour in EHD lubrication [3, 4, 13, 25]. As described earlier, the reason for this is unknown as many researchers claim that in grease lubricated contacts, the oil released from the grease is the dominant mechanism of lubrication in the early stages of grease life [19, 91, 93, 94].

As shown in Sections 3.7 and 3.8.1 bleed-oil composition and properties are different from base oil properties. Apart from their differences, LiM1 and LiCaE base oils and bleed-oils showed a Newtonian behaviour in the rheological measurements (see Figure 3.14) and an increase of film thickness with a $\approx U^{0,67}$ entrainment speed, suggesting a Newtonian behaviour. Consequently, the same methodology applied to predict the base oil film thickness (Section 4.3.1) was used to predict the LiM1 and LiCaE bleed-oil film thickness.

PPAO bleed-oil showed a non-Newtonian behaviour (see Figure 3.14) and could be predicted with the same equations developed for Newtonian fluids. Although these equations were found to be quite accurate for Newtonian lubricants, they largely overestimate the film thickness for shear-thinning lubricants [130].

PPAO bleed-oil was therefore modelled according to the equation proposed by Katyal and Kumar [130]. This model predicts the central film thickness for shear thinning lubricants in EHL point contacts under pure rolling (see Equation 4.9). The model is a numerical regression based on a full numerical simulation where the Reynolds equation is solved with the Carreau viscosity model and Barus' exponential pressure-viscosity relation (see Equation 2.6). The thermal correction factor ϕ_T was also considered (see Equation 4.8)

$$\begin{aligned} H_{ock} &= \phi_T \times 1,098538 \cdot R_{xk} \times U_k^{0,652} \times G_k^{0,557} \times W_k^{-0,0415} \times \bar{R} \\ \bar{R} &= \left(1 + 1,32528 \times \frac{U_k^{0,69} \times W_k^{0,264}}{G_k^{0,77} \times G_{cr}^{1,92}/E_k^*}\right)^{-1,2(1-n)^2} \end{aligned} \tag{4.9}$$

where $\bar{R}$ is the shear thinning factor, which depends on dimensionless parameters U_k, W_k, G_k and on the Carreau viscosity model, given by Equation 4.10,

$$\eta = \eta_\infty + (\eta_0 - \eta_\infty) \times \left[1 + \left(\frac{\eta_0 \dot{\gamma}}{G_{cr}}\right)^2\right]^{(n-1)/2} \tag{4.10}$$

where η_0 is the first Newtonian viscosity at low shear rates (considered bleed-oil viscosity at low shear rates) and η_∞ is the second Newtonian viscosity at high shear rates (considered zero). G_{cr} is the bleed-oil critical stress (reported previously as yield stress - τ_y) and n is the power-law index.

G_{cr} and n were calculated in order to obtain the best R^2 fitting with the viscosity measurements shown in Figure 4.4. Few attempts were made considering $\eta_\infty = \eta_{\text{BaseOil}}$ and calculating η_∞ in order to obtain the best R^2 fitting. These different assumptions used in an attempt to define η_∞ lead to slightly different values of G_{cr} and n, but barely alter the R^2 correlation factor. Since, the true value of η_∞ is unknown and Katyal and Kumar showed that η_∞ can be set as zero without prejudging the results, such an assumption was made.

Adjustable variables (G_{cr} and n) are shown in Table 4.3.

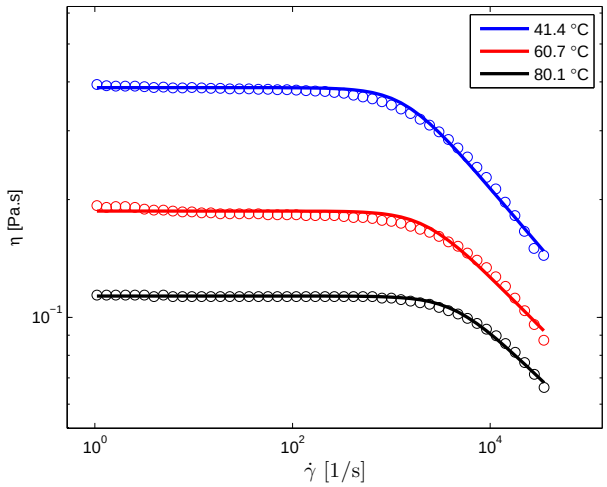

Figure 4.4.: Application of Carreau model to the PPAO bleed-oil viscosities measured at ≈ 40, 60 and 80 °C .

Table 4.3.: Bleed-oil parameters for the Carreau viscosity model at ≈ 40, 60 and 80 °C .

PPAO	G_{cr} [Pa]	n [-]
≈ 40 °C	569.6	0.699
≈ 60 °C	538.0	0.727
≈ 80 °C	500.3	0.752

4.3.4. Bleed-oil film thickness - Results

Figure 4.5 presents the film thickness measurements and predictions versus the entrainment speeds for all bleed-oils ≈ 40, 60 and 80 °C . In all cases, the film thickness measurements increased with the entrainment speed at a rate of $\approx U^{0,67}$. The bleed-oil film thickness followed the same trend observed with the base oil (LiM1 ⩾ LiCaE ⩾ PPAO), but with significantly different values. The coefficients of pressure-viscosity α_{film} were determined on the basis of the best R^2 fit between measurements and predictions, and are given in Table 4.4 for each operating temperature.

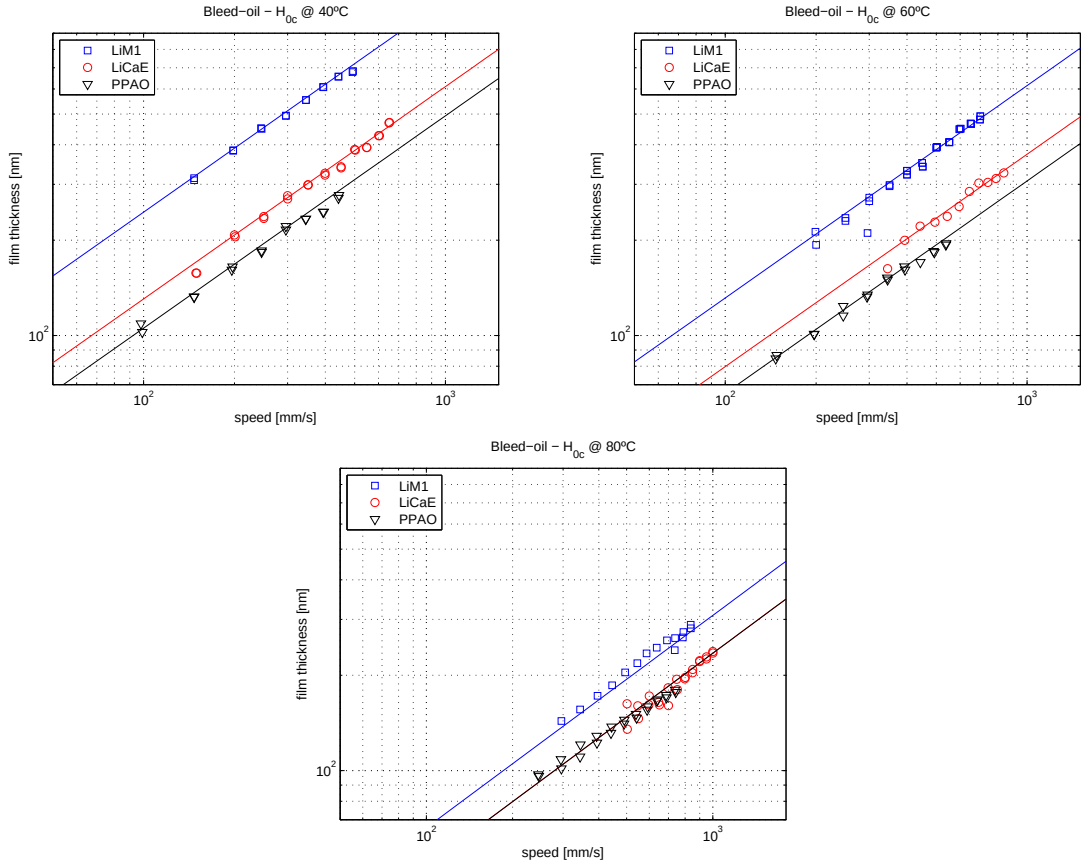

Figure 4.5.: Film thickness versus entrainment speed: Experimental and predicted values at 40, 60 and 80 °C . Bleed-oils.

Table 4.4.: Pressure-viscosity coefficients of the bleed-oils at ≈ 40, 60 and 80 °C .

α_{film}·[GPa^{-1}]	LiM1	LiCaE	PPAO
≈ 40 °C	43.5	27.8	24.4
≈ 60 °C	40.0	25.8	17.3
≈ 80 °C	36.8	20.3	12.8

4.3.5. Grease film thickness - Background

The EHL theory for rolling contacts is well established in the case of fully flooded, oil-lubricated contacts [138]. In the case of grease-lubricated contacts, however, this theory is far from complete. Many studies with lubricating greases suggest that:

- thickeners pass through rolling EHD contacts and hence contribute to EHD formation [127, 153]. Some thickeners seem to enter the contact easier then others [13];
- film thickness depends basically on the thickener structure and is thinner in the following order: aliphatic, aromatic and alicyclic greases when the same ether-type synthetic oil is used as base oil [154];
- polymer additives seem to pass through the contact whatever the composition of the initial grease [13, 155];
- thickener layers are also present on the contact surface at the end of full bearing tests and ball-on-disc tests [11, 99, 156];
- lubricating greases with the same formulations generate higher film thickness for higher base oil viscosities and thickener concentrations [19];
- the film thickness difference between a grease and its base oil depends on base oil viscosity, thickener type and concentration [19];
- the thickener of high shear stability greases is more able to survive inside the contact, thus contributing more to EHD film thickness than low shear stability greases [19];
- grease builds a higher film thickness than its base oil under fully flooded lubrication [127, 139, 154, 157];
- film thickness varies little in function of time due to mechanical work (shear degradation) [158];
- grease yield stress has a negligible effect on fully flooded EHL film thickness [159];
- thixotropic and poor convective cooling can significantly reduce film thickness [160].

It is important to note that not all of the above assumptions are widely accepted and that most of these studies were carried out over short periods of time and thus, represent only the earlier stages of grease lubrication.

Nowadays, it is understood that bulk grease fluid may indeed lubricate the contact during the initial phase of operation but that it will also act as a reservoir, releasing lubricant either by bleeding, shear, or shear-induced bleeding. The result is that the active lubricant will ultimately have a different rheology than bulk grease. Unfortunately, there is no consensus in the scientific literature regarding the rheological properties of the active lubricant.

Regarding EHL models, in the early 1970s Kauzlarich and Greenwood [159] had already developed a model for fully flooded grease lubricated line contacts, by assuming that grease is a semi-fluid with strong non-linear rheology (Herschel-Bulkley rheological model). A more appropriate rheological grease model was proposed by Bauer [68] and used by Dong and Qiang in 1988 [18] to model the film thickness of line contacts. The same rheological model was used by Bordenet *et al.* in 1990 [126] but this time, for point contacts. From these EHL models and considering a strong non-Newtonian rheology, it was found that at high shear rates, base oil viscosity is the most important parameter and yield stress does not have an impact on film thickness.

Many other researchers have developed simple models for film predictions in fully flooded grease lubricated contacts, as shown in Equations 4.11 [19], 4.12 [20] and 4.13 [161].

$$\Delta h = (1 + B\Phi)^{0,67} \tag{4.11}$$

$$\frac{h}{h_{oil}} = \left(\frac{K}{\eta_{bo}}\right)^{0,74} \tag{4.12}$$

$$h = h_R + h_{oil} \tag{4.13}$$

where Δh is the relative film increase of the grease in comparison with its base oil, B a constant taken as 2,5 from [162], Φ the volume fraction of soap (equivalent to soap concentration), h the film thickness of the grease (Figure 4.6), h_{oil} the film thickness of the base oil (Figure 4.3), K the Bingham grease consistency (obtained from Figure 3.25), η_{bo} the base oil viscosity (Table 3.11) and h_R the residual layer measured at the end of the test at zero speed (unknown). The h_R value used is the highest residual layer measured with lubricating grease found in the literature [163].

Table 4.5.: Comparison between film thickness calculated with Equations 4.11 to 4.13 and the measured values presented at Figure 4.6. Grease PPAO, U_e = 0,5 m/s.

	Param.	Values	Calc. h_{grease}/h_{oil}	Meas. h_{grease}/h_{oil}	Error [%]
	B	2.5			
Eq. 4.11	Φ	15.30 %	1.24	2.22	-44.14
	K	4.02 Pa.s			
Eq. 4.12	h_{oil}	167 nm	33.4	2.22	1404
	η_{bo}	0.035 Pa.s			
Eq. 4.13	h_R	80 nm	1.48	2.22	-33.3

These models were compared to the experimental results shown in Figure 4.6 but no agreement was found. Table 4.5 provides the input needed for solving Equations 4.11, 4.12 and 4.13. In the same table, the outputs of these equations were compared to the grease film thickness measurements in terms of h_{grease}/h_{oil}. The results measured were obtained with PPAO grease at $U_e = 0,5$ m/s.

4.3.6. Grease film thickness - Results

Figure 4.6 shows the film thickness measurements versus the entrainment speeds for all lubricating greases at 40, 60 and 80 °C . Again, it was observed that the typical film thickness increased with speed, suggesting a Newtonian behaviour in the inlet region [164]. Although the continuous lines are presented in Figure 4.6 only to emphasizes this trend ($h \propto U^{0,67}$), it is *NOT* a grease film thickness prediction. The film thickness values of lubricating greases were similar to the bleed-oil values and consequently, also followed the LiM1 $\geqslant$ LiCaE $\geqslant$ PPAO order.

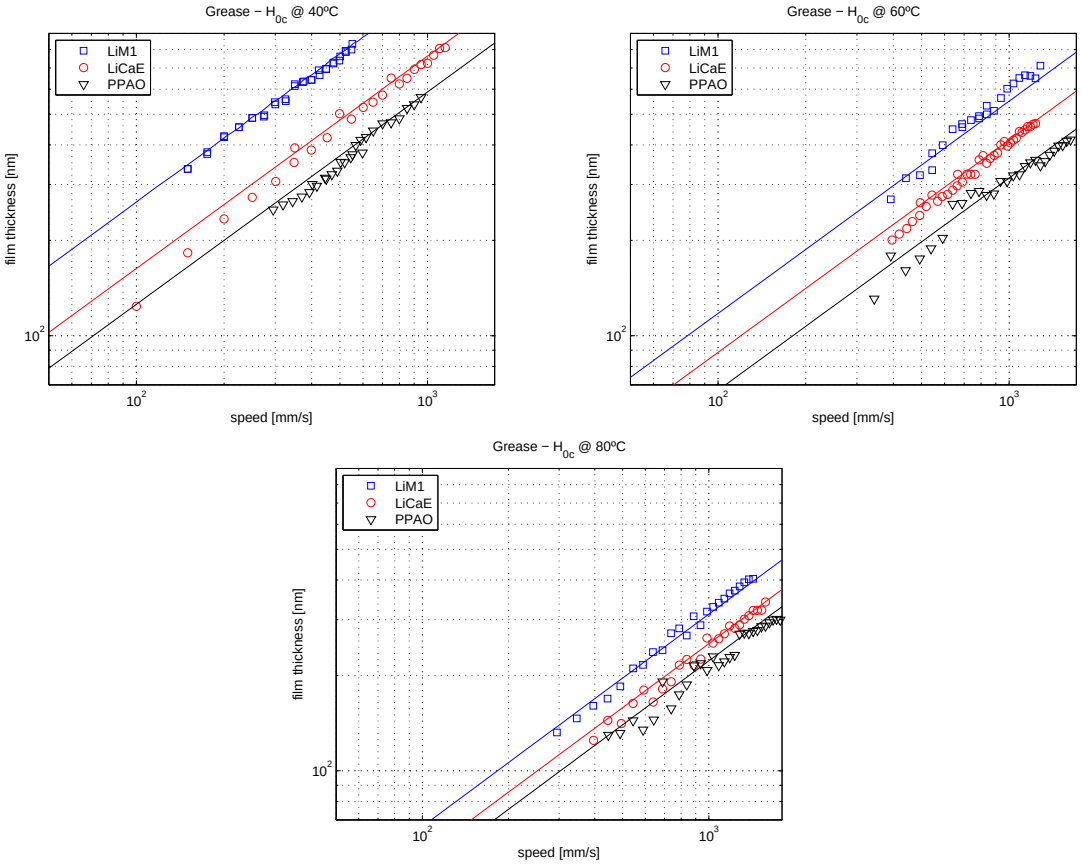

Figure 4.6.: Film thickness versus entrainment speed: Experimental values at 40, 60 and 80 °C . Greases.

4.4. Discussion on fully flooded film thickness results

An attempt to define the active lubricant in EHL contacts in fully flooded lubrication was performed by comparing the central film thickness of the lubricating greases to those of their base oils and bleed-oils at 40, 60 and 80 °C , as shown in Figures 4.7 to 4.9. The film thickness prediction of base oils and bleed-oils are also presented. These figures show that each grease and its bleed-oil generated a similar central film thickness, which is higher than the film thickness generated by the base oils.

The differences between base oils and bleed-oils (or greases and their base oils, since $h_{grease} \approx h_{bleed-oil}$) are specific to each lubricant. Such differences might be expressed by the relative film thickness increment Δh, as defined by

$$\Delta h\,[\%] = \frac{h_{bleed} - h_{base}}{h_{base}} \times 100 \tag{4.14}$$

Figure 4.10 gives the average values and deviations of the relative film thickness increment (Δh - Eq. 4.14) for each lubricant at 40, 60 and 80 °C . Δh is approximately constant for the whole range of entrainment speeds, although some deviations were noted due to a scattering of the film thickness measurements.

It was also observed that the relative film thickness increment (Δh) was very high in the case of PPAO (between 80 % and 180 %, depending on the temperature) and much lower in the case of LiM1 (between 10 % and 25 %). LiCaE Δh is between LiM1 and PPAO. Figure 4.10 also shows that all bleed-oils (and consequently all the lubricating greases) had a significantly higher capacity to build-up a lubricating film than the corresponding base oils, and their performance was even better at higher temperatures. This was true for all the operating conditions used.

Cann *et al.* [19] also studied the difference in central film thickness between greases and their base oils, and suggested that the relative film increment depends on the thickener type and its concentration, on the base oil viscosity and, above all, on the inlet lubricant supply. In the present work a temperature dependency was also evident, as shown in Figure 4.10. Δh increased with temperature, despite the fact that LiCaE presented slightly lower Δh at 60 °C than at 40 °C . This is likely related to the viscosity improver additives, which are present in the lubricating greases and bleed-oils, but absent in the base oils.

Cann *et al.* [19] also observed Δh from 2.5 to 24.8 % at 20 °C for Lithium greases formulated with conventionally refined base stocks ($\nu = 309,8$ cSt at 20 °C) and that Δh increased up to 88 % when Calcium was blended with the Lithium, although thickener concentration, base oil type and viscosity were kept constant.

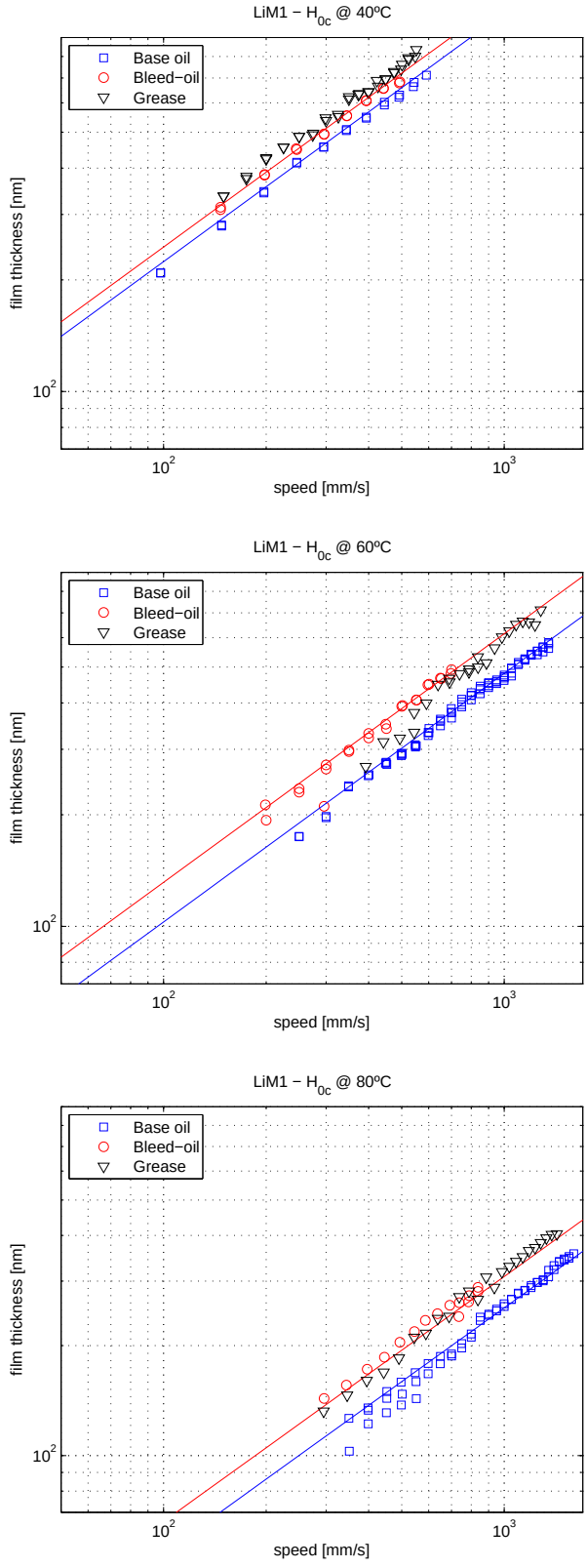

Figure 4.7.: Film thickness versus entrainment speed: Comparison between grease, base oil and bleed-oil at 40, 60 and 80 °C . LiM1.

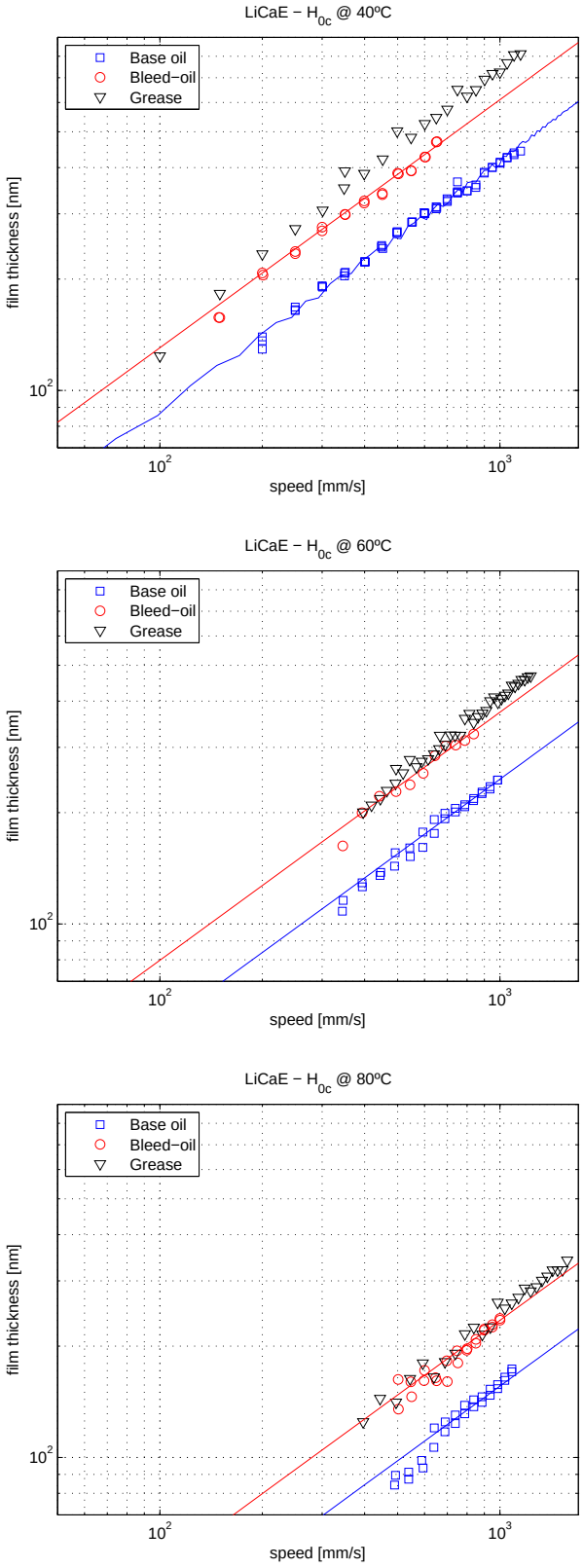

Figure 4.8.: Film thickness versus entrainment speed: Comparison between grease, base oil and bleed-oil at 40, 60 and 80 °C . LiCaE.

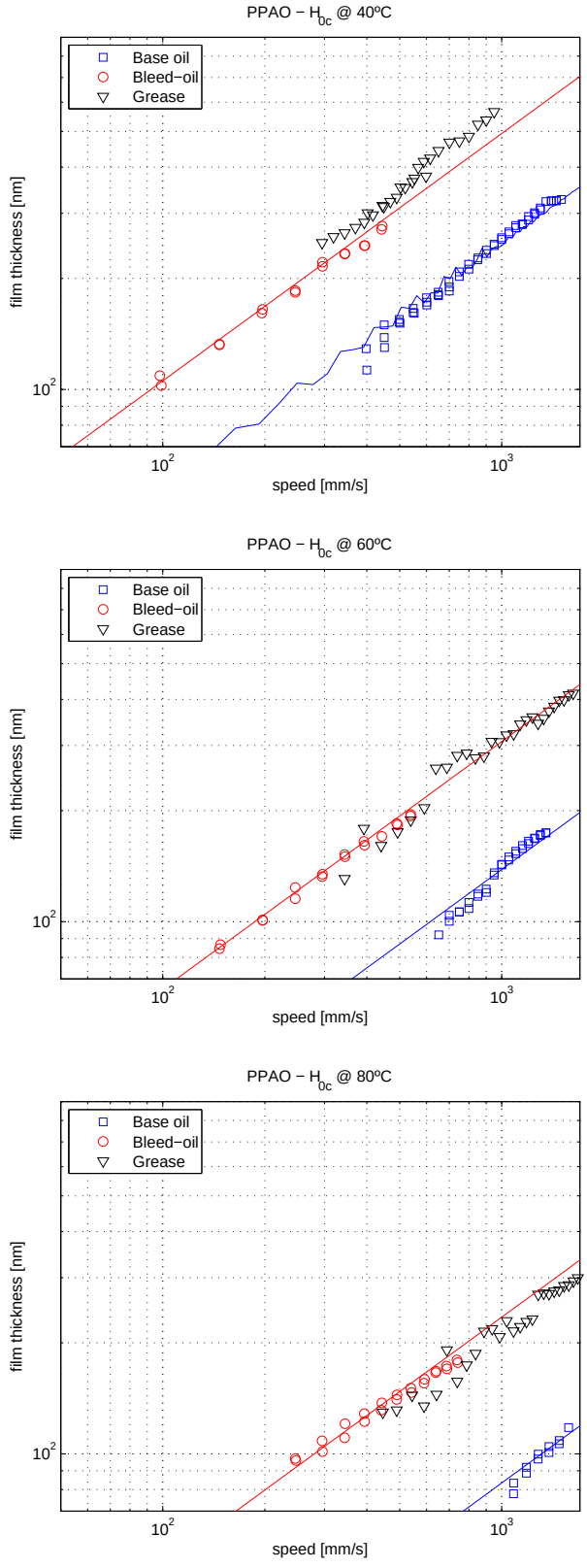

Figure 4.9.: Film thickness versus entrainment speed: Comparison between grease, base oil and bleed-oil at 40, 60 and 80 °C . PPAO.

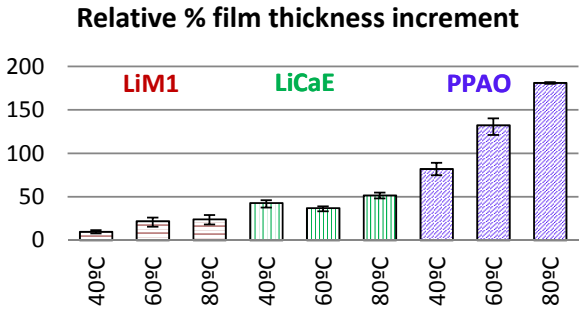

Figure 4.10.: $\Delta h\,[\%]$ – Relative film thickness increment between base and bleed-oils.

In spite of the scattering of the film thickness measurements that was observed, the use of the bleed-oil properties provided a better correlation with the grease measurements as compared to the base oil; therefore, the bleed-oil might be considered the active lubricant in EHL contacts under fully flooded lubrication.

Other evidence of bleed-oil importance in film formation was shown by Couronné *et al.* [3] and Per-Orlof Larsson [4], both of whom obtained bleed-oil through static bleed tests.

Couronné also showed film thickness measurements with base oil, bleed-oil and greases in a ball-on-disc machine and, indeed, similar film thickness values between greases and their bleed-oils were measured. Couronné, however, directed the conclusions of her work to the grease lubricating phase, and the bleed-oil performance was not highlighted (see Figure 4.11, from [3]).

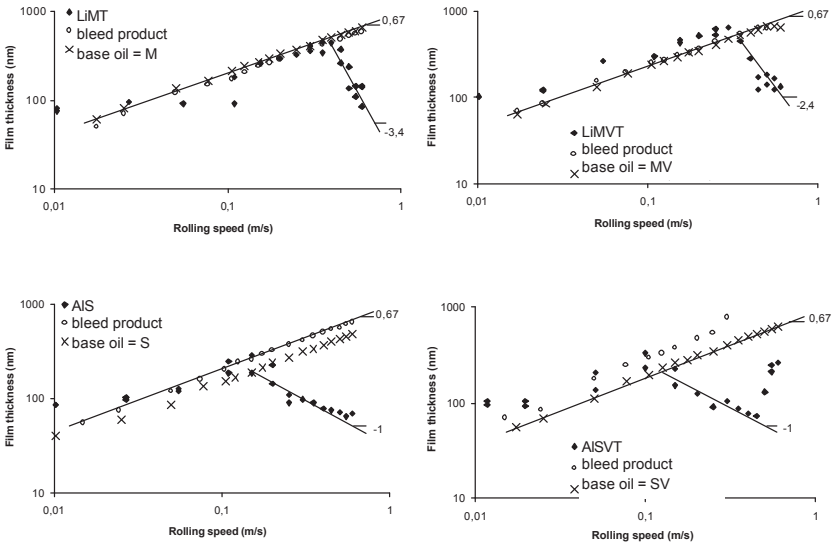

Figure 4.11.: Film thickness results for greases, base oils and bleed products [3].

Per-Orlof Larsson measured the lift-off-speed[1] and breakthrough-speed[2] of four deep groove ball bearings in an SKF R2F test rig lubricated with base oil, bleed-oil and greases. Again, no correlation between base oil and grease was found in the lift-off-speed and breakthrough-speed, however the bleed-oils showed almost exactly the same results as the greases, as their differences were within the margin of errors for experiments (see Figure 4.12, from [4]).

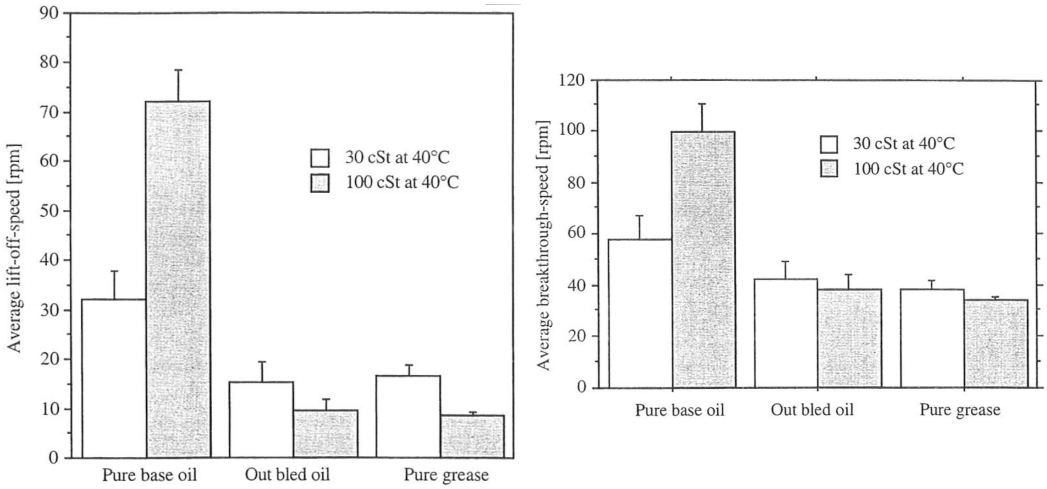

Figure 4.12.: Avarage lift-off speed (left) and break-through-speed (right) for pure base oil, bleed-oil and grease [4].

[1]Speed at which a transition from boundary to mixed lubrication is observed when the speed increases from zero up to a certain value.

[2]Speed at which a transition from full film to mixed lubrication is observed when the speed decreases towards zero.

4.5. Results and discussion on grease thin-films under fully flooded lubrication

4.5.1. Grease thin-films - Background

Grease film thickness behaviour (e.g., $h \propto U^{0,67}$) mostly differs from that of its base oil at very thin films and low speeds. In this case, base oils (not blended or fully additivated) have the same $h \propto U^{0,67}$ decrease rate when speed goes towards zero until the moment when the hydrodynamic effect is not sufficient and $h = 0$. In fact, it has been shown that highly refined, non-polar base fluids exhibit classical hydrodynamic behaviours down to less than 2 nm film thickness [165]. Lubricating greases on the other hand, shows a decrease rate that goes from $\approx U^{0,67}$ at high speeds, passes by at a minimum rate and increase again at rates up to $\approx U^{-1,4}$ when speed goes towards zero (calculated from the results presented by Cann [166]). In this last region measurements fluctuate wildly, standard deviation is very high and increasing film thickness with decreasing speeds is not always linear (in a log-log plot). Depending on the lubricant, operating conditions and surface properties, film thickness dependence on speed can vary significantly.

Such phenomena are explained by considering that the film thickness is composed by the sum of a static and a dynamic film component [161, 167]. The static film is a layer that is adsorbed by the metal surfaces whether they move or not, and the dynamic film is the one predicted by the EHL equations (oil film). In the case of the lubricating greases tested, increasing film thickness with decreasing speed indicates that the static film depends on time and/or speed.

Spikes observed the same behaviour shown in Figure 4.13 for several different additivated fluids [168], where high films that appear to be highly viscous are seen at low speeds, although these level out as speed increases and make a negligible contribution to film thickness at higher speeds. Spikes also verified that when the entrainment speed is rapidly reduced from a high value, the boundary film starts to develop again, but at lower speeds, and builds back to its original, low-speed level over some minutes. When the motion is halted, most (but not all) of the developed film remains to separate the stationary contact.

Cann [164] also observed these effects in grease lubricated rolling contacts and justified it by the passage of lumps of thickener through the contact. At low speeds, hence low shear rates and shear stresses, the largest lumps are more likely to survive and their effects are more obvious because of the thin films.

In this case, where the contribution of the "static" layer at low speeds does not

contribute (or makes a negligible contribution) to film thickness at higher speeds, a thin film with enhanced viscosity (due to additives-thickener/co-thickener-surface interaction) is believed to be the active lubricant in EHL contacts [168]. This permits a fluid film to be entrained at a lower speed than would otherwise be the case. It is known that adsorbing polymer solutions, blends of a higher viscosity polar component in a lower viscosity, less polar ones and organic friction modifiers behave in this way [168].

4.5.2. Grease thin-films - Results

The film thickness measurements presented in Figure 4.6 were again measured one year later for wider ranges of entrainment speed in order to compare fresh and degraded grease performance, as will be shown in Chapter 7. The measurements of the fresh greases showed really well grease behaviour when thin-films and low entrainment speeds occur, and these will be used here to illustrate the grease mechanisms of lubrication under these circumstances.

These film thickness measurements were carried out in a WAM 6A with a smaller diameter ($2R = 19{,}05$ mm) ball and a $P \approx 20$ N load. Contact pressure, temperature and operating procedures were the same as those described in Section 4.2.2.

Figure 4.13 shows the measured values (markers) and the predictions (continuous lines) over entrainment speed. Predicted values were calculated with the bleed-oil properties at 40 °C (η, α, G_{cr}, n - see Table 3.11) and Equation 4.7 in the case of LiM1 and LiCaE, and Equation 4.9 in the case of PPAO.

All the lubricating greases showed a minimum film thickness value over the entrainment speed. The speed value with which the film thickness changes its manner (U_{hmin}) depends on grease formulation. LiM1 changed the traditional Newtonian behaviour when $U_{hmin} \approx 0,7$ mm/s, LiCaE at $U_{hmin} \approx 1$ mm/s and PPAO at $U_{hmin} \approx 300$ mm/s. At speeds lower than U_{hmin} lubricating greases showed an increasing trend, with PPAO grease reaching values of $h_{oc} \approx 750$ nm.

The PPAO lubricating grease showed a better capacity for forming a thick film at low speeds, followed by the LiCaE and LiM1 (see Figure 4.13). This is most likely related to the thickener type and concentration since such behaviour was not as evident in the bleed-oils (see Figure 4.9 at 40 °C), where several additives, but no or hardly no thickener, were evidenced (see Figure 3.12). The adhesiveness of PPAO, despite its low polarity thickener, was highly improved by the elastomer[3].

[3]Information provided by the grease manufacturer.

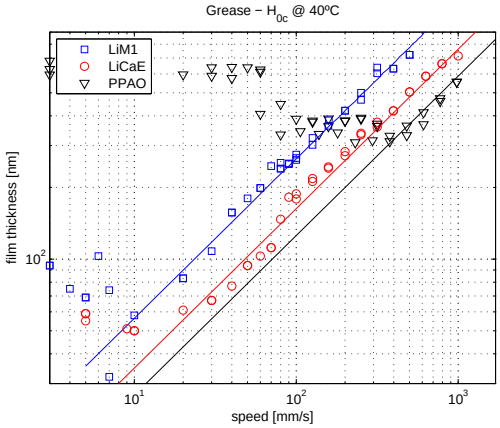

Figure 4.13.: Thin film thickness measurements versus entrainments speed at 40 °C and $P_0 = 0{,}5$ GPa. Greases.

4.6. Results and discussion on grease film thickness under starved lubrication

4.6.1. Grease film thickness under starved lubrication - Background

Starvation was visually observed using optical interferometry in the seventies [146, 169, 170]. One observation was that as starvation proceeds an oil-air meniscus forms in the inlet region and this moves towards the Hertzian contact circle as the severity condition increases (starved contact is illustrated in Figure 4.1). Film thickness reduction coefficient was thus derived by many researchers on the basis of the position of the inlet meniscus. Although this approach initially appeared promising, the meniscus position could only be observed in model tests and could not be used to predict film thickness in practical applications. Different models have therefore been proposed, namely the thin layer flow [158, 171, 172], a novel and very promising way to predict film thickness decay in starved EHL contacts. Unfortunately, this model has not yet been applied to a significant amount of lubricating greases.

Starved film thickness is often time dependent and its value is governed by competing lubricant supply and loss mechanisms. This balance is not constant in time and can present a chaotic behaviour, see Lugt, *et al.* [173]. The lubricant supply and loss mechanisms on rolling bearings depend on several mechanisms at the same time, as summarized by [2]:

- contact forces between the rolling elements and the raceway;

- contact forces between the rolling elements and the cage, see Damiens *et al.* [174];
- centrifugal forces, see Gershuni *et al.* [175] and van Zoelen, *et al.* [172];
- gravity: Horizontal or vertical shaft arrangements;
- surface tension, see Åstrom *et al.* [176] and Gershuni *et al.* [175];
- capillary forces, see Jacod [177];
- ball spin [178];
- air flow;
- shocks/vibrations ;
- transient loading, see Cann and Lubrecht [179];
- start-stop operation.

Furthermore, the amount of oil available for lubrication may differ, depending on grease formulation. This is determined by:

- the initial filling and distribution of lubricant, see Lugt *et al.* [173];
- grease bleeding: from the cage and the side reservoirs;
- grease rheology;
- grease degradation, see Cann, *et al.* [102];
- evaporation;
- oxidation.

In the case of the ball-on-disc device, the first two items are substituted by the contact forces between the steel ball and the glass disc. Cann and co-workers have extensively studied the lubrication mechanisms in a ball-on-disc contact, e.g. see, [69,156,163,180,180], and references therein. They noted that different physical mechanisms may predominate depending on geometry, operating conditions and grease type.

The most common trends in grease film thickness when replenishment is not imposed were reported by Mérieux, *et al.* [5] and are illustrated in Figure 4.14.

In the case of the three tested greases (Figure 4.15), only behaviour C (starved with stabilization) was observed. According to Cann [161], the level in which film

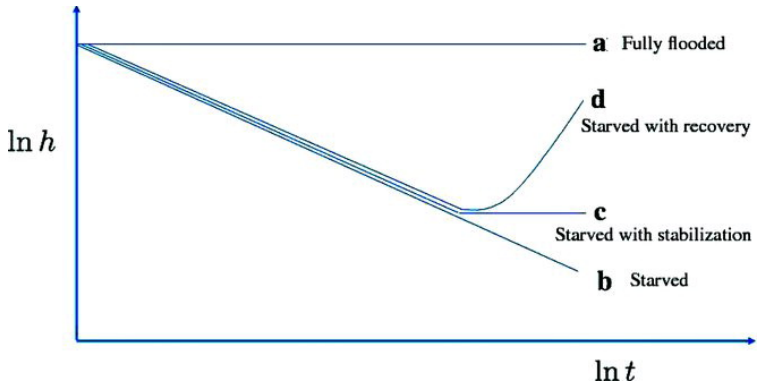

Figure 4.14.: Characteristic starvation behaviour for grease lubrication [5].

thickness stabilizes (residual layer) is composed by a liquid layer of base oil on top of a solid-like, thickener-rich layer, with thicknesses between 6 nm and 80 nm [163]. That layer, measured at the end of the test at zero speed, is a portion (or all) of the static layer, referred in Section 4.5.

Such behaviour was well predicted by the thin layer flow model developed by Venner, *et al.* [171] using the base oil viscosity as input and the thickener layer thickness as zero level. Such comparisons can be found in [21]. This is a remarkable result and points to new lines of research aiming at studying thickener-additives-surface interaction and their characteristics when thick boundary layers are formed.

4.6.2. Grease film thickness under starved lubrication - Results

Figure 4.15 shows film thickness measurements under starved conditions versus time at 40 °C , P_0 = 0.5 GPa and Ue = 0.1 m/s. All lubricating greases revealed a quick film thickness decay followed by a significant reduction of the decay rate with time (stabilization), as shown in Figure 4.14. The values of the stabilized film thickness of each grease represent averages of all film thickness measurements for time > 1250 s, and are given in Table 4.6. LiCaE grease presented the lowest stabilized value, followed by LiM1 and PPAO.

The very high standard deviation in these measurements is related to grease materials crossing the contact, as already reported by several authors [127,164,181,182]. This may indicate that the constituents of PPAO grease pass through the contact more often and in larger lumps than the constituents of LiCaE and LiM1, and is in agreement with the findings of Couronné *et al.* [3] and Cann *et al.* [156].

Couronné *et al.* [3] when comparing 4 lubricating greases with different formulations, had already verified that polymers tend to pass through the contact at a higher

Table 4.6.: Film thickness versus time under starved lubrication. P_0 = 0.5 GPa, T = 40 °C , Ue = 100 mm/s.

	LiM1	LiCaE	PPAO
Film thickness [nm]	50.4	28.3	63.2
Variation [nm]	±16	±12	±45

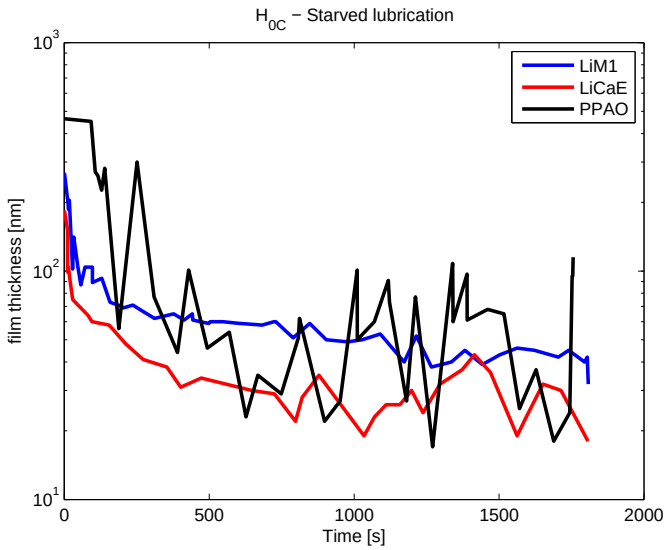

Figure 4.15.: Grease film thickness versus time under starved conditions at P_0 = 0.5 GPa, T = 40 °C and Ue = 100 mm/s.

rate as compared to lithium. Likewise, Cann *et. al* [156], when comparing several Lithium, Calcium and Lithium-Calcium greases with the same base oil type, verified that the contribution of Calcium to film formation was much greater than that of Lithium. This behaviour was attributed to Calcium crystals, which are probably larger than the lumps of Lithium in the contact inlet.

Longer test periods and measurements at zero speed should be performed for a better evaluation of a greases capacity to form a film under starved lubrication. The results shown in Figure 4.15 only indicate that Polypropylene seems to contribute the most to increase the film locally, Lithium seems to contribute the least, whilst Calcium is in between the two. This could be related to the thickener's capacity to survive the mechanical work to which it is submitted and thus, the thickener that survives this work with larger lumps is more likely to generate an increase of higher

local film.

In case the local increase in film thickness were to be disregarded after stabilization (time > 1250 s), film thickness would be higher for LiM1 grease ($\approx$ 40 nm), followed by LiCaE, which is only slightly higher than PPAO (both of $\approx$ 20 nm). This suggests that the lubricant film is formed by a thin layer of bleed-oil and is constantly, but momentarily, increased by the thickener's passing through the contact.

4.7. Discussion and conclusions on grease film thickness

The authors' analysis of the film thickness measurements is in agreement with several authors' previous observations and adds some important aspects regarding separate film properties in EHL contacts.

Under fully flooded lubrication, which can be related to the churning phase and the early stages of the bleeding phase in grease lubricated rolling contacts, it was observed that:

- lubricating greases and their corresponding bleed-oils generate similar film thickness values under the same operating conditions;
- grease and bleed-oil generate higher film thickness than the corresponding base oil;
- bleed-oil properties depend on base oil nature and viscosity, thickener and co-thickener type and concentration, additive package, the interaction between grease constituents and the manufacturing process;
- FTIR analysis showed that base oil and bleed-oil are chemically different, however it was not possible to correlate their IR spectra differences with their film thickness performance;
- pressure-viscosity coefficients of bleed-oil can be estimated by correlating the film thickness measurements with an appropriate centre film thickness equation, if the flow curve of the bleed-oil is known, i.e., if the flow parameters (η_0, G_{cr} and n) are known;
- grease thin-film measurements at very low rolling speeds showed unusually thick films and increasing film values with decreasing speed, contrary to usual fluid film behaviour. Such behaviour was not observed for base oils and bleed-oils, indicating that such behaviour is associated with the thickener / co-thickener;

- the speed at which lubricating greases change their trend (U_{hmin}) depends on grease formulation; the thickener type and concentration are most likely the dominant factors;
- the grease thicker films observed at low speeds do not contribute to the film thickness at high speeds, which approach the bleed-oil ones and follow a typical Newtonian trend ($h \propto U^{0,67}$);
- the thick films observed at low speeds seem to increase in time suggesting subsequent thickener deposition on the track.

These results suggest that the grease mechanism of lubrication under fully flooded lubrication is governed by the bleed-oil, and therefore the grease film thickness can be predicted by considering the bleed-oil properties. The accuracy of this prediction depends on how the lubricant parameters were obtained and the film thickness equation selected. A more accurate solution should include flow curves at higher pressures and shear rates.

The main advantage of using bleed-oil properties over grease ones to describe grease film thickness is the application of already developed and well established technologies to characterize and model lubricating oils. At very low speeds and thin films, however, bleed-oil does not represent grease film behaviour for any longer time. Under these conditions, the dominant lubrication mechanism seems to be governed by the thickener/co-thickener.

Under the starved elastohydrodynamic regime, which is the dominant condition that many grease lubricated rolling contacts operate under after the initial stages of the bleeding phase, it was observed that:

- film thickness decreased rapidly over time followed by stabilization;
- the stabilized values fluctuated wildly and the standard deviation was very high;
- the stabilized film probably consisted of a liquid layer of bleed-oil with thickener material passing through the contact;
- the liquid layer resulted in a loss of equilibrium (mostly due to pressure ejection) and resupply mechanisms (mostly due to re-flow effects);
- thickeners with more susceptibility to cross the contact, that contributed the most to local increases in the film thickness follow a PP > Ca > Li order;
- the higher the thickener's susceptibility to cross the contact, the higher the likelihood of residual film due to subsequent deposition (enhanced-viscous or thickener-rich layer);

- the thickener layers are most likely physically deposited rather than result of a chemical reaction, since there were no visible boundary layers in the samples after washing.

These results suggest that the grease mechanism of lubrication under starved conditions is initially governed by the bleed-oil + thickener/co-thickener that passes through the contact. During its passage through the contact this may be deposited on the surfaces due to the severe conditions in the high pressure zone. The more the thickener that passes through the contact, the higher the possibility of thickener deposition and thicker residual layers. Thickener / co-thickener effects on locally increasing the film follows the PP/rubber > Ca > Li. However, as the starved tests were carried out over a very short period of time (30 minutes), the lubrication mechanisms may change after that. For instance, in cases of severe operating conditions, it is expected that the additives will interact with the surface and change the way that grease performs.

5. Traction coefficient in a grease lubricated contact

5.1. Introduction

Traction properties, characterized by the low shear viscosity, limiting elastic shear modulus, and limiting shear stress the material can withstand, are of great interest in the development of lubricants, in the design of traction drives, dynamic behaviour design and failure analysis of some machine elements and for the proper choice of lubricants for a given application [22, 183]. Although prediction of the traction behaviour of lubricating oils is well documented [183, 184], it is not well established for lubricating greases, mostly due to the as yet unknown properties of the lubricant film, as described in the previous section.

Actually, even for oil lubrication, two main approaches have been used to determine the parameters that describe oil traction behaviour, very often leading to different results. One approach defines traction parameters by adjusting them in order to obtain the best R^2 fitting with traction measurements [59, 185, 186]. The other approach employs primary laboratory data and no fitting procedure is required, although the correlation factor (R^2) of this approach is still unsatisfactory [187–189]. Both approaches have their followers and there is no consensus here. In addition, the properties of the boundary layers, which considerably affect traction values, depend largely on the lubricant-additive-surface interaction that is not yet well known. Surface topography is another important aspect that considerably influences rolling and sliding friction in EHL contacts and which is difficult to model [138].

As described before, there is no overall agreement on how grease lubricates the contact and there is some uncertainty regarding the rheological properties of the lubricant film [22,23]. Most of the grease single-contact tests have therefore aimed at understanding film formation and properties, whilst very few works on grease traction behaviour have been published.

Consequently, the authors only experimentally analysed the grease traction behaviour in a ball-on-disc device in order to complement the understanding of the

friction torque model (Chapter 6), which requires inputs of friction coefficients under full film and boundary lubrication. The effect of entrainment speed, slide-to-roll ratio, temperature and lubricant properties on the traction coefficient were thus analysed.

5.2. Materials and methods

Grease traction coefficient measurements were conducted in a Wedeven Associates Machine (WAM) ball-on-disc test device, model 11A with controlled temperature under fully flooded and starved conditions. The machine was described in the previous chapter but a brief description will be given here because traction measurements require a different arrangement.

During traction measurements the ball runs against the upper part of the disc, as shown in Figure 5.1. Here, the load is applied by moving the disc upwards towards the ball and since both contacting bodies are made of steel, the contact pressure may rise to 2.91 GPa. The remaining conditions related to machine operation capabilities were described in Section 4.2.

Figure 5.1.: WAM 11A ball-on-disc test device: Traction measurement arrangement. Luleå University of Technology.

5.2.1. Test specimens

The ball and disc used were made from AISI 52100 bearing steel, with 13/16″ (20,637 mm) and 100 mm diameters, respectively. The roughness of the disc was measures with a Wyko NI1100 optical profiling system from Veeco. Measurements were done using $10\times$ magnification and $0,5\times$ field of view (FOV). The ball roughness was provided by the manufacturer.

The ball and disc properties are presented in Table 5.1 and the grease properties, in Table 3.11.

Table 5.1.: Ball and disc data.

	Ball	Disc
Elastic Modulus $-E$ [GPa]	210	210
Poison Coefficient $-\nu$ [-]	0.29	0.29
Radius $-R$ [mm]	10.3185	50
Surface roughness $-\sigma$ [μm]	0.02	0.20

5.2.2. Test procedure

Two different test sets were carried out to measure the traction coefficient of the lubricating greases described in Chapter 3. In the first set, fully flooded conditions were ensured by using a scraper; the scraper was not used in the second set and the tests were performed under starved lubrication.

The load applied was 266 N, which corresponds to a maximum Hertz pressure of $P_0 = 1.86$ GPa. Three operating temperatures were used: 40, 60 and 80 °C . The test cycle of each set covered entrainment speeds between $0.37 - 2.8$ m/s and slide-to-roll ratios from 0,05 to 5,45 %. In all cases the ball rotated faster than the disc. The temperature control is described in Section 4.2.2.

The test cycle contained several loops where the *SRR* was held constant and the entrainment speed increased from 0.37 to 2.8 m/s. The *SRR* was held at 0.05 % in the first loop and increased in each loop until it reached 5.45 %. The same test cycle was repeated twice for each grease and temperature; repeatability was good. The maximum difference between the two tests was 8 % under fully flooded conditions and 12 % under starved conditions. Error values were calculated disregarding the friction values measured for $SRR < 0.5$ %, where the error rises to 250 %. Logged data from each test was processed separately, but the results presented here are an average of the two test cycles.

5.3. Friction map analysis

The measured values of the test cycles are shown in a 3D friction map for each lubricating grease and temperature. As friction maps contain *SRR*, entrainment speed and traction coefficient values, they can replace several Traction and Stribeck curves and offer a better overview of the grease friction characteristics.

Figure 5.2 represents the friction map for LiM1 grease at 80 °C , under fully flooded lubrication. This figure was chosen as it represented better the general trends observed in the fully flooded tests. A friction map can be divided in 5 parts according to the factors governing / influencing the friction [187]. TThe friction regimes in full film lubrication (1-3, 5) were proposed by W. Habchi, *et al.* [190].

1. *Linear regime*: Friction varies linearly against *SRR* indicating that frictional response of the contact is governed by the Newtonian behaviour of the lubricant (or Newtonian + Elastic behaviour according to Bair and Kotzalas [191]).

2. *Non-linear viscous regime*: Friction departs from linear behaviour indicating that shear-thinning and/or thermal dissipation and/or limiting shear stress behaviour of the lubricant is affecting the friction response of the contact.

3. *Plateau region*: Friction reaches an asymptotic value and shows very little variation indicating that the frictional response of the contact is governed by the limiting shear stress behaviour of the lubricant.

4. *Mixed regime*: Friction varies due to a transition from mixed to full film lubrication. Here, friction behaviour is governed by asperity interaction and hydrodynamic effect.

In case the combinations of speed and *SRR* go beyond the ones shown in Figure 5.2, the *5 - Thermoviscous regime* is observed [190]. In this regime, friction decreases with increasing sliding speeds, indicating that both thermal dissipation and shear thinning effects are governing the frictional response of the contact and overwhelming all other effects, including limiting shear stress.

Note that as these regimes depend on operating conditions and lubricant properties, they do not necessarily come together in a friction map.

According to the flow chart proposed by W. Habchi, *et al.* [190], for the operating conditions (high loads, slow to high speeds and low *SRR* values) used under full film conditions, the dominant parameter in frictional response of EHL contacts is the limiting shear stress (LSS). Shear-thinning effects may also occur before LSS is reached, but thermal effects have little influence.

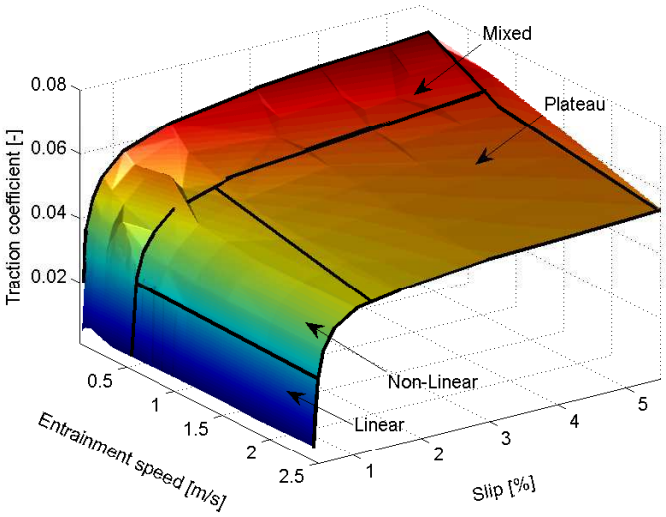

Figure 5.2.: Typical 3D friction map obtained under fully flooded lubrication with the different traction regimes highlighted.

5.4. Results

5.4.1. Fully flooded tests

The average values of the test cycles under fully flooded lubrication are shown as a 3D friction map for each grease and temperature in Figures 5.3 to 5.5. The greases are positioned in a well defined order of magnitude of the traction coefficient, where the LiM1 consistently generates the highest traction coefficient, followed by the grease LiCaE, that is only slightly higher than the PPAO grease (LiM1 > LiCaE ≈ PPAO).

The first three friction regimes previously described (*1-linear, 2-non-linear viscous and 3-plateau*) are seen for all tested greases whatever the operating temperature. The *4-mixed regime*, where the traction decreases with increasing film thickness, is hardly observed at the 40 °C measurements, but it is significant at higher operating temperatures. It occurs due to a lubrication regime transition (from mixed to full film lubrication) that takes place at 60 and 80 °C , while at 40 °C the tests run mostly in full film condition. This is well depicted by the specific film thickness predictions showed in Figure 5.6 for all lubricating greases, operating temperatures and for the highest *SRR*. The predictions were performed using the Equation 5.1 and the bleed-oil properties presented in Table 3.11.

$$\Lambda = \frac{H}{\sigma_c}; \qquad \sigma_c = \sqrt{\sigma_{disc}^2 + \sigma_{ball}^2} \tag{5.1}$$

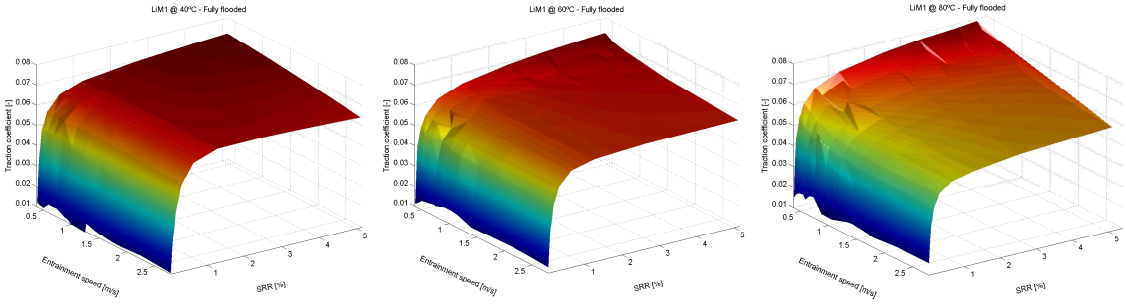

Figure 5.3.: LiM1 friction map at 40, 60 and 80 °C . Fully flooded lubrication.

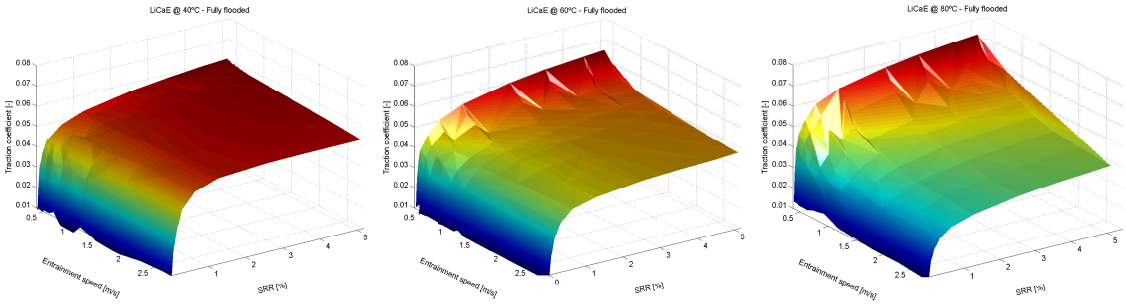

Figure 5.4.: LiCaE friction map at 40, 60 and 80 °C . Fully flooded lubrication.

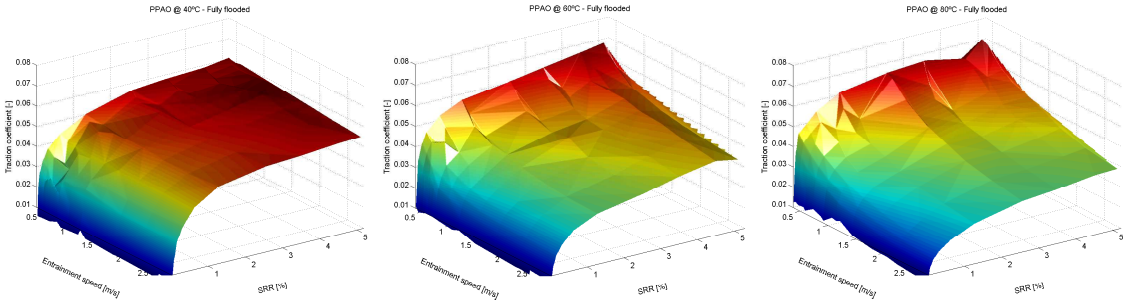

Figure 5.5.: PPAO friction map at 40, 60 and 80 °C . Fully flooded lubrication.

where H is equal to H_{oc} from Equation 4.7 for LiM1 and LiCaE bleed-oils (Newtonian), and H is equal to H_{ock} from Equation 4.9 for PPAO bleed-oil (non-Newtonian). Surface roughness are given in Table 5.1. The thermal correction (ϕ_T - Equation 4.8) was considered in both equations.

The specific film thickness values correlated well with the transition of the friction regimes from *4 - Mixed regime* ($\Lambda < 1$) to *3 - Plateau region* ($\Lambda > 1$), as observed by comparing Figure 5.3 to 5.5 with Figure 5.6. Were the specific film thickness predictions to be carried out considering the base oil viscosity, PPAO would reach full film (Λ >1) at U = 1 m/s at 40 °C , U = 2,25 m/s at 60 °C and it would not do so over Λ >1 at 80 °C , which would not corroborate the traction measurements.

The 5-*thermoviscous regime* is only slightly visible in the LiM1 friction map at 40 °C for the combination of high speeds and *SRRs* (see Figure 5.3 - left).

The slight decrease of the traction values with increasing speed when $\Lambda > 1$, which was mainly observed with PPAO and LiCaE at 80 °C , no longer depends on film thickness. In these conditions, the friction response may be governed by shear thinning effects and thermal dissipation.

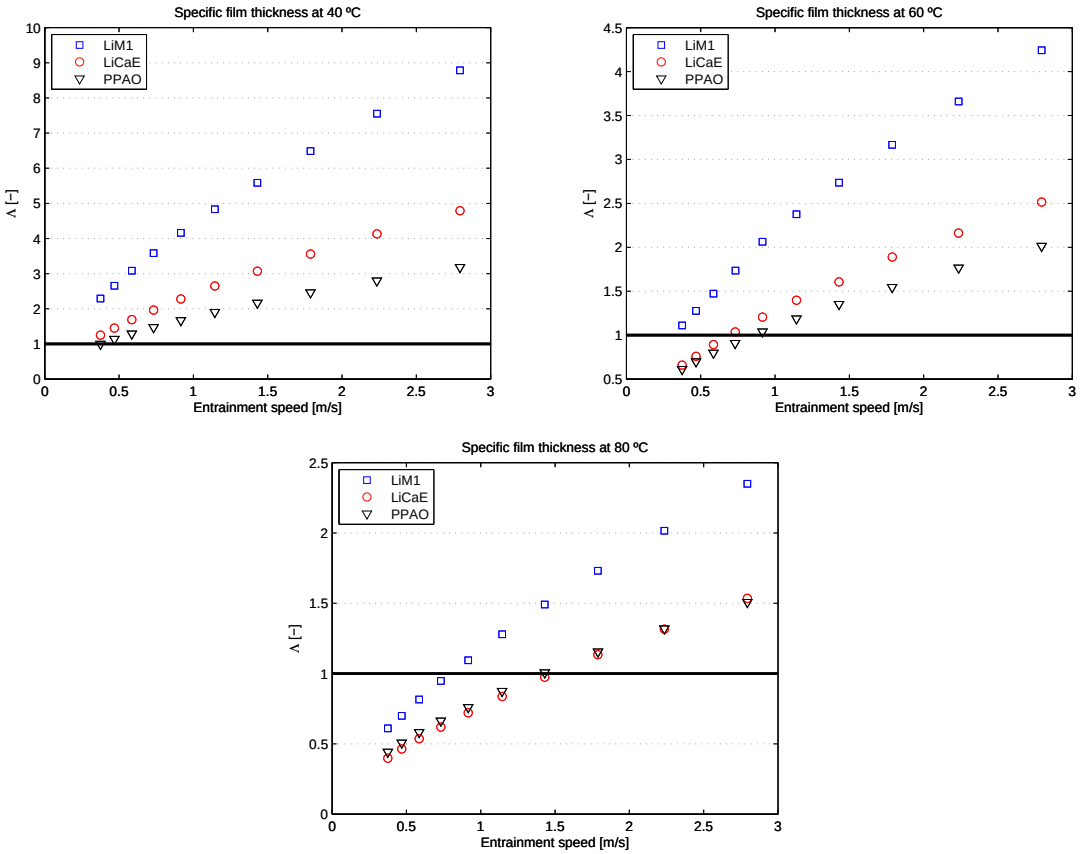

Figure 5.6.: Specific film thickness at 40, 60 and 80 °C of all lubricating greases. Fully flooded lubrication

5.4.2. Starved tests

Likewise, the average values of the test cycles under starved lubrication are shown in Figures 5.8 to 5.10.

Friction maps obtained under starved and fully flooded lubrication shared some features. Both presented a high traction coefficient gradient when little sliding was induced from pure rolling. According to Bair and Kotzalas [191], under these operating conditions (high pressure $\approx$ 1.85 GPa and very low $SRR \leqslant 0.5$ %) there is another regime that will supersede the Linear regime (Newtonian viscous regime). This regime is called elastic creep of the contact bodies and is characterized for being independent of the lubricant properties. Here, in spite of the high instability of the measurements at very low SRR, dependency of the lubricant and lubrication regime (or a non evidence of the elastic creep contact bodies behaviour) was evidenced in the traction curves, indicating that such regime did not supersede the Newtonian viscous one (see Figure 5.7). For example, traction values measured under starved lubrication always presented faster increase rates with SRR than those obtained under fully flooded conditions in the linear regime.

Under starved lubrication, friction maps are not as "smooth" as under a fully flooded regime because of the uncontrolled starved conditions that lead to sudden and significant changes to film thickness over time (see Figure 4.15) that are shown to affect the traction behaviour of the lubricating greases. Consequently, repeatability in the starved tests was worse than the fully flooded ones, as described in Section 5.2.2.

Contrary to that which was observed in the fully flooded tests, it was noted no trends regarding the traction coefficient's order of magnitude. At 40 °C the highest

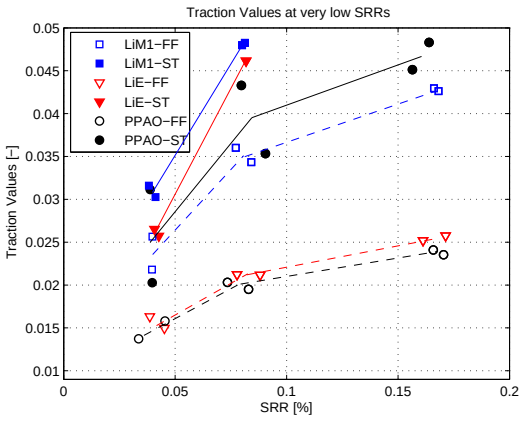

Figure 5.7.: Traction curves at very low $SRR's$, T =80 °C , Ue = 2.8 m/s.

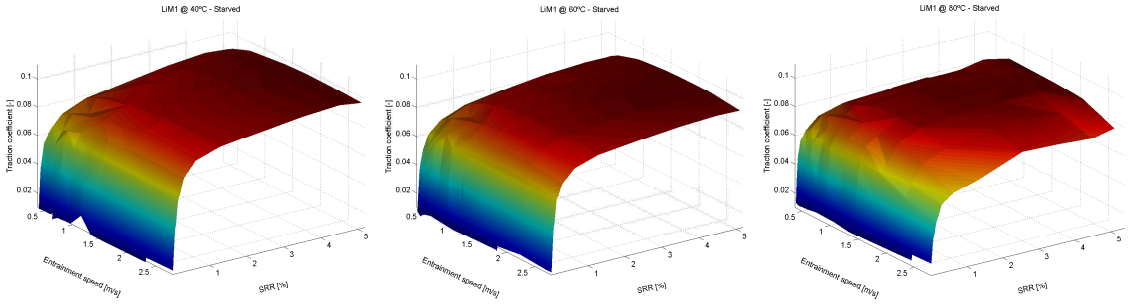

Figure 5.8.: LiM1 friction maps at 40, 60 and 80 °C . Starved lubrication.

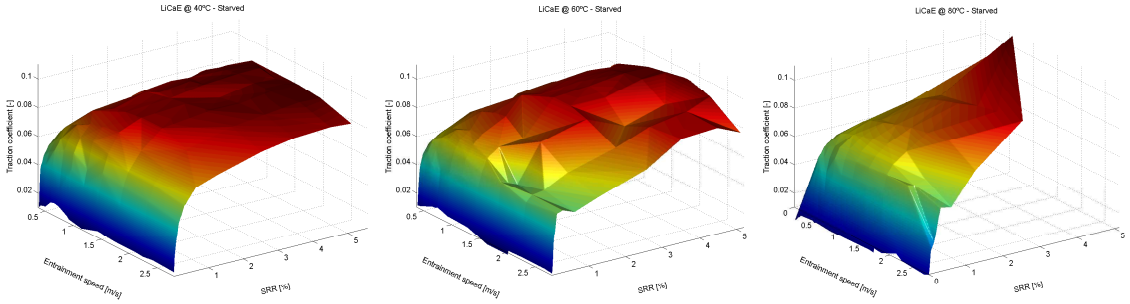

Figure 5.9.: LiCaE friction maps at 40, 60 and 80 °C . Starved lubrication.

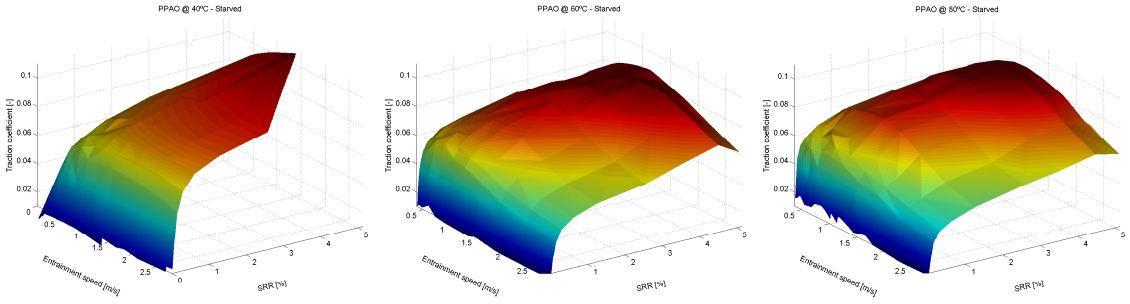

Figure 5.10.: PPAO friction maps at 40, 60 and 80 °C . Starved lubrication.

traction coefficient was reached with PPAO grease (test aborted due to high friction, taking place at exactly the same combination of *SRR* and speed (or time) in both tests - see Figure 5.10) and the lowest one with LiCaE. At 60 °C the highest traction coefficient was reached with LiM1 grease, followed by LiCaE and PPAO, which were similar. At 80 °C the highest traction coefficient was reached with LiCaE grease (test aborted due to high friction, taking place at exactly the same combination of SRR and speed (or time) in both tests - see Figure 5.9) and the lowest one with PPAO.

Traction values measured under starved lubrication were always higher than the ones measured under fully flooded conditions. As described earlier, film thickness is expected to show a very rapid decay with low film thickness values after stabilization (mix / boundary lubrication). This leads to increased asperity interactions, thin films with unknown properties (but probably governed by thickener-additive-surface interaction) and consequently higher traction coefficients.

Due to the differences in film generation, here it was observed divergent trends from the ones seen under fully flooded condition at low speeds ($\leqslant 1.5$ m/s). Instead of the *Mixed* to *Plateau* (film regimes: mixed to full film) transition of the friction regimes that is characterized by increasing traction values with decreasing speed, the traction values dropped as speed decreased. This was most likely related to film thickness decay over time, which kept higher films (or similar ones) during the firsts test loops (low speeds) up to the moment it reached a stable condition (thickener-layer with bleed-oil in the top). The decrease of traction values with increasing speed afterwards is not fully understood but it could be related with the increasing formation of a solid-like or enhanced viscous film by additives, thickener and oil over time, as the thickener / additives pass through the contact and are physically deposited on the surfaces [155].

5.4.3. Influence of temperature

Operating temperature influences the traction coefficient by changing lubricant properties such as viscosity, pressure-viscosity and by limiting shear strength. In the case of lubricating greases, the higher the operating temperature, the lower the lubricant properties. Increasing temperature leads to lower film thickness and consequently higher shear rate, which in turn increases the traction coefficient. On the other hand, a reduction of the lubricant properties also reduces the traction coefficient.

Figure 5.11 displays the percentage differences between the traction coefficient values at 40 °C and 80 °C under fully flooded lubrication ($(TV_{80} - TV_{40}) \times 100$). The negative values in the lower speed region indicate that the traction coefficient is higher at 80 °C .

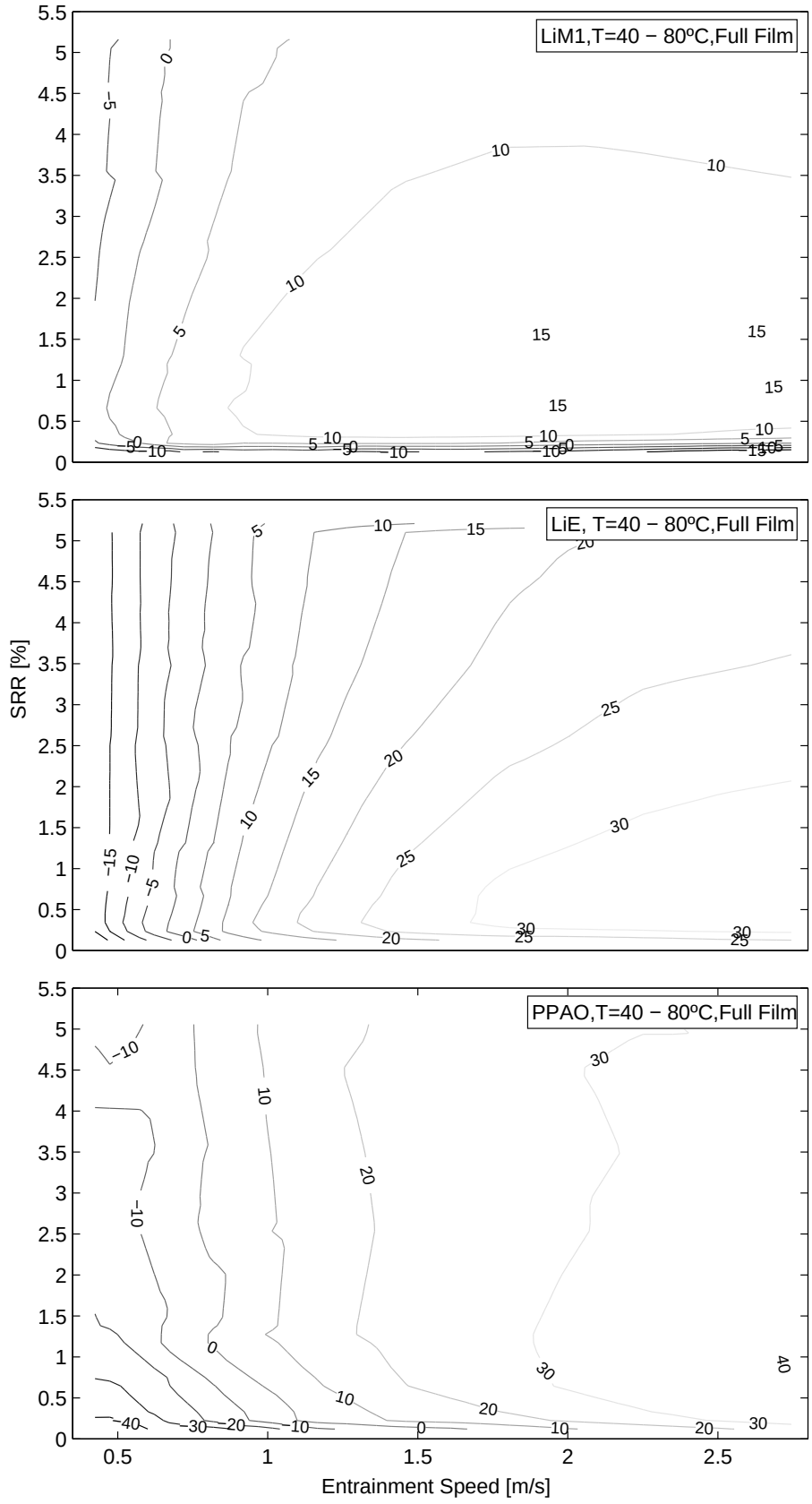

Figure 5.11.: Difference in percentage between the traction coefficient values at 40 °C and 80 °C under fully flooded conditions.

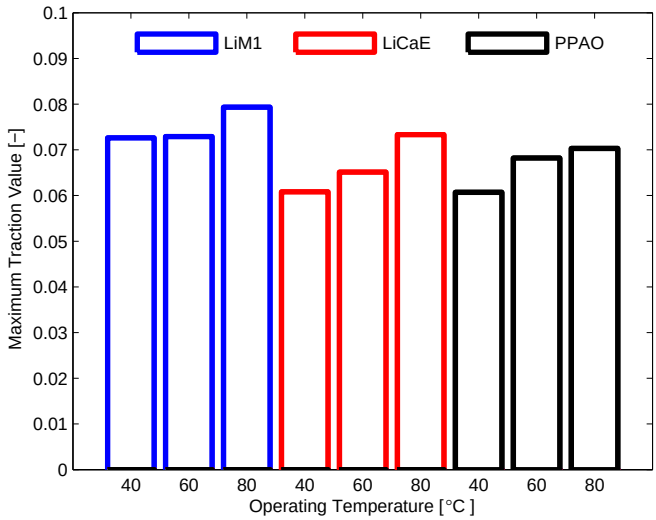

Figure 5.12.: Maximum traction coefficient at 40, 60 and 80 °C of each grease under fully flooded lubrication.

The traction values at 80 °C are higher than the ones at 40 °C in the low speed region due to their different lubrication regimes. At 80 °C the contact is operating under mixed / boundary lubrication, while at 40 °C it is under full film conditions. On the other hand, at higher speeds, traction values at 80 °C are lower than at 40 °C because full film lubrication has been reached, asperity contacts are reduced and high shear rates are less significant than the decrease in lubricant properties (viscosity, pressure-viscosity and limiting shear stress).

Figure 5.12 shows the maximum TV_{FF} for each grease and operating temperature. It is important to mention that the maximum traction coefficient was always measured at the lowest entrainment speed (≈ 0.375 m/s), highest SRR (≈ 5.2 %) and highest temperature. It clearly shows that when the operating conditions approached the lubrication boundary (low speed, high SRR and high temperature) the traction coefficient attained its maximum value.

5.5. Discussion and conclusions on grease traction coefficient

Two interesting facts emerge from the analysis of Figures 5.3 to 5.5 and 5.8 to 5.10: *i)* under fully flooded conditions, the greases are positioned in a well-defined order of magnitude for the traction coefficient and *ii)* LiM1 greases consistently generates the highest friction coefficient, followed by LiCaE greases, which are slightly higher than PPAO greases. This trend does not remain under starved lubrication, which is different depending on the operating conditions. PPAO greases did not replenish the contact under low speed and temperature and therefore failed in such conditions. This may be related to their low oil bleed rate and high consistency. LiCaE on the other hand failed at high temperatures. Under these conditions the system is operating under severe boundary conditions and probably, the low additivation of LiCaE was not enough to form a low-shear boundary layer; metal to metal contact occurred, significantly increasing the traction values.

The trends observed under fully flooded lubrication ($Mineral > Ester \cong PAO$) had already been observed by Brandão *et al.* [192] when comparing the traction curves for 6 different gear oils. These authors claimed that traction curves more or less follow the grouping by base oil types. This trend was also verified in bearing tests by Fernandes *et al.* [193] and in the friction torque measurements presented in 6.

Grease or bleed-oil film thickness measurements under fully flooded lubrication followed the same trends as the traction measurements ($Mineral > Ester \cong PAO$). The lubrication regime transition (mixed to full film) predicted by the film thickness equations using bleed-oil properties correlated nicely with the traction regimes (mixed to plateau) transition. This may indicate that limiting shear strength is most likely proportional to the pressure-viscosity coefficient and somehow connected to low-shear viscosity. Several authors have already reported a relationship between the lubricant parameter (viscosity and pressure-viscosity coefficient) and the limiting shear strength [194–196].

Lubricating greases running under fully flooded conditions behaved similarly to lubricating oils. Analysis of these curves revealed the influence of the operating variables, namely:

- traction coefficient decreases significantly with increasing speed if lubrication regime transition takes place, and slightly at full film lubrication;
- increasing SRR influences the traction coefficient in the same way but at dif-

ferent levels for fully flooded and starved tests;

- at very low entrainment speeds, traction coefficients under fully flooded and starved lubrication are very similar;
- *SRR* and operating temperature influences are more significant under fully flooded lubrication;
- starved lubrication produces a higher traction coefficient;
- increasing entrainment speed increases the traction coefficient in starved tests for all *SRRs* tested, unless replenishment occurs;

High traction values observed for PPAO at 40 °C and LiCaE at 80 °C in both test cycles that were shut-aborted, occurred for exactly the same combinations of *SRR* and speed (or time) due to severe starvation. This suggests that the grease mechanisms of lubrication under starved lubrication can be predicted when the initial lubrication condition is controlled.

6. Rolling bearing friction torque

6.1. Introduction

The internal friction torque that occurs in rolling bearings is a major concern, since the main function of rolling bearings is to transmit load at very low friction. Thus, understanding internal friction in rolling bearings becomes relevant when energy saving and bearing performance optimization are required. A more efficient transmission, in general, generates less heat, less wear, less power loss and, consequently, implies a lower impact on nature due to fewer waste materials (worn out mechanical transmissions and lubricants).

There are several models for predicting the internal friction torque of rolling bearings in the literature [6, 94, 197–199]. The models based on a large number of experimental results, including thrust ball bearings, however, are those provided by bearing companies, such as FAG [24] and SKF [8]. Of these, the new SKF friction torque model is the only one that considers the true physical sources of the friction torque, hence it provides a better understanding of the bearing operating conditions. This model, however, does not take into account the grease formulations (thickener type and concentration) that may influence the torque measurements.

Again, the challenge of predicting the friction torque of rolling bearings is the uncertainty regarding the properties of the active lubricant in the contact and consequently, the impossibility of accurately predicting the lubrication regime and friction behaviour. In fact, very little has been published on grease analysis in full bearing tests and there is no consensus as to how grease operates in rolling bearings. According to Cann *et al.* [11, 102], grease lubrication mechanisms after the churning phase depend on bearing type, operating conditions and grease properties; base oil oxidation, thickener degradation, and anti-wear/boundary properties will all play a role. A general trend based on few experimental results from Cann and co-workers [11, 102] suggests that after running long periods at high speeds (> 10000 rpm), high temperatures ($\geqslant 100$ °C) and low loads, the active lubricant becomes degraded / oxidized grease containing a significant amount of thickener, whilst a similar bearing running at similar operating conditions but at low speeds (≈ 1500 rpm) is mostly lubricated

by a "free" oil containing little thickener.

Scarlett [91] verified the formation of pads of grease with a higher soap content than fresh grease under the cage bars of rolling bearings and concluded that this occurred due to bleeding in the first $\approx$ 100 h of operation. After that, he claimed that grease no longer bleeds, hence it does not contribute to the lubrication process. Scarlett also verified that lubricating greases near to the seals also do not supply the rolling contact with bleed-oil, but they prevent the bleed-oil released from different parts of the bearing to escape.

Aside from the difficulty in understanding grease film formation since it depends on several factors, there is an overall agreement that grease lubricated bearings are generally running under starved lubrication conditions after the churning phase. This has been shown in full bearing tests by Wilson in 1979 [157] and Wikström and Jacobson in 1997 [200] and in many single-contact tests [139, 154, 201]. On the other hand, the starved situation does not actually mean boundary lubrication as after 240 hours of full bearing tests, the average minimum film thickness measured by Wilson [157] was around 0.4 μm, which gives a specific film thickness greater than 1 ($\Lambda \geqslant 1$) considering the typical value of the composite surface roughness of spherical and cylindrical roller bearings at that time ($\sigma_s \approx 0,35$ μm - worst case scenario). Many other short period (few hours) tests in bearing simulation devices also demonstrated that grease retains a separating film [15, 201] for a wide range of operating conditions.

Therefore, based on the above arguments and the results from Chapter 4, one can say that grease lubricated rolling bearings operate mostly under starved lubrication but retain a separating film, which is characterized by the bleed-oil in the earlier stages of the bearing operation and by a little-known lubricant material after that.

One of the principle constraints to better understanding grease operation especially during the late stages of lubrication, is the extensive tests that are required, as well as the limited academic availability of full bearing test-rigs.

As only the first stages of the bearing operation are studied in this chapter, the possibility of using bleed-oil properties for predicting friction torque is discussed.

6.2. Materials and methods

The behaviour of the new generation of lubricating greases, such as biodegradable greases, polymeric greases, greases with nano-particles (and even the usual lithium mineral greases) is not yet well known, particularly in terms of rolling bearing wear and power loss. Consequently, new experimental methods and analytical tools have to be developed to study the tribological and energetic behaviour of these greases.

Full-bearing experiments are the closest to the real application, as they give a good indication as to how real system performance is influenced by changing certain operating parameters and grease Furthermore, this complements the measured data obtained from the single contact tests presented in Chapters 3, 4 and 5. Although several full bearing test rigs can be found in bearing companies, they are not widely available for research. A test rig was designed and manufactured, therefore, for performing rolling bearing tests with accurate friction torque and temperature measurements.

6.2.1. Rolling bearing assembly

Rolling bearing tests were performed with a modified Four-Ball Machine (Cameron-Plint TE 82/7752) where the standard four-ball arrangement was substituted by a rolling bearing assembly, as shown in Figure 6.1. The new arrangement was developed to measure the friction torque and operating temperatures in rolling bearings. The device consists of: a shaft adaptor (6), which connects the machine input shaft to the upper race (5); a support (2) and the lower race (3), both clamped to the bearing house (1); a torque cell (11) protected by two plates (9, 13), which connect the bearing house (1) to the lower support of the Four-Ball Machine through the pins (10, 12). The retainer (7) and the cover (8) prevent lubricant leakage and contamination by external sources.

During operation, load (P) is applied on the lower plate (12) and the rotational speed (n) is transmitted to the shaft adapter (6), which is connected to the drive shaft of the machine (see Figure 6.1). The rotating motion is led through the upper race (5) to the rolling elements and cage assembly (4). The motion generates the bearing internal friction torque, which is transmitted through the lower race (3) to the bearing house (1), to the upper plate (9) and to the torque cell (11), all of which are clamped together. During the test, the rolling bearing assembly is submitted to continuous forced air convection by two fans, 38 mm in diameter and running at 2000 rpm, to remove the heat generated during the bearing operation.

The assembly also includes seven thermocouples located in strategic places to measure the lubricant and bearing housing temperatures, so that lubricant viscosity can be calculated with reasonable accuracy. Two of these thermocouples (VI and VII, not shown in Figure 6.1) are used to record the temperatures of the air flow surrounding the bearing housing and the room temperature.

The bearing assembly permits lubrication by oil or grease; four types of rolling bearings with different sizes can be tested, namely: thrust ball bearings (SKF ref. 51103 and 51107), tapered roller bearings (SKF ref. 30302 J2 and 30203 J2), angular

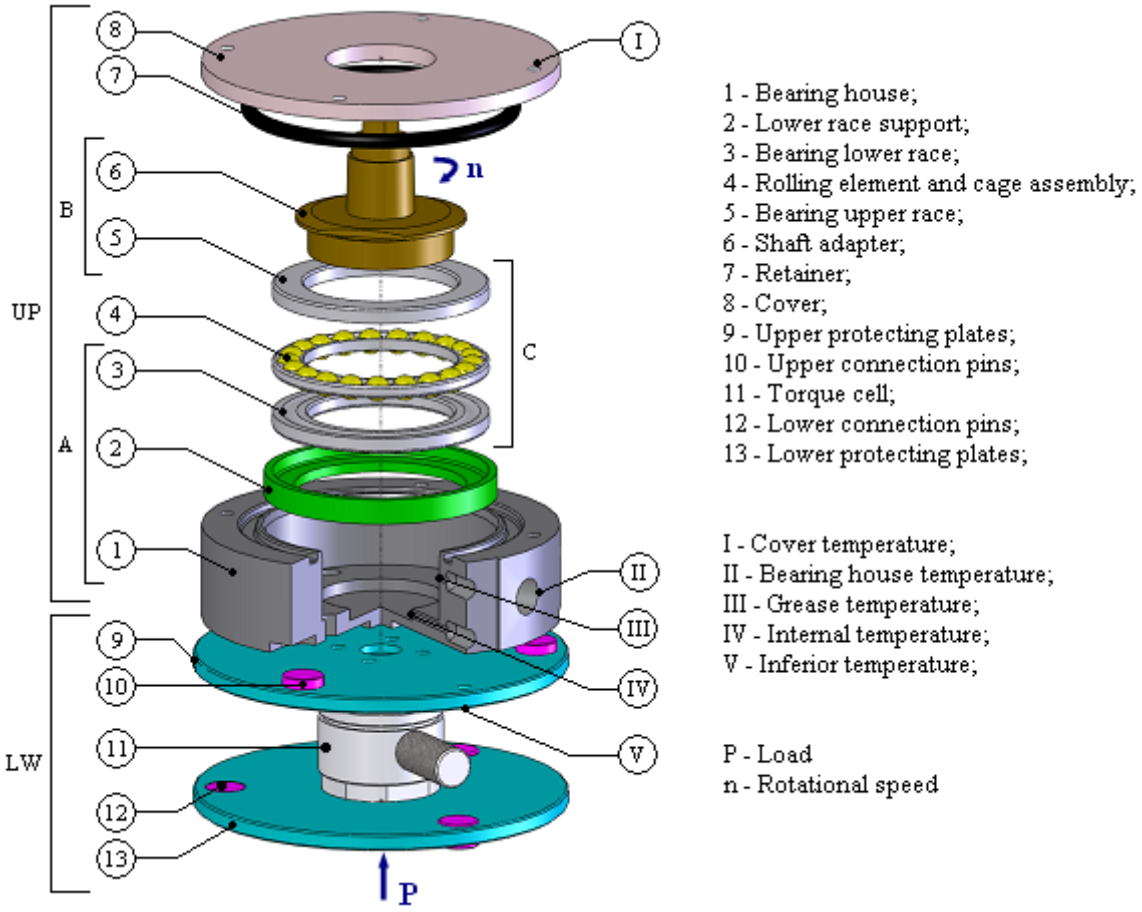

Figure 6.1.: Schematic view of the rolling bearing assembly with a THBB 51107.

contact ball bearings (SKF ref. 7203 and 7204) and cylindrical roller thrust bearings (SKF ref. 81102 TN and 81107 TN). Depending on the type of bearing, items (2) and (6), shown in Figure 6.1, must be replaced. In this work only the tests carried out with lubricating greases and thrust ball bearings SKF ref. 51107[1]are reported (see bearing characteristics in Figure 6.2 and Table 6.1). Surface roughness measurements were carried out after a running-in period of 1 hour with some balls in three different locations and a raceway fitted with a *Hommelwerke T4000* device.

The bearing assembly was recently re-designed by the author to operate with more bearing types and sizes, heating control and with the *Stanhope-Seta 19900-0* Four-Ball Machine.

In the case of grease lubrication, SKF recommends that the bearing should be complete filled, while the free space in the housing should be only partly filled [8]. For the THBB 51107 and the bearing house (1), the volume of grease that satisfies

[1]Thrust ball bearing SKF ref. 51107 will be reported from here on as THBB 51107.

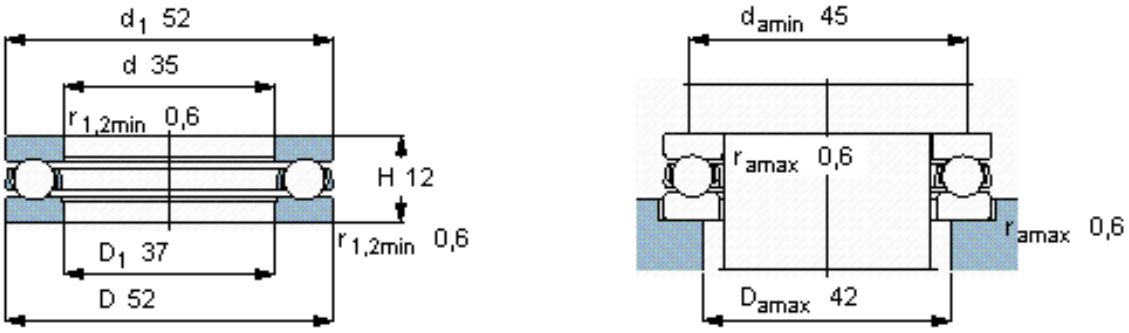

Figure 6.2.: THBB 51107 schematic view and dimensions.

Table 6.1.: Main characteristics of the thrust ball bearing SKF ref. 51107.

Princip. Dimens.			Basic load ratings		Speed ratings		Surf. Roughness	
d	D	H	Dynamic C	Static C_0	Ref. speed	Lim. speed	σ_{race}	σ_{balls}
mm	mm	mm	kN	kN	rpm	rpm	μm	μm
35	52	12	19.9	51	5600	7500	0.07	0.12

these requirements in 2 cm^3. This grease volume was used in all tests and should ensure proper replenishment without causing excessive churning and heat generation.

The friction torque measurements are constrained by several factors, in particular, the operating limits of the Four-Ball Machine and the torque cell characteristics (*Reaction Torque Sensor - KISTLER Type 9339A* [202]). The operating conditions imposed by the Four-Ball Machine allow texts with axial loads and rotational speeds up to 6867 N and 5500 rpm, respectively. The torque cell is affected by a phenomenon known as drift[2]. To avoid the drift effect, friction torque measurements must be performed for short period of time (120 s) and stabilized temperatures (± 2 °C).

6.2.2. Test procedure

All the measurements were performed according to the following procedures:

1. The new THBB 51107 was lubricated with 2 cm^3 of fresh grease for each test;
2. Forced air convection was used;

[2]Drift is an undesirable change of the output signal that depends on measurement time and temperature gradient.

3. The running-in period was carried out with an axial load of 1000 N and rotational speed varying from 100 to 5500 rpm during 10 min to accommodate the grease inside the bearing;

4. The desired load and rotational speed are set to the required value;

   Load, $P = 6867$ N;

   Rotational speed, $n = 100$, 350, 500, 1000, 2000, 4000 and 5500 rpm.

5. Temperature data acquisition starts. The operating temperatures rise continuously until stabilization is reached ($\approx$ 1.5 hours);

6. When the temperatures have stabilized, the machine is turned off and immediately restarted, together with torque data acquisition;

7. Torque is measured during 120 s, and temperature stabilization is again reacquired ($\approx$ 5-10 min) before the next torque measurements at the same speed;

8. Stages 6 and 7 are repeated three more times in order to obtain four measurements of the friction torque under the same conditions;

9. Another rotational speed is set and stages 5 to 8 are followed.

The running-in period advised for lubricating greases is greater than the one used here (1.5 h for the first measurement). Nonetheless, such methodology is justified due to the constant friction torque values measured over 36 h (measurements carried out after 2, 3, 4, 6, 12, 24 and 36 h, at 1000 rpm and 7000 N, for all three lubricating greases), as shown in Figure 6.3.

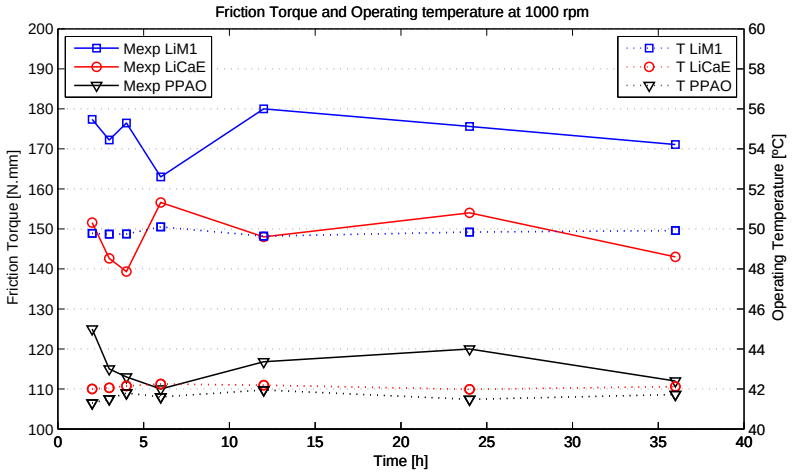

Figure 6.3.: Friction torque and operating speed versus time at 1000 rpm and 7000 N.

In fact, for the THBB 51107 (without seals or shields) and with a free space between the rolling bearing and the bearing house, the time for grease accommodation (churning phase) is probably less than 1.5 hours. All the torque measurements were performed within a running time lower than 10 h to prevent grease degradation, oxidation, thickener deposition or changing of the lubrication mechanisms from significantly affecting the measurements. Even so, when boundary films were visually observed at the end of the tests with some greases, their influence or when they were generated is unknown.

Due to the short running time before torque measurements, it is believed that the rolling bearing is operating during the grease bleeding phase. Under this condition the lubrication mechanisms are governed by the oil that bleeds from the grease.

6.3. Experimental results

Figure 6.4(a) shows the internal friction torque measured in a THBB 51107, for each entrainment speed and lubricating grease. The corresponding operating temperatures, measured with thermocouple III (see Figure 6.1) are shown in Figure 6.4(b).

Figure 6.4(a) shows that the internal bearing friction torque reached the highest values with the mineral greases (LiM1) and the lowest values with the polymeric greases (PPAO), whereas the torque values corresponding to the ester-based greases (LiCaE) fall between the mineral and polymeric grease values. This also shows that the bearing friction torque decreases as the rolling bearing speed increases.

Figures 6.4(b) shows that operating temperatures increase with the bearing speed. The highest temperature values correspond to the mineral grease (LiM1) and the

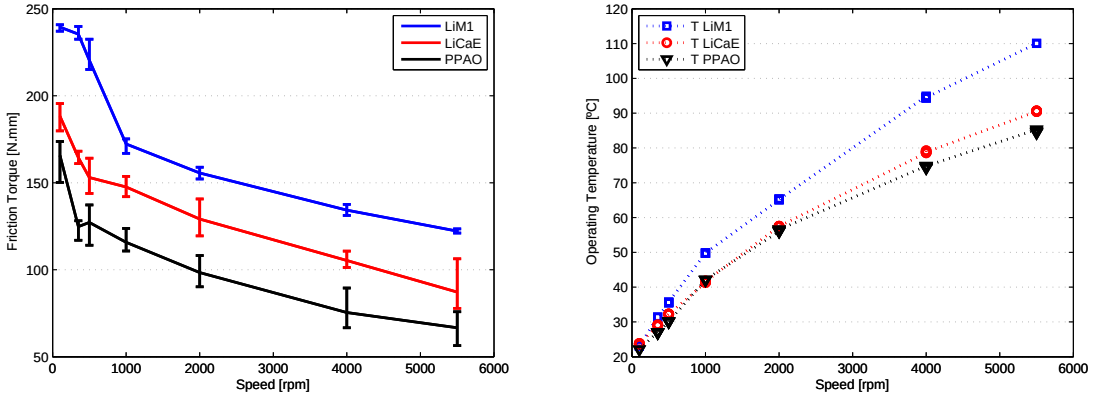

(a) (b)

Figure 6.4.: (a) Friction and (b) operating temperature versus rotational speed

lowest ones to the polymeric grease (PPAO), whereas the ester-based grease (LiCaE) presented temperatures between the other two, which is in agreement with the friction torque measurements. In fact, under the same operating conditions and constant surrounding temperature, a higher bearing friction torque generates higher power loss, higher bearing operating temperatures, and, consequently a greater evacuation of heat to the surrounding area.

Bearing friction torque values are significantly different between the greases for the entire operating speed range. At 2000 rpm for example, the bearing friction torque and the operating temperature of the LiM1 were 59.4 % and 16.5 % higher than for polymeric grease PPAO, respectively.

Friction torque behaviour is the sum of several sources of friction and this will be discussed in the next section by means of the new SKF friction torque model.

6.4. Friction torque - SKF Model

The bearing friction torque model developed by SKF [6, 8] separates the friction torque in the true physical sources of friction, namely the rolling torque (M_{rr}), the sliding torque (M_{sl}), the mechanical drag torque (M_{drag}) and the torque loss on the seals (M_{seal}), as shown in Equation 6.1,

$$M_t = \varphi_{ish} \times \varphi_{rs} \underbrace{\left(G_{rr}(n \times \nu)^{0,6}\right)}_{M_{rr}} + \underbrace{\left(G_{sl} \times \mu_{sl}\right)}_{M_{sl}} + \underbrace{\left(V_M \times K_{ball} \times d_m^5 \times n^2\right)}_{M_{drag}} + \underbrace{\left(K_{S1} \times d_s^{\beta} + K_{S2}\right)}_{M_{seal}} \tag{6.1}$$

As THBB 51107, however, has no seals and its drag loss is zero in the case of grease lubrication, M_{seal} and M_{drag} torque loss terms can be disregarded. Thus, the total internal friction torque expressed in Equation 6.1 can be summarized to Equation 6.2 for a grease lubricated THBB 51107.

$$M_t = \varphi_{ish} \times \varphi_{rs} \underbrace{\left(G_{rr}(n \times \nu)^{0,6}\right)}_{M_{rr}} + \underbrace{\left(G_{sl} \times \mu_{sl}\right)}_{M_{sl}} \tag{6.2}$$

The full explanation of the model for a THBB 51107 is given in Appendix B, which summarizes the information available in [6, 8].

TSKF bearing friction torque predictions are compared to the experimental measurements in Figure 6.5(a). The predictions were carried out using the **base oil** kinematic viscosity, as shown in Figure 6.5(b) and data from Table 6.2.

As the friction torque predictions (continuous lines) exceeded by far the measured values (dashed lines) for most of the operating conditions, a different application

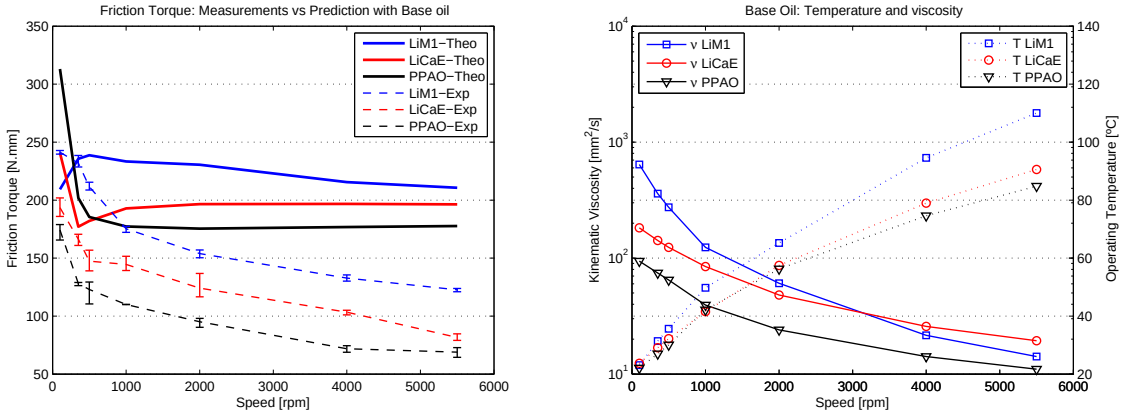

(a) (b)

Figure 6.5.: (a) Friction torque measurements and predictions versus rotational speed; (b) Operating temperature and base oil kinematic viscosity versus rotational speed.

Table 6.2.: SKF parameters for bearing friction torque predictions [8].

Parameters	Units	Value
Krs	-	6×10^{-8}
Kz	-	3.8
R_1	-	1.03×10^{-6}
S_1	-	1.60×10^{-2}
Fa	N	6867
D	mm	52
d	mm	35
d_m	mm	43.5
G_{rr}	-	0,1211
G_{sl}	-	2521.9
μ_{bl}	-	0.15
μ_{EHL} mineral oils	-	0.05
μ_{EHL} synthetic oils	-	0.04

of the model is suggested. This consists of calculating the coefficient of friction in full film conditions (μ_{EHL}) instead of using the constant value recommended for the model (see μ_{EHL} in Table 6.2), as it is well known that μ_{EHL} depends on the operating conditions and lubricant properties, as previously shown in Chapter 5.

In order to do so, the sliding torque component (M_{sl}) was calculated using Equation 6.3, where the experimental bearing friction torque is used as input for the total bearing friction torque ($M_t \equiv M_{exp}$) and M'_{rr} is calculated with equation B.6.

$$M_{sl} = M_{exp} - M'_{rr} \tag{6.3}$$

thus providing the following coefficient of friction in full film conditions (μ_{EHL}):

$$\mu_{EHL} = \frac{M_{sl}/G_{sl} - \varphi_{bl} \times \mu_{bl}}{1 - \varphi_{bl}} \tag{6.4}$$

Nevertheless, bearing friction torque measurements were systematically lower than the corresponding predictions (see Figure 6.5(a)), which implies that negative μ_{EHL} values were calculated for some operating conditions; this should not have happened. This led to the analysis of the relative importance of some constants of the model. At first, the internal geometric constants of the THBB 51107 bearing were identified as among the very few types of bearings with "universal" constant values, regardless of the series and type (see constants R_1 and S_1 at Appendix B, Equation B.3 and B.8). This means that R_1 and S_1 values are the same for small bearings such as the THBB 51107, as well as for medium and large size bearings.

Further analysis of R_1 and S_1 values was made by running new bearing tests with fully formulated mineral, PAO and ester oils, for which the corresponding traction curves under full film lubrication were known under similar operating conditions. The bearing friction torque model was then run with known traction data for μ_{EHL}, and R_1 and S_1 were optimized on the basis of a best R^2 fit between the friction torque measurements and the friction torque model. This produced R_1 and S_1 values of about 21.1 % lower than the ones shown in Table 6.2.

Some simulations with the full SKF friction torque model - Bearing BEACON (not available for end users) were later performed at SKF-ERC in Nieuwegein, The Netherlands[3]. This confirmed that there was a significant difference between the model provided with the SKF General Catalogue GC6000 [8] and the full model (Bearing BEACON), which considers true bearing geometry instead of R_1 and S_1.

The constraints used as inputs in both models are given in Table 6.3 and Figure 6.6. Differences of about 18.5 % for the rolling torque (M'_{rr}) and 37 % for the sliding torque

[3]The author thanks SKF specialist Andriy Rychahivskyy for the calculations he performed with SKF-Bearing BEACON model.

Table 6.3.: Input parameters for friction torque predictions.

Grease thickener	Lithium
Grease base oil	Mineral
Grease additives	EP, AW, AO (fully formulated)
Base oil viscosity at 40 °C	208.5 mm^2/s
Base oil viscosity at 100 °C	17.5 mm^2/s
Load	7 kN

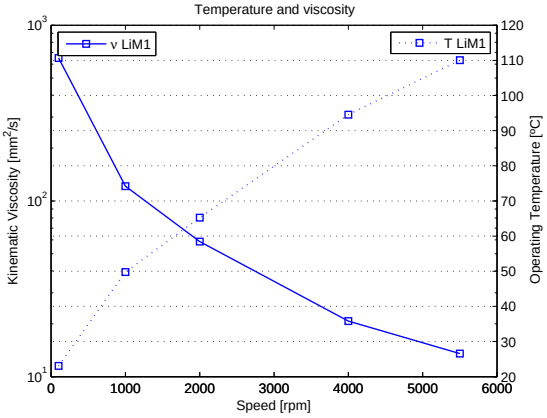

Figure 6.6.: Operating temperature and kinematic viscosity versus rotational speed. Inputs to run SKF Bearing BEACON.

(M_{sl}) were observed, as shown in Figure 6.7. Such differences were nearly constant for the whole range of temperature (thus viscosity) and speed. Other simulations were carried out varying the load, grease types, μ_{EHL} and μ_{sl} values; the same differences were observed.

An analysis of the "Bearing BEACON" results and rolling torque Equation B.6 led to an 18.5 % reduction of geometric constant R_1. That was the only constant in equation B.6that would constantly shift M'_{rr} whatever the other inputs, i.e. a reduction of 18.5 % in R_1 will decrease 18,5 % in M'_{rr}. Likewise, geometric constant S_1 was reduced by 37 %. The changes in geometric constants agree with the fact that THBBs are amongst the very few types of bearings with "universal" constant values and, most likely, should not be so.

According to SKF specialists, any substantial correction to the geometric factors without re-doing the whole fitting procedure to express the true internal geometry of

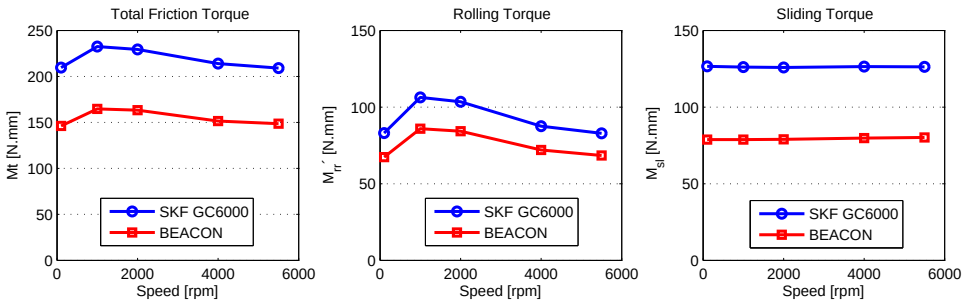

Figure 6.7.: Friction torque versus rotational speed: comparison between the results from SKF BEACON and from SKF GC 6000.

the bearing may ruin the true relation between the internal and external geometry. As the true geometric parameters of the THBB 51107, however, are unknown, the reduction factors proposed for R_1 and S_1 will be used in this work as an approximation.

In addition to changing the geometric constants, bleed-oil properties were used instead of base oil ones because of the evidence presented in Section 4.4. In the case of PPAO bleed-oil, viscosity was measured for each bearing operating temperature as shown in Figure 6.8. The low-shear viscosity was used as input in the model because all the equations where the viscosity is present are related to the lubricant properties in the surroundings of the contact inlet (see Equations B.2, B.4, B.5 and B.10), where the shear rate is very small. Furthermore, the friction torque predictions correlated much better with the measured values when the low-shear viscosity of the bleed-oil was used instead of the base oil viscosity. The replenishment / starvation constant K_{rs} was increased to 11×10^{-8} in order to account for the opened geometry of the THBB 51107, which is more prone to lose oil than sealed rolling bearings.

Finally, the new bearing SKF friction torque model was applied taking the following assumptions into account:

- a 18.5 % reduction of the R_1 parameter;
- a 37 % reduction of the S_1 parameter;
- low shear bleed-oil viscosity instead of low-shear base oil viscosity;
- K_{rs} set to 11×10^{-8};
- μ_{EHL1} calculated according to Equation 6.4 instead of using the constant values given in Table 6.2 (option 1).

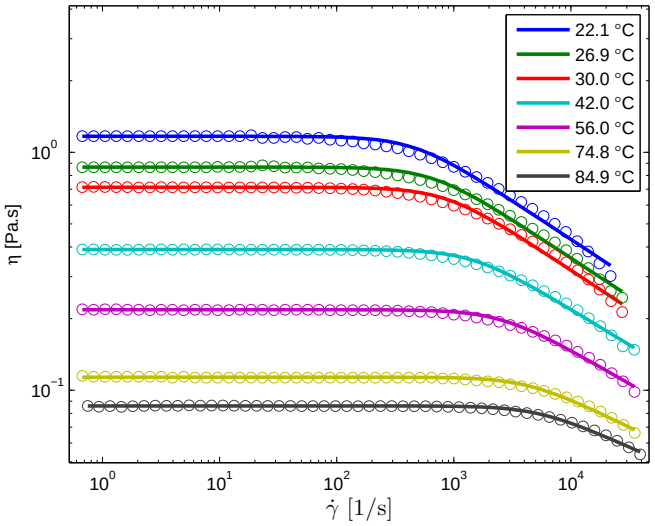

Figure 6.8.: PPAO bleed-oil viscosity versus shear rate. Measured values (markers), Carreau equation 4.10 (lines).

In order to verify whether μ_{EHL1} follows the same trends observed during the traction measurements presented in Chapter 5, a second approach was used to determine rolling bearing friction torque. This consists of using the traction values measured in the WAM tests as input (μ_{EHL2}) in the friction torque model (Equation B.9).

μ_{EHL2} values were extracted from the friction maps presented in Figures 5.3 to 5.5, for all the operating conditions (speed and temperature) in which full film was observed, but only at SRR of 1.3 %, due to the small sliding expected in THBB 51107, as these are most likely in this order of magnitude. These values were therefore interpolated and extrapolated to account for the operating conditions under which the bearing tests were performed (see Equation 6.5). This Equation well described ($R^2 \geqslant 0{,}94$) the experimental observation of the friction maps, i.e., a slight linear decrease of traction values with increasing speeds (n) and a second degree polynomial decrease of traction values with rising temperatures (T). This is better depicted in Figures 6.9 to 6.11, which show friction as a function of speed (n) and temperature(T). The markers indicate the coefficient of friction in full film conditions (μ_{EHL2}) under bearing operating conditions. This approach is only intended to verify whether the coefficient of friction (μ_{EHL1}) obtained from Equation 6.4 follows similar trends to the measured ones, since the operating conditions in which they were obtained differ from the bearing tests in terms of contact geometry and pressure.

$$\mu_{EHL2}(T,n) = a + b \times T + c \times n + d \times T^2 + e \times T \times n \tag{6.5}$$

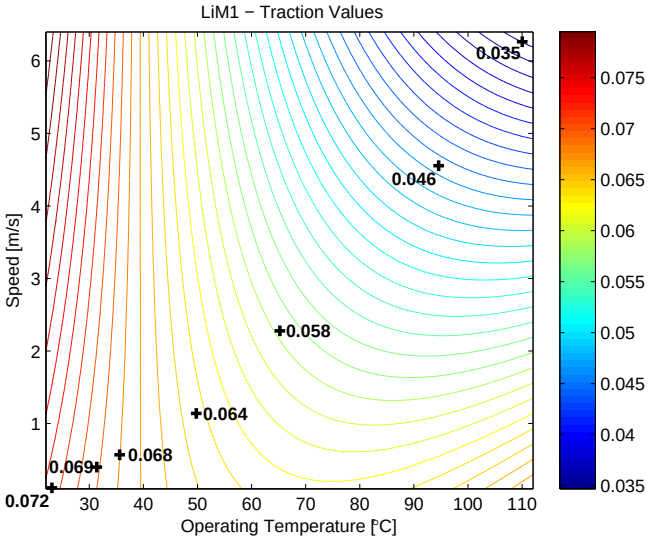

Figure 6.9.: LiM1: μ_{EHL2} values extrapolated from Figure 5.3 with $R^2 = 0{,}94$. The markers represent the μ_{EHL2} for each bearing operating condition.

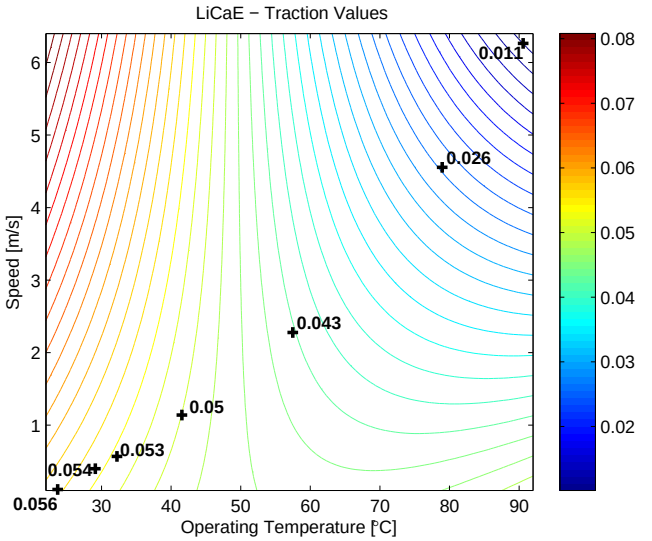

Figure 6.10.: LiCaE: μ_{EHL2} values extrapolated from Figure 5.4 with $R^2 = 0{,}97$. The markers represent the μ_{EHL2} for each bearing operating condition.

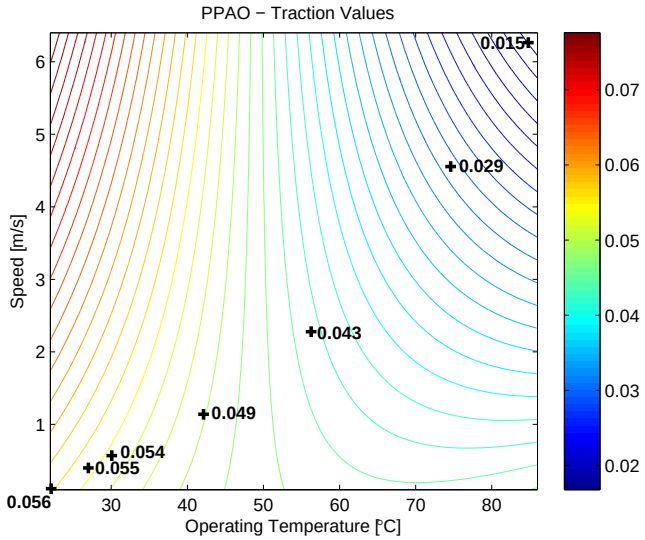

Figure 6.11.: PPAO: μ_{EHL2} values extrapolated from Figure 5.5 with $R^2 = 0{,}97$. The markers represent the μ_{EHL2} for each bearing operating condition.

The lubrication regime should be known in order to obtain a better understanding of the friction torque model results. Therefore, the lubrication quality factor k (used in rolling bearing technology) and the specific film thickness Λ (generally applied in machine design) are determined in Section 6.5, as follows.

6.5. Lubricant film thickness inside the THBB 51107

As discussed in Chapter 4, predicting film thickness in grease lubricated ball bearings is a major challenge and still not well known. The following assumptions were considered for such predictions:

- lubricant film is characterized by the bleed-oil oil properties (initial stage of grease lubrication);
- LiM1 and LiCaE bleed-oils are considered Newtonian and PPAO bleed-oil is considered non-Newtonian;
- LiM1 and LiCaE bleed-oil viscosities vary with temperature according to ASTM D314, Equation 2.4;
- PPAO (non-Newtonian) dynamic bleed-oil viscosities were measured at each bearing operating temperature (see Figure 6.8);

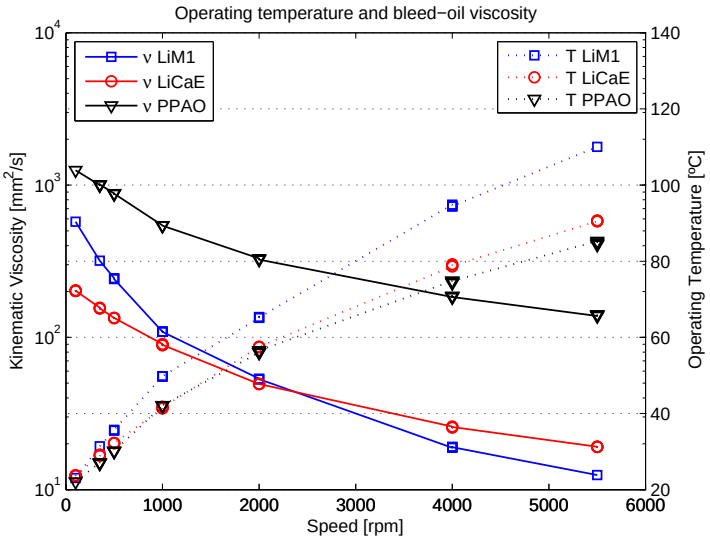

Figure 6.12.: Operating temperature and bleed-oil kinematic viscosity versus rotational speed.

- The measured pressure-viscosity coefficient (α) was extrapolated for different viscosities according to Gold *et al.* [60];

LiM1 and LiCaE bleed-oil dynamic viscosity measurements were carried out at 40°C and 80 °C as described in Section 3.8.1. From that, the kinematic viscosities were calculated using Equation 2.2. Equation 2.4 was then used to obtain the bleed-oil viscosity at each bearing operating temperature. PPAO bleed-oil viscosity was measured with a Physica MCR 301 - Anton Paar rheometer, smooth parallel plates with 50 mm diameter (geometry PP-50) and a 0.2 μm gap for all bearing operating temperatures, as shown in Figure6.8. From that, the kinematic viscosities were calculated with Equation 2.2, using the low-shear viscosity values (average ν for $\dot{\gamma}$ <10^2 s^{-1}). It was also noted that the low-shear viscosity of PPAO bleed-oil also varies with temperature according to ASTM D314.

The bleed-oil viscosity and operating temperature values versus the bearing rotational speeds are shown in Figure 6.12.

The pressure-viscosity coefficient values (α_{film}) of all bleed-oils were calculated from the film thickness measurements at ≈ 40, 60 and 80 °C and are given in Table 4.4. From that, a Gold-like equation [60] was used to extrapolate the pressure-viscosity coefficients for each bearing operating viscosity.

$$\alpha_{bear} = s \cdot \nu^t \tag{6.6}$$

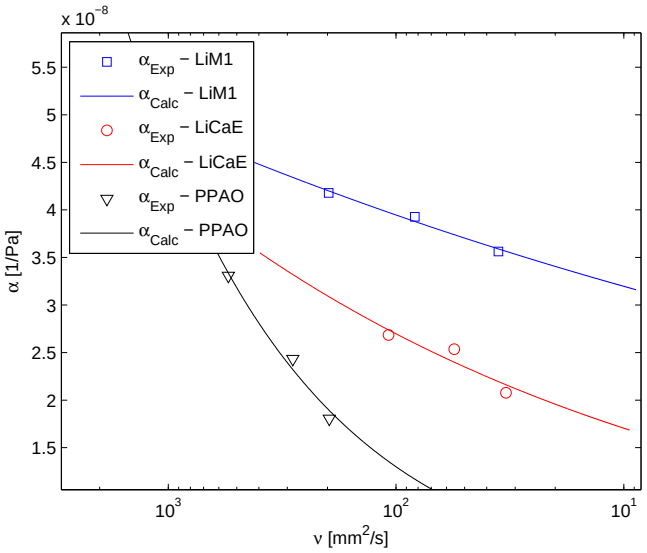

Figure 6.13.: Pressure-viscosity coefficient versus operating viscosity calculated from the film thickness measurements (markers) and extrapolated with Eq. 6.6 (continuous lines).

where ν is the bearing operating kinematic viscosity in mm^2/s and s and t are constants determined on the basis of a best $\mathbf{R}^2$ fit with the α_{film} in GPa. The variation of the pressure-viscosity coefficient with the operating viscosity is shown in Figure 6.13 and the values of s and n are given in Table 6.4.

Table 6.4.: Parameters n and t for all bleed-oils.

Bleed-Oil	s	t
LiM1	25.89	0.092
LiCaE	10.78	0.199
PPAO	1	0.556

The dynamic viscosity and the pressure-viscosity coefficient of the bleed-oils shown in Figure 6.14 were then used to calculate film thickness in the THBB 51107. LiM1 and LiCaE film thicknesses were predicted with Equation 4.7 (Hamrock *et al.*) and PPAO film thickness with Equation 4.9 (Katyal and Kumar). Moreover, as Equation 4.9 was developed for pure rolling point contacts, Katyal and Kumar [130], based on their previous works [203–205], claimed that sliding adds only little to the extend of film-thinning observed with pure rolling. Greenwood and Kauzlarich [125] observed that shear affects the central film thickness of point and line contacts similarly, there-

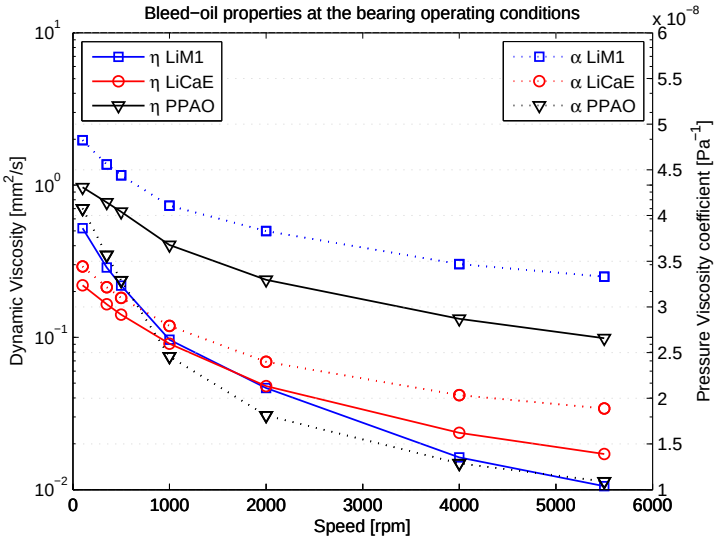

Figure 6.14.: Dynamic viscosity and pressure-viscosity coefficient versus rotational speed.

fore use of Equation 4.9 9 when little sliding is expected (as in the case of THBB 51107) and for elliptical contacts, will present a reasonable approximation of the film thickness. Tables 6.1 and 6.5, and Figure 6.14 provide the necessary parameters for performing film thickness calculations.

Finally, the specific film thickness Λ in the centre of the contact was calculated with Equation 6.7. The ball and race roughness ($\sigma_{ball}, \sigma_{race}$) are given in Table 6.1.

$$\Lambda = \frac{H_{oc}}{\sigma_c}; \qquad \sigma_c = \sqrt{\sigma_{race}^2 + \sigma_{ball}^2} \tag{6.7}$$

The specific film thickness Λ is shown in Figure 6.15. This indicates that the lubrication regime according to which the bearing is operating is mostly full film lubrication ($\Lambda > 1$). The lubrication regime in the friction torque model is related to the weighting factor for the sliding friction coefficient (φ_{bl}), which is given by equation B.10 and shown in Figure 6.16. As described in Appendix B, when $\varphi_{bl} \rightarrow 0$ the lubrication regime tends to full film lubrication, and when $\varphi_{bl} \rightarrow 1$ the lubrication regime tends to boundary lubrication.

Figures 6.15 and 6.16 show that Λ and φ_{bl} are in good agreement. Mostly, Λ >1 and the $\varphi_{bl} \rightarrow 0$ (full film), with an exception at 100 rpm, where LiCaE showed $\Lambda \approx$1.22 and $\varphi_{bl} \approx 0.22$, and PPAO showed $\Lambda \approx$0.61 and $\varphi_{bl} \approx 0$.

There is another lubrication quality factor often used for rolling bearings - viscosity ratio k. This is calculated with Equation 6.8,

Table 6.5.: Geometric and material parameters of the THBB 51107 for film thickness prediction.

	Ball	Raceway
R_x [m]	$3{,}0 \times 10^{-3}$	∞
R_y [m]	$3{,}0 \times 10^{-3}$	-3.3×10^{-3}
E [Pa]	$2{,}1 \times 10^{11}$	2.1×10^{11}
ν [-]	0.29	0.29
SRR [%]	1.3	

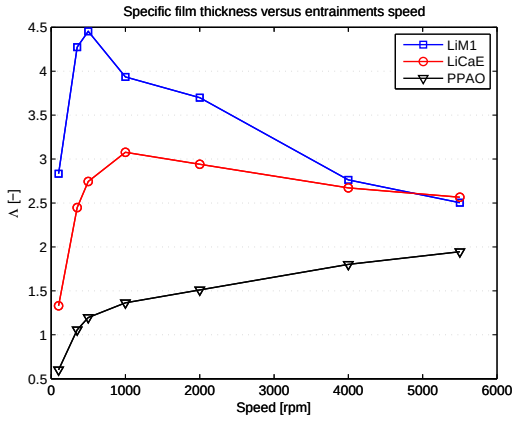

Figure 6.15.: Specific film thickness versus rotational operating speed.

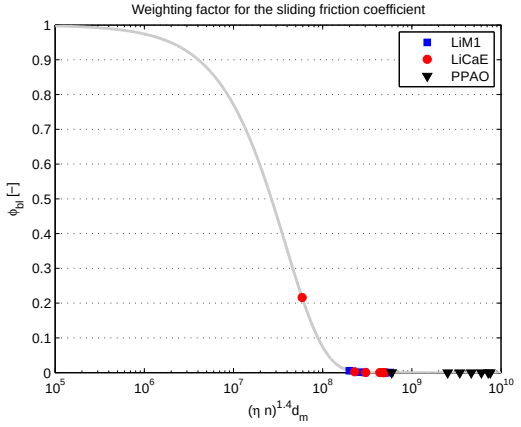

Figure 6.16.: Weighting factor for the sliding friction coefficient (φ_{bl}) versus rotational speed.

$$k = \frac{\nu}{\nu_1} \tag{6.8}$$

where ν is the actual operating kinematic viscosity in mm^2/s and ν_1 is the rated kinematic viscosity depending on the mean diameter of the bearing and rotational speed. ν_1 was obtained from SKF website [206] and ν is considered the low-shear kinematic viscosity. Figure 6.17 shows viscosity ratio k versus rotational speed for all lubricating greases.

Viscosity ratio k is also in close agreement with φ_{bl} for most of the operating conditions. The discrepancies between Λ and k in the case of PPAO are due to the PPAO's shear thinning behaviour, which is not considered in the viscosity ratio k, but in the specific film thickness Λ.

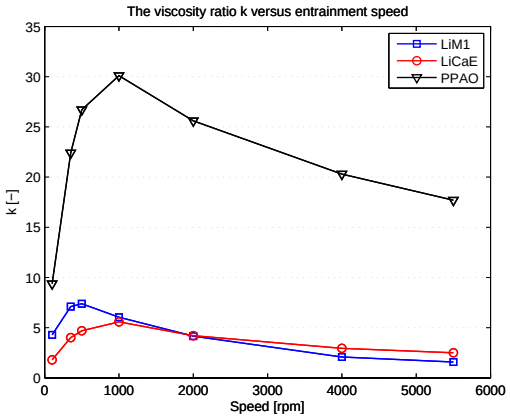

Figure 6.17.: Viscosity ratio versus bearing operating speed.

6.6. Friction torque model results

The results obtained from the model (after the proposed changes) are compared with the measured values in Figures 6.18 to 6.20 for the lubricating greases LiM1, LiCaE and PPAO, respectively. Each figure shows the measured friction torque with deviations (M_{exp}), total friction torque, rolling torque and sliding torque predicted using the traction coefficient calculated with Equation 6.4 (M_{teo-1}, M'_{rr-1}, M_{sl-1}), and total friction torque, rolling torque and sliding torque predicted with the traction coefficient measured at WAM (M_{teo-2}, M'_{rr-2}, M_{sl-2}).

Application of the model using the traction coefficients measured in the WAM tests (μ_{EHD2}) presented very similar results to the ones obtained when μ_{EHD1} was calculated with equation 6.4, and both predicted quite well the friction torque measurements. This may indicate that traction coefficients measured under similar operating

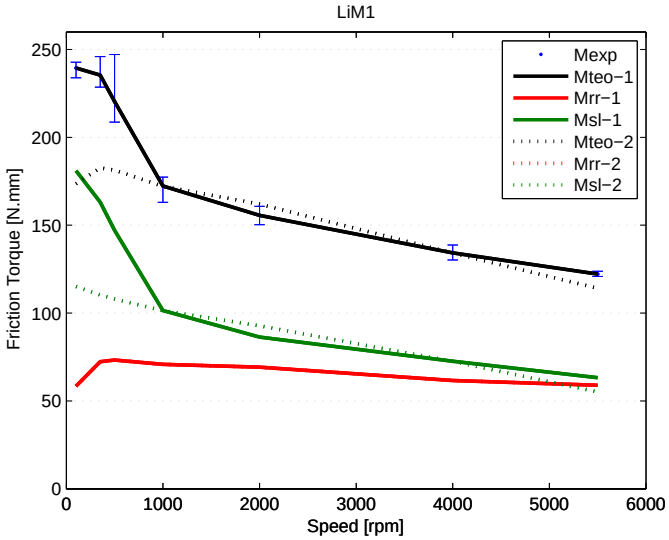

Figure 6.18.: LiM1: Measured and predicted rolling bearing friction torque versus rotational speed.

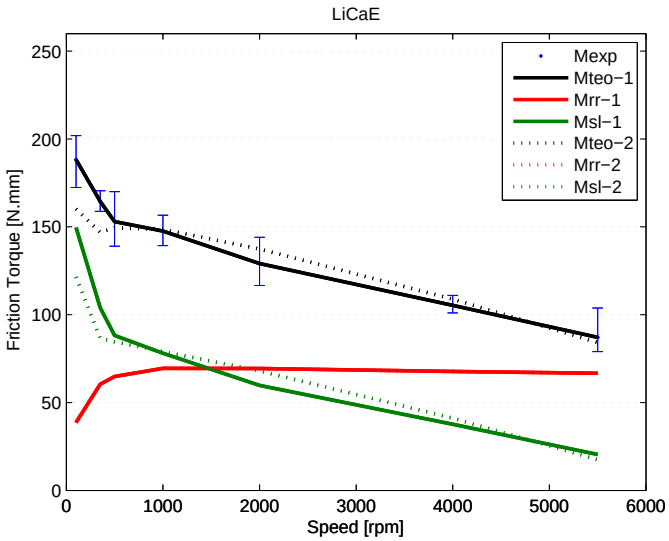

Figure 6.19.: LiCaE: Measured and predicted rolling bearing friction torque versus rotational speed.

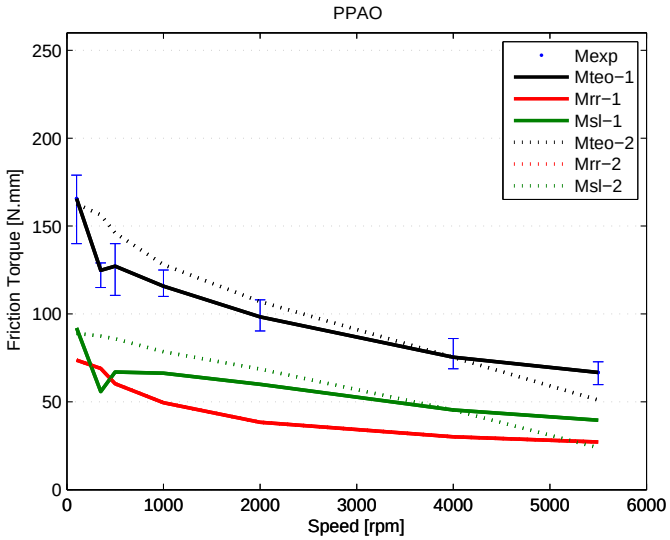

Figure 6.20.: PPAO: Measured and predicted rolling bearing friction torque versus rotational speed.

conditions in a ball-on-disc device could be used, as a rough approximation, as input in the bearing friction torque model for a THBB 51107.

The divergence between measurements and predictions at low speeds in the case of LiM1 grease (see Figure 6.18)suggests that the rolling bearing was operating under mixed or boundary lubrication, although the weighting factor calculated, specific film thickness and viscosity ratio, shown in the Figures 6.15 to 6.17, indicate full film condition.

Friction sources M'_{rr} and M_{sl} are governed by different factors. The rolling torque (M'_{rr} Eq, B.6) is mainly dependent on the bleed-oil viscosity at the operating temperature, on the operating speed and on the replenishment of the contact (φ_{rs}), while the sliding torque (M_{sl} Eq. B.7) is mainly dependent on the weighting factor (φ_{bl}) and on the friction coefficient in full film EHL lubrication (μ_{EHL}). These two source of friction losses (M'_{rr} and M_{sl}) are analysed in the following sections.

6.6.1. Rolling torque - M'_{rr}

Figure 6.21 shows that rolling losses grow from zero (at zero speed) and become very quickly dominant, with maximum values at about 350 - 1000 rpm depending on the lubricating grease. Such an increase is related to the increase in film thickness (see Figures 6.15 and 6.17). As speed increases further, rolling friction decreases because of kinematic starvation (φ_{rs}) and/or inlet shear heating (φ_{ish}) becomes relevant. A high decrease of the M'_{rr} with increasing speed indicates the use of an excessively high viscosity grease in the application.

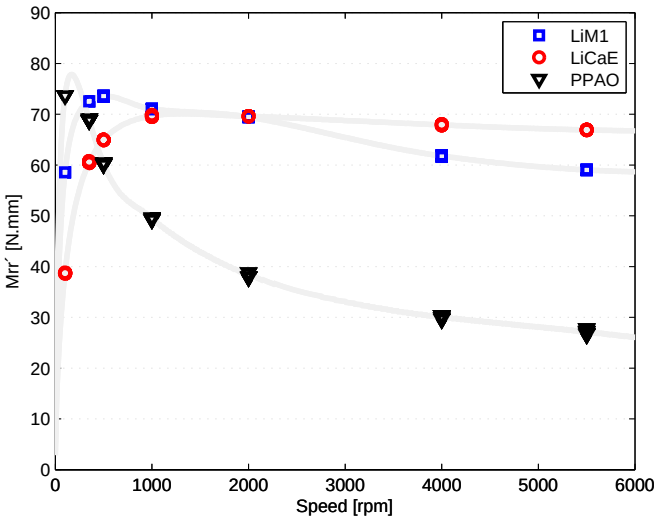

Figure 6.21.: Rolling Torque ($M_{rr'}$) versus rotational speed.

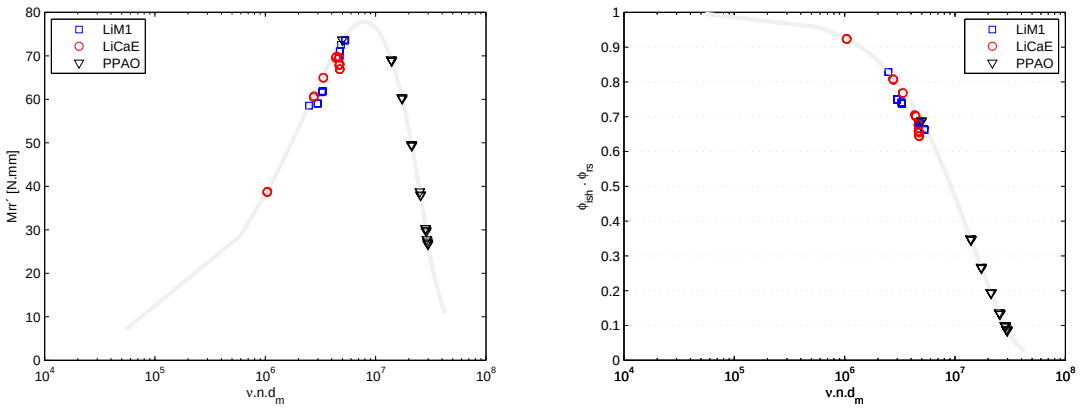

(a) (b)

Figure 6.22.: (a) Rolling Torque ($M_{rr'}$) and (b) Reduction factors product ($\varphi_{rs} \times \varphi_{ish}$) versus the parameter ($\nu \times n \times d_m$).

The influence of the reduction factors φ_{rs} and φ_{ish} in the rolling torque component (M'_{rr}) is better observed in Figure 6.22. Figure 6.22(a) compares rolling friction torque M'_{rr} to the operating parameter $\nu \times n \times d_m$ and the Figure 6.22(b) shows the product $\varphi_{rs} \times \varphi_{ish}$ compared to the same operating parameter. These figures clearly show that $\varphi_{rs} \times \varphi_{ish}$ strongly influences the rolling torque. In the case of PPAO grease, $\nu \times n \times d_m \geqslant 10^7$, thus $\varphi_{rs} \times \varphi_{ish} \leqslant 0,5$; consequently, the rolling torque is reduced by a factor $\geqslant 2$.

6.6.2. Sliding torque - M_{sl}

Figure 6.23 shows (M_{sl1}) and (M_{sl2}) versus rotational speed, respectively. At low speeds, there is a small area of high sliding loss, due to asperity interaction; very quickly the sliding losses decrease as the film increases at rates of about 350 - 1000 rpm depending on the lubricating grease. After that, as speed continues to rise, the M_{sl} alters its trend for a lower decrease rate with entrainment speed. In this last stage full film has already been reached and the decreasing sliding torque values with speed are due to increasing temperatures, which reduces the μ_{EHL} as shown in Chapter 5.

The sliding torque (M_{sl}) shows a direct relationship with the coefficient of friction in full film conditions (μ_{EHL}), since the weighting factor (φ_{bl}) is nearly zero for all lubricating greases in most of the operating conditions (see Figure 6.16). Such relationship is seen when comparing Figures 6.23 with 6.24.

Close to the boundary regime ($k \leqslant 2$) the weighting factor (φ_{bl}) increases considerably, the boundary friction coefficient (μ_{bl}) gains importance and the sliding torque increases. This explains why LiCaE M_{sl1} is high at 100 rpm, whilst μ_{EHD1} is not high.

The discrepancies between μ_{EHD1} and μ_{EHD2} (hence M_{sl1} and M_{sl2}) are not easily explained. First, there is an uncertainty about the lubrication regime in which the bearing is operating. Second, it is evident that the traction values measured at WAM (μ_{EHD2}) should not be directly applied in the model due to the differences of the contact geometry, centrifugal forces, over-rolling periods and operating conditions. On the other hand, although the approach presented for predicting the rolling bearing friction torque needs some improvements, its predictions were in very good agreement with the measured torques, as shown in Figures 6.18 to 6.20. Furthermore, the boundary coefficient of friction, which was also considered constant ($\mu_{bl} = 0{,}15$), may be influenced by boundary layers of thickener or additives.

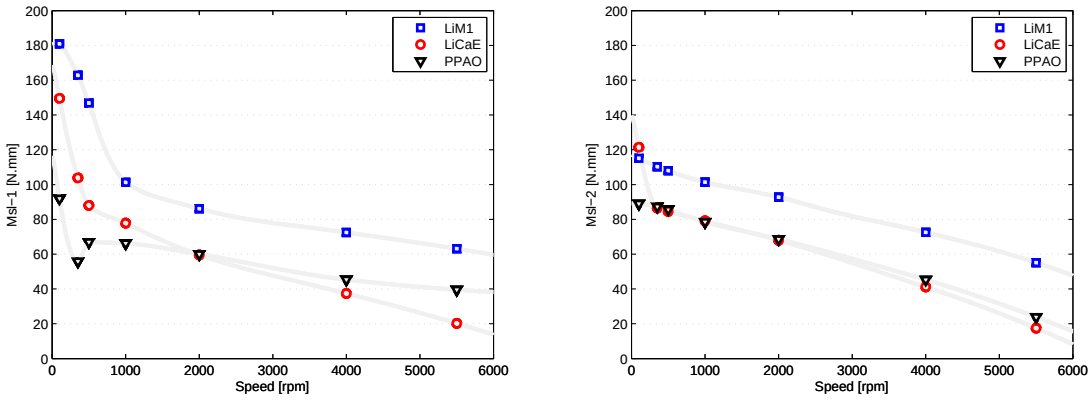

(a) (b)

Figure 6.23.: (a) Sliding Torque - M_{sl1} and (b) M_{sl2} versus versus rotational speed.

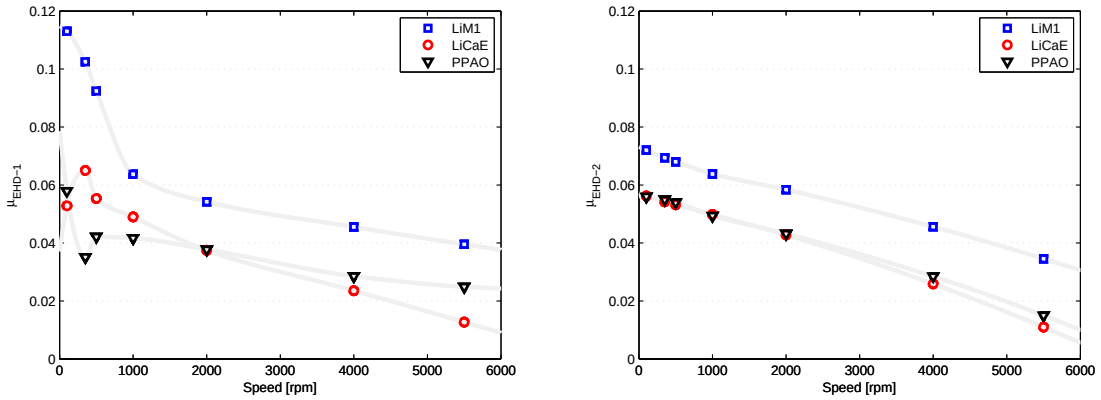

(a) (b)

Figure 6.24.: (a) μ_{EHL1} and (b) μ_{EHL2} versus versus rotational speed.

6.7. Discussion and conclusions on rolling bearing friction torque

Grease formulation and particularly, the interaction between thickener, base oil and additives (bleed-oil), can significantly influence contact replenishment/starvation (φ_{rs}), inlet shear heating effect (φ_{ish}), the lubrication regime (φ_{bl}) and thus, the rolling ($M_{rr'}$) and sliding friction torque (M_{sl}). This means that two greases with identical base oil types and viscosities, but different thickener and additive packages (or manufacturing processes) may generate bleed-oil with different properties that the base oils and consequently, different rolling and sliding torques.

These conclusions are better supported when a larger number of lubricating greases are compared. Hence, the total bearing friction torques and operating speed measurements of seven (7) different lubricating greases, which were published in a previous work [207], are presented in Figure 6.25. Those measurements were carried out with the same procedures described in Section 6.2; the grease properties are shown at the end of the chapter in Table 6.7.

Figure 6.25 shows the operating temperature (T), operating low-shear bleed-oil viscosity (ν_{bleed}), viscosity ratio (k), total experimental friction torque (M_t), rolling torque (M'_{rr}) and sliding torque (M_{sl}), respectively. The lubricating grease properties are shown in Table 6.7.

Several interesting trends emerged from the analysis of these figures. First, that lubricating greases with the same base oil type (mineral, ester, PAO) showed very similar bearing friction torque values for most of the operating conditions (see Figure

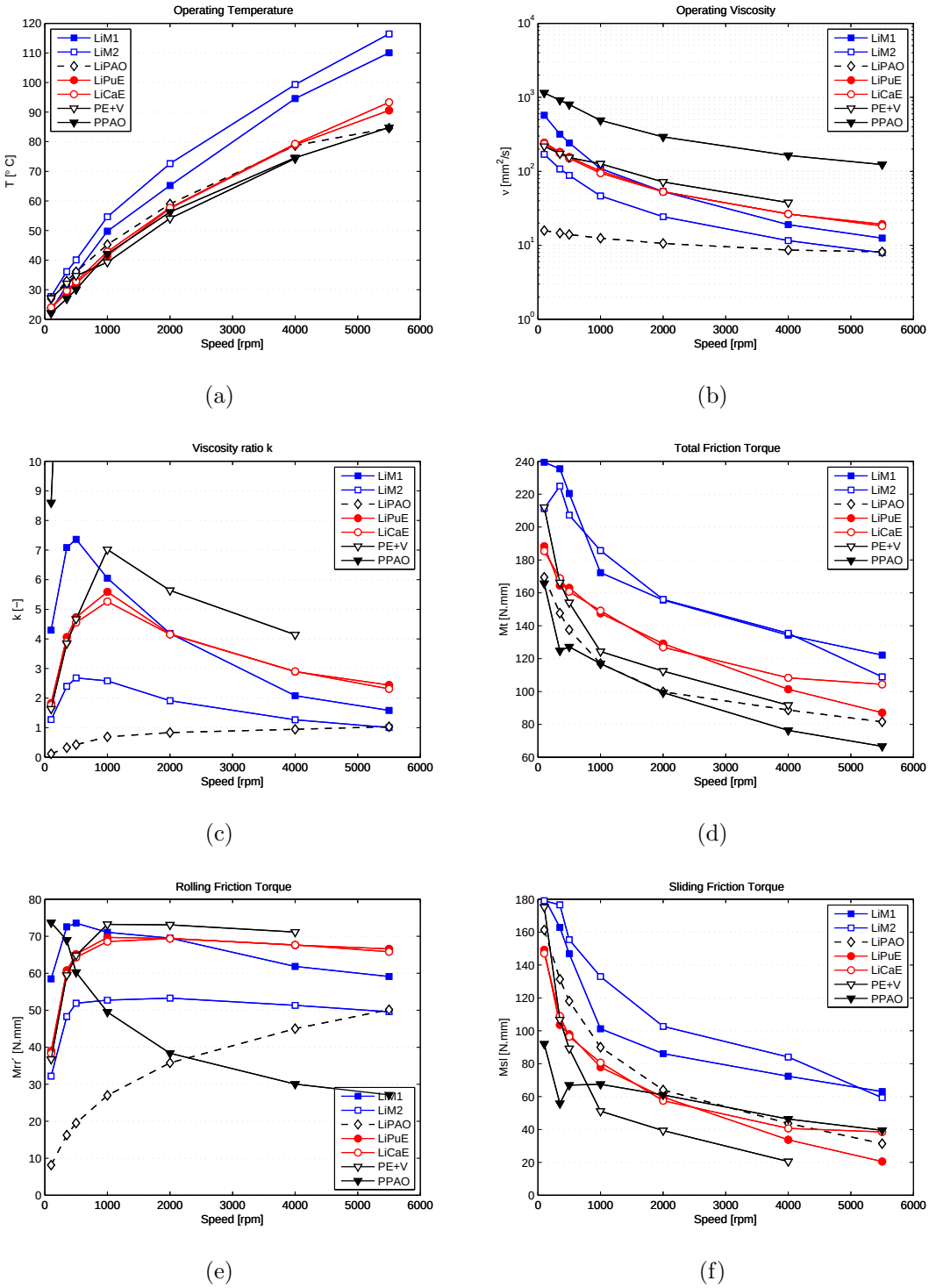

Figure 6.25.: Operating temperature T, bleed-oil viscosity ν_{bleed}, viscosity ratio k, total experimental friction torque $M_t \equiv M_{exp}$, rolling torque M'_{rr} and sliding torque M_{sl} versus rotational speed

6.25(d)), whatever their base or bleed-oil viscosity (Figure 6.25(b)), thickener type or additive package. Second, that the friction torque follows a well defined order of magnitude according to the base oil type, where mineral oils showed the highest friction torque values, followed by ester oils and PAO oils (LiM1>LiCaE>PPAO). From these two findings one might ask: if the total friction torque depends mostly on the base oil type, but the thickener type, additive package and base or bleed-oil properties do not play a major role on the total friction torque, why put so much effort into grease characterization, friction torque models and measurements?

This question is explained by analysing bearing friction loss components (M'_{rr} - Figure 6.25(e) and M_{sl} - Figure 6.25(f)) and their influence on bearing performance in terms of wear and failure. Whether or not viscosity seems to significantly affect total friction torque, it still governs rolling torque by affecting M_{rr}, φ_{rs} and φ_{ish} and sliding torque M_{sl} through φ_{bl}. Table 6.6 clarifies the influence of grease formulation and properties on friction losses. For example, when comparing lubricating greases with the same base oil type but different operating viscosities (LiM1 - LiM2 and LiPAO - PPAO at 1000 and 2000 rpm), different M'_{rr} are obtained. But when comparing lubricating greases with different base oil and thickener types, similar operating viscosities (LiM1-LiCaE-LiPuE at 2000 rpm), similar M'_{rr} are obtained. This shows that the rolling torque is mostly influenced by the operating viscosity of the bleed-oil. Sliding torque on the other hand is barely affected by the operating viscosity when $k > 1$, because in this situation $\varphi_{bl} \rightarrow 0$ and M_{sl} is governed by μ_{EHL}, which is not significantly affected by the viscosity.

In the case of lubricating greases with similar total friction torque (LiM1 - LiM2 and LiPAO - PPAO at 1000 and 2000 rpm), the ones with lower operating viscosity will generate lower films (viscosity ratio k), hence lower rolling torques and higher sliding torques (such as for LiM2 and LiPAO as compared to LiM1 and PPAO, respectively). Rolling bearings running under low film thickness and high sliding torque value conditions are more prone to severe wear.

These conclusions are based on friction torque measurements carried out over a short period of time (< 10 h), where the bleed-oil available for lubricating the contact is most likely abundant (or at least enough) and probably the dominant lubrication mechanism, as verified in Chapter 4. Furthermore, for most of the operating conditions and lubricating greases, the lubrication regime sits on the full film (see Figure 6.25(c)). However, under different operating conditions, where there is not enough oil to ensure full film lubrication (e.g., long tests), friction torque is most likely governed by the thickener-additives-surface interaction and the trends observed may be significantly different.

Table 6.6.: Bleed-oil viscosity, viscosity ratio and friction torque values at 1000 and 2000 rpm.

		LiM1	LiM2	LiPAO	PPAO	LiCaE	LiPuE
1000 rpm	ν [mm^2/s]	108.97	46.50	12.47	487.55	100.63	94.76
	k [-]	6.05	2.58	0.70	27.07	5.58	5.26
	M_t [Nmm]	172.27	185.70	117.00	117.00	147.55	149.15
	M'_{rr} [Nmm]	71.05	52.74	26.98	49.52	69.67	68.55
	M_{sl} [Nmm]	101.22	132.96	90.02	67.48	77.87	80.60
2000 rpm	ν [mm^2/s]	53.31	24.37	10.62	291.70	53.08	52.87
	k [-]	4.18	1.91	0.83	22.89	4.17	4.15
	M_t [Nmm]	155.61	155.99	99.79	99.35	129.12	126.88
	M'_{rr} [Nmm]	69.49	53.27	35.78	38.37	69.43	69.36
	M_{sl} [Nmm]	86.11	102.72	64.02	60.98	59.69	57.52

Table 6.7.: Characterization and properties of seven lubricating greases.

Designation	***LiM1***	**LiM2**	***LiPAO***	***PPAO***	***PE+V***	***LiCaE***	***LiPuE***
Base oil	Mineral	Mineral	PAO	PAO	Ester+veg.	Ester	Ester
Thickener	Li	Li	Li	PP	PP	Li/Ca	Li/Ca-Polyurea
Biodegradability [%]	-	-	-	-	>60	>60	>60
Toxicity [%]	-	-	-	-	>45	>45	>45
Base oil properties							
Specific gravity [g/cm^3]	0.903	0.9	0.9	0.828	0.915	0.952	0.952
Viscosity at 40 °C [mm^2/s]	211	110	30	42.8	32.5	89.9	91.8
Viscosity at 100 °C [mm^2/s]	18.5	9	11.5	8	6.7	15.7	14.5
Bleed oil properties							
Specific gravity [g/cm^3]	0,903	0,9	0.9	0.828	0.915	0.952	0.952
Viscosity at 40 °C [mm^2/s]	186.2	71.9	10.8	529.8	102.8	107.8	86.3
Viscosity at 100 °C [mm^2/s]	16.3	9.3	5.8	84.28	16.7	15.8	14.2
Grease properties							
NLGI Number (DIN 518181)	2	2	2	2	2	2	2
Dropping point [°C]	185	>190	>185	>140	154	>180	>181
Operat. tempe. [°C]	-20 to +130	-30 to +120	-60 to +120	-35 to +120	-25 to +80	-30 to +120	-30 to +120

7. Grease degradation

7.1. Introduction

FFrom the previous chapters, one may conclude that the lubrication mechanism that seems to be dominant in single contact tests and full bearing tests during the first hours of grease life (churning and initial stage of the bleeding phase) under full film conditions is the bleed-oil properties. However, as running time passes, the mechanical and thermal stresses to which the grease is submitted will give rise to several physical, chemical and structural changes to the lubricating grease, which in turn will modify the grease lubrication mechanisms [26, 105, 129]. The lubrication mechanisms at this stage are not well known [17].

One obvious consequence of the running time is the gradual loss of bleed-oil up to the moment that available bleed-oil no longer ensures full film lubrication, after which the thickener-additives-surface interaction will play a significant role on the lubrication process. Oil loss is only one amongst many other changes that occur during grease aging.

Grease aging can be defined as permanent changes in the grease properties. These changes go from simple long storage periods, where oil separation is observed, to severe mechanical and thermal work to which lubricating greases are subjected in rolling bearings. Grease aging depends mostly on its own formulation, bearing type (size, geometry and material), bearing house geometry (free space around the bearing), operating conditions (mainly speed and temperature), wear debris (and other contaminants such as water) and running time, as observed by many researchers [11, 69, 93, 102].

Actual work in this field falls into two categories: analysis of used grease from bearing tests [11, 102, 104, 208, 209] and thermal degradation of bulk grease samples in laboratory tests [26,105,166,210,211]. The lubricating grease samples from bearing tests are, in general, insufficient for performing any tribological test, and therefore grease is only physico-chemically characterized. The thermal degradation of lubricating greases in a laboratory provides large samples suitable for physico-chemical and tribological characterization, but in general, these tests poorly simulate the conditions

within a bearing where thin greae films and mechanical shear stresses are present. Recently, some improved tests were performed on thin films of grease spread on metal surfaces [105], which although closer to the bearing tests, are still unsatisfactory due to the lack of mechanical stress applied to the grease. Further improvements combining thermal/rubbing experiments have been performed with a ball-on-disc device that although it provided a larger amount of grease than that obtained in bearing tests, was still not enough for a complete characterization of the aged grease [212]. Furthermore, the laboratory tests do not attempt to age the lubricating greases on the basis of the degraded grease properties obtained from full bearing tests.

In order to overcome the problem of the small amounts of lubricating greases obtained from bearing tests and the dissimilarity between grease samples from bearing and laboratory tests, a different method/procedure, shown in Appendix C, was developed at SKF-ERC. This method was applied to LiM1, LiCaE and PPAO greases and their fresh and aged performances were compared.

7.2. Aging: Practical approach

Different phenomena occur during the aging process, which can be classified in two main groups - mechanical and chemical.

Mechanical aging promotes oil separation and deterioration of grease thickener structure [17]. It leads lubricating greases to soften (reduction in consistency) or harden (increase in consistency). Grease softening is caused by degradation of the thickener material by shear, and grease hardening is caused by oil loss ("thickener content increase"). These two phenomena occur simultaneously and affect each other. In general, shear degradation effects prevail over oil loss in rolling bearings operating under low temperatures, as suggested by the results presented by Lundberg and coworkers [10, 27, 129, 213]. However, under very long running periods, oil loss (plus wear particles mixed with the grease) may prevail, generating an increase in grease consistency, as already reported by Mas and Magnin [214].

Changes in consistency can be defined by grease rheological properties such as τ_y, G', G'' and $\tau \times \dot{\gamma}$ (see section 3.8), and are related to the oil loss, as measured by the remaining oil percentage method (see section 3.6). IR spectroscopy also qualitatively indicates the oil loss by an increase in the absorbance intensity of the band at 1580 cm^{-1} in relation to the normalised peak at 1460 cm^{-1} for lithium thickened greases [105]. In addition, FTIR technique provides information about thickener breakdown due to shearing, although this is barely perceptible. According to Hurley *et al.* [215], the chain-breaking reactions are characterized by an increase in peak

absorbance intensity at 1377 cm^{-1} in relation to the normalised peak at 1460 cm^{-1}. The decrease in the weight/size of the molecules, due to chain-breaking, facilitates lubricant mobility (softening), but on the other hand, their low weight molecules (formed after breaking) are more susceptible to evaporation (oil loss-hardening).

Chemical aging development on lubricating greases is still not well known. Most of the research work in this field concerns lubricating oils, while information about the role of the thickener on the aging process is rare. It is known that thickener and oil oxidation are not independent problems, since thickener-oil interaction depends on grease constituents (properties and morphology) that change during the aging process.

In spite of the uncertainty as to how oxidation develops in lubricating greases, this is known to promote reaction/consumption of additives, acid formation, thermo-oxidative degradation of thickeners, polymerization of base oils, thermo-oxidative degradation of the base oils and varnish and sludge formation [17].

Consumption of additives (mostly antioxidants at high temperatures) is usually followed by a rapid increase in Total Acid Number (TAN) to the point where antioxidant additives are exhausted [209].

AAntioxidant consumption can be monitored by Fourier Transform Infrared - FTIR, Inductive Coupled Plasma spectroscopy - ICP (ASTM D 5185) and Ruler^{TM} (ASTM D6971), among others. All these techniques used to be applied to the oil extracted from the grease, and some of them can be directly applied to the grease. FTIR for example, presents a reasonable consistency between additive consumption observed in the grease and the extracted oil spectra. Antioxidant consumption used to be observed (and were in this work) in the ranges of 960 - 1020 cm^{-1} and 650 - 690 cm^{-1} for ZDDP [110], at $\approx$ 1515, 1310 and 744 cm^{-1} for amine antioxidants [108,109] and at $\approx$ 1600 cm^{-1} for phenolic antioxidants [106]. Other additives, different from the antioxidants, also react during the aging process and can be monitored using FTIR spectroscopy.

As antioxidants are being exhausted, a number of chemical reactions leads to the formation of a series of oxidation products depending on the grease formulation. The main oxidation products of lubricating greases are aldehydes, ketones and alcohols, which may be further oxidized to give rise of carboxylic acid. These oxidation products are observed by FTIR in the bands of 1740-1725 cm^{-1}, 1725-1705 cm^{-1}, 1200-1050 cm^{-1} and 1725-1700 cm^{-1}, respectively [69].

The main grease changes observed with FTIR after the aging process are summarized below.

- Increase in intensity of the thickener band (Lithium 1580 and 1560 cm^{-1}, Calcium $\approx$ 872 and 712 cm^{-1} and Polypropylene 2722, 998 and 972 cm^{-1}) in comparison with the peak at 1460 cm^{-1}. This is attributed to an increase in the thickener/oil ratio caused by oil loss due to bleeding or evaporation of short chain, volatile hydrocarbons from the base oil [215].

- Increased thickener content is also apparent by the appearance of a shoulder (or doublet at 1451 cm^{-1}) at the peak at 1456 cm^{-1} peak in the bulk lithium grease spectrum. This is due to an increase in the contribution of the soap band (1451 cm^{-1}) and a reduction in the contribution of the base oil band (1461 cm^{-1}), as described in Section 3.7. The larger the increase in the thickener content, the more prevalent the thickener band ($\approx$ 1451 cm^{-1}) and the less pronounced the base oil band at 1461 cm^{-1}.

- The decrease in intensity at 1560 cm^{-1} denotes some breakdown of the thickener structure. This is usually accompanied by a shift to higher frequencies of the 1580 cm^{-1} peak. During thin-film aging experiments, however, this is hardly noticeable due to the increased evaporation of the base oil [103]. Grease breakdown is also related to a decrease in the intensity of the peaks in the region of 2853-2953 cm^{-1}, which is attributed to the breaking of C-H and C-C long chains and to the increasing in the CH_3/CH_2 ($\approx$ 1377/1460 cm^{-1}) ratio [215].

- There is also a slightly decrease in the broad -OH group absorbance centred at around 3330 cm^{-1} that is most likely caused by the evaporation of water trapped in the thickener during the manufacturing process [216].

- The broadening and increase in intensity in the region of 3700-3000 cm^{-1} is probably caused by O-H vibrations of hydroxyl groups in the thickener, by alcohol species from the oxidation reaction or by water contamination [71, 102, 104, 217].

- Decrease in the intensity of the peaks related to the additive package due to additive depletion/reaction are observed at the $\approx$ 1515, 1310 and 744 cm^{-1} bands, which are most likely amine antioxidants [108,109]; at 1747 cm^{-1}, which is a carbonyl (C=O) of the ester group and often used in AW additives; at 1710 cm^{-1}, which is often used as an EP/AW additive and signed as Bismuth; at 1600 cm^{-1}, which is attributed to phenolic antioxidants [106, 107]; at $\approx$ 1162 cm^{-1}, which used to be used as viscosity improver [106] and at $\approx$ 1004 cm^{-1}, ZDDP, which also acts as antioxidant [11, 110].

- The rise of a broad absorbance band between 1750 - 1685 cm^{-1} due to the presence of a range of oxidation products such as esters (1750-1725 cm^{-1}), aldehydes (1740-1725 cm^{-1}), ketones (1725-1705 cm^{-1}), carboxylic acids (1725-1700 cm^{-1}), alcohols (1200-1050 cm^{-1}) [218] and the formation of other carbonyl species [102, 219].

7.3. Results: Comparison between aged and fresh greases

All the techniques and experiments applied to the fresh lubricating greases in the Chapters 3 to 6 were also applied to the AGED samples; their comparison is presented in the sections that follow.

7.3.1. FTIR

7.3.1.1. LiM1

Figure 7.1(a) shows the infrared spectra of aged and fresh LiM1 grease samples. As described in section 3.7, all spectra were normalized to the CH_2 peak at approximately 1460 cm^{-1} in order to prevent disparities between spectra due to different sample thicknesses.

No formation of oxidation products (arising from peaks in the 1750-1700 cm^{-1} range) was observed, which indicates that grease LiM1 was not or just slightly oxidised. A chemical reaction observed in the spectra was a decrease in the absorbance intensity of the -OH grouped centred around the 3330 cm^{-1} band. This was probably caused by a dehydration of the thickener, as it is known that lithium-12-hydroxysteared dehydrates over a temperature range of 110 and 170 °C [216].

Fresh and aged thickener and bleed-oil samples were also analysed in order to determine where the oxidation products remained (oil or thickener) and obtain a better observation of additive depletion.

Figure 7.1(b) shows the IR spectra of fresh and aged extracted oil from LiM1 grease samples. Only few changes were observed. This indicates that the extracted oil was not or just slightly oxidised. One of the differences was indicated by a slight increase of the 1740 cm^{-1} band caused by oxidation products such as aldehyde (1740-1725 cm^{-1}) and ester (1750-1725 cm^{-1}). The other was related to the decrease in the peaks at 1600, 1516, 1164 and 1004 cm^{-1}, which are attributed to additive consumption.

Figure 7.1(c) shows the IR spectra of the thickener extracted from fresh and aged LiM1 grease. Due to the solid state of the thickener sample, the IR spectra had to be collected in "reflectance mode" instead of the absorbance mode. Consequently, the IR spectra are presented in $Log(1/R)$, which is equivalent to absorbance.

The most noticeable differences were the decrease of several peaks in the 1150-1000 cm^{-1} region and a considerable reduction in peak width and intensity at $\approx$ 3335 cm^{-1}, which was attributed to thickener dehydration. The absence of peaks in the oxidation products region indicates that the thickener was not oxidised.

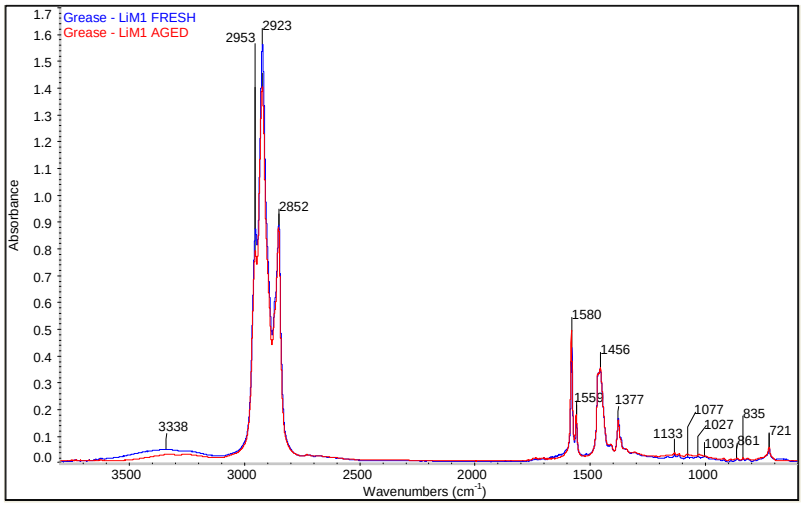

(a)

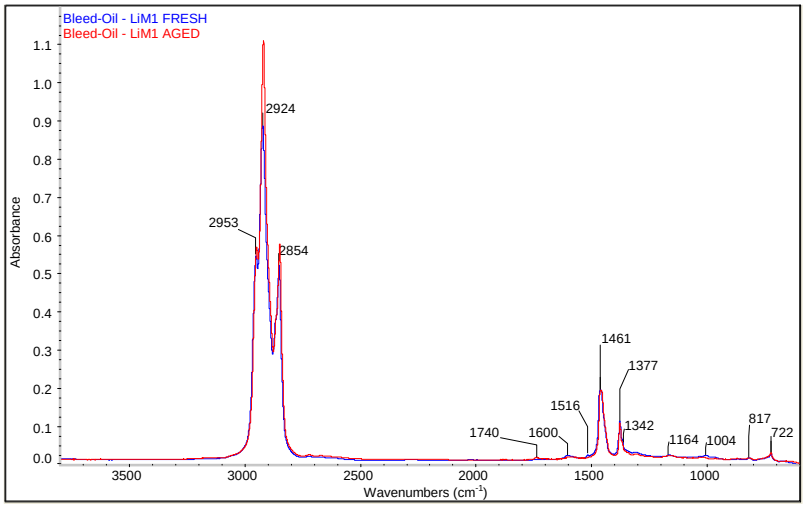

(b)

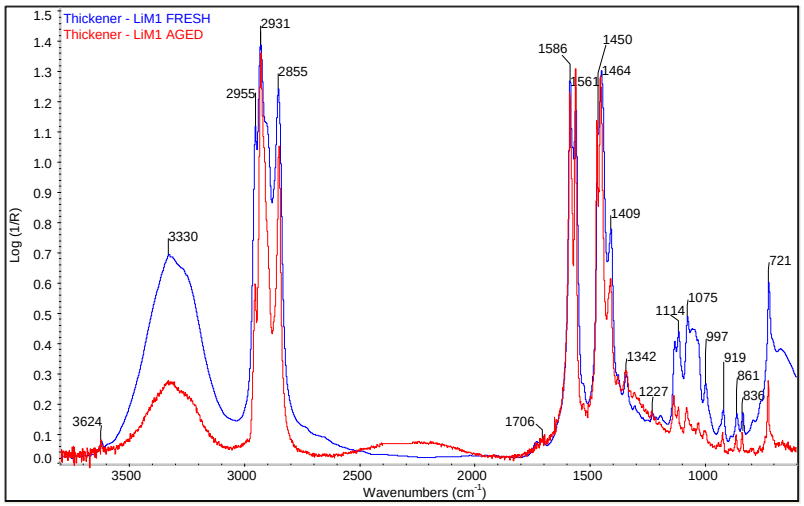

(c)

Figure 7.1.: (a) Grease, (b) Bleed-oil and (c) Thickener spectra.

7.3.1.2. LiCaE

Figure 7.2(a) shows the spectra of the fresh and aged LiCaE grease samples. The oxidation products of the LiCaE were not seen at the same ranges of the LiM1 grease. Here, the main signs of oxidation were the increase of the base line at the 1900-800 cm^{-1} range, broadening of the 1740 and 1460 cm^{-1} bands and increase in intensity of absorbance of the 1239 and 1165 cm^{-1} ester peaks [220].

The IR spectra show changes in thickener concentration due to a relative decrease in intensity of the lithium peak at 1580 cm^{-1} and an increase in the calcium peak at 872 cm^{-1} with a normalized peak at approximately 1460 cm^{-1}. This suggests a breakdown of the lithium thickener structure and a relative increase in the calcium content due to oil loss. An increase in the CH_3/CH_2 (1377/1460 cm^{-1}) absorbance band ratio was noted, which indicates chain-scission reactions [215].

TThe aged LiCaE grease spectrum presented moderate to high levels of oxidation, which is depicted by the significant increase in the base line, broadening and increase in intensity around 3700-3000 cm^{-1}, height increase at 1240, 1165 cm^{-1}, and broadening of the 1740 cm^{-1} and 1460 cm^{-1} bands. Such differences were probably due to the oxidation products of several different structures, such as esters, ketones, alcohols, and so forth. Absorbance around 3700-3000 cm^{-1}, characteristic of hydroxyl groups and possibly indicating the presence of a hydroperoxide group, corroborated the increase in intensity of the 925-1060 cm^{-1} band [221].

Figure 7.2(b) shows the IR of the oil extracted from the fresh and aged grease samples. As opposed to LiM1 bleed-oil, LiCaE blood-oil was is oxidised. This is seen by the increasing height of the 3467, 1417, 1240 cm^{-1} bands and the broadening of the peak at 1740 cm^{-1}. Peaks at 1602 and 1517 cm^{-1} were reduced in the aged spectrum due to additive depletion.

Figure 7.2(c) shows the IR spectra of the fresh and aged thickener. Several chemical changes were observed around 1800-600 cm^{-1}. The most noticeable differences were broadening and increase in intensity of the 1741, 1243 and 1170 cm^{-1} bands and the concomitant increase in the 1300-900 cm^{-1} region. It is not clear whether those changes were due to thickener aging or to the oxidised ester oil, which may have remained together with the thickener during the separation process.

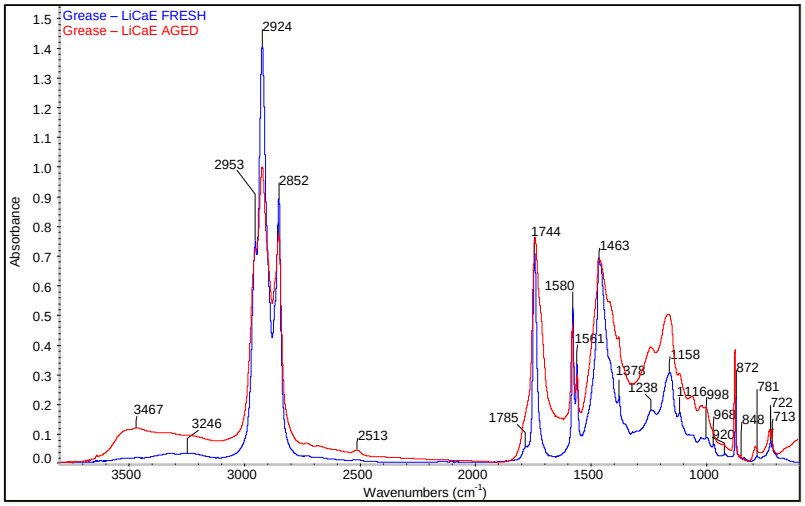

(a)

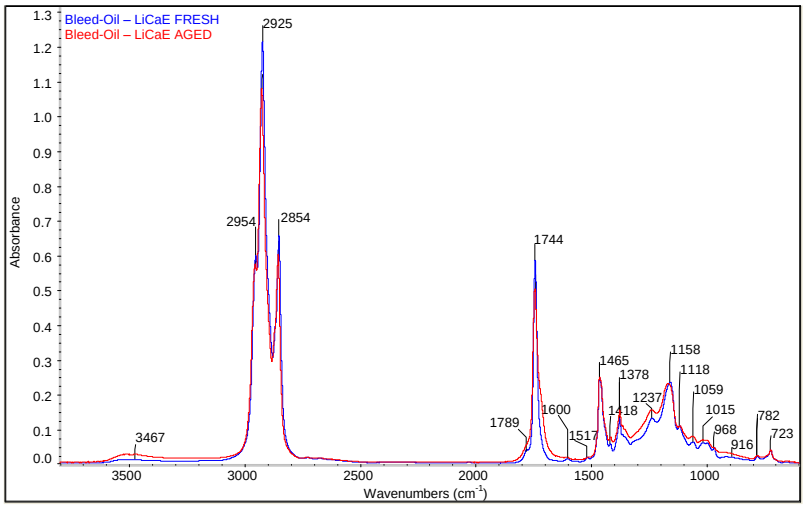

(b)

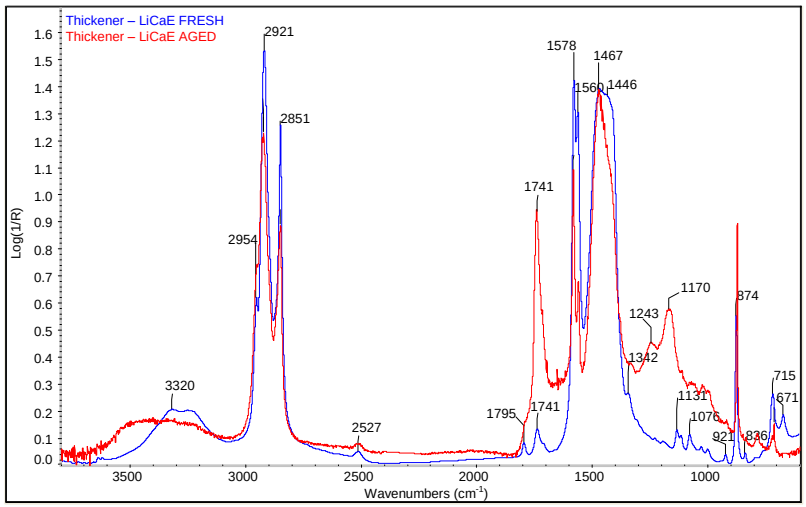

(c)

Figure 7.2.: (a) Grease, (b) Bleed-oil and (c) Thickener spectra.

7.3.1.3. PPAO

Figure 7.3(a) shows the spectra of the fresh and aged PPAO grease samples. It is noticeable that no or just slight oxidation occurs. However the consumption of AW additives at 1745 cm^{-1} and the depletion of the extreme pressure and anti-wear additive at 1709 cm^{-1} (Bismuth) are clear. Furthermore, a significant decrease in intensity of the peaks in the region of 2853-2953 cm^{-1} indicates that the C-H and C-C long chains of PP and/or PAO were broken [222]. In fact, polymers submitted to high shear and high temperature may undergo structural modification, mainly scission, generally accompanied with deterioration of the physical and mechanical properties, which results in a reduction of its rheological properties, such as apparent viscosity and shear stress [223].

When comparing the aged and fresh bleed-oil in Figure 7.3(b), it is observed a small decrease at the peaks at 1745, 1710, 1304 and 1167 cm^{-1}, which are related to additives consumption. The decrease in intensity of the peaks in the region of 2853-2953 cm^{-1} also represents scission and evaporation of the more volatile compounds of the oil. However, no or just slight oxidation is observed.

Figure 7.3(c) shows the IR spectra of the thickener extracted from the fresh and aged grease samples. Again, the only significant chemical changes observed indicates scission reaction. The sinusoidal shape at the base line is due to internal equipment noise and does not represent the thickener characteristics.

From the spectra presented before, the following simplifications can be done:

- LiM1 grease is not or just slightly oxidised, but additive consumption and the beginning of an oxidation process were observed in the aged bleed-oil spectrum; several chemical changes were observed at the thickener spectrum.
- LiCaE grease showed moderate to high level of oxidation, chain-scission reactions and additives consumption.
- PPAO grease is not or just slightly oxidised, but chain-scission reactions and additives consumption were observed.

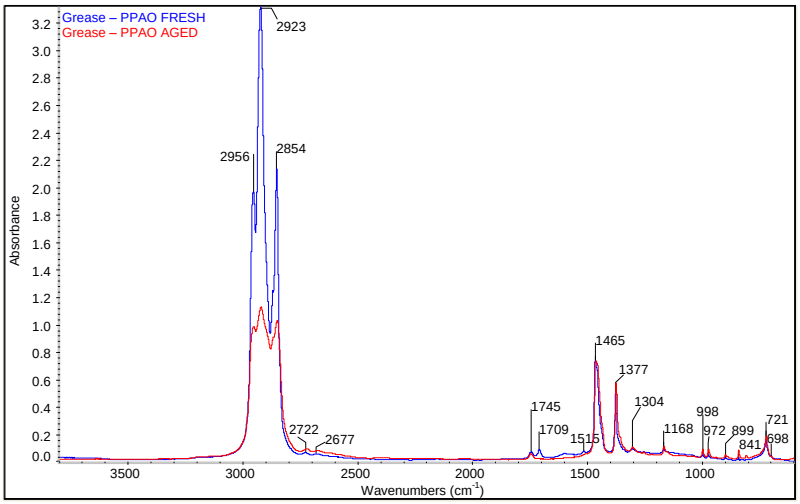

(a)

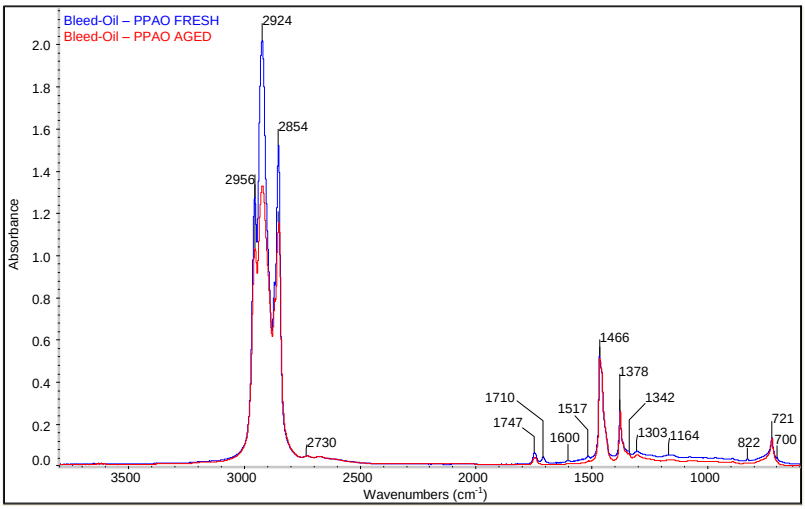

(b)

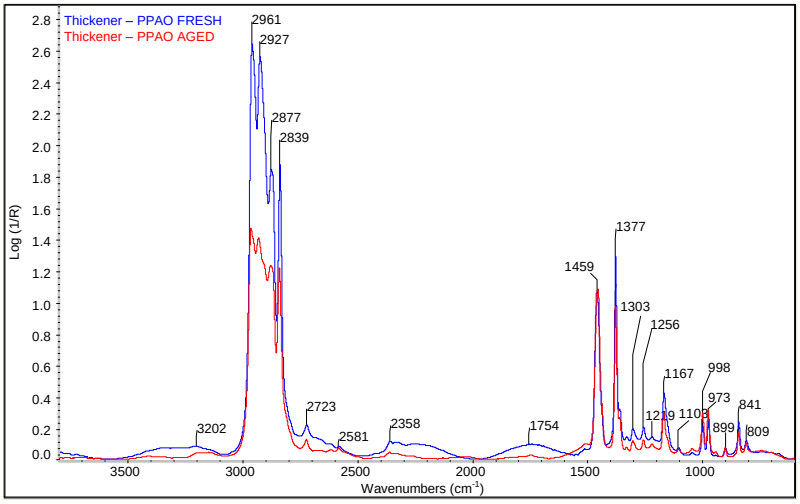

(c)

Figure 7.3.: (a) Grease, (b) Bleed-oil and (c) Thickener spectra.

7.3.2. X-ray fluorescence - XRF

Table 7.1 shows the most common elements used on grease additivation and their concentration as a function of the total mass [wt % $\times 10^3$], before and after the aging process. The relative decrease/increase in percentage of each element after the aging process is also given in the table by $\Delta_c = (Fresh - Aged)/Fresh \times 100$.

The decreased content of some common elements usually used as additives (P, S, Ca, Zn, Pb, Bi) was observed by comparing the XRF data of fresh and aged grease samples. This supports the FTIR analysis presented in the previous section. Table 7.1 also shows an increase of the iron content (Fe) in the LiM1 (28.2 %) and LiCaE (535.7 %) greases. As shown by Hurley *et al.* [105], oxidation occurs more rapidly and reaches higher levels in the presence of metallic debris. Therefore, the high content of Fe together with the low additivation of the LiCaE grease are likely to be the main reason for the high level of oxidation.

The iron (Fe) content also indirectly indicates the grease's ability to protect the contacting surfaces, either by forming a hydrodynamic film or a boundary film (thickener and/or additives). In this sense, the iron content suggests that PPAO has the highest capacity for forming a film, followed by LiM1 and LiCaE.

Table 7.1.: Concentration in percentage of total mass [wt % $\times 10^{-3}$] of the chemical content of fresh and aged grease samples.

	P	S	Ca	Zn	Pb	Bi	Fe
Fresh LiM1	120.0	1649.0	3.0	285.0	8.0	0.0	4.9
Aged LiM1	82.5	696.5	3.0	156.4	8.0	0.0	6.3
Δ_c	31.3	57.8	0.0	45.1	0.0	0.0	-28.2
Fresh LiCaE	37.0	102.0	3145.0	29.0	0.0	0.0	2.8
Aged LiCaE	23.5	63.4	1958.0	12.3	0.0	0.0	17.8
Δ_c	36.6	37.8	37.7	57.6	0.0	0.0	-535.7
Fresh PPAO	6.0	581.0	22.0	0.0	14.0	717.0	2.9
Aged PPAO	2.2	123.4	0.2	0.0	11.4	643.6	2.9
Δ_c	64.2	78.8	99.0	0.0	18.8	10.2	0.0

7.3.3. Remaining oil percentage and bleed-oil viscosity

The remaining oil percentage analyses were performed in order to evaluate the grease oil loss due to the aging process. The method is described in Section 3.6 and the results obtained are summarized in Table 7.2 and 7.3. Where Δ_{oil} and Δ_{thick} are obtained from Equation 7.1

$$\Delta_{oil} = \frac{Aged_{oil} - Fresh_{oil}}{Fresh_{oil}} \times 100; \;\; \Delta_{thick} = \frac{Aged_{thick} - Fresh_{thick}}{Fresh_{thick}} \times 100 \qquad (7.1)$$

Table 7.2.: Oil Content. Comparison between fresh and aged grease samples.

	LiM1	**LiCaE**	**PPAO**
Fresh [%]	88.71	79.51	84.52
Aged [%]	86.43	72.90	84.01
$\lvert\Delta_{oil}\rvert$ [%]	2.6	8.3	0.6

Table 7.3.: Thickener Content. Comparison between fresh and aged grease samples.

	LiM1	**LiCaE**	**PPAO**
Fresh [%]	11.29	20.49	15.48
Aged [%]	13.57	27.10	15.99
Δ_{thick} [%]	20.2	32.3	3.3

Δ_{oil} indicates the oil loss due to evaporation and/or bleeding that occurred during the aging process. Figure 7.4 shows that the absolute value of the oil loss ($\lvert\Delta_{oil}\rvert$) decreases in a power law fashion with the dynamic viscosity of the fresh bleed-oil measured at 40 °C (η). Although a relationship between oil viscosity and its evaporation rate [224] are usually observed, several other factors play a role in the oil evaporation process, such as the thickener-oil chemical and physical interaction.

Figure 7.5 shows the measured dynamic viscosity of the fresh and aged samples measured at 40 °C , and Table 7.4 summarizes their viscosity differences in the low shear range, expressed by Equation 7.2.

$$\Delta\eta\,[\%] = \frac{\eta_{aged} - \eta_{fresh}}{\eta_{fresh}} \times 100 \qquad (7.2)$$

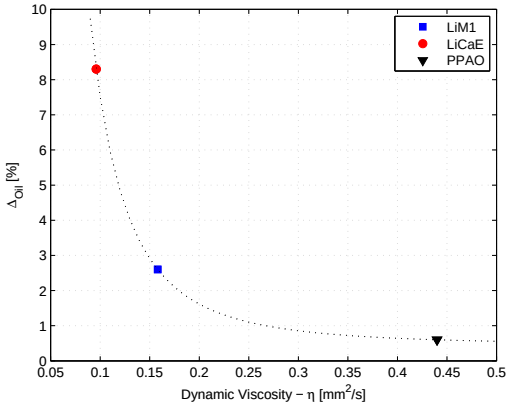

Figure 7.4.: Fresh bleed-oil dynamic viscosity versus oil loss ($\eta_{\text{bleed-oil}} \times |\Delta_{oil}|$).

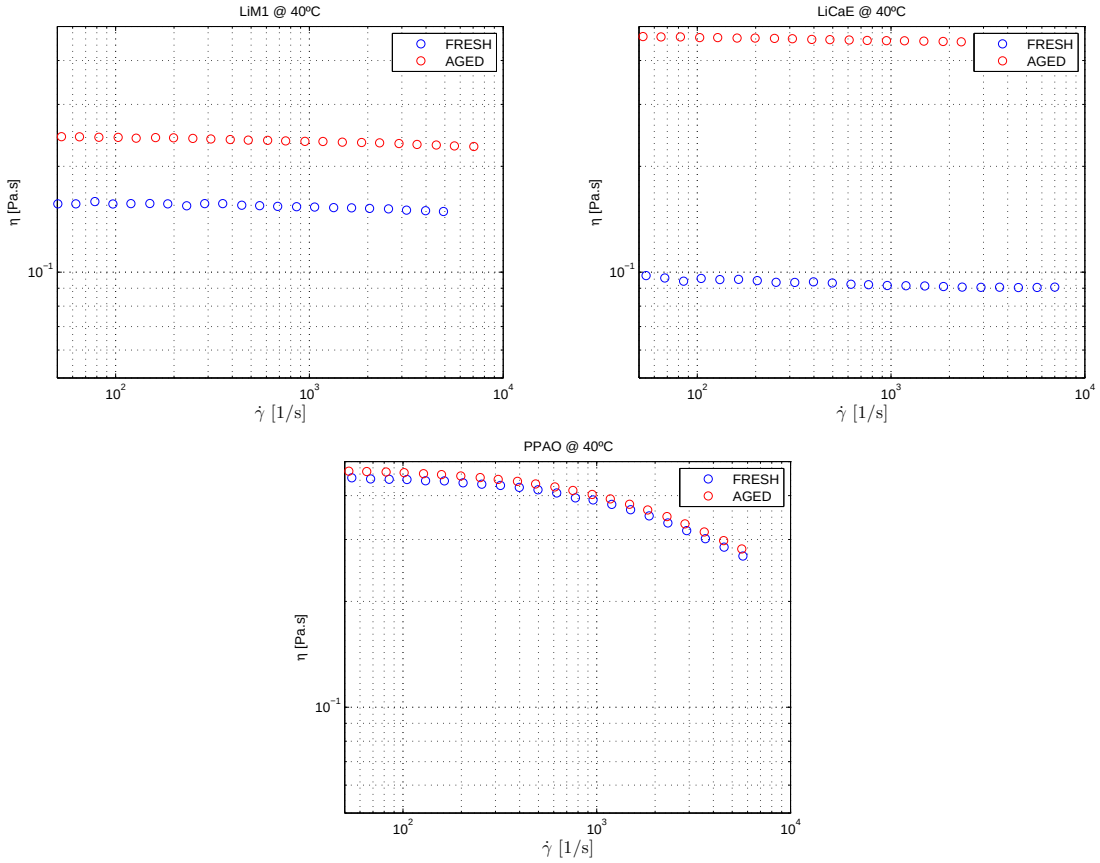

Figure 7.5.: Bleed-oil viscosity at 40 °C . Comparison between fresh and aged samples.

Table 7.4.: Bleed-oil viscosity at 40 °C . Comparison between fresh and aged samples.

	LiM1	**LiCaE**	**PPAO**
Fresh [Pa.s]	0.158	0.096	0.440
Aged [Pa.s]	0.243	0.470	0.470
Δ_η [%]	54.6	382.3	6.8

The increase in viscosity observed can be related to different reactions that occur during the aging process such as evaporation of the low weight compounds of the base oil and formation of high molecular weight molecules (polymerization). Due to the low level of oxidation observed in LiM1 and PPAO lubricating greases and bleed-oils, the increase in viscosity is probably due to the evaporation of the low weight compounds of the base oil, while the significant increase in the bleed-oil viscosity observed in the case of LiCaE is also attributed to polymerization, since LiCaE is highly oxidised. Figure 7.6 shows that Δ_η increases in a power law fashion with increasing oil loss ($|\Delta_{oil}|$), which suggests that evaporation of the low weight compounds of the base oil prevailed over the bleeding process.

It is important to clarify that the aged LiCaE, when submitted to static and dynamic bleed tests (IP 121 and ASTM D4425, respectively) during 3 days at 70 °C , did not release any oil, while LiM1 and PPAO did. Therefore, the aged LiCaE bleed-oil was obtained with the remaining oil percentage technique. This does not invalidate the comparisons presented in this section because it was verified, for the other samples, that the viscosity obtained from the different methods is similar.

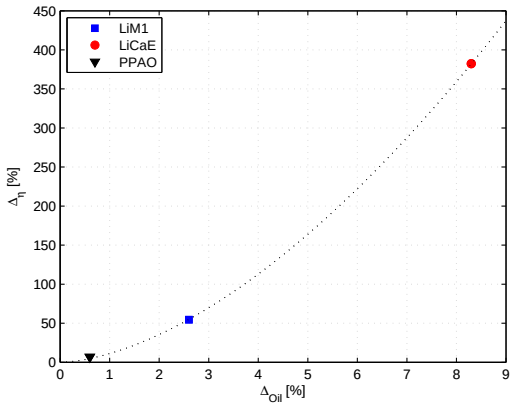

Figure 7.6.: Absolute value of the relative dynamic bleed-oil viscosity versus oil loss ($|\Delta\eta| \times \Delta_{oil}$).

7.3.4. Rheometry

The yield stress τ_y, storage G' and loss G'' moduli and the flow curve $\tau \times \dot{\gamma}$ of the aged samples were measured with the methodology presented in Section 2.10 and compared with the corresponding fresh samples.

Figures 7.7 to 7.9 show the results from the creep tests at 40 °C for the fresh and aged samples of LiM1, LiCaE and PPAO, respectively. Table 7.5 summarizes the results presented in these figures.

Figure 7.10 and Table 7.6 present a comparison between the storage G' and loss G'' moduli of aged and fresh samples at 40 °C .

Figure 7.11 shows the shear stress versus the shear rate of the aged and fresh samples at 40 °C .

Table 7.5.: Yield stress limits. Comparison between fresh and aged sample at 40 °C .

	LiM1		LiCaE		PPAO	
	Fresh	Aged	Fresh	Aged	Fresh	Aged
τ_{ymin}	100	200	200	200	600	$<<$ 100
τ_{ymax}	200	400	400	400	800	$<<$ 100

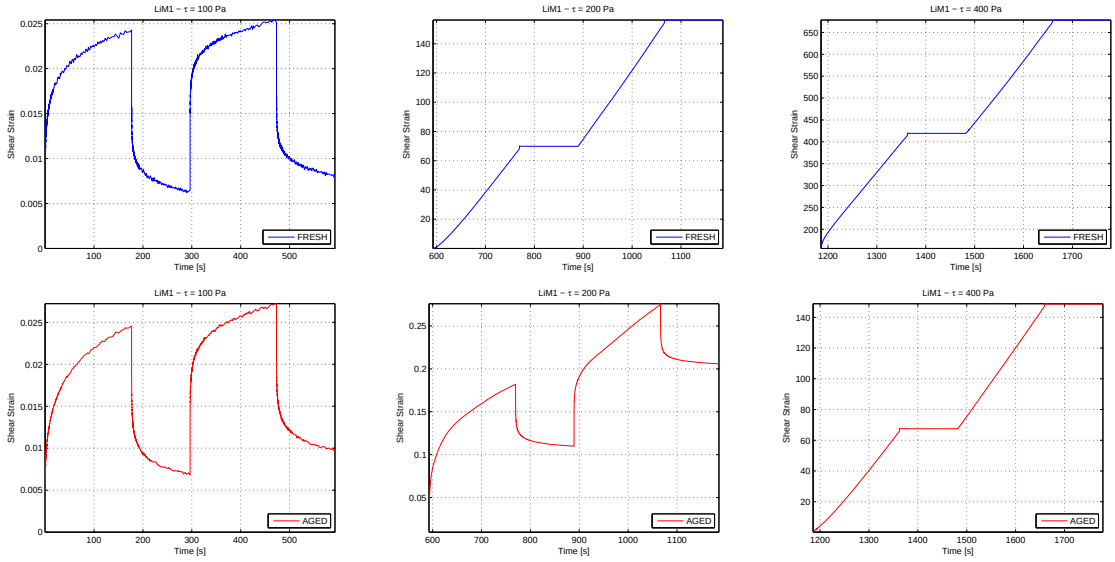

Figure 7.7.: Creep test: Shear strain vs. time for different applied shear stresses. Comparison between fresh and aged sample of LiM1 grease.

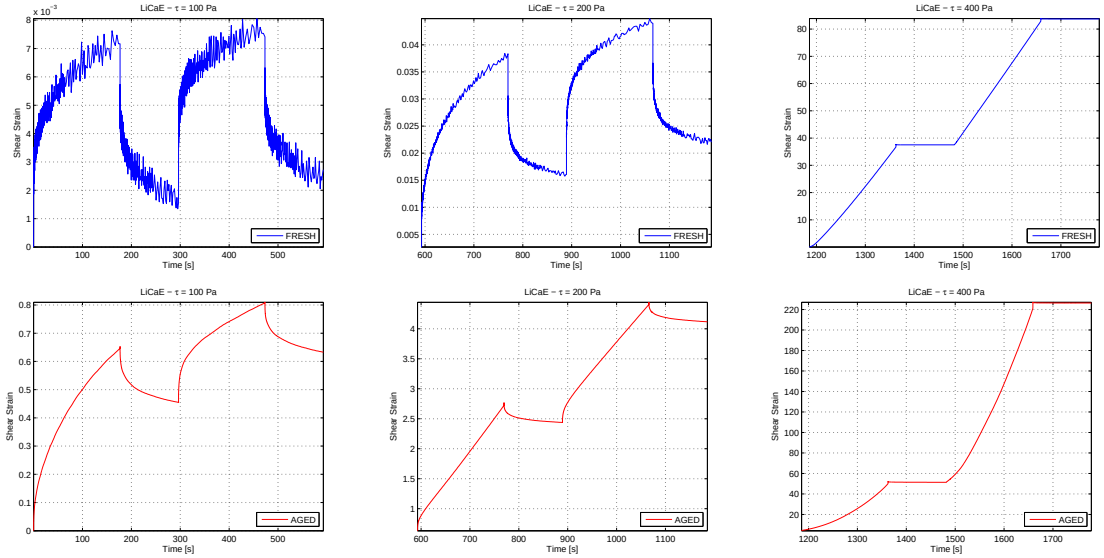

Figure 7.8.: Creep test: Shear strain vs. time for different applied shear stresses. Comparison between fresh and aged sample of LiCaE grease.

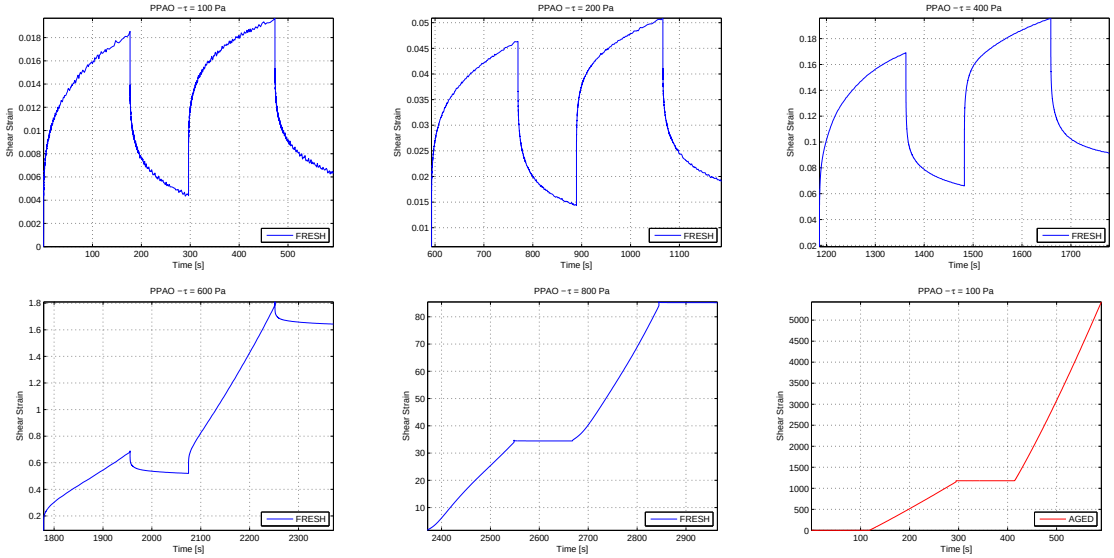

Figure 7.9.: Creep test: Shear strain vs. time for different applied shear stresses. Comparison between fresh and aged sample of PPAO grease.

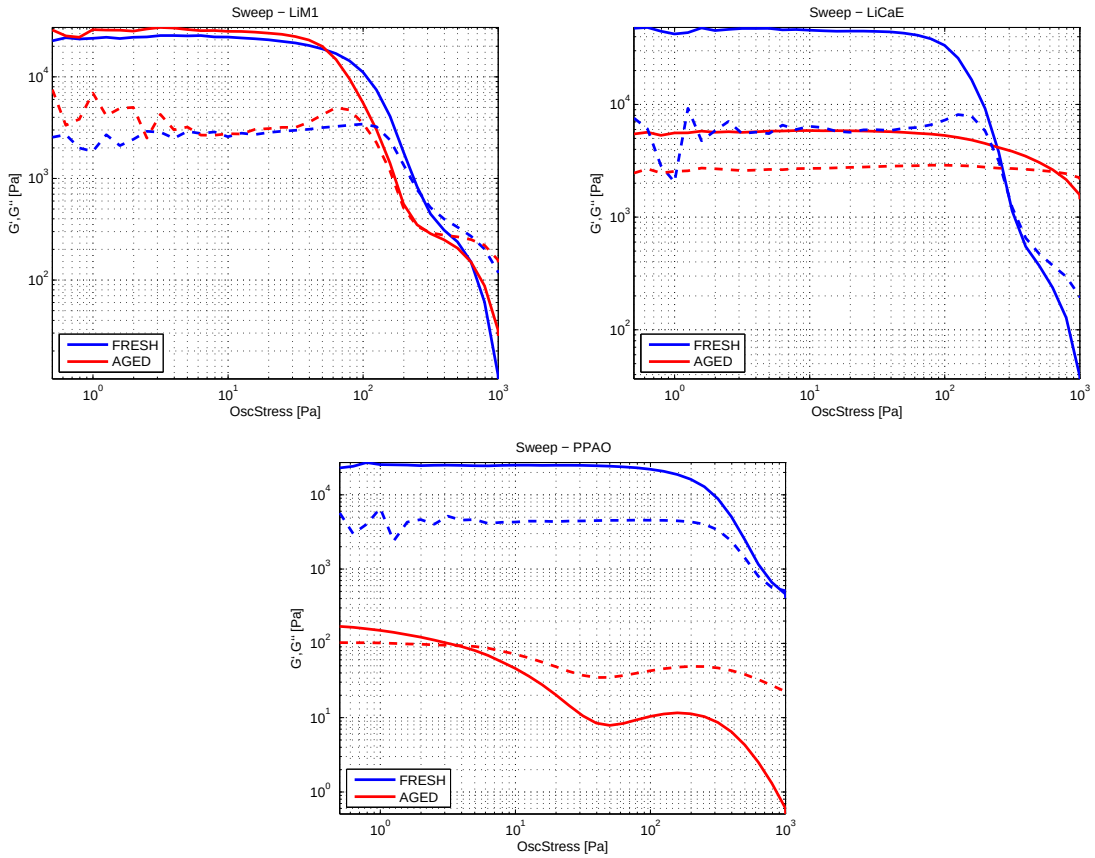

Figure 7.10.: Storage G' (—) and Loss G'' ($\cdots$) moduli. Comparison between fresh and aged grease samples.

Table 7.6.: Storage and loss moduli versus oscillatory stress. Comparison between fresh and aged samples at 40 °C in the LVE region.

Grease	G' **Fresh [Pa]**	G' **Aged [Pa]**	G'' **Fresh [Pa]**	G'' **Aged [Pa]**
LiM1	23690	27523	2778	2958
LiCaE	44893	5847	5895	2740
PPAO	24957	28	4394	56

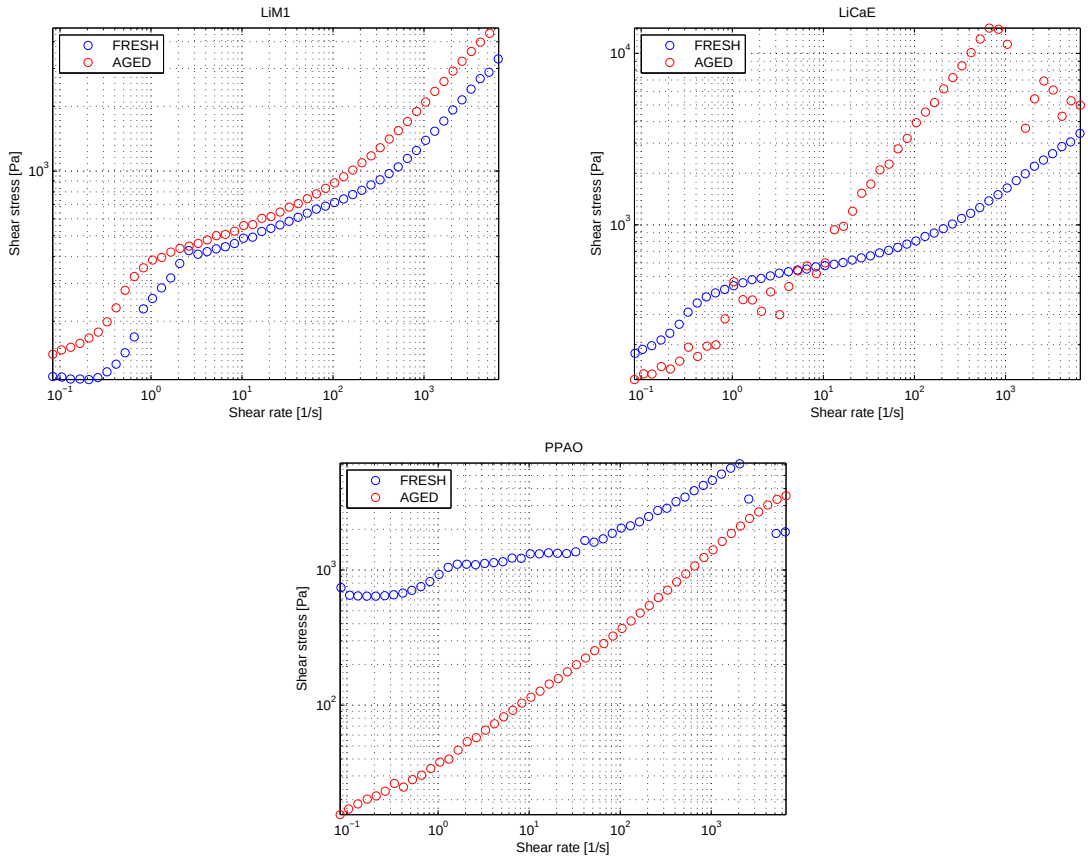

Figure 7.11.: Shear stress versus shear rate. Comparison between fresh and aged samples.

Although aged samples of LiM1 are not or just slightly oxidised, additive consumption, oil loss and increased bleed-oil viscosity were observed. This suggests evaporation of the low weight compounds in the base oil. The oil loss, due to bleeding and evaporation, promotes grease stiffening, which was observed by the increase of all rheological parameters (τ_y, G', G'' and $\tau \times \dot{\gamma}$) - grease stiffening.

Aged samples of LiCaE showed significant oxidation, thickener degradation and oil loss. Consequently, it was observed a significant increase in bleed-oil viscosity. At low stresses (low shear rate or low shear stress), where the rheological response of lubricating greases are dominated by their thickener structure, the aged LiCaE sample showed a softening behaviour, which is likely due to thickener breakdown (chain-scission reactions) and might be related to the formation of oxidation products. This was observed in the rheological measurements of the aged LiCaE grease by its lower recovering capacity (Figure 7.8), lower oscillatory parameters (G' and G'') and lower shear stress values at the low shear rate range ($\dot{\gamma} \ < 10\ \mathrm{s}^{-1}$) in the flow curve (Figure 7.11). However, at higher stresses (high oscillatory stress and high shear rate)

where the rheological responses of the lubricating greases are dominated by their oil, LiCaE aged samples showed a stiffening behaviour due to their increased bleed-oil viscosity. This was verified by their higher oscillatory parameters (G' and G'') and higher shear stress values values at high shear rates $\dot{\gamma} > 10$ s^{-1} in the flow curve.

Aged samples of PPAO were not or just slightly oxidised, oil loss and viscosity increase were low, but significant chemical changes in the range of 2853-2953 cm^{-1}, representing chain-scission reactions, were observed. Chain scission reactions shorten PP chain length and consequently lead to decreasing values of apparent viscosity and other rheological properties [225]. This was noted in all rheological parameters (τ_y, G', G'' and $\tau \times \dot{\gamma}$) that were measured.

7.3.5. Grease film thickness measurements

As discussed in Chapter 4, under fully flooded lubrication, grease and its bleed-oil have similar film thickness values. Thus, grease film thickness may be predicted by using the bleed-oil viscosity and pressure-viscosity coefficient in the case of Newtonian lubricants (fresh and aged samples of LiM1 and LiCaE bleed-oil) and the bleed-oil low-shear viscosity, pressure-viscosity coefficient, critical stress and power-law index in the case of non-Newtonian lubricants (fresh and aged samples of PPAO bleed-oil).

Throughout this chapter, it was shown several significant changes to the lubricating greases and their bleed-oil viscosities due to aging (degradation). Changes to the pressure-viscosity coefficient, therefore, are also expected, as verified by Bair *et al.* [135]. Consequently, the capability of aged greases to form and keep a separating film might be different from fresh greases.

Film thickness measurements were carried out under fully flooded conditions where a scraper was used to redistribute the grease back to the rolling track; and under starved conditions, where the scraper was not used. All the tests were performed at 40 °C . The load applied was 20 N, which corresponds to a maximum hertzian pressure of $P_0 = 0.5$ GPa for a ball with a $2R = 19{,}05$ mm diameter. First, the film thickness measurements were performed under fully flooded conditions (with the scraper) at an operating speed varying from 100 to 1000 mm/s, and then from 1000 to 100 mm/s. At that point (speed = 100 mm/s), the scraper was removed (starved conditions) and the film thickness was measured over time during 30 minutes.

Figure 7.12 shows the film thickness measurements under fully flooded (left) and starved (right) lubrication for fresh and LiM1, LiCaE and PPAO greases. All the aged greases generated film thickness values above the measuring limit ($\approx$ 750 nm) of the optical device during the fully flooded lubrication measurements. This is depicted by the constant film thickness values of $\approx$ 750 nm observed in the figures.

The differences between fresh and aged lubricating greases will be expressed by the relative film thickness increment Δh in the centre of the contact, defined by:

$$\Delta h\,[\%] = \frac{h_{aged} - h_{fresh}}{h_{fresh}} \times 100 \tag{7.3}$$

Under fully flooded lubrication, both fresh and aged samples of LiM1 showed increasing film thickness at an entrainment speed of $\approx U^{0,67}$, although the aged sample presented higher film thickness values ($\Delta h \approx 40$ %), as shown in Figure 7.12(a).

In the case of aged LiM1 grease, oil loss and low levels of oxidation and of rheological changes, together with the significant increase in bleed-oil viscosity $\Delta_\eta \approx 54{,}6$ % suggest that the grease lubrication mechanisms are still similar to the fresh ones although the bleed-oil is more viscous. The bleed-oil, therefore, may still be the active lubricant, which would explain the increased film thickness. When using the methodology described in Section 4.3.3, where the pressure-viscosity coefficient is determined on the basis of the best R^2 fit between film thickness measurements and predictions, the pressure viscosity coefficient should increase $\Delta\alpha_{film} \approx 12$ %, which is reasonable.

UUnder starved conditions, fresh and aged LiM1 samples showed similar film thickness decay with time. According to the thin layer flow model developed by Venner, *et al.* [171], lubricating greases with higher base oil (bleed-oil) viscosity at the contact inlet should present a lower decay rate with time (considering that the active lubricant is the bleed-oil). This was not observed here, which may indicate that the other constituents of the grease play a role in the film decay rate.

LiCaE greases also showed higher film thickness values after the aging process (see Figure 7.12(b)). Even at low speeds (100 mm/s), measured film thickness values were above the limit of the optical device ($\approx$ 750 nm). At 100 mm/s, the relative film thickness increment is at least $\Delta h \approx 310$ %. Contrary to the LiM1, aged LiCaE was highly oxidised, lost a significant amount of oil, presented several rheological changes and additive consumption. Furthermore, when submitted to the centrifugal oil bleed test (ASTM D4425), it did not release any oil during 72 h running at high speeds (2000 rpm, that is $\approx$ 20 m/s) and at a 70 °C temperature. This suggests that the lubrication mechanisms of the aged LiCaE grease are not solely governed by the bleed-oil properties any longer, but also by a material with enhanced viscosity or a solid-like thick film, which may be formed by oxidation products and/or thickener material and/or bleed-oil.

Under starved lubrication, the aged sample of LiCaE retained a significantly high film thickness over time, while the fresh sample decayed rapidly. The film thickness values of the aged sample is approximately one hundred times higher than the fresh

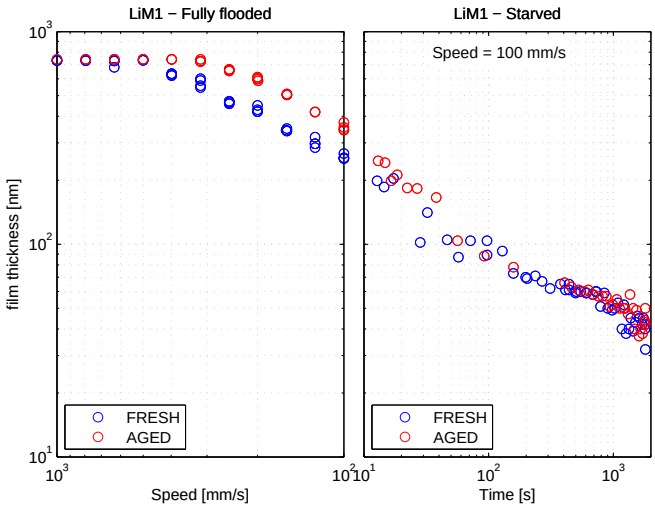

(a)

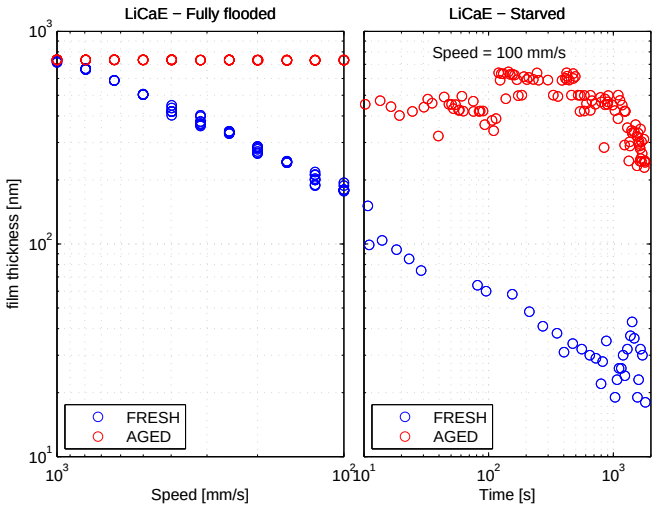

(b)

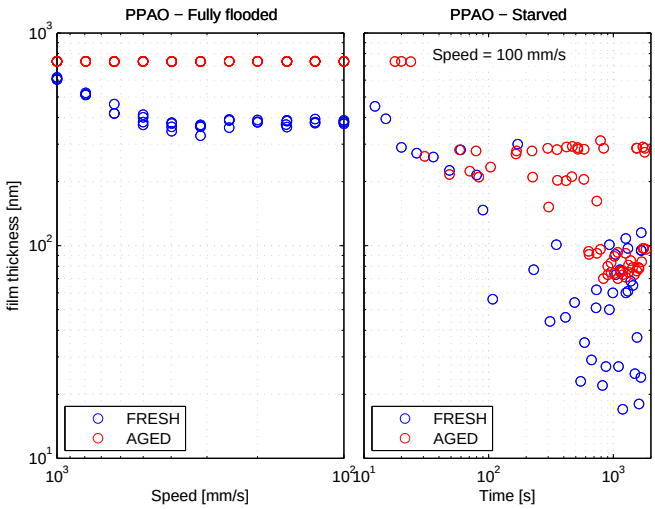

(c)

Figure 7.12.: Film thickness versus entrainment speed. Comparison between fresh and aged samples (a) LiM1, (b) LiCaE and (c) PPAO.

sample when t = 30 minutes. The almost time independent film thickness of the aged sample supports the idea of the active film having an enhanced viscosity that is not easily ejected by pressure or centrifugal forces or being a deposited solid-like layer.

In fact, Cann [103] showed that the presence of additives seems to prevent thickener deposition and that non-additivated greases generated deposited films consisting mostly of degraded thickener as high as 600 nm (after 300 min), while additivated greases did not form such films. In the case of LiCaE, where most of additives were consumed after aging, it is likely that the film is not solely controlled by the bleed-oil properties, but also by a solid-like or enhanced viscous film formed mostly of degraded grease with a high thickener content deposited in the track.

Under fully flooded lubrication, PPAO also showed higher film thickness values after the aging process, as shown in Figure 7.12(b). At a speed of 300 mm/s (before low speed effect starts, i.e., film thickness no longer follows the $h \propto U^{0,67}$ relation), the relative film thickness increment is at least $\Delta h \approx 110$ %.

The film thickness increment Δh is not clear. This does not seem to be related to the bleed-oil properties, because the viscosity that increased after aging was small $\Delta\eta \approx 6,8\%$, which most likely implies small $\Delta\alpha_{film}$, when for a perfect $\mathbf{R}^2$ fitting with the measured film thickness values, a $\Delta\alpha_{film}$ of at least ≈ 112 % it would be required . This also does not seem to be related to the level of oxidation, because PPAO grease was not or just slightly oxidised. Grease softening, which is often related to contact replenishment [154], may not show significant effects in the case of fully flooded tests because the replenishment is imposed. This suggests that the film thickness increment is mostly related to additive consumption, which "allowed" for the deposition of thick layers of grease material.

Under starved lubrication, the aged sample of PPAO retained higher film thickness values than the fresh sample. According to Kaneta *et al.* [154], grease shear degradation (when bleed-oil viscosity does not change significantly) results in thicker films due to the suppression of starvation, i.e., softening of the grease will improve grease reflow, thus improving grease replenishment. Besides, as stated earlier, consumption of additives allows for the deposition of degraded grease in the track, which also increases film thickness. Aged PPAO also showed high local fluctuations in film thickness values, although lower than the fresh sample. The reduction of local fluctuations in film thickness may also be attributed to thickener degradation [154], thus reducing the size of grease material entering the contact and therefore, local fluctuation.

7.3.6. Traction coefficient measurements

Traction measurements were carried out in a ball-on-disc contact (steel × steel) under fully flooded conditions, where a scraper was used to redistribute the grease back to the rolling track. All the tests were performed at 40 °C . The load applied was 75 N, which corresponds to a maximum hertzian pressure of $P_0 \approx 1.29$ GPa for a ball with a $2R = 19{,}05$ mm diameter. The traction measurements were performed at first with an operating speed varying from 0.1 to 1000 mm/s and $SRR = 5$ %, then with constant speed of 1000 mm/s and SRR varying from 0,1 to 20 %.

Figure 7.13 shows the traction values of fresh and aged greases under fully flooded lubrication.

All lubricating greases presented lower traction values after the aging process. The highest reduction rate was observed for grease LiCaE, while greases LiM1 and PPAO presented lower reduction rates. It is not clear how aging affected the traction values, although make some assumptions are given.

The formation of oxidation products, such as alcohols and carboxylic acids, may adsorb in the surface leading to friction reduction [32]. The higher film thickness of the aged samples (see Figure 7.12) generates lower shear rates, thus lower shear stresses and consequently, lower traction coefficients. Grease softening also presented lower shear stress values (at least at low shear rates) and therefore, lower traction values would be expected. On the other hand, the increased bleed-oil viscosity of the aged samples can be expected to increase the traction values [194], although it is known that viscosity and traction values are not necessarily connected.

This suggests that for all aged lubricating greases, increased film thickness contributed to traction decreasing by reducing the shear rate in the contact, and in the case of LiCaE, an additional reduction may be due to the action of the oxidation products.

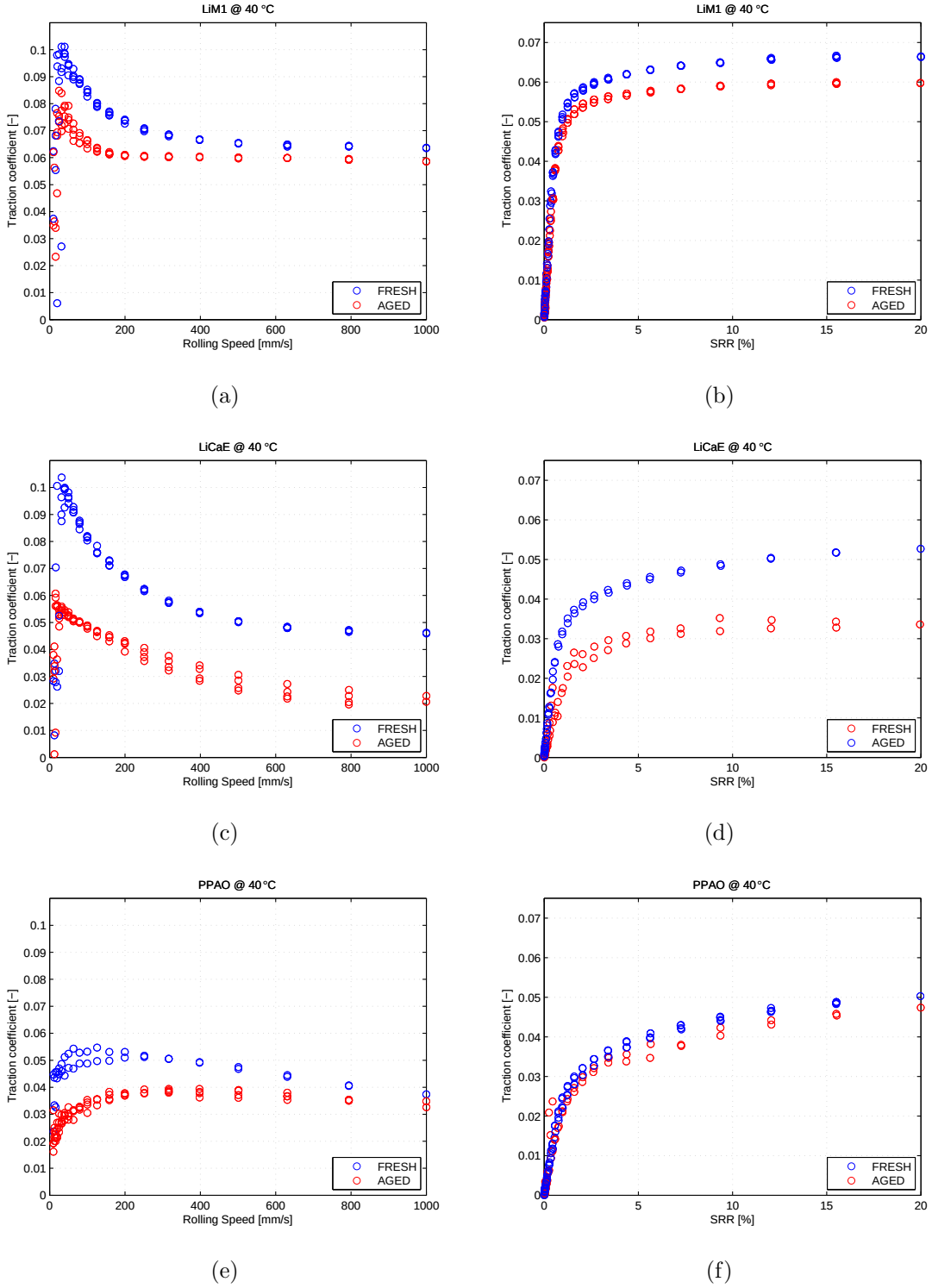

Figure 7.13.: Traction coefficient. Comparison between fresh and aged samples (a) and (b) LiM1, (c) and (d) LiCaE, (e) and (f) PPAO.

7.3.7. Rolling bearing friction torque measurements

Friction torque measurements were carried out according to the process described in Section 6.2.1. All the tests were performed at self-induced temperatures with forced air convection. The load applied was 5000 N ($P_0 \approx 2.08$ GPa); three different rotational speeds were used, 500, 1000 and 1500 rpm.

Figure 7.14 shows the rolling bearing friction torque values for fresh and aged greases as compared to the rotational speed. All the aged lubricating greases generated higher friction torques than the fresh ones. At first, this appeared to be counter intuitive since the aged greases also showed lower traction values than the fresh ones, as shown in Figure 7.13. Nonetheless, bleed-oil viscosity plays a significant role in the friction torque model and may overcome the coefficient of friction effect, thus raising the friction torque values.

The friction torque model could not be applied to these measurements because the aged bleed-oil viscosity was only measured at 40 °C and the bearing tests were run under self-induced temperature, which generated operating temperatures other than 40 °C . The influence of changes in the viscosity ($\Delta\eta$), however, shown in Table 7.4 and in the traction values shown in Figure 7.13, can be analysed in comparison by running the friction torque model with the fresh and aged properties at 40 °C to verify whether the experimental trends agree with the predictions or not.

Table 7.7 provides all the inputs to perform such comparisons at 40 °C and 1000 rpm, and Table 7.8 provides the results. The full film coefficient of friction of fresh and aged greases (μ_{EHL}) were obtained from Figures 7.13 at $SRR = 1.3$ %.

Rolling bearing friction torque predictions for the aged greases were slightly lower than the predictions for the fresh greases, while the measurements showed the opposite.

In the case of LiM1 and PPAO greases, the fresh and aged friction torque predictions were quite similar, likely due to the experimental observations. In these cases, where aged lubricating greases are not so degraded, the small differences between predictions and measurements may be as a result of the different operating temperatures of the bearing tests against the constant values used in the predictions ($T = 40$ °C). In the case of LiCaE, which is much oxidised, however, the differences were significant and cannot be only related to the different operating temperatures of the bearing tests.

In fact, the difference between the aged LiCaE predictions and the measured values indicates that the lubrication mechanism of this sample was no longer governed by the bleed-oil.

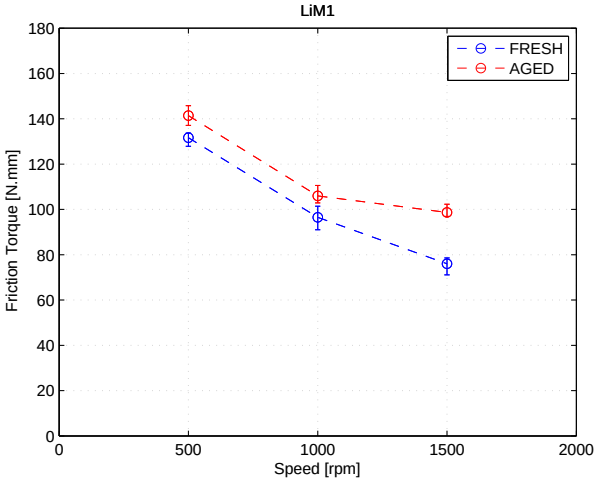

(a)

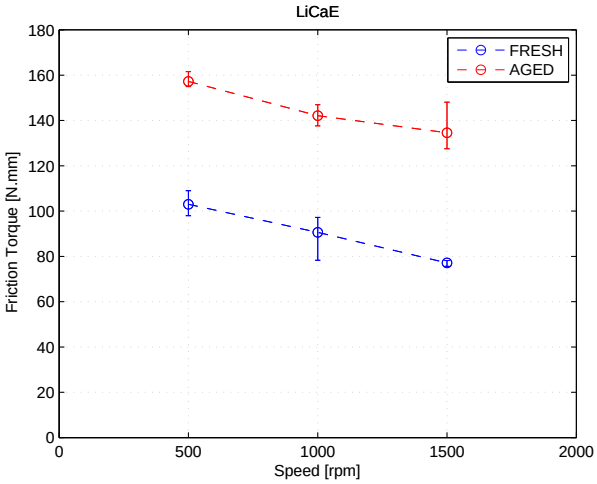

(b)

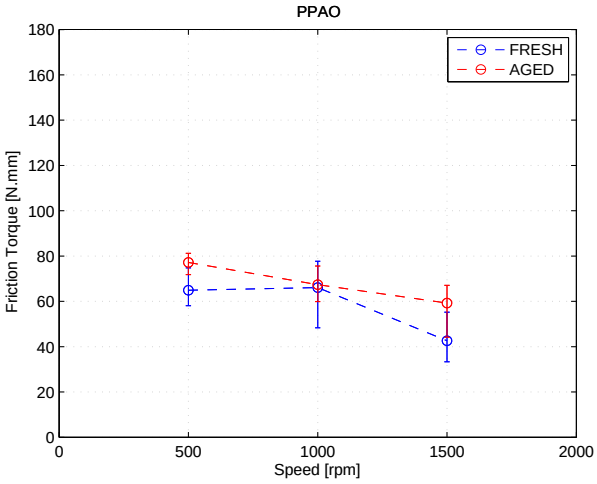

(c)

Figure 7.14.: Rolling bearing friction torque versus entrainment speed. Comparison between fresh and aged samples (a) LiM1, (b) LiCaE and (c) PPAO.

Table 7.7.: Used parameters for friction torque predictions.

Parameters	Units	LiM1	LiCaE	PPAO
n	rpm	1000	1000	1000
K_{rs}	-	$11{\cdot}10^{-8}$	$11{\cdot}10^{-8}$	$11{\cdot}10^{-8}$
K_z	-	3.8	3.8	3.8
R_1	-	$1.03{\cdot}10^{-6}$	$1.03{\cdot}10^{-6}$	$1.03{\cdot}10^{-6}$
S_1	-	$1.60{\cdot}10^{-2}$	$1.60{\cdot}10^{-2}$	$1.60{\cdot}10^{-2}$
F_a	N	6867	6867	6867
D	mm	52	52	52
d	mm	35	35	35
d_m	mm	43.5	43.5	43.5
G_{rr}	-	0.1211	0.1211	0.1211
G_{sl}	-	2521.9	2521.9	2521.9
ν_{40} fresh	mm^2/s	186	95	530
ν_{40} aged	mm^2/s	290	465	569
μ_{bl}	-	0.15	0.15	0.15
μ_{40} fresh	-	0.0530	0.0375	0.0264
μ_{40} aged	-	0.0507	0.0217	0.0241

Table 7.8.: Friction torque predictions at 40 °C . Comparison between fresh and aged samples.

N.mm	**LiM1**	**LiCaE**	**PPAO**
M_{rr} Fresh	61.88	56.18	37.08
M_{rr} Aged	57.36	42.50	34.08
M_{sl} Fresh	50.63	35.83	25.22
M_{sl} Aged	48.44	20.73	23.02
M_t Fresh	112.52	92.01	60.30
M_t Aged	105.80	63.23	57.10
$M_{tfresh} - M_{taged}$	6.72	28.78	3.2

7.4. Discussion and conclusions on grease degradation

Grease properties vary constantly during operation. Most of the changes to the rheological properties and oil loss occur at the beginning of grease life due to mechanical stress (mostly churning). Chemical changes, such as additive exhaustion and formation of oxidation products, occur after approximately half of grease life [226]. All these changes affect the tribological performance of lubricating greases in a different manner.

From the analysis of the experimental results, it was verified that whatever the physico-chemical changes that occurred in lubricating greases, whilst they are still able to release enough oil to replenish the contact, bleed-oil appears to be the active lubricant, thus the use of its properties to predict tribological performance might be satisfactory. As soon as the oil available for lubricating the contact becomes insufficient, however, in situations of thin films or at very low entrainment speeds, the bleed-oil is no longer the active lubricant and film formation seems to depend on grease properties. Consequently, tribological behaviour will depend on the active lubricant, which in turn depends on the type of grease and the operating conditions. The different types of active lubricants suggested in the literature are grease material, degraded or not, deposited in the track (physical absorption) [103] or a material with enhanced viscosity of additives and/or thickener [168].

Consequently, the greases' capacity to form and sustain thick boundary layers with good lubricity during the later stages of grease lubrication, depends mostly on thickener-additives-surface interaction, plus the hydrodynamic effect generated by the small amounts of bleed-oil presented in the contact.

8. General conclusions and future work

8.1. Conclusions

Chapters 1 - 3 present the main properties of lubricating greases and their components in terms of grease formulation and performance (film thickness and friction). The importance of characterizing grease and its bleed-oil, instead of only characterizing its components separately, was outlined. It was also shown that base and bleed-oil properties might be different depending on grease formulation. Furthermore, it was shown that direct correlation between fresh grease rheological behaviour and base oil properties with grease tribological performance in short-period tests has not being achieved so far; this suggests that new approaches need to be developed.

In Chapter 4 the results of the film thickness measurements performed at moderate temperatures, speeds and pressures showed that the main mechanism of lubricating greases, under full film conditions, is the oil released either by bleeding, shear, or shear-induced bleeding. Under these conditions, grease film thickness might be predicted by using the bleed-oil properties.

In the event that the speed goes below a critical value, film formation is affected by the thickener passing through the contact. This critical speed and the film thickness values under this condition depend on grease formulation and, in the case of the lubricants used, were higher in the following order of thickener types PP > Li+Ca > Li.

Under starved lubrication, oil availability is reduced and the separating film appears to be formed by a limited amount of oil that is constantly, but momentarily, increased by the thickener as it passes through the contact. The frequency with which the thickener passes through the contact and the increase rate it promotes, for the lubricants used, also follow the PP > Li+Ca > Li order.

In Chapter 5 the results of the ball-on-disc traction tests, performed under fully flooded and starved grease lubrication, at moderate temperatures and moderate to

high speeds and pressures, were presented. These results were used as an input for the SKF friction torque model, thus contributing to a good agreement between the friction torque measurements and the model. Under fully flooded lubrication, the transition of the traction regimes from mixed to plateau (shown in the 3D friction maps) agreed with the calculated specific film thickness (from $\Lambda < 1$ to $\Lambda > 1$). It was also shown that grease traction behaviour follows the usual and well known trends of lubricating oils under fully flooded lubrication. The different trends observed under starved conditions were attributed to the grease film formation.

Chapter 6 showed that the modified Four-Ball machine is an interesting test rig for measuring the internal friction torque of rolling bearings under a wide range of operating conditions. This provided a simple way for evaluating lubricant performance in terms of power loss. Together with the SKF rolling bearing friction torque model, it provided useful information with which to evaluate the conditions under which the bearing operates, in terms of sliding / rolling bearing friction torque.

The rolling bearing friction torque developed by SKF was optimized on the basis of the findings presented in Chapters 3, 4 and 5. This optimization was in good agreement with the friction torque measurements.

It also shown that grease formulation and in particular the interaction between thickener, base oil and additives might generate bleed-oils with properties that are different from the corresponding base oils. These can influence the total rolling bearing friction torque through the replenishment/starvation factor (φ_{rs}), inlet shear heating effect (φ_{ish}), lubrication regime (φ_{bl}) and rolling friction torque ($M_{rr'}$). It was also observed that the traction coefficient varies with speed and temperature (Chapter 5), according to the sliding friction torque component (M_{sl}) under full film condition.

In Chapter 7 an aging procedure was developed to degrade the lubricating greases under similar conditions as those for the grease degradation that occurs in rolling bearings that are run for long periods at high speeds and temperatures. Aged greases were described and showed significant changes in their physico-chemical properties that consequently modified the grease lubrication mechanisms. Aged greases might show significant oil loss, which restricts the oil availability in the contact, reducing the hydrodynamic film thickness and consequently, increasing the severity of the contact. Furthermore, additive consumption may also be significant, which allows for the adhesion of thickener films but restricts the additive boundary film formation. Under such conditions bleed-oil barely plays a role in film formation and the contact is mostly lubricated by an enhanced viscous or solid-like film of degraded thickener with a very small amount of oil entrapped in it. The prediction of the tribological

performance in this situation requires an understanding of boundary film formation and its properties.

Grease performance: It was observed that, under full film lubrication, traction values, i.e., the coefficient of friction under full film lubrication μ_{EHD} and the sliding friction torque M_{sl} mostly depend on the nature of the grease base oil, which follows the order Mineral > Ester ≈ PAO oil, whilst grease film thickness h_{oc} and the total rolling bearing friction torque M_t [1] mostly depend on bleed-oil viscosity.

8.2. Future work

Considering that bleed-oil is the main grease lubrication mechanism in the earlier stages of grease lubrication, it is clear that is necessary to:

- develop a model for predicting the oil bleed rate of lubricating greases, that takes into account the grease formulation, properties and morphology, the bearing type and operating conditions, in order to estimate the bleeding phase, in terms of the number of cycles;
- investigate bleed-oil more thoroughly in order to determine how the interaction between grease components affects the bleed-oil viscosity and pressure-viscosity coefficient;
- characterize the bleed-oil properties at high pressures and shear rates;
- predict the rolling bearing friction torque of grease lubricated roller bearings (line contact) to improve our knowledge of grease lubricated line contacts. This work has a significant advantage over the work presented in this thesis, because film thickness, traction coefficient and rolling bearing friction torque measurements can be performed with the same contact geometry and operating conditions, thus avoiding so many extrapolations.

On the other hand, the estimation of grease performance after the bleeding stage, which is the condition that rolling bearings operate under for the longest part of their lives is of extreme importance. Therefore, it is also required to:

- study the grease lubrication mechanisms after significant oil loss;

[1] M_t is influenced by the bleed-oil viscosity mainly through the rolling friction torque $M_{rr}^{'}$ and weighting factor φ_{bl}.

- study the properties of the boundary layers, which appear to be initially formed by additives and then by degraded thickeners;
- analyse the tribological performance of these boundary layers in terms of film thickness and traction behaviour;
- study the influence of the products of oxidation on film formation and traction behaviour.

Bibliography

[1] P. Baart, *Grease lubrication mechanisms in bearing seals.* PhD thesis, Luleå University of Technology, 2011.

[2] M. T. van Zoelen, *Thin layer flow in rolling element bearings.* PhD thesis, University of Twente, December 2009.

[3] I. Couronné, P. Vergne, D. Mazuyer, N. Truong-Dinh, and D. Girodin, "Effects of grease composition and structure on film thickness in rolling contact," *Tribology Transactions*, vol. 46, no. 1, pp. 31–36, 2003.

[4] P. Larsson, *Lubricant Replenishment in the Vicinity of an EHD Contact.* PhD thesis, Tekniska högskolan i Luleå, 1996.

[5] J.-S. Mérieux, S. Hurley, A. Lubrecht, and P. Cann, "Shear-degradation of grease and base oil availability in starved EHL lubrication," *Proc. 26th Leeds-Lyon Symp. on Trib.*, pp. 581–588, 1999.

[6] G. M. Espejel, "Using a friction model as an engineering tool," *Evolution*, vol. 1, pp. 27–30, June 2006.

[7] G. Schimidt, "Chemie und herstellung der metallseifenfette am beispiel der metallseifenfette," *W. J. Bartz (ed.), Schmierfette, expert, Renningen-Malmsheim*, pp. 55–63, 2000.

[8] SKF, *SKF General Catalogue 6000EN*, November 2005.

[9] P. M. LUGT, "A review on grease lubrication in rolling bearings," *Tribology Transactions*, vol. 52, no. 4, pp. 470 – 480, 2009.

[10] J. Lundberg and E. Höglund, "A new method for determining the mechanical stability of lubricating greases," *Tribology International*, vol. 33, no. 34, pp. 217 – 223, 2000.

[11] P. Cann, J. Doner, M. Webster, and V. Wikström, "Grease degradation in rolling element bearings," *Tribology Transactions*, vol. 44, no. 3, pp. 399–404, 2001.

[12] S. Hurley and P. Cann, "Examination of grease structure by SEM and AFM techniques," *NLGI Spokesman*, vol. 65, no. 5, pp. 17–26, 2001.

[13] I. Couronné, P. Vergne, D. Mazuyer, N. Truong-Dinh, and D. Girodin, "Nature and properties of the lubricating phase in grease lubricated contac," *Tribology Transactions*, vol. 46, p. 37 43, 2003.

[14] M. Delgado, M. Sánchez, C. Valencia, J. Franco, and C. Gallegos, "Relationship among microstructure, rheology and processing of a lithium lubricating grease," *Chemical Engineering Research and Design*, vol. 83, no. 9, pp. 1085 – 1092, 2005.

[15] H. Baly, G. Poll, P. Cann, and A. Lubrecht, "Correlation between model test devices and full bearing tests under grease lubricated conditions," in *IUTAM Symposium on Elastohydrodynamics and Micro-elastohydrodynamics* (R. Snidle and H. Evans, eds.), vol. 134 of *Solid Mechanics and Its Applications*, pp. 229–240, Springer Netherlands, 2006.

[16] M. Delgado, J. Franco, and E. Kuhn, "Effect of rheological behaviour of lithium greases on the friction process," *Industrial Lubrication and Tribology*, vol. 60, pp. 37–45, 2008.

[17] P. Lugt, *Grease Lubrication in Rolling Bearings*. Tribology Series, Wiley, 2013.

[18] D. Dong and X. Qian, "A theory of elastohydrodynamic grease-lubricated line contact based on a refined rheological model," *Tribology International*, vol. 21, no. 5, pp. 261 – 267, 1988.

[19] P. Cann, B. Williamson, R. Coy, and H. Spikes, "Behaviour of greases in elastohydrodynamic contacts," *Journal of Physics D: Applied Physics*, vol. 25, no. 1 A, pp. A124–A132, 1992.

[20] Z. Yang and X. Qian, "A solution to grease lubricated EHD film thickness in an elliptical rolling contact," *ImechE Conference Publication*, vol. 1, no. 5, pp. 97–104, 1987.

[21] M. T. Van Zoelen, C. H. Venner, and P. M. Lugt, "The prediction of contact pressure induced film thickness decay in starved lubricated rolling bearings," *Tribology Transactions*, vol. 53, no. 6, pp. 831–841, 2010.

[22] W. Yanshuang and Y. Boyuan, "An investigation into grease behavior in thermal EHL circular contacts," *Tribology Transactions*, vol. 49, no. 3, pp. 449–453, 2006.

[23] X. Lu and M. M. Khonsari, "An experimental investigation of grease-lubricated journal bearings," *Journal of Tribology*, vol. 129, no. 1, pp. 84–90, 2007.

[24] F. K. Group, *FAG Catalogue - Rolling Bearing Lubrication (WL 81 115/4 EA)*. FAG OEM und Handel AG, P.O. Box 1260 D-97 419 Schweinfurt, 2004 ed., 1997.

[25] T. Cousseau, M. Björling, B. Graça, A. Campos, J. Seabra, and R. Larsson, "Film thickness in a ball-on-disc contact lubricated with greases, bleed oils and base oils," *Tribology International*, vol. 53, no. 0, pp. 53–60, 2012.

[26] I. Couronn É and P. Vergne, "Rheological behavior of greases: Part ii - effect of thermal aging, correlation with physico-chemical changes," *Tribology Transactions*, vol. 43, no. 4, pp. 788–794, 2000.

[27] J. Lundberg, "Grease lubrication of roller bearings in railway waggons. part 1: field tests and systematic evaluation to determine the optimal greases," *Industrial Lubrication and Tribology*, vol. 52, pp. 36–44, 2000.

[28] H. P. Jost, "Lubrication tribology - education and research," tech. rep., Department of Education and Science, HMSO, London, 1966.

[29] K. Holmberg, "Friction science saves energy," *Finnish Journal of Tribology*, vol. 28, pp. 16–25, 2009.

[30] X. Hu, *Separation of oil-in-water wmulsion for environmental protection.* PhD thesis, Szent stván Egytem. Budai Campus, 2002.

[31] SCImago, "SJR - scimago journal & country rank," July 2007.

[32] T. Mang and W. Dresel, *Lubricants and lubrication.* Wiley-vch, 2007.

[33] D. Dowson, *History of Tribology.* John Wiley & Sons, Limited, 2013.

[34] E. Britannica, ed., *Lubricants*, vol. 14. W. F. Parish, 14 ed., 2013.

[35] Partridge, "British patent 6945," 07.12.1835.

[36] J. Lewkowitsch, *Chemical technology and analysis of oils, fats, and waxes.* Macmillan, 1904, Vol 2.

[37] W. Little, "Brithish patent 12571," 16.04.1849.

[38] C. Balan and Grease Specialists from ELGI, "ELGI publication: The rheology of lubricating grease." CD-ROM.

[39] "ASTM standard D288-61(1978) Definitions of terms relating to petroleum (withdrawn 1980)."

[40] W. Dresel and R.-P. Heckler, *Ullmann's Encyclopedia of Industrial Chemistry*, ch. Lubricants, 8. Lubricating Greases. Wiley-VCH Verlag GmbH & Co. KGaA, 2000.

[41] H. Huang, J. Tu, T. Zou, L. Zhang, and D. He, "Friction and wear properties of IF-MoS2 as additive in paraffin oil," *Tribology Letters*, vol. 20, pp. 247–250, 2005. 10.1007/s11249-005-8552-z.

[42] S. Tarasov, A. Kolubaev, S. Belyaev, M. Lerner, and F. Tepper, "Study of friction reduction by nanocopper additives to motor oil," *Wear*, vol. 252, no. 12, pp. 63 – 69, 2002.

[43] L. Rapoport, N. Fleischer, and R. Tenne, "Fullerene-like WS2 nanoparticles: Superior lubricants for harsh conditions," *Advanced Materials*, vol. 15, no. 7-8, pp. 651–655, 2003.

[44] M. R. Lovell, M. A. Kabir, P. L. Menezes, and C. F. Higgs, "Influence of boric acid additive size on green lubricant performance," *Philosophical Transactions of the Royal Society A: Mathematical, Physical and Engineering Sciences*, vol. 368, no. 1929, pp. 4851–4868, 2010.

[45] G. E. Totten, S. R. Westbrook, and R. J. Shah, *Fuels and lubricants handbook: technology, properties, performance, and testing*, vol. 37. ASTM International, 2003.

[46] C.-S. Koh and J. B. Butt, "Experimental and modeling study of kinetics and selectivity in the oxidation of a poly(alpha-olefin) lubricant," *Industrial & Engineering Chemistry Research*, vol. 34, no. 2, pp. 524–535, 1995.

[47] V. Štěpina and V. Vesel'y, "Tribology series," in *Lubricants and Special Fluids* (V. Štěpina and V. Vesel'y, eds.), vol. 23 of *Tribology Series*, pp. ii –, Elsevier, 1992.

[48] R. F. Crouch and A. Cameron, "Viscosity-temperature equations for lubricants," *Journal of the Institute of Petroleum*, vol. 47, pp. 307–313, 1961.

[49] "ASTM D341 - 09, Standard practice for viscosity - temperature charts for liquid petroleum products."

[50] H. Vogel, "The law of the relation between the viscosity of liquids and the temperature," *Physikalische Zeitschrift*, vol. 22, p. 645, 1921.

[51] "ASTM standard D2270-10e1, 2010, Standard practice for calculating viscosity index from kinematic viscosity at 40 and 100 °C."

[52] C. Barus, "Isothermals, isopiestics and isometrics relative to viscosity," *American Journal of Sciences*, vol. Third Series XLV (266), pp. 87–96, 1893.

[53] C. Roelands, *Correlational aspects of the viscosity-temperature-pressure relationship of lubricating oils*. PhD thesis, Delft University of Technology, 1967.

[54] S. Bair and P. Kottke, "Pressure-viscosity relationships for elastohydrodynamics," *Tribology Transactions*, vol. 46, no. 3, pp. 289–295, 2003.

[55] D. Dowson and G. R. Higginson, "A numerical solution to the elastohydrodynamic problem," *Journal of Mechanical Engineering Science*, vol. 1, no. 1, pp. 6–15, 1959.

[56] A. W. Crook, "The lubrication of rollers," *Philosophical Transactions of the Royal Society of London. Series A, Mathematical and Physical Sciences*, vol. 250, no. 981, pp. 387–409, 1958.

[57] A. W. Crook, "The lubrication of rollers ii. film thickness with relation to viscosity and speed," *Philosophical Transactions of the Royal Society of London. Series A, Mathematical and Physical Sciences*, vol. 254, no. 1040, pp. 223–236, 1961.

[58] A. W. Crook, "The lubrication of rollers iii. a theoretical discussion of friction and the temperatures in the oil film," *Philosophical Transactions of the Royal Society of London. Series A, Mathematical and Physical Sciences*, vol. 254, no. 1040, pp. 237–258, 1961.

[59] A. W. Crook, "The lubrication of rollers iv. measurements of friction and effective viscosity," *Philosophical Transactions of the Royal Society of London. Series A, Mathematical and Physical Sciences*, vol. 255, no. 1056, pp. 281–312, 1963.

[60] P. W. Gold, A. Schmidt, H. Dicke, J. Loos, and C. Assmann, "Viscosity-pressure-temperature behaviour of mineral and synthetic oils," *Journal of Synthetic Lubrication*, vol. 18, no. 1, pp. 51–79, 2001.

[61] B. So and E. Klaus, "Viscosity-pressure characteristis of lubricating oils," *ASLE Transactions*, vol. 23, pp. 409–421, 1980.

[62] A. Handbook, "Friction, lubrication and wear technology," *American Society for Metals*, vol. 18, p. 942, 1992.

[63] H. van Leeuwen, "The determination of the pressure-viscosity coefficient of a lubricant through an accurate film thickness formula and accurate film thickness measurements," *Proceedings of the Institution of Mechanical Engineers, Part J: Journal of Engineering Tribology*, vol. 223, pp. 1143–1163, 2009.

[64] S. Bair and P. Gordon, "Rheological challenges and opportunities for EHL," in *IUTAM Symposium on Elastohydrodynamics and Micro-elastohydrodynamics* (R. Snidle and H. Evans, eds.), vol. 134 of *Solid Mechanics and Its Applications*, pp. 23–43, Springer Netherlands, 2006.

[65] H. Eyring, "Viscosity, plasticity, and diffusion as examples of absolute reaction rates," *The Journal of Chemical Physics*, vol. 4, no. 4, pp. 283–291, 1936.

[66] J. B. Hamrock and D. Dowson., *Ball Bearing Lubrication, The Elastohydrodynamics of Elliptical Contacts*. John Willey & Sons, 1981.

[67] D. Pirro and A. Wessol, *Lubrication fundamentals*, vol. 137. CRC Press, 2010.

[68] W. H. Bauer, A. P. Finkelstein, and S. E. Wiberley, "Flow properties of lithium stearate-oil model greases as functions of soap concentration and temperature," *ASLE Transactions*, vol. 3, no. 2, pp. 215–224, 1960.

[69] S. Hurley, *Fundamental Studies of Grease Lubrication in Elastohydrodynamic Contacts*. PhD thesis, University of London, Imperial College of Science, Technology and Medicine, UK., 2000.

[70] E. Forster, J. Kolfenbach, and H. Leland, "Fibers, forces and flow," *NLGI Spokesman*, vol. 20, no. 3, pp. 16–22, 1956.

[71] R. Mortier, M. Fox, and S. Orszulik, *Chemistry and technology of lubricants*. SpringerLink: Springer e-Books, Springer Netherlands, 2010.

[72] C. Lu, H. Shen, P. Jiang, and R. Jiang, "A study on anti-wear and anti-friction performance of lithium-calcium base greases," *NLGI Spokesman*, vol. 57, pp. 65–69, 1993.

[73] ASTM International, *Annual Book Of ASTM Standards*, vol. 05.01-05.03. American Society for Testing & Materials, 2004.

[74] "ASTM standard D217-10, 2007, Standard test methods for cone penetration of lubricating grease."

[75] "ASTM standard D1403-10, 2007, Standard test methods for cone penetration of lubricating grease using one-quarter and one-half scale cone equipment."

[76] L. Hamnelid, "Consistency consists in σ_y," *NLGI Spokesman*, vol. 62(4), pp. 17–30, 1998.

[77] H. A. Barnes, "The yield stress - a review or $\pi\alpha\nu\tau\alpha$ $\rho\varepsilon\iota$ - everything flows ?," *Journal of NonNewtonian Fluid Mechanics*, vol. 81, no. May 1998, pp. 133–178, 1999.

[78] "ASTM standard D1092 - 12, 2011, Standard test method for measuring apparent viscosity of lubricating greases."

[79] M. Keentok, "The measurement of the yield stress of liquids," *Rheologica Acta*, vol. 21, pp. 325–332, 1982. 10.1007/BF01515720.

[80] C. W. Macosko, *Rheology - Principles, Measurements and Applications*, pp. 217–222. John Wiley & Sons, 1994.

[81] M.-C. Yang, L. E. Scriven, and C. W. Macosko, "Some rheological measurements on magnetic iron oxide suspensions in silicone oil," *Journal of Rheology*, vol. 30, no. 5, pp. 1015–1029, 1986.

[82] H. J. Walls, S. B. Caines, A. M. Sanchez, and S. A. Khan, "Yield stress and wall slip phenomena in colloidal silica gels," *Journal of Rheology*, vol. 47, no. 4, pp. 847–868, 2003.

[83] W. Y. Shih, W.-H. Shih, and I. A. Aksay, "Elastic and yield behavior of strongly flocculated colloids," *Journal of the American Ceramic Society*, vol. 82, no. 3, pp. 616–624, 1999.

[84] S. Yeong, P. Luckham, and T. Tadros, "Steady flow and viscoelastic properties of lubricating grease containing various thickener concentrations," *Journal of Colloid and Interface Science*, vol. 274, no. 1, pp. 285 – 293, 2004.

[85] C. Balan and K. Hutter, "A procedure to determine the material constants and the viscosity function for a fluid with yield shear stress," *Acta Mechanica*, vol. 109, pp. 65–78, 1995.

[86] P. Cann and S. Hurley, "Started lubrication of EHL contacts - relationship to bulk grease properties," *NLGI Spokesman*, vol. 64(2), pp. 15–23, 2000.

[87] L. Figura and A. Teixeira, *Food Physics: Physical Properties - Measurement and Applications*. Springer London, Limited, 2007.

[88] M. Delgado, J. Franco, P. Partal, and C. Gallegos, "Experimental study of grease flow in pipelines: wall slip and air entrainment effects," *Chemical Engineering and Processing: Process Intensification*, vol. 44, no. 7, pp. 805 – 817, 2005.

[89] M. M. Cross, "Rheology of non-newtonian fluids: A new flow equation for pseudoplastic systems," *Journal of Colloid Science*, vol. 20, no. 5, pp. 417 – 437, 1965.

[90] T. Cousseau, B. Graça, A. Campos, and J. Seabra, "Friction torque in grease lubricated thrust ball bearings," *Tribology international*, vol. 44, no. 5, pp. 523–531, 2011.

[91] N. Scarlett, "Use of grease in rolling bearings," *Proc. Inst. Mech. Eng.*, vol. 182, no. PART 3A, pp. 585–593, 1967.

[92] M. A. Delgado, C. Valencia, M. C. Sánchez, J. M. Franco, and C. Gallegos, "Influence of soap concentration and oil viscosity on the rheology and microstructure of lubricating greases," *Industrial & Engineering Chemistry Research*, vol. 45, no. 6, pp. 1902–1910, 2006.

[93] D. Booser, E.R. Wilcock, "Minimum oil requirements of ball bearings," *Lubric. Engng, June*, vol. 9, p. 156, 1953.

[94] V. Wikström and E. Höglund, "Starting and steady-state friction torque of grease-lubricated rolling element bearings at low temperatures-part ii: Correlation with less-complex test methodsá," *Tribology Transactions*, vol. 39, no. 3, pp. 684–690, 1996.

[95] J. Wolska, B. Vrebos, and P. Brouwer, "Analysis of fuels, lubricants, and greases using x-ray fluorescence spectrometry," *ASTM Special Technical Publication*, vol. 2005, no. 1468, pp. 98–107, 2005.

[96] B. Beckhoff, B. Kanngießer, N. Langhoff, R. Wedell, and H. Wolff, *Handbook of Practical Xray Fluorescence Analysis - Chapter 5*. SpringerLink : Bücher, Springer, 2006.

[97] P. Griffiths and J. De Haseth, *Fourier Transform Infrared Spectrometry*. Chemical Analysis: A Series of Monographs on Analytical Chemistry and Its Applications, Wiley, 2007.

[98] I. Fuks, T. Medvedeva, and Y. Ishchuk, "Application of ir spectroscopy in studying grease composition and properties (review)," *Chemistry and Technology of Fuels and Oils*, vol. 8, pp. 152–156, 1972.

[99] P. M. Cann and H. A. Spikes, "In lubro studies of lubricants in EHD contacts using FTIR absorption spectroscopy," *Tribology Transactions*, vol. 34, no. 2, pp. 248–256, 1991.

[100] K. Takahashi, Y. Shitara, and S. Mori, "Direct observation of thermo-reversible gel-lubricants in EHL by ft-ir micro-spectroscopy," *Tribology Online*, vol. 3, no. 2, pp. 131–136, 2008.

[101] P. Cann and S. Hurley, "IR spectroscopic analysis of grease lubricant films in rolling contacts," *Tribology Series*, vol. 36, pp. 589–600, 1999.

[102] P. Cann, M. Webster, J. Doner, V. Wikström, and P. Lugt, "Grease degradation in R0F bearing tests," *Tribology Transactions*, vol. 50, no. 2, pp. 187–197, 2007.

[103] P. Cann, "Grease degradation in a bearing simulation device," *Tribology International*, vol. 39, no. 12, pp. 1698 – 1706, 2006. Interactions of Tribology and the Operating Environment: Proceedings of the 32nd Leeds-Lyon Symposium on Tribology (Lyon, 2005).

[104] D. J. Carré, R. Bauer, and P. D. Fleischauer, "Chemical analysis of hydrocarbon grease from spin-bearing tests," *ASLE Transactions*, vol. 23, p. 475, 1983.

[105] S. Hurley, P. M. Cann, and H. A. Spikes, "Lubrication and reflow properties of thermally aged greases," *Tribology Transactions*, vol. 43, pp. 9 –14, 2000.

[106] M. Diaby, M. Sablier, A. L. Negrate, M. E. Fassi, and J. Bocquet, "Understanding carbonaceous deposit formation resulting from engine oil degradation," *Carbon*, vol. 47, no. 2, pp. 355 – 366, 2009.

[107] A. Rivaton, S. Cambon, and J.-L. Gardette, "Radiochemical ageing of ethylenepropylenediene elastomers. 4. evaluation of some anti-oxidants," *Polymer Degradation and Stability*, vol. 91, no. 1, pp. 136 – 143, 2006.

[108] N. Gracia, S. Thomas, F. Thibault-Starzyk, O. Lerasle, and L. Duponchel, "Combination of mid-infrared spectroscopy and curve resolution method to

follow the antioxidant action of alkylated diphenylamines," *Chemometrics and Intelligent Laboratory Systems*, vol. 106, no. 2, pp. 210 – 215, 2011.

[109] A. Kupareva, P. Mäki-Arvela, H. Grénman, K. Eränen, R. Sjöholm, M. Reunanen, and D. Y. Murzin, "Chemical characterization of lube oils," *Energy & Fuels*, vol. 27, no. 1, pp. 27–34, 2013.

[110] A. Aranzabe, E. Aranzabe, A. Marcaide, R. Ferret, J. Terradillos, J. Ameye, and R. Shah, "Comparing different analytical techniques to monitor lubricating grease degradation," in *NLGI Spokesman-Including NLGI Annual Meeting-National Lubricating Grease Institute*, vol. 70(6), pp. 17–30, [Kansas City, Mo.] National Lubricating Grease Institute., 2006.

[111] K. D. O. Jackson, "A guide to identifying common inorganic fillers and activators using vibrational spectroscopy," *Journal of natural rubber research*, vol. 12(2), pp. 102–11, 1997.

[112] E. T. Akintayo, O. Olaofe, C. O. Akintayo, and C. O. Adefemi, "Potential of fourier transform infrared spectroscopy for characterising vegetable oils.," *International Jour. Chem*, vol. 12, no. 2, p. 151, 2002.

[113] X. Zhu, D. Yan, and Y. Fang, "In situ FTIR spectroscopic study of the conformational change of isotactic polypropylene during the crystallization process," *The Journal of Physical Chemistry B*, vol. 105, no. 50, pp. 12461–12463, 2001.

[114] H. J. Walls, S. B. Caines, A. M. Sanchez, and S. A. Khan, "Yield stress and wall slip phenomena in colloidal silica gels," *Journal of Rheology*, vol. 47, no. 4, pp. 847–868, 2003.

[115] G. Davies and J. Stokes, "Thin film and high shear rheology of multiphase complex fluids," *Journal of Non-Newtonian Fluid Mechanics*, vol. 148, no. 13, pp. 73 – 87, 2008.

[116] G.-S. Chang, J.-S. Koo, and K.-W. Song, "Wall slip of vaseline in steady shear rheometry," *Korea-Australia Rheology Journal*, vol. 15, pp. 55–61, 2003.

[117] H. Barnes, *A handbook of elementary rheology*. University of Wales, Institute of Non-Newtonian Fluid Mechanics, 2000.

[118] S. Yeong, P. Luckham, and T. Tadros, "Steady flow and viscoelastic properties of lubricating grease containing various thickener concentrations," *Journal of Colloid and Interface Science*, vol. 274, no. 1, pp. 285 – 293, 2004.

[119] "ASTM standard D445-12 , 2011, Standard test method for kinematic viscosity of transparent and opaque liquids (and calculation of dynamic viscosity)."

[120] G. Gow, "The CEY to grease rheology," *Transactions of Mechanical Engineering*, pp. 202–205, 1991.

[121] T. Karis, R.-N. Kono, and M. Jhon, "Harmonic analysis in grease rheology," *Journal of Applied Polymer Science*, vol. 90, no. 2, pp. 334–343, 2003.

[122] G. Froishteter, *Rheological and Thermophysical Properties of Greases*. Taylor & Francis, 1988.

[123] G. B. Froishteter, ÉL. Smorodinskii, Y. L. Ishchuk, L. O. Yurtin, and N. V. Radionova, "Calculation of hydraulic resistance in transport of lubricating greases through pipelines," *Chemistry and Technology of Fuels and Oils*, vol. 12, pp. 129–133, 1976. 10.1007/BF00714261.

[124] D. Doraiswamy, A. N. Mujumdar, I. Tsao, A. N. Beris, S. C. Danforth, and A. B. Metzner, "The cox–merz rule extended: A rheological model for concentrated suspensions and other materials with a yield stress," *Journal of Rheology*, vol. 35, no. 4, pp. 647–685, 1991.

[125] J. Greenwood and J. Kauzlarich, "Elastohydrodynamic film thickness for shear-thinning lubricants," *Proceedings of the Institution of Mechanical Engineers, Part J: Journal of Engineering Tribology*, vol. 212, no. 3, pp. 179–191, 1998.

[126] L. Bordenet, G. Dalmaz, J. Chaomleffel, and F. Vergne, "A study of grease film thicknesses in elastorheodynamic rolling point contacts," *Lubrication Science*, vol. 2, no. 4 , Jul., 1990, pp. 273–284, 1990.

[127] H. Aström, O. Isaksson, and E. Höglund, "Video recordings of an EHD point contact lubricated with grease," *Tribology International*, vol. 24, no. 3, pp. 179–184, 1991.

[128] W. B.P., K. D.R., and C. P.M., "Influence of grease composition on film thickness in EHD contacts," *NLGI Spokesman*, vol. 57, no. 8, pp. 13–18, 1993.

[129] J. Lundberg, A. Parida, and P. Söderholm, "Running temperature and mechanical stability of grease as maintenance parameters of railway bearings," *Int. J. Autom. Comput.*, vol. 7, pp. 160–166, May 2010.

[130] P. Katyal and P. Kumar, "Central film thickness formula for shear thinning lubricants in EHL point contacts under pure rolling," *Tribology International*,

vol. 48, no. 0, pp. 113 – 121, 2012. 14th Nordic Symposium on Tribology, NORDTRIB 2010.

[131] S. Bair and F. Qureshi, "The generalized newtonian fluid model and elastohydrodynamic film thickness," *Journal of Tribology-transactions of The Asme*, vol. 125, 2003.

[132] P. Anuradha and P. Kumar, "New film thickness formula for shear thinning fluids in thin film elastohydrodynamic lubrication line contacts," *Proceedings of the Institution of Mechanical Engineers, Part J: Journal of Engineering Tribology*, vol. 225, no. 4, pp. 173–179, 2011.

[133] P. Kumar and M. Khonsari, "Combined effects of shear thinning and viscous heating on EHL characteristics of rolling/sliding line contacts," *Journal of tribology*, vol. 130, no. 4, 2008.

[134] S. Bair, "Actual eyring models for thixotropy and shear-thinning: experimental validation and application to EHD," *Journal of tribology*, vol. 126, no. 4, pp. 728–732, 2004.

[135] S. Bair, I. Krupka, P. Sperka, and M. Hartl, "Quantitative elastohydrodynamic film thickness of mechanically degraded oil," *Tribology International*, vol. 64, pp. 33 – 38, 2013.

[136] I. Krupka, S. Bair, P. Kumar, P. Svoboda, and M. Hartl, "Mechanical degradation of the liquid in an operating EHL contact," *Tribology Letters*, vol. 41, no. 1, pp. 191–197, 2011.

[137] I. Krupka, S. Bair, P. Kumar, M. Khonsari, and M. Hartl, "An experimental validation of the recently discovered scale effect in generalized newtonian EHL," *Tribology Letters*, vol. 33, pp. 127–135, 2009.

[138] H. A. Spikes, "Sixty years of EHL," *Lubrication Science*, vol. 18, no. 4, pp. 265–291, 2006.

[139] P. Sy, "Experimental study of grease in elastohydrodynamic lubrication," *J Lubr Technol Trans ASME*, vol. 94 Ser F, no. 1, pp. 27–34, 1972.

[140] P. M. Cann, H. A. Spikes, and J. Hutchinson, "The development of a spacer layer imaging method (SLIM) for mapping elastohydrodynamic contacts," *Tribology Transactions*, vol. 39, pp. 915 – 921, 1996.

[141] G. J. Johnston, R. Wayte, and H. A. Spikes, "The measurement and study of very thin lubricant films in concentrated contacts," *STLE Tribology Transaction*, vol. 34, p. 187194., 1991.

[142] G. Guangteng, P. Cann, A. V. Olver, and H. A. Spikes, "Lubricant film thickness in rough surface, mixed elastohydrodynamic contact," *Journal of Tribology*, vol. 122, pp. 65–76, 2000.

[143] L. Gustafsson, E. Hoglund, and O. Marklund, "Measuring lubricant film thickness with image analysis," *Proceedings - IMechE: J, Journal of Engineering Tribology*, vol. 208, pp. 199–205, 1994.

[144] M. Hartl, I. Krupka, and M. Liska, "Differential colorimetry: tool for evaluation of chromatic interference patterns," *Optical Engineering*, vol. 36, no. 9, pp. 2384–2391, 1997.

[145] H. S. Cheng, "A numerical solution of the elastohydrodynamic film thickness in an elliptical contact," *Journal of Tribology*, vol. 1, pp. 155–161, 92.

[146] L. Wedeven, D. Evans, A. Cameron, and A. S. of Mechanical Engineers, *Optical Analysis of Ball Bearing Starvation*. American Society of Mechanical Engineers, ASME, 1970.

[147] B. J. Hamrock and D. Dowson, "Isothermal elastohydrodynamic lubrication of point contacts, part iii - fully flooded results.," *Trans. ASME Series F, J. Lubr. Technol.*, vol. 99(2), pp. 264–276, 1977.

[148] R. J. Chittenden, D. Dowson, J. F. Dunn, and M. Taylor, C., "A theoretical analysis of the isothermal elastohydrodynamic lubrication of concentrated contacts, part i: direction of lubricant entrainment coincident with the major axis of the hertzian contact ellipse.," *Proc. R. Soc. Lond*, vol. A397(1813), pp. 245–269, 1985.

[149] B. J. Hamrock, S. R. Schmid, and B. Jacobson, *Fundamentals of fluid film lubrication, 2nd edition*. Dekker, Basel, 2004.

[150] C. Venner and W. Napel, "Multilevel solution of the elastohydrodynamically lubricated circular contact problem part 2: Smooth surface results," *Wear*, vol. 152, no. 2, pp. 369 – 381, 1992.

[151] D. Dowson and G. Higginson, *Elasto-hydrodynamic lubrication*. International series on materials science and technology, Pergamon Press, 1977.

[152] P. K. Gupta, H. S. Cheng, D. Zhu, N. H. Forster, and J. B. Schrand, "Viscoelastic effects in mil-l-7808-type lubricant, part i: Analytical formulation," *Tribology Transactions*, vol. 35, no. 2, pp. 269–274, 1992.

[153] P. O. Larsson, R. Larsson, A. Jolkin, and O. Marklund, "Pressure fluctuations as grease soaps pass through an EHL contact," *Tribology International*, vol. 33, no. 3-4, pp. 211 – 216, 2000.

[154] M. Kaneta, T. Ogata, and M. Takubo, Y.AND Naka, "Effects of a thickener structure on grease elastohydrodynamic lubrication films," *Proceedings of the Institution of Mechanical Engineers, Part J: Journal of Engineering Tribology*, vol. 214, no. 4, pp. 327–336, 2000.

[155] R. W. M. Wardle, R. C. Coy, P. M. Cann, and H. A. Spikes, "An in lubro study of viscosity index improvers in EHD contacts," *Lubrication Science*, vol. 3, no. 1, pp. 45–62, 1990.

[156] P. M. Cann, B. P. Williamson, R. C. Coy, and H. A. Spikes, "The behaviour of greases in elastohydrodynamic contacts," *Journal of Physics D: Applied Physics*, vol. 25, no. 1A, p. A124, 1992.

[157] A. Wilson, "Relative thickness of grease and oil films in rolling bearings.," *Proceedings - Institution of Mechanical Engineers*, vol. 193, pp. 185–192, 1979.

[158] C. Venner, M. van Zoelen, and P. Lugt, "Thin layer flow and film decay modeling for grease lubricated rolling bearings," *Tribology International*, vol. 47, no. 0, pp. 175 – 187, 2012.

[159] J. J. Kauzlarich and J. Greenwood, "Elastohydrodynamic lubrication with herschel-bulkley model greases.," *ASLE Trans*, vol. 15, no. 4, pp. 269–277, 1972.

[160] B. K. Karthikeyan, M. Teodorescu, H. Rahnejat, and S. J. Rothberg, "Thermoelastohydrodynamics of grease-lubricated concentrated point contacts," *Proceedings of the Institution of Mechanical Engineers, Part C: Journal of Mechanical Engineering Science*, vol. 224, no. 3, pp. 683–695, 2010.

[161] P. M. Cann, "Starvation and reflow in a grease-lubricated elastohydrodynamic contact," *Tribology Transactions*, vol. 39, no. 3, pp. 698–704, 1996.

[162] J. Mansot, P. Terech, and J. Martin, "Structural investigation of lubricating greases," *Colloids and Surfaces*, vol. 39, no. 2, pp. 321 – 333, 1989.

[163] P. Cann and H. Spikes, "Film thickness measurements of lubricating greases under normally starved conditions," *NLGI Spokesman*, vol. 56, p. 21, 1992.

[164] P. M. Cann, "Starved grease lubrication of rolling contacts," *Tribology Transactions*, vol. 42, no. 4, pp. 867–873, 1999.

[165] H. A. Spikes, "Direct observation of boundary layers," *Langmuir*, vol. 12, no. 19, pp. 4567–4573, 1996.

[166] P. M. Cann, "Grease lubrication of rolling element bearings role of the grease thickener," *Lubrication Science*, vol. 19, no. 3, pp. 183–196, 2007.

[167] J. Luo, S. Wen, and P. Huang, "Thin film lubrication. part i. study on the transition between EHL and thin film lubrication using a relative optical interference intensity technique," *Wear*, vol. 194, no. 1á2, pp. 107 – 115, 1996.

[168] H. A. Spikes, "Film-forming additives - direct and indirect ways to reduce friction," *Lubrication Science*, vol. 14, no. 2, pp. 147–167, 2002.

[169] J. Pemberton and A. Cameron, "A mechanism of fluid replenishment in elastohydrodynamic contacts," *Wear*, vol. 37, no. 1, pp. 185 – 190, 1976.

[170] Y. P. Chiu, "An analysis and prediction of lubricant film starvation in rolling contact systems," *A S L E Transactions*, vol. 17, no. 1, pp. 22–35, 1974.

[171] M. T. van Zoelen, C. H. Venner, and P. M. Lugt, "Prediction of film thickness decay in starved elasto-hydrodynamically lubricated contacts using a thin layer flow model," *Proceedings of the Institution of Mechanical Engineers, Part J: Journal of Engineering Tribology*, vol. 223, no. 3, pp. 541–552, 2009.

[172] M. van Zoelen, C. Venner, and P. Lugt, "Free surface thin layer flow on bearing raceways," *Journal of Tribology*, vol. 130, no. 2, pp. 1–10, 2008.

[173] P. Lugt, S. Velickov, and J. Tripp, "On the chaotic behavior of grease lubrication in rolling bearings," *Tribology Transactions*, vol. 52, no. 5, pp. 581–590, 2009.

[174] B. Damiens, A. Lubrecht, and P. Cann, "Influence of cage clearance on bearing lubrication," *Tribology Transactions*, vol. 47, no. 1, pp. 2–6, 2004.

[175] L. Gershuni, M. G. Larson, and P. M. Lugt, "Lubricant replenishment in rolling bearing contacts," *Tribology Transactions*, vol. 51, no. 5, pp. 643–651, 2008.

[176] H. Åström, J. O. Östensen, and E. Höglund, "Lubricating grease replenishment in an elastohydrodynamic point contact," *Journal of tribology*, vol. 115, no. 3, pp. 501–506, 1993.

[177] B. Jacod, F. Pubilier, P. Cann, and A. Lubrecht, "An analysis of track replenishment mechanisms in the starved regime," *Proceedings of 25 Leeds-Lyon Symposium on Tribology*, pp. 483–492, 1998.

[178] X. Li, F. Guo, and B. Fan, "Influence of spinning effect on the rolling EHL films," in *Advanced Tribology* (J. Luo, Y. Meng, T. Shao, and Q. Zhao, eds.), pp. 134–135, Springer Berlin Heidelberg, 2010.

[179] P. Cann and A. Lubrecht, "The effect of transient loading on contact replenishment with lubricating greases," *Tribology Series*, vol. 43, pp. 745–750, 2003.

[180] P. M. Cann, "Thin-film grease lubrication," *Proceedings of the Institution of Mechanical Engineers, Part J: Journal of Engineering Tribology*, vol. 213, no. 5, pp. 405–416, 1999.

[181] H. Kageyama, W. Machidori, and T. Moriuchi, "Grease lubrication in elastohydrodynamic contacts," *NLGI Spokesman*, vol. 48(3), pp. 72–81, 1984.

[182] P. Eriksson, V. Wikström, and R. Larsson, "Grease passing through an elastohydrodynamic contact under pure rolling conditions," *Proceedings of the Institution of Mechanical Engineers, Part J: Journal of Engineering Tribology*, vol. 214, no. 4, pp. 309–316, 2000.

[183] N. Fang, L. Chang, M. Webster, and A. Jackson, "A non-averaging method of determining the rheological properties of traction fluids," *Tribology International*, vol. 33, no. 11, pp. 751 – 760, 2000.

[184] G. E. Morales and A. W. Wemekamp, "An engineering approach on sliding friction in full-film, heavily loaded lubricated contacts," *Proceedings of the Institution of Mechanical Engineers, Part J: Journal of Engineering Tribology*, vol. 218, no. 6, pp. 513–527, 2004.

[185] K. L. Johnson and J. L. Tevaarwerk, "Shear behaviour of elastohydrodynamic oil films," *Proceedings of the Royal Society of London. A. Mathematical and Physical Sciences*, vol. 356, no. 1685, pp. 215–236, 1977.

[186] W. Hirst and A. J. Moore, "Elastohydrodynamic lubrication at high pressures," *Proceedings of the Royal Society of London. A. Mathematical and Physical Sciences*, vol. 360, no. 1702, pp. 403–425, 1978.

[187] M. Björling, W. Habchi, S. Bair, R. Larsson, and P. Marklund, "Towards the true prediction of EHL friction," *Tribology International*, vol. 66, pp. 19 – 26, 2013.

[188] S. Bair and W. O. Winer, "A rheological model for elastohydrodynamic contacts based on primary laboratory data," *Journal of Lubrication Technology*, vol. 101, no. 3, pp. 258–264, 1979.

[189] S. Bair and W. O. Winer, "Shear strength measurements of lubricants at high pressure," *Journal of Lubrication Technology*, vol. 101, no. 3, pp. 251–257, 1979.

[190] W. Habchi, S. Bair, and P. Vergne, "On friction regimes in quantitative elastohydrodynamics," *Tribology International*, vol. 58, no. 0, pp. 107 – 117, 2013.

[191] S. Bair and M. Kotzalas, "The contribution of roller compliance to elastohydrodynamic traction," *Tribology Transactions*, vol. 49, no. 2, pp. 218–224, 2006.

[192] J. A. Brando, M. Meheux, J. H. O. Seabra, F. Ville, and M. J. D. Castro, "Traction curves and rheological parameters of fully formulated gear oils," *Proceedings of the Institution of Mechanical Engineers, Part J: Journal of Engineering Tribology*, vol. 225, no. 7, pp. 577–593, 2011.

[193] C. M. Fernandes, R. C. Martins, and J. H. Seabra, "Friction torque of thrust ball bearings lubricated with wind turbine gear oils," *Tribology International*, vol. 58, no. 0, pp. 47 – 54, 2013.

[194] S. Gunsel, S. Korcek, M. Smeeth, and H. A. Spikes, "The elastohydrodynamic friction and film forming properties of lubricant base oils," *Tribology Transactions*, vol. 42, no. 3, pp. 559–569, 1999.

[195] T. Kyotani, H. Yoshitake, T. Ito, and Y. Tamai, "Correlation between flow properties and traction of lubricating oils," *A S L E Transactions*, vol. 29, no. 1, pp. 102–106, 1986.

[196] J. Igarashi, T. Kagaya, M.and Satoh, and T. Nagashima, "High viscosity index petroleum base stocks - the high potential base stocks for fuel economy automotive lubricants," *SAE Technical Paper 920659*, 1992.

[197] L. Houpert, "Ball bearing and tapered roller bearing torque: Analytical, numerical and experimental results," *Tribology Transactions*, vol. 45, no. 3, pp. 345–353, 2002.

[198] V. Paleu, S. Cretu, and D. Nelias, "Friction moment in oil and kerosene mist lubricated all-steel and hybrid ball bearings," in *16th International Colloquium Tribology - Lubricants, Materials and Lubrication Engineering*, 2008.

[199] X. T. Xia and T. M. Lv, "Dynamic prediction of rolling bearing friction torque using lyapunov exponent method," *Applied Mechanics and Materials*, vol. 44-47, pp. 1120–1124, 2010.

[200] B. Wikström, V. Jacobson, "Loss of lubricant from oil-lubricated near-starved spherical roller bearings," *Proceedings of the Institution of Mechanical Engineers, Part J: Journal of Engineering Tribology*, vol. 211, no. 1, pp. 51–66, 1997.

[201] P. M. E. Cann and A. A. Lubrecht, "Bearing performance limits with grease lubrication: the interaction of bearing design, operating conditions and grease properties," *Journal of Physics D: Applied Physics*, vol. 40, no. 18, p. 5446, 2007.

[202] *Kistler Instruments AG. Reaction Torque Sensor 9339A and Charge Meter 5015A Instruction Manual, 2008 Edition.*

[203] P. Kumar, M. M. Khonsari, and S. Bair, "Full EHL simulations using the actual reeeyring model for shear-thinning lubricants," *Journal of Tribology-transactions of The Asme*, vol. 131, 2009.

[204] P. Kumar and M. M. Khonsari, "Combined effects of shear thinning and viscous heating on EHL characteristics of rolling/sliding line contacts," *Journal of Tribology-transactions of The Asme*, vol. 130, 2008.

[205] P. Kumar and M. M. Khonsari, "EHL circular contact film thickness correction factor for shear-thinning fluids," *Journal of Tribology-transactions of The Asme*, vol. 130, 2008.

[206] http://webtools3.skf.com/BearingCalc/selectCalculation.action, 2013.

[207] T. Cousseau, B. M. Graça, A. V. Campos, and J. H. Seabra, "Influence of grease rheology on thrust ball bearings friction torque," *Tribology International*, vol. 46, no. 1, pp. 106–113, 2012.

[208] S. Hosoya and M. Hayano, "Deterioration of lithium soap greases and functional life in ball bearings," *NLGI spokesman*, vol. 53, no. 6, pp. 246–251, 1989.

[209] H. Ito, M. Tomaru, and T. Suzuki, "Physical and chemical aspects of grease deterioration in sealed ball bearings," *Lubrication engineering*, vol. 44, no. 10, pp. 872–879, 1988.

[210] C. Araki, H. Kanzaki, and T. Taguchi, "A study on the thermal degradation of lubricating greases," *NLGI Spokesman*, vol. 59, pp. 15–23, 1995.

[211] I. Couronné, G. Blettner, and P. Vergne, "Rheological behavior of greases: Part ieffects of composition and structure," *Tribology Transactions*, vol. 43, no. 4, pp. 619–626, 2000.

[212] S. Hurley and P. M. Cann, "Infrared spectroscopic characterisation of grease lubricant films on metal surfaces.," *NLGI Spokesman*, vol. 64, pp. 13–21, 2000.

[213] J. Lundberg and S. Berg, "Grease-lubrication of roller bearings in railway waggons. part 2: laboratory tests and selection of proper test methods," *Industrial Lubrication and Tribology*, vol. 52, pp. 76–86, 2000.

[214] R. Mas and A. Magnin, "Rheological and physical studies of lubricating greases before and after use in bearings," *Journal of Tribology*, vol. 118, no. 3, pp. 681–686, 1996.

[215] S. Hurley, P. Cann, and H. Spikes, "Thermal degradation of greases and the effect on lubrication performance," in *Tribology for Energy Conservation Proceedings of the 24th Leeds-Lyon Symposium on Tribology* (D. Dowson, C. Taylor, T. Childs, G. Dalmaz, L. F. Y. Berthier, J.-M. Georges, and A. Lubrecht, eds.), vol. 34 of *Tribology Series*, pp. 75 – 83, Elsevier, 1998.

[216] M. Barbooti and D. Al-Sammerrai, "Thermoanalytical investigations on lithium stearate, lithium 12-hydroxystearate and related greases," *Journal of thermal analysis*, vol. 30, pp. 587–595, 1985.

[217] N. Eng-Poh and M. Svetlana, "Quantitative moisture measurements in lubricating oils by FTIR spectroscopy combined with solvent extraction approach," *Microchemical Journal*, vol. 98, no. 2, pp. 177 – 185, 2011.

[218] J. Coates, "Interpretation of infrared spectra, a practical approach," *Encyclopedia of analytical chemistry*, 2000.

[219] J. P. Coates and L. C. Setti, "Infrared spectroscopic methods for the study of lubricant oxidation products," *ASLE transactions*, vol. 29, no. 3, pp. 394–401, 1986.

[220] T. Bley, E. Pignanelli, and A. SchUtze, "Multichannel ir sensor system for determination of oil degradation," in *14th International Meeting on Chemical Sensors - IMCS 2012*, pp. 974 – 977, 2012.

[221] W. Castro, J. Perez, S. Erhan, and F. Caputo, "A study of the oxidation and wear properties of vegetable oils: Soybean oil without additives," *Journal of the American Oil Chemists' Society*, vol. 83, no. 1, pp. 47–52, 2006.

[222] Q. Li, P. Jiang, and P. Wei, "Thermal degradation behavior of poly(propylene) with a novel silicon containing intumescent flame retardant," *Macromolecular Materials and Engineering*, vol. 290, no. 9, pp. 912–919, 2005.

[223] V. González-González, G. Neira-Velázquez, and J. Angulo-Sánchez, "Polypropylene chain scissions and molecular weight changes in multiple extrusion," *Polymer Degradation and Stability*, vol. 60, no. 1, pp. 33 – 42, 1998.

[224] S. Wen and P. Huang, *Principles of Tribology*. Wiley, 2012.

[225] Z. M. Ariff, A. Ariffin, S. S. Jikan, and N. A. A. Rahim, *Polypropylene*, ch. 3 - Rheological Behaviour of Polypropylene Through Extrusion and Capillary Rheometry, pp. 29–48. In Tech, 2012.

[226] A. van den Kommer and J. Ameye, "Prediction of remaining grease life - a new approach and method by linear sweep voltammetry," *Proceeding of the 7th International Colloquim Tribology*, pp. 891–896, 2001.

[227] M. Keentok and S.-C. Xue, "Edge fracture in cone-plate and parallel plate flows," *Rheologica Acta*, vol. 38, pp. 321–348, 1999.

Appendix

A. Data correction of the rheological measurements

The error on rheological measurements can arise from non-parallelism, wall slip, non- concentricity, edge effects, non-flatness of the plates, gap error and non-constant shear rate [1].

A.1. Edge effects, wall slip, parallelism, concentricity and flatness of the plates

The rheometer rotating shafts and plates were checked for run-out, dimensional and geometric tolerances, excluding or at least reducing the errors associate with non-parallelism, non-concentricity and non flatness of the plates.

Not so small gaps and rough plates follow by post-analysis of the flow curves were used to minimize wall slip.

Edge effects include rim fracture and radial migration of grease [227]. These effects give an important contribution to the shear stress because shear rates and thus shear stresses are highest at the rim. After each measurement the rim was visually checked out for edge effects and when needed some of the measured values at high shear rates were disregarded.

A.2. Gap error

The gap errors were eliminated by a carefully zero gap procedure (see Section 3.8) together with post-processing of the data using the method described by Davies and Stokes [115], and briefly described here.

Newtonian fluid was used before and after a series of experiments at the required temperature to determine the gap error. The measured gap error is used for a correction of the shear rates. The real shear rate can then be calculate as

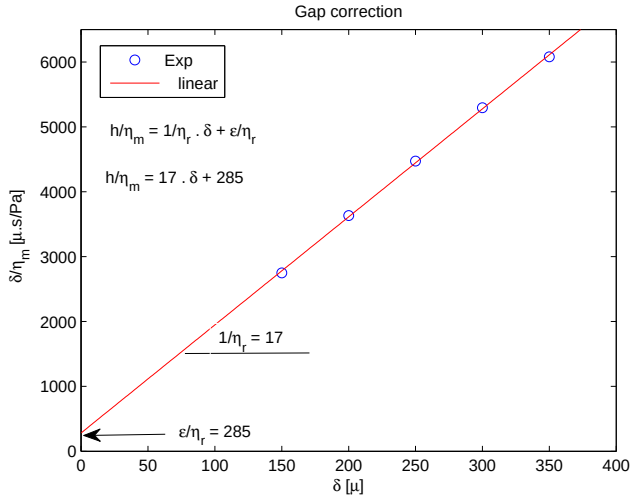

Figure A.1.: Gap correction graph at 40°C - Newtonian oil.

$$\dot{\gamma}_{actual} = \dot{\gamma}_m \frac{\delta}{\delta + \epsilon} \tag{A.1}$$

where $\dot{\gamma}_{actual}$ is the actual shear stress, $\dot{\gamma}_m$ the measured shear rate, δ the gap height, and ϵ the gap error.

Newtonian oil with well known viscosity was used to determine the gap error at 40 °C . The viscosity was measured for 5 different gap heights - 350, 300, 250, 200 and 150 μm. The gap error was determined with the graphical solution explained by Davies and Stokes [115] and equation A.2

$$\frac{\delta}{\eta_m} = \left(\frac{1}{\eta_{actual}}\right)\delta + \left(\frac{\epsilon}{\eta_{actual}}\right), \tag{A.2}$$

where η_m is the measured viscosity and η_{actual} the real viscosity. The quotient δ/η_m is plotted against the gap setting δ in Figure A.1. The slope of the straight line (linear fitting through the measurements) determines the actual viscosity $1/\eta_{actual}$. The intercept at $\delta = 0$ gives the ϵ/η_{actual} term from which the gap error can be determined. In the given example the quotient $1/\eta_{actual} \approx 16,7$ and $\epsilon/\eta_{actual} \approx 285$, from where the real viscosity $\eta_{actual} = 0,06$ Pa.s and the gap error $\epsilon = 17\ \mu\ m$ were obtained, respectively. The positive gap error of $\epsilon = 17\ \mu$m was used for gap correction. Such gap error shift the results in ≈ 9 %, once the used gap for the flow tests was 175 μm.

Once the gap error ϵ is known, the shear rate, viscosity and shear stress are easily corrected using equations A.3 to A.5.

$$\dot{\gamma}_{actual} = \dot{\gamma}_m \frac{\delta}{\delta + \epsilon} \tag{A.3}$$

$$\eta_{actual} = \eta_m \frac{\delta}{\delta + \epsilon} \tag{A.4}$$

$$\tau_{actual} = \eta_{actual} \cdot \dot{\gamma}_{actual} \tag{A.5}$$

Since the commanded or measured strain is also affected by gap error in the same way as the shear rate, the measured values of storage (G') and loss (G'') moduli must also be corrected when performing oscillatory experiments according to equation A.6 [115]. The used gap in the oscilattory tests was 250 μm and therefore the results were reduced in $\approx$ 6.5 %.

$$G = G_{actual} = G_m \frac{\delta}{\delta + \epsilon} \tag{A.6}$$

where G refers to either G' and G''.

A.3. Non-constant shear rate

To correct for the non-constant shear rate over the plate radius the shear stress is calculated from the measured torque as Macosko [80]. Such corrections should be done after gap correction, and therefore the used input values for shear stress, shear rate and apparent viscosity are gap-corrected.

$$T = 2\pi \int_0^R \tau r^2 dr, \tag{A.7}$$

$$\tau = \frac{T}{2\pi R^3} \left(3 + \frac{\partial \ln T}{\partial \ln \dot{\gamma}_R} \right), \tag{A.8}$$

where τ is the shear stress, $\dot{\gamma}_R$ the shear rate at the rim, T the measured torque, and R the plate radius. Similarly, the apparent viscosity can be calculated,

$$\eta = \frac{T/2\pi R^3}{\dot{\gamma}_R} \left(3 + \frac{\partial \ln(T/2\pi R^3)}{\partial \ln \dot{\gamma}_R} \right) \tag{A.9}$$

B. Rolling bearing friction torque

B.1. SKF rolling friction torque model

A summary of the SKF friction torque model information available in [8] and [6] is presented here in the case of grease lubricated thrust ball bearing - THBB 51107 mounted in vertical shafts. Therefore, all constants and equations presented should **not** be used for different bearings, lubrication methods or assembly arrangements.

All the figures presented in this appendix depict the typical behaviour of a THBB 51107 running under constant operating temperature of 60 °C , loaded with 7 kN, lubricated with mineral based grease with base oil viscosity of 50 mm^2/s at the operating temperature and entrainment speed from 50 to 100000 rpm. The used rotational speed values over by far the limits advised for the THBB 51107, but were used just to characterize all the friction torque variables from very low to very high $\nu \times n \times d_m$ parameter.

The total internal friction torque of a grease lubricated THBB 51107 is composed by the rolling (M_{rr}) and sliding torque (M_{sl}) components, according to equation B.1.

$$M_t = \varphi_{ish} \times \varphi_{rs} \underbrace{(G_{rr}(n \times \nu)^{0,6})}_{M_{rr}} + \underbrace{(G_{sl} \times \mu_{sl})}_{M_{sl}} \tag{B.1}$$

B.1.1. Rolling torque - M_{rr}

There are several sources of rolling friction losses in the rolling contacts, such as the energy spent to introduce the lubricant into the contact and to reject the excess (elastohydrodynamic lubrication process) and the elastic hysteresis losses in the steel (energy dissipation in the deformation process) as shown in Figure B.1. Adhesion forces between surfaces are another mechanism that can generate rolling friction.

The rolling frictional moment is calculated from equation B.2,

$$M_{rr} = G_{rr}(n.\nu)^{0,6} \tag{B.2}$$

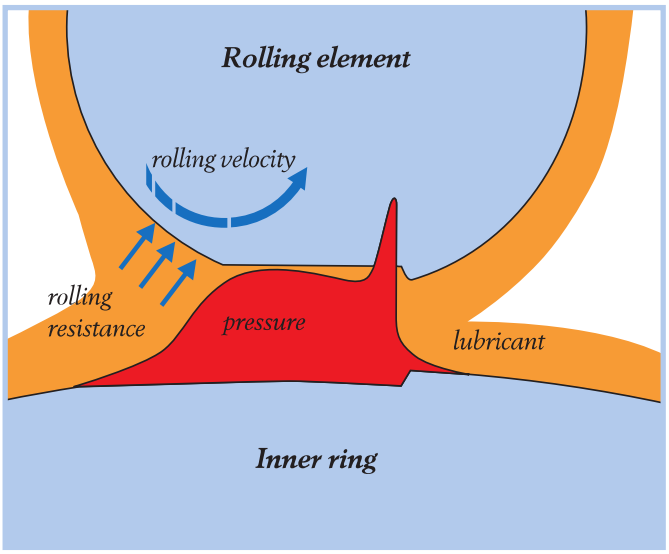

Figure B.1.: Rolling resistance due to pressure distribution and elastic deformation [6].

where ν is the kinematic viscosity of the lubricant at the operating temperature in mm^2/s (for grease lubrication base oil viscosity must be used), n is the rotational speed in rpm and G_{rr} represents the influence of the bearing load on the rolling resistance and depends on the bearing type, the bearing mean diameter and the axial load. The load distribution in the different rolling element contacts is added all together. G_{rr} is given by

$$G_{rr} = R_1 . {d_m}^{1,83} . {F_a}^{0,54} \tag{B.3}$$

where R_1 is a geometry constant for rolling frictional moment with value of $1,03 \times 10^{-6}$, d_m is the bearing mean diameter in mm and F_a is the axial load in N.

The rolling friction resistance is also affected by two reduction factors, the inlet shear heating (φ_{ish}) and the kinematic replenishment/starvation (φ_{rs}):

B.1.1.1. Inlet shear heating - φ_{ish}

Inlet shear heating occurs because not all the lubricant present at the inlet of the contact manages to get inside; some of it will recirculate in the inlet because of the reverse flow. This recirculation produces heat, since the viscosity of the lubricant is highly reduced by the temperature; lower viscosity at the inlet of the contact means lower film thickness and, therefore, lower rolling resistance. This effect is taken into

account in the SKF friction model by means of the reduction factor φ_{ish}, which is calculated by

$$\varphi_{ish} = \frac{1}{1 + 1,84 \times 10^{-9}(nd_m)^{1,28}\nu^{0,64}} \tag{B.4}$$

B.1.1.2. Kinematic replenishment/starvation - φ_{rs}

The kinematic replenishment/starvation occurs when high speeds or high lubricant viscosities hamper the replenishment of lubricant in the raceway after a rolling element has passed, since the lubricant will not have sufficient time to flow back from the sides to the centre of the raceway. This is kinematic starvation, which will produce a reduction of the lubricant availability in the inlet of the contact and reduce the film thickness and the rolling resistance. The replenishment/starvation effect is considered in the SKF friction model by means of the multiplication factor φ_{rs}. This factor is a function of the lubricant supply mechanism as well and is calculated by

$$\varphi_{rs} = \frac{1}{e^{K_{rs}\nu n(d+D)\sqrt{\frac{K_z}{2(D-d)}}}} \tag{B.5}$$

where K_{rs} is the replenishment/starvation factor with values of 6×10^{-8} for greases or oil-spot lubrication and K_Z is a bearing type related geometry with value of 3,8.

The typical curve of φ_{ish} and φ_{rs} for the same inputs of speed, viscosity and bearing geometry are shown in Figure B.2

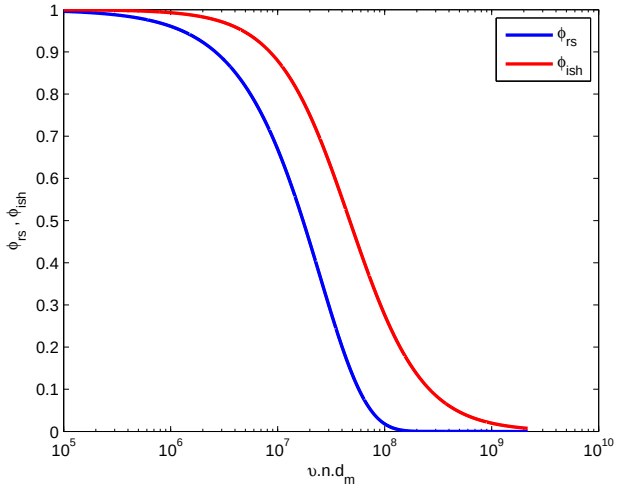

Figure B.2.: Typical variation of the reduction factors φ_{ish} and φ_{rs} with the operating parameter $\nu \times n \times d_m$.

This figure clearly shows that the kinematic replenishment/starvation factor (φ_{rs}) has a greater influence on the rolling torque that the inlet shear heating factor φ_{ish} at the same operating condition.

Including the inlet shear heating and the kinematic replenishment/starvation effects, the rolling resistance can be expressed by

$$M'_{rr} = \varphi_{ish} \times \varphi_{rs} \times G_{rr}(n \times \nu)^{0,6} \tag{B.6}$$

The typical behaviour of the rolling torque is shown in Figure B.3 including (M'_{rr}) and not including (M_{rr}) the reduction factors.

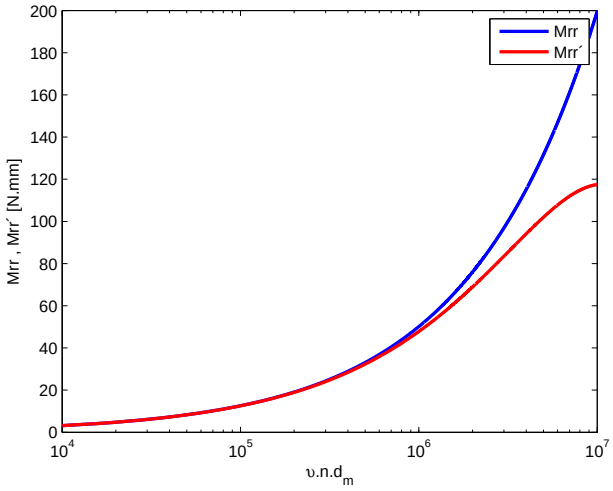

Figure B.3.: Typical variation of the rolling torque M'_{rr} and M_{rr} with the operating parameter $\nu \times n \times d_m$.

B.1.2. Sliding torque - M_{sl}

The slide-to-roll ratio in thrust ball bearings is very small, but it is always present and it generates significant friction. One of the sources of this friction is the macro-sliding caused by contact conformity due to macro-geometry features of the bearing, e.g., the contact between balls and curved raceways and spinning. The other source is the micro-sliding, which is caused by geometrical distortions from elastic deformation. Figure B.4 depicts how sliding friction is produced due to elastic deformation.

The sliding frictional moment is calculated from equation B.7

$$M_{sl} = G_{sl}.\mu_{sl} \tag{B.7}$$

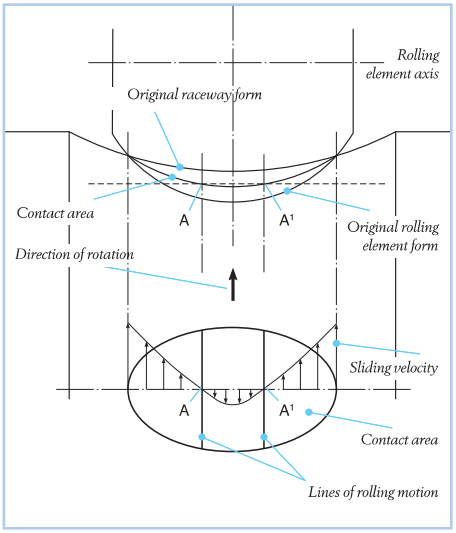

Figure B.4.: Sliding resistance due to elastic deformation in a rolling element with a curved contact surface [6].

where G_{sl} represents the influence of the bearing load on the sliding resistance and depends on the bearing type, the bearing mean diameter and the axial load. The load distribution in the different rolling element contacts is added together and it is given by equation B.8

$$G_{sl} = S_1 . {d_m}^{0,05} . {F_a}^{4/3} \tag{B.8}$$

where S_1 is a geometry constant for sliding frictional moment with value of $1,6 \times 10^{-2}$. μ_{sl} is the global coefficient of friction of the rolling bearing (lubricant shearing - μ_{EHL} plus asperity contacts - μ_{bl}). It strongly depends on the lubrication regime, which is defined here by φ_{bl}. For full film lubrication μ_{sl} mostly depends on lubricant shearing and for boundary lubrication on asperity contacts. It is given by

$$\mu_{sl} = \varphi_{bl} . \mu_{bl} + (1 - \varphi_{bl}) . \mu_{EHL} \tag{B.9}$$

where μ_{bl} is the coefficient of friction in boundary lubrication and therefore strongly depends on lubricant additive package; and μ_{EHL} is the coefficient of friction in full film lubrication and therefore strongly depends on lubricant rheology and contact area. φ_{bl} is the weighting factor for the influence of asperity contact and lubricant shearing mechanisms. Its meaning is analogous to the specific film thickness Λ and viscosity ratio k, shown in equations 6.7 and 6.8, and is determined by

$$\varphi_{bl} = \frac{1}{e^{2{,}6\times10^{-8}(n.\nu)^{1{,}4}d_m}} \tag{B.10}$$

The typical curve of φ_{bl} for the same inputs of speed, viscosity and bearing geometry are shown in Figure B.5

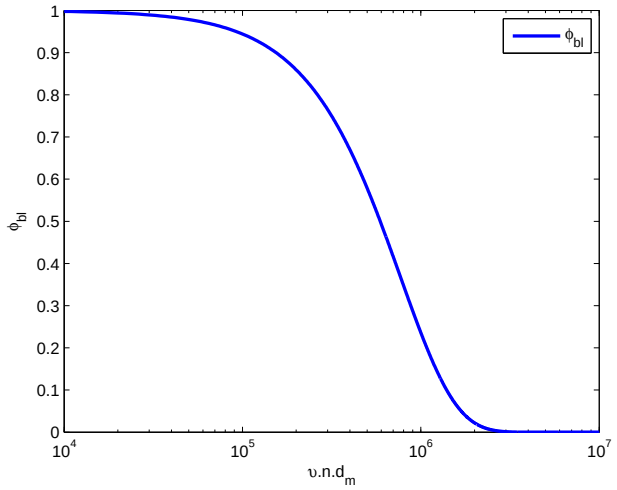

Figure B.5.: Typical variation of the weighting factor (φ_{bl}) with the operating parameter $\nu \times n \times d_m$.

Figure B.5 indicates that the transition from full film lubrication to mixed lubrication starts when $\varphi_{bl} \neq 0$. For the given example, it happens when $\nu \times n \times d_m \leqslant 2 \times 10^6$.

SKF recommends μ_{bl} =0,15 and μ_{EHL} =0,05 for mineral oils and μ_{EHL} =0,04 for synthetic oils.

The typical behaviour of the sliding torque is shown in Figure B.6 .

The total friction torque (M_t), given by equation B.1, is the sum of the curves presented in Figures B.3 and B.6. Its typical behaviour is shown in Figure B.7. One can note that the total friction torque behaves just like a Stribeck curve, presenting high friction torque values for low $\nu \times n \times d_m$ (boundary lubrication), followed by a significant decrease in the friction torque as $\nu \times n \times d_m$ increases (mixed lubrication) up to the moment it reaches full film conditions at higher $\nu \times n \times d_m$.

The presented frictional behaviours are slightly different for rolling bearing tests with self-induced temperature, where the viscosity rather than constant varies drastically with increasing rotational speed.

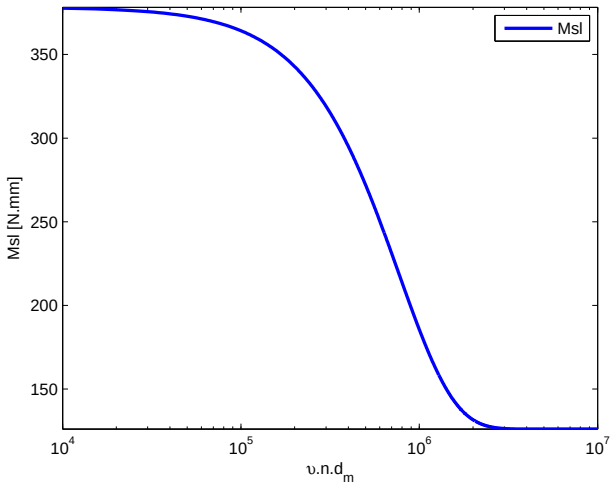

Figure B.6.: Typical variation of the sliding torque (M_{sl}) with the operating parameter $\nu \times n \times d_m$.

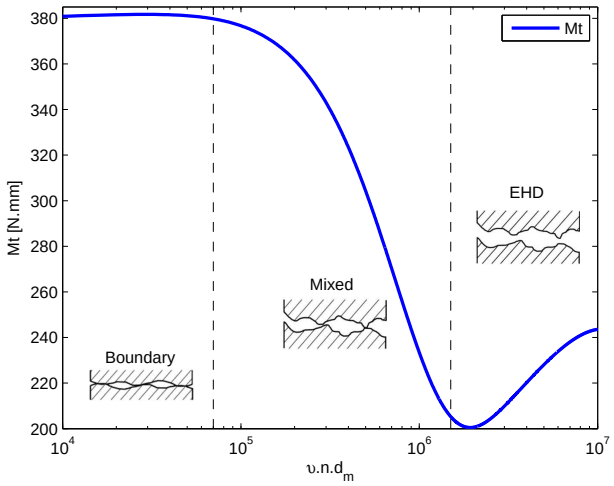

Figure B.7.: Typical variation of the total torque (M_t) with the operating parameter $\nu \times n \times d_m$.

C. Degradation process (Confidential)

D. Publications

D.1. Articles in international peer reviewed scientific journals

- T. Cousseau, M. Björling, B. Graça, A. Campos, J. Seabra and R. Larsson, Film thickness in a ball-on-disc contact lubricated with greases, bleed oils and base oils, Tribology International, 53 (0) (2012) 53-60.

- T. Cousseau, B. Graça, A. Campos and J. Seabra, Influence of grease rheology on thrust ball bearings friction torque, Tribology International, 46 (1) (2012) 106-113.

- T. Cousseau, B. Graça, A. Campos and J. Seabra, Friction torque in grease lubricated thrust ball bearings, Tribology International, 44 (5) (2011) 523-531.

- T. Cousseau, B. Graça, A. Campos and J. Seabra, Influence of grease formulation on thrust bearings power loss, Proceedings of the Institution of Mechanical Engineers, Part J: Journal of Engineering Tribology , 224 (9) (2010) 935-946.

- T. Cousseau, B. Graça, A. Campos and J. Seabra, Friction and wear in thrust ball bearings lubricated with biodegradable greases, Proceedings of the Institution of Mechanical Engineers, Part J: Journal of Engineering Tribology , 225 (7) (2011) 627-639.

- T. Cousseau, B. Graça, A. Campos and J. Seabra, Experimental measuring procedure for the friction torque in rolling bearings, Lubrication Science, 22 (4) (2010) 133-147.

D.2. Articles in conference proceedings

- T. Cousseau, B. Graça, A. Campos and J. Seabra, Friction torque in rolling bearings lubricated with biodegradable greases. In: ECOTRIB 2009 - European Conference on Tribology, Pisa, 2009.

- T. Cousseau, A. Gama, B. Graça, A. Campos and J. Seabra, Analysis of grease lubrication mechanisms on a roller-on-disc contact. In: VII IBERTRIB - Iberian Conference on Tribology, Porto, 2013.

- T. Cousseau, A. Seabra, B. Graça, A. Campos and J. Seabra, Film thickness analysis through friction torque measurements. In: VII IBERTRIB - Iberian Conference on Tribology, Porto, 2013.

- T. Cousseau, M. Björling, B. Graça, A. Campos, J. Seabra and R. Larsson, Film thickness and friction torque prediction of lubricating greases using bleed oil properties. In: ICEM 15 - International Conference on Experimental Mechanics, Porto, 2012.

- T. Cousseau, B. Graça, A. Campos and J. Seabra, Thrust ball bearings lubricated with biodegradable greases. In: 17th International Colloquium Tribology TAE: 'Solving friction and wear problems', Stuttgart/Ostfildern, 2010.

- J. Seabra, T. Cousseau, C. Fernandes, B. Graça, A. Campos and R. Martins, Testing rolling bearings in a modified Four-Ball machine. In: Proceedings of the 18^{th} International Colloquium Tribology TAE: 'Industrial and Automotive Lubrication', Ostfildern, Germany, 2012.

- T. Cousseau, B. Graça, A. Campos and J. Seabra, Friction torque and rheological behaviour of greases thrust bearings. In: 6^{th} Arnold-Tross-Kolloquium, Hamburg, 2010.

- T. Cousseau, B. Graça, A. Campos and J. Seabra, Método experimental para determinação do momento de atrito em rolamentos. In: Segunda Jornada Luso-Brasileira de Ensino e Tecnologia em Engenharia - JLBE09, Porto, 2009.

D.3. Master thesis

- T. Cousseau, Análise comparativa do comportamento de massas lubrificantes num rolamento axial de esferas. Master's thesis, Faculdade de Engenharia da Universidade do Porto (2009).

D.4. Products development

- T. Cousseau, A. Campos and J. Seabra, Bearing assembly for rolling bearing tests in a 4-ball machine, Faculdade de Engenharia da Universidade do Porto (2009).
- T. Cousseau, A. Campos and J. Seabra, Bearing assembly for rolling bearing tests in a 4-ball machine with temperature control, Faculdade de Engenharia da Universidade do Porto (2012).